

SPECTROSCOPIC METHODS OF PROCESS MONITORING  
FOR SAFEGUARDS OF USED NUCLEAR  
FUEL SEPARATIONS

By

Jamie Lee Warburton

Bachelor of Science  
Massachusetts Institute of Technology  
2007

A dissertation submitted in partial fulfillment of  
the requirements for the

**Doctor of Philosophy in Radiochemistry**

**Department of Chemistry  
College of Sciences  
The Graduate College**

**University of Nevada, Las Vegas  
December 2011**

Copyright by Jamie Warburton 2012  
All Rights Reserved



**THE GRADUATE COLLEGE**

We recommend the dissertation prepared under our supervision by

**Jamie Lee Warburton**

entitled

**Spectroscopic Methods of Process Monitoring for Safeguards of Used Nuclear Fuel Separations**

be accepted in partial fulfillment of the requirements for the degree of

**Doctor of Philosophy in Radiochemistry**

Department of Chemistry

Ken Czerwinski, Committee Chair

Paul Forster, Committee Member

Patricia Paviet-Hartmann, Committee Member

Mary Anne Yates, Committee Member

Anthony Hechanova, Graduate College Representative

Ronald Smith, Ph. D., Vice President for Research and Graduate Studies  
and Dean of the Graduate College

**December 2011**

## ABSTRACT

### **Spectroscopic Methods of Process Monitoring for Safeguards of Used Nuclear Fuel Separations**

by

Jamie Lee Warburton

Dr. Ken Czerwinski, Committee Chair  
Professor of Chemistry  
Chair of the Department of Radiochemistry  
University of Nevada, Las Vegas

To support the demonstration of a more proliferation-resistant nuclear fuel processing plant, techniques and instrumentation to allow the real-time, online determination of special nuclear material concentrations in-process must be developed. An ideal materials accountability technique for proliferation resistance should provide nondestructive, real-time, on-line information of metal and ligand concentrations in separations streams without perturbing the process. UV-Visible spectroscopy can be adapted for this precise purpose in solvent extraction-based separations.

The primary goal of this project is to understand fundamental URanium EXtraction (UREX) and Plutonium-URanium EXtraction (PUREX) reprocessing chemistry and corresponding UV-Visible spectroscopy for application in process monitoring for safeguards. By evaluating the impact of process conditions, such as acid concentration, metal concentration and flow rate, on the sensitivity of the UV-Visible detection system, the process-monitoring concept is developed from an advanced application of fundamental spectroscopy. Systematic benchtop-scale studies investigated the system relevant to UREX or PUREX type reprocessing systems, encompassing 0.01-1.26 M U and 0.01-8 M HNO<sub>3</sub>. A laboratory-scale TRansUranic Extraction (TRUEX)

demonstration was performed and used both to analyze for potential online monitoring opportunities in the TRUEX process, and to provide the foundation for building and demonstrating a laboratory-scale UREX demonstration.

The secondary goal of the project is to simulate a diversion scenario in UREX and successfully detect changes in metal concentration and solution chemistry in a counter current contactor system with a UV-Visible spectroscopic process monitor. UREX uses the same basic solvent extraction flowsheet as PUREX, but has a lower acid concentration throughout and adds acetohydroxamic acid (AHA) as a complexant/reductant to the feed solution to prevent the extraction of Pu. By examining UV-Visible spectra gathered in real time, the objective is to detect the conversion from the UREX process, which does not separate Pu, to the PUREX process, which yields a purified Pu product. The change in process chemistry can be detected in the feed solution, aqueous product or in the raffinate stream by identifying the acid concentration, metal distribution and the presence or absence of AHA. A fiber optic dip probe for UV-Visible spectroscopy was integrated into a bank of three counter-current centrifugal contactors to demonstrate the online process monitoring concept. Nd, Fe and Zr were added to the uranyl nitrate system to explore spectroscopic interferences and identify additional species as candidates for online monitoring. This milestone is a demonstration of the potential of this technique, which lies in the ability to simultaneously and directly monitor the chemical process conditions in a reprocessing plant, providing inspectors with another tool to detect nuclear material diversion attempts.

Lastly, dry processing of used nuclear fuel is often used as a head-end step before solvent extraction-based separations such as UREX or TRUEX. A non-aqueous process,

used fuel treatment by dry processing generally includes chopping of used fuel rods followed by repeated oxidation-reduction cycles and physical separation of the used fuel from the cladding. Thus, dry processing techniques are investigated and opportunities for online monitoring are proposed for continuation of this work in future studies.

## ACKNOWLEDGEMENTS

Many individuals influenced the forming of this document, and I'm thankful for all of the different perspectives, opinions and fields of expertise that I've been able to learn from throughout this endeavor. My professors, supervisors and colleagues at the University of Nevada Las Vegas provided me with the facilities, network and instruction to succeed. Ken Czerwinski, Patricia Paviet-Hartmann, Anthony Hechanova, Mary Anne Yates and Paul Forster were kind enough to sit on my dissertation committee and fly from around the world to attend my defense. Additionally, the patience necessary to get through multiple iterations of this document as committee members should not go unnoticed. Michelle Bossler and Kris Davidson helped me so many times at UNLV, from getting me a desk when I first arrived on campus to showing me how to mail a FedEx envelope when my brain failed during the somewhat tortuous path leading up to my defense. Thanks for being the go-getters who cut through red tape to get the job done (gasp!), and for laughing at me when I'm an idiot. Thanks to Nick Smith for paving the beginning of the path of this project and imparting a tremendous amount of knowledge to me, and to Amber Wright who spent a tremendous amount of time explaining chemistry to this nuclear engineer, and without whom this document wouldn't exist (literally). Additionally, all radiochemists and nuclear scientists should be lucky enough to have Tom O'Dou, Julie Bertoia and Trevor Low as an example to follow for diligence in safety and laboratory management.

From my internships at Argonne National Laboratory, the Idaho National Laboratory and General Atomics, thanks to Allen Bakel, John Krebs and Monica Regalbuto (ANL); Troy Garn, Mitch Greenhalgh, Scott Herbst, Jack Law, Nick Mann, Dave Meikrantz and

Troy Tranter (INL); Tina Back, Tim Bertch, Don McEachern and Bob Schleicher (GA). To my new supervisors as part of the Nonproliferation Graduate Fellowship Program at the National Nuclear Security Administration, Marco Di Capua and Rhys Williams – I'm so very grateful that you've supported this endeavor and provided regular, enthusiastic encouragement for me to finish.

Of course, all the encouragement in the world would not be enough to achieve this milestone without the love and support of my family and friends. Thank you all so very much for continuously supporting my endeavors around the country, putting up with my (sometimes?) headstrong nature and making me the person that I am today. Our dynamic family is an inspiration to me, and I feel incredibly fortunate to have all of you in my life. Maj, your patience with me is never-ending. You have encouraged, challenged and pushed me to choose and pursue my path with confidence and passion. My gratitude and love for you is endless. To my friends and roommates, thanks for listening to me talk about safeguards in used nuclear fuel recycling for so long, for cheering me on, and for looking the other way on my long days and nights with Diet Coke and no showers.

I am deeply appreciative of the financial support I've received throughout my graduate studies. This work was funded by the Nuclear Forensics Graduate Fellowship Program which is sponsored by the U.S. Department of Homeland Security's Domestic Nuclear Detection Office and the U.S. Department of Defense's Domestic Threat Reduction Agency, and by the Nuclear Energy University Programs (NEUP) subcontract No. 89654 from Battelle/INL entitled: Quantification of UV-Visible and Laser Spectroscopic Techniques for Materials Accountability and Process Control under prime contract with the Department of Energy No. DE-AC07-05ID14517.

## TABLE OF CONTENTS

ABSTRACT.....	iii
ACKNOWLEDGEMENTS.....	vi
LIST OF TABLES.....	xi
LIST OF FIGURES .....	xii
CHAPTER 1 INTRODUCTION .....	1
1.1    Project Overview .....	1
1.2    Research Goals.....	2
1.3    Dissertation Outline .....	3
CHAPTER 2 BACKGROUND .....	5
2.1    Nuclear Fuel Cycles.....	5
2.1.1    Nuclear Fuel Cycle Challenges.....	7
2.2    Used Nuclear Fuel Composition.....	11
2.3    Reprocessing Options .....	12
2.3.1    UREX.....	14
2.3.2    TRUEX .....	15
2.3.3    AIROX.....	18
2.4    Proliferation Resistance and Safeguards.....	20
2.4.1    Process Monitoring .....	21
CHAPTER 3 INSTRUMENTATION AND METHODS .....	24
3.1    UV-Visible Spectroscopy .....	24
3.1.1    Fundamentals .....	24
3.1.2    Sample Preparation and Data Analysis.....	29
3.2    X-ray Absorption Fine Structure (XAFS) Spectroscopy .....	31
3.2.1    Fundamentals .....	32
3.2.2    Sample Preparation and Data Analysis.....	33
3.3    Inductively Coupled Plasma – Atomic Emission Spectroscopy (ICP-AES) ...	35
3.3.1    Fundamentals .....	35
3.3.2    Sample Preparation and Data Analysis.....	37
3.4    Titration.....	37
3.4.1    Fundamentals .....	37
3.4.2    Sample Preparation and Data Analysis.....	38
3.5    Centrifugal Countercurrent Contactors .....	38
3.5.1    Fundamentals .....	40
3.5.2    Settings and Options .....	42
3.6    Raman Spectroscopy.....	44
3.6.1    Fundamentals .....	44
3.6.2    Sample Preparation and Data Analysis.....	46
CHAPTER 4 PROCESS MONITORING UNDER UREX CONDITIONS .....	47

4.1	Introduction.....	47
4.1.1	Uranyl Spectroscopy .....	47
4.1.2	Relevance to reprocessing.....	52
4.2	Scoping Experiments and Preliminary Application to Reprocessing .....	55
4.3	High Fidelity Uranyl Nitrate System Studies .....	62
4.4	Experimental Implementation of UV-Visible Process Monitor .....	72
4.5	Conclusions.....	78
CHAPTER 5 TRUEX EXPERIMENTS .....		80
5.1	Introduction.....	81
5.1.1	Equipment .....	83
5.2	Experimental Techniques and Setup.....	85
5.2.1	TRUEX Flowsheet.....	85
5.2.2	Demonstration and Data Collection.....	88
5.3	Results and Discussion .....	91
5.3.1	Steady-State Determination .....	92
5.3.2	Removal Efficiencies .....	97
5.3.3	Mass Transfer Stage Efficiency .....	98
5.3.4	Temperature Profiles.....	100
5.4	Conclusions.....	104
CHAPTER 6 DEVELOPMENT OF A DRY PROCESSING FLOWSHEET AND SAFEGUARDS APPROACH.....		107
6.1	Introduction to EM <sup>2</sup> .....	107
6.1.1	EM <sup>2</sup> fuel cycle goals .....	109
6.2	Previous dry processing studies .....	112
6.2.1	AIROX.....	114
6.2.2	OREOX and DUPIC .....	121
6.2.3	CARBOX/CARDIO .....	124
6.2.4	Summary of processing conditions and results.....	125
6.3	Development of EM <sup>2</sup> flowsheet.....	128
6.4	Characterization of waste and recycled streams .....	131
6.5	Proliferation resistance in dry processing .....	134
6.5.1	Raman spectroscopy for dry process monitoring.....	138
6.6	Classification of dry processed waste products .....	144
6.7	Conclusions.....	148
6.8	Future work .....	149
CHAPTER 7 CONCLUSIONS .....		152
7.1	Process Monitoring Under UREX Conditions.....	152
7.2	TRUEX Experiments .....	154
7.3	Dry processing flowsheet and safeguards approach .....	155
NOMENCLATURE .....		157
REFERENCES .....		158

VITA .....	188
------------	-----

## LIST OF TABLES

Table 1: Summary of used nuclear fuel treatment options [15].....	13
Table 2: PUREX and UREX comparison [43-46].....	15
Table 3: UREX+ Suite of Processes [52] .....	17
Table 4: Conservative estimates of elemental removal by dry processing [60, 61] .....	20
Table 5: Oxidation states, Raman and UV-Visible wavelengths of common process stream actinides [88].....	22
Table 6: Molar absorptivities and Lower Limit of Detection (LLD) for Pu major absorption bands in 1 M HClO <sub>4</sub> , diluted from 0.005 M Pu stock .....	53
Table 7: Comparison of calculated and averaged ICP-AES determined values for U concentration.....	63
Table 8: Prepared sample conditions .....	64
Table 9: Metal concentration in UREX aqueous feeds.....	73
Table 10: Summary of UREX aqueous feed variables .....	73
Table 11: Aqueous feed target and actual compositions .....	87
Table 12: TRUEX demonstration sample plan summary .....	90
Table 13: Detection limits for ICP-MS metals analysis .....	92
Table 14: Percentage of metals in effluent streams just prior to shutdown and calculated removal efficiencies. ....	97
Table 15: Individual stage efficiencies for selected stages.....	99
Table 16: Selected boiling points reported for fission products [192].....	119
Table 17: Mean observed removal fractions of selected elements under CARDIO [194] .....	125
Table 18: EM <sup>2</sup> dry process flowsheet fission product removal goals.....	129
Table 19: Selected summary of EM <sup>2</sup> used fuel at Discharge, 5 and 10 years .....	132
Table 20: Summary of selected elements present in EM <sup>2</sup> discharge fuel.....	132
Table 21: Isotopes expected in LWR dry processing waste and recycled streams in quantities greater than g/MTHM with half lives greater than 100,000 years .....	134
Table 22: Selected elements in used nuclear fuel and relative concentrations .....	138
Table 23: Vibrational frequencies (cm <sup>-1</sup> ) of UO <sub>2</sub> (NO <sub>2</sub> )·2TBPO [213].....	141
Table 24: Resulting wastes from AIROX plant [57] .....	147

## LIST OF FIGURES

Figure 1: Nuclear fuel cycle schematic [10] .....	6
Figure 2: 2003 UNF inventory by state [24, 25].....	9
Figure 3: Approximate mass distribution of LWR used nuclear fuel .....	12
Figure 4: TBP molecule [51] .....	16
Figure 5: CMPO molecule [51] .....	16
Figure 6: Schematic of potential solvent extraction UNF reprocessing scheme .....	17
Figure 7: Diagram of UV-Visible system [91] .....	27
Figure 8: UV-Visible spectra of 0.11 M U in ~2 M HNO <sub>3</sub> .....	28
Figure 9: Peak ratio example comparing 403 and 426 nm over a range of [HNO <sub>3</sub> ] [89]	30
Figure 10: Segment of Advanced Photon Source synchrotron [114] .....	33
Figure 11: XAFS sample holders.....	35
Figure 12: ICP-AES diagram [116] .....	36
Figure 13: Cutaway view of CINC V-02 contactor [121] .....	40
Figure 14: Example Diagram of Countercurrent Centrifugal Contactors [125] .....	41
Figure 15: Residence time as a function of flowrate in the V-02 CINC contactor [121].	43
Figure 16: Molecular vibration modes [91] .....	45
Figure 17: Molecular orbital diagram of uranyl ion [139].....	49
Figure 18: UV-Visible Absorbance of 0.63 M U at 0.01 M HNO <sub>3</sub> , 0.1 cm pathlength ...	51
Figure 19: Fiber optic dip probe range study with UO <sub>2</sub> <sup>2+</sup> .....	56
Figure 20: Effect of addition of NH <sub>4</sub> OH on UV-Visible spectra .....	57
Figure 21: UV-Visible absorption spectra of Nd solution showing the time response study with fiber optic dip probe.....	58
Figure 22: Resolution studies of uranyl nitrate solutions (0.023 to 0.115 M) with the fiber optic dip probe in Swagelok flow cell .....	59
Figure 23: Fiber optic dip probe mounted in aqueous product outlet.....	60
Figure 24: UO <sub>2</sub> <sup>2+</sup> growth in UREX product stream [154].....	61
Figure 25: Inverse relationship between strip flow rate adjustment and UO <sub>2</sub> <sup>2+</sup> concentration seen in aqueous product stream [154].....	62
Figure 26: UV-Visible Absorbance of 0.126 ± 0.02 M U at 0.01-8 M HNO <sub>3</sub> , 0.1 cm pathlength.....	64
Figure 27: Example ICP-AES calibration curve.....	65
Figure 28: UV-Visible absorbance of 1.26 ± 0.10 M U at 0.01-5 M HNO <sub>3</sub> , 0.1 cm pathlength.....	66
Figure 29: UV-Visible Absorbance of 0.01-1.26 M U concentrations at 0.01 M HNO <sub>3</sub> , 0.1 cm pathlength.....	68
Figure 30: UV-Visible Absorbance of 0.01-1 M U concentrations at 7 M HNO <sub>3</sub> , 0.1 cm pathlength.....	69
Figure 31: UV-Visible Absorbance of 0.01-1.26 M U at 3 M HNO <sub>3</sub> , 0.1 cm pathlength	70
Figure 32: Molar absorptivities at 414 nm for uranyl in varied nitric acid solutions .....	71
Figure 33: Bench of 3 V-02 contactors at UNLV .....	72
Figure 34: UV-Visible absorbance of uranyl peaks over time under UREX process conditions.....	74
Figure 35: ICP-AES measured metal concentrations over time in the aqueous product of a UREX extraction (0-17 minutes) and strip (17-37 minutes) .....	75

Figure 36: Peak ratios over time in UREX extraction and strip .....	76
Figure 37: Foaming in organic interstage tubing.....	77
Figure 38: No foaming in aqueous interstage tubing.....	78
Figure 39: Thirty stage centrifugal contactor pilot plant .....	84
Figure 40: Typical fluid feed system with components.....	85
Figure 41: Contactor pilot plant flowsheet diagram .....	86
Figure 42: Foaming evident in interstage tubing throughout pilot plant .....	89
Figure 43: Steady-state plots for raffinate outlet .....	93
Figure 44: Approach to steady-state at strip product outlet.....	94
Figure 45: Lanthanide concentration profile across the cascade in organic phase at steady-state .....	95
Figure 46: Concentration profiles for fission products across the cascade in aqueous phase at steady-state.....	96
Figure 47: Aqueous and organic phase temperature (°C) profile averaged across respective extraction, scrub and strip sections .....	101
Figure 48: Temperature profile of solution outlets and ambient laboratory .....	102
Figure 49: Used nuclear fuel accumulation scenarios .....	110
Figure 50: Elemental makeup of LWR and EM <sup>2</sup> used fuel [180].....	112
Figure 51: Sample AIROX flowsheet [57] .....	115
Figure 52: Summary of maximum removal percentages reported in the literature for dry processes: green≥75%, 75%>yellow≥65% and red≤5% .....	126
Figure 53: Literature reported removal percentages for elements with maximum reported percentages of ≥75%.....	127
Figure 54: Summary of removal percentages for elements with maximum removal percentages between 65% and 75% .....	128
Figure 55: Flowsheet for dry processing of used nuclear fuel for recycle into EM <sup>2</sup> .....	130
Figure 56: Normalized elemental composition of recycled and waste streams from dry processing of LWR discharge .....	131
Figure 57: $[\text{UO}_2(\text{NO}_3)_3]^-$ molecule [14].....	142
Figure 58: $[\text{UO}_2\text{Cl}_4]^{2-}$ molecule [14].....	142

## CHAPTER 1

### INTRODUCTION

#### 1.1 Project Overview

This project was developed for the purpose of utilizing UV-Visible spectroscopy in a process monitoring setting to provide a method for confirming and tracking chemistry in solvent extraction separations of used nuclear fuel. The direct application of this is for an increase in the proliferation resistance of nuclear fuel reprocessing through both materials accountability and process monitoring. This project fits into the overall task of the investigation of optical techniques for on-line materials accountability in the used nuclear fuel treatment processes.

UV-Visible spectroscopy can be utilized in an on-line fashion to directly measure the concentrations of special nuclear materials, thus allowing real-time accountability and tracking for the solvent extraction processes. UV-Visible spectroscopy is an optical technique that is attractive for online monitoring applications because it permits on-line, real-time analysis of a solution and is easily adaptable to multiple sampling geometries. The implementation of UV-Visible spectroscopy for concentration measurements in flowing systems has been demonstrated at the laboratory-scale [1-4]. Therefore, the fundamental basis for this project is proven, and coupled with the radiation-tolerance potential of the setup [5, 6], this technology provides a great opportunity to simultaneously and directly monitor chemical process conditions as well as concentrations of special nuclear materials. In order to achieve this objective, the UV-Visible spectroscopic technology, used nuclear fuel composition, reprocessing options,

solvent extraction equipment technology, U spectroscopy and spectral attribution methods must be studied and understood.

## 1.2 Research Goals

The preliminary purpose of this research is to evaluate the effectiveness of UV-Visible spectroscopy in a process monitoring setting to track U through a UREX reprocessing scheme. As such, detection limits, process conditions and metal speciation relevant to UREX are studied in a systematic fashion. This evaluation includes determining the impact of process conditions, such as acid concentration and flow rate, on the sensitivity of the UV-Visible detection system. Understanding this relationship will enable an online materials accountability system as well as provide an attribution methodology for identifying diversion scenarios.

Following the success of the uranyl nitrate UV-Visible spectroscopic study, the spectroscopic methods for the evaluation of actinide concentrations and solution conditions are expanded to other used fuel treatment schemes such as TRUEX and AIROX (dry processing). Aspects of this research effort are investigated in the UNLV laboratory, Argonne National Laboratory, Idaho National Laboratory and at General Atomics.

The primary goal of this project is to understand fundamental UREX and PUREX reprocessing chemistry and corresponding spectroscopy for application in process monitoring for safeguards. Due to the impact of process chemistry on the molar absorptivity of U, the potential application of UV-Visible spectroscopy as an online technique for materials accountability must be examined separately for the relevant conditions of 0.01-1.26 M U and 0.01-8 M HNO<sub>3</sub>. The limits of quantization, including

the impact of process chemistry (metal, nitrate and acid concentrations) are explored to determine suitability of these techniques for real-time interrogation of the process streams. The potential for applying the qualitative spectroscopic information to evaluate the chemical environment of the process stream is also examined.

The secondary goal of the project is to simulate a diversion scenario in UREX (a change to PUREX conditions) and successfully detect changes in metal concentration and solution chemistry in a centrifugal counter-current contactor system with a UV-Visible spectroscopic process monitor. Towards this end, the UREX and PUREX solvent extraction flowsheets are investigated and compared, a benchtop scale pilot plant for a cascade of solvent extraction separations is designed and constructed, and a UREX to PUREX flowsheet conversion experiment is performed. Parameters monitored in this experiment as indicators of a potential diversion are flow rate modification, acid concentration, and concentration of the complexant/reductant AHA. Perturbations in the UV-Visible spectroscopy of the flowsheet product are correlated with known process changes to show that these diversion attempts can be detected in real time.

Finally, these studies are extrapolated to propose and demonstrate feasibility of process monitoring for safeguards used in other reprocessing flowsheets such as TRUEX and AIROX, to be studied more extensively in the future. Fundamental investigations are performed to consider the effects of metal interferences, temperature and the presence of other ligands on flowsheet performance and thus potential process monitors.

### 1.3 Dissertation Outline

Chapter 1 presents the project goals and dissertation overview. Chapter 2 provides an extensive background and review of prior work for the topics covered in this dissertation,

including the nuclear fuel cycle, used nuclear fuel treatment options, details of the processes relevant to this work and process monitoring for safeguards. Chapter 3 outlines the instrumentation and methods used in this research, with further experimental details on the application of these procedures given in Chapters 4-6. Each of Chapters 4-6 is presented in manuscript format, subdivided into sections of introduction, experimental, results, conclusions and discussions on future work. Chapter 4 discusses safeguards relative to UV-Visible spectroscopy in UREX. Chapter 5 covers a TRUEX demonstration, and Chapter 6 presents information relevant to dry processing. Chapter 7 provides a general summary of the conclusions discussed in previous chapters, and reviews options for future research areas.

## CHAPTER 2

## BACKGROUND

An overview of nuclear fuel cycles (NFCs), used nuclear fuel (UNF) compositions, treatment options for UNF recycling and proliferation resistance in NFCs is provided within this chapter. The motivation for the research in this dissertation is to provide opportunities for safeguards in used nuclear fuel recycling scenarios. As such, the composition of discharged fuel, relevant used nuclear fuel treatment methods and previous research on process monitoring for safeguards must be understood and discussed.

### 2.1 Nuclear Fuel Cycles

As energy demands soar, nuclear power's ability to provide baseload electricity becomes increasingly attractive resulting in the construction and licensing of more nuclear power reactors. In turn, these reactors generate used nuclear fuel which revitalizes the interest in modifying the U.S. open nuclear fuel cycle and utilizing a reprocessing scheme. Nuclear energy's presence in the U.S. energy portfolio and the choice of fuel cycle are crosscutting issues encompassing fundamental and applied science and engineering, energy independence and national security, and as such they are topics of discussion in multiple realms including academia, private industry and state and federal governments [7-9]. Thus, the development and advancement of all aspects of nuclear fuel cycles are rich areas for research.

There are several potential nuclear fuel cycles, generally identified as “open,” “modified open” or “closed.” Figure 1 illustrates all potential parts of a nuclear fuel

cycle. An “open” or “once-through” cycle would begin with U mining and milling, move to UF<sub>6</sub> conversion, enrichment, fuel fabrication, nuclear power generation, used fuel storage, and then proceed directly to final disposal. A “modified open” cycle would be the same as the “open” cycle from mining through used fuel storage, but then utilize some form of used fuel partitioning or reprocessing, such as dry processing or fast reactor burning, and then proceed to both new fuel fabrication and final disposal.

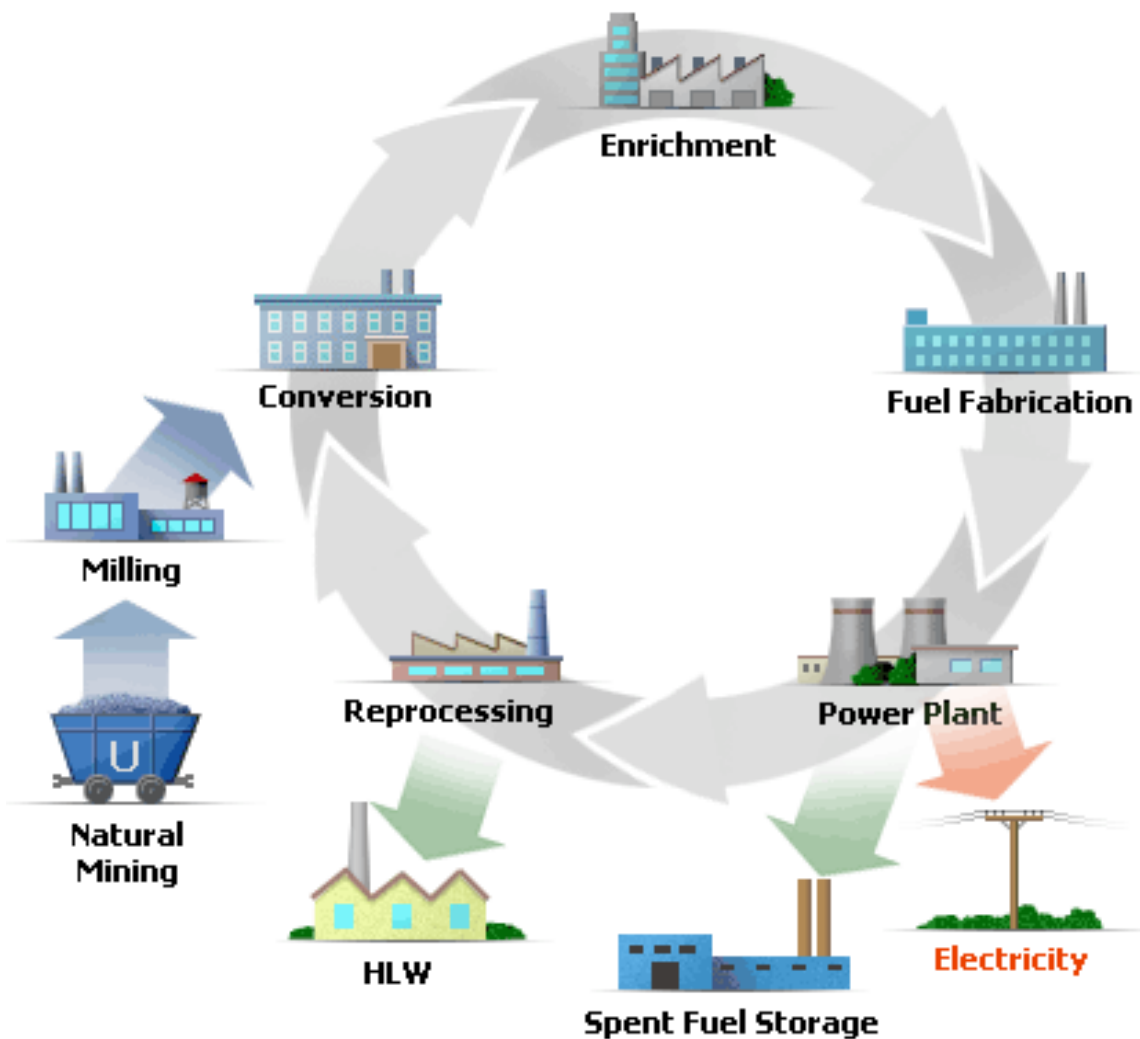


**Figure 1:** Nuclear fuel cycle schematic [10]

A “closed” cycle would be the same as the “open” and “modified open” through used fuel storage, however then all of the fuel would go through a reprocessing scheme, with extensive portioning allowing for new fuel fabrication, fast reactor transmutation and only HLW being sent to a repository for final disposal. Within these general fuel cycles, there are various methods and options at each step, for example there are many ways of U mining and milling [11], approaches to transmutation in both thermal and fast reactors [12], and a plethora of used fuel treatment or reprocessing options [13-18].

One assumption for the future U.S. nuclear fuel cycle, as described in U.S. policy defining Generation IV reactors, is that in order for any reprocessing scheme to be adapted successfully, it will need to utilize sufficient safeguards against proliferation [19, 20]. Towards this end, in addition to off-the-shelf technologies that can be used for process monitoring such as pH meters, mass balances, flow rate meters and temperature controllers, online UV-Visible spectroscopy can be used to effectively monitor certain radionuclide concentrations along with process chemistry, yielding real-time results. Some competitive techniques have been proposed [21], but few offer the real-time, online capability under reprocessing conditions combined with speciation sensitivity provided here.

### 2.1.1 Nuclear Fuel Cycle Challenges

As long as nuclear power has been used to generate electricity, "the management of the radioactive wastes produced in the course of electricity generation from nuclear fission [has been] a problem of concern to the electric-power sectors, governments and publics of all of the 25 nations that obtain some of their electricity in this way, as well as to people in other countries who might be affected by choices about how and where such

wastes will be shipped, processed and store [22]." Concerns about the safety of the nuclear fuel cycle have always been at the forefront of public and policy-maker resistance to the expansion of nuclear energy. These concerns, combined with those in regards to radioactive wastes and weapons proliferation played a major role in the decline of nuclear energy's prospects in the U.S. in the 1970s and 1980s. Specifically, "decisions in the late 1970s to defer indefinitely the reprocessing of used fuel, to discourage the transition to breeder reactors, and to forbid the export of enrichment and reprocessing technologies...were motivated by the concerns of the administration about nuclear-weapons proliferation [22]." More recently, the goals in the nuclear fuel cycle have shifted, likely due to increased energy demands, and now look to ensure that U resources are efficiently utilized and electricity supplies are guaranteed in the future. In fact, many believe that the establishment of a closed nuclear fuel cycle is one of the most important issues from the viewpoints of long-term energy supply with "high reliability, reduction of environmental impact due to radioactive waste disposal, and cost reduction for nuclear power generation [23]."

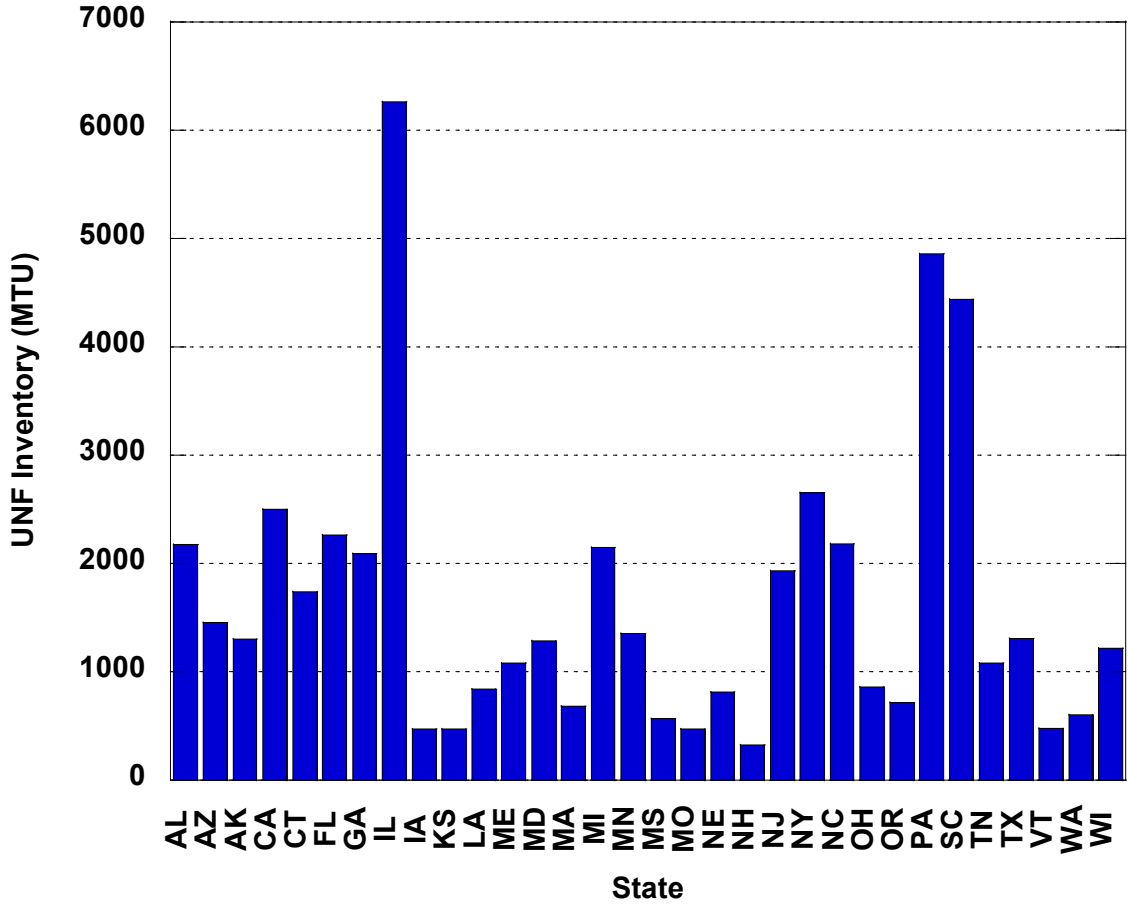


**Figure 2:** 2003 UNF inventory by state [24, 25]

Currently, no commercially generated used fuel is reprocessed in the U.S., therefore it is all stored in various forms across the country (Figure 2). A small commercial reprocessing plant was operated in New York from 1966 to 1972, but was closed for modifications and expansion in 1972 and never reopened. A second commercial reprocessing plant in Illinois did not work properly during testing and was shut down without ever going into commercial operation, and lastly a third plant in South Carolina was completed but did not operate [22]. Thus, in general, the used fuel generated at the operating commercial nuclear reactors in the U.S. is stored at the reactor sites, making

used fuel treatment or disposition a pressing matter (Figure 2). The 11 March 2011 Tohoku 9.0 earthquake and resulting tsunami experienced at the Fukushima Daiichi plant in Japan has also increased interest internationally in the issue of UNF storage. In the BWR Mark 1 design used at the Daiichi site, the spent fuel pools are located well above ground and suffered varying loss of coolant scenarios [26]. Due to their location, the spent fuel pools at Fukushima Daiichi were more susceptible to damage to hydrogen explosions as compared to below-grade spent fuel storage. In general, some amount of spent fuel storage is necessary at all reactor sites for immediate cooling of fuel upon removal from the reactor core. However, if spent fuel were stored at a centralized facility offsite after sufficient on-site cooling, the quantity of the spent fuel stored in the pools would be greatly reduced, mitigating much of the potential risks of damage to spent fuel pools in accident conditions, regardless of their location at the reactor site [27].

In contrast to commercial used nuclear fuel, defense high level waste (HLW) is stored in tanks at three federal facilities: the Hanford Nuclear Reservation (Richland, Washington) and the Savannah River Laboratory (Aiken, South Carolina), both of which operated reprocessing plants for the weapons-material production reactors on the respective sites; and the Idaho National Laboratory (Idaho Falls, Idaho), which has reprocessed naval-reactor fuel [22].

One of the main benefits of closing the nuclear fuel cycle is that recycling provides utilities with an additional source of domestic nuclear fuel, thus providing a hedge against global U prices and promoting energy security [28]. Additionally, recycling "allows for early movement of freshly discharged used fuel from utilities' sites...and provides more efficient use of geologic repositories, avoiding the need for an additional repository

beyond this century and expanding repository options [28]." Recent events at the Fukushima nuclear plant in Japan have brought renewed interest in moving used nuclear fuel away from reactor sites for storage. Lastly, in speculating beyond current U.S. policy, recycling of light water reactor (LWR) used fuel could impact the whole nuclear fuel cycle by reducing the number of fast reactors needed to burn minor actinides [28].

## 2.2 Used Nuclear Fuel Composition

Literature is available on computer modeled and actual radionuclides in a LWR core and the resulting gaseous, liquid and solid chemical species present both during normal operation, under accident conditions and at discharge [29, 30]. Nominally, LWR discharge fuel is assumed to have 60 GWd/t burnup and have the general composition of 95% U, 1% Pu and minor actinides, and 4% fission products, with a mass distribution shown in Figure 3 [31, 32]. The variations in reactor type, initial fuel composition and loading, burnup, core life and decay time prevent more specific generalizations on these characteristics, however the composition estimates should remain approximately the same even within these variables. Numerous databases and inventories are available for specific used nuclear fuel compositions, and a number of computer codes, such as ORIGEN, are available for calculating isotopically detailed nuclide transmutation, radiation emission characteristics and decay heat of irradiated nuclear fuel [33-36].

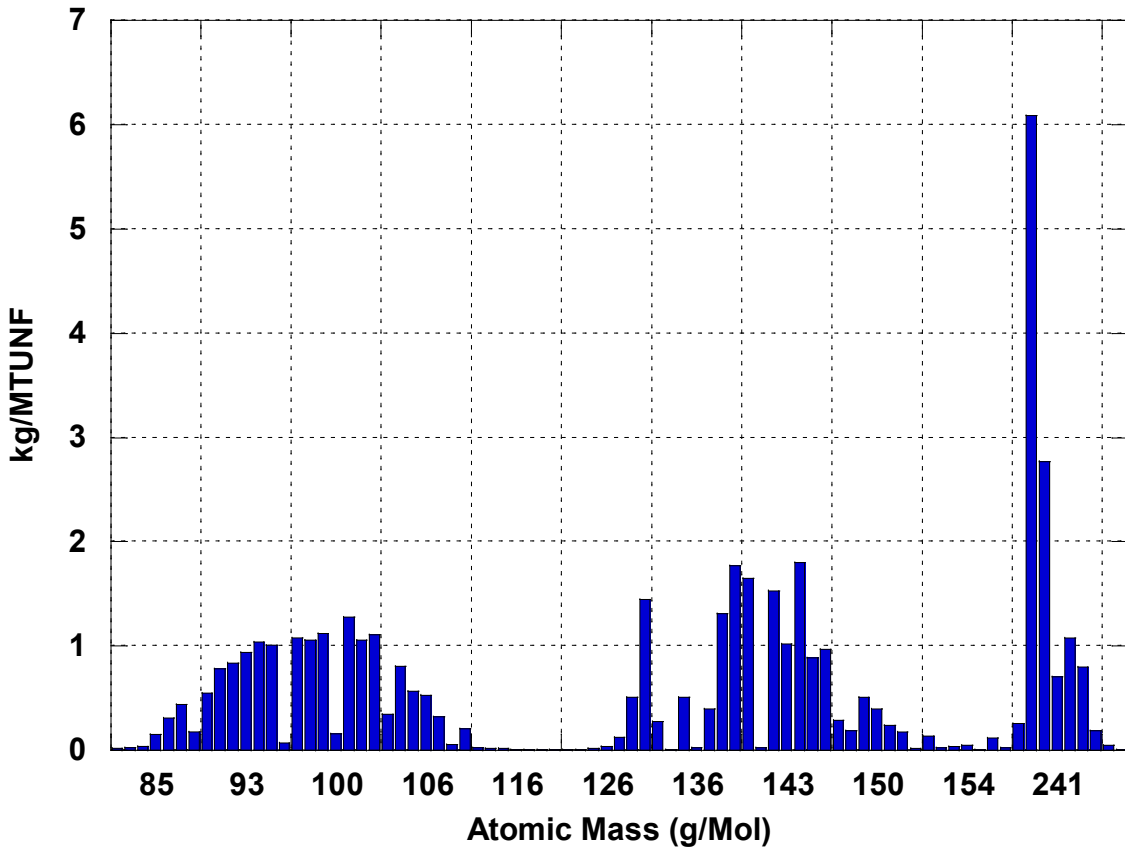


**Figure 3:** Approximate mass distribution of LWR used nuclear fuel

### 2.3 Reprocessing Options

Reprocessing originated during the Manhattan Project in which two broad approaches were used: isotopic enrichment to concentrate fissile  $^{235}\text{U}$  from natural U and transmutation of  $^{238}\text{U}$  to produce fissile  $^{239}\text{Pu}$ . At the time, the bismuth phosphate process was developed based on carrying Pu along with other metals in solution as precipitates, and other classical separation methods were studied such as ion exchange and solvent extraction [37]. Historically, reprocessing has existed in many countries such as the UK (Butex and THORP at Sellafield), France (PUREX at Marcoule and La Hague), Germany (WAK at Karlsruhe), Belgium (Eurochemic at Mol), Russia (Mayak) and Japan

(Rokkasho). All of these reprocessing operations have investigated and/or demonstrated chemical processes such as bismuth phosphate precipitation, ion exchange or solvent extraction [36].

Proliferation resistance relies on the knowledge of the nuclear fuel cycle under consideration, therefore successful safeguards must be tailored for each separations process within a nuclear fuel cycle. France has a relatively long reprocessing history, and lessons can be learned from both the separations processes and opportunities for special nuclear materials safeguards. For example, the separation activities at La Hague result in about two truck shipments per week of separated Pu to the Melox MOX fuel fabrication plant at Marcoule [38].

Generally, used nuclear fuel separations efforts are geared towards first separating actinides from fission products, and then separating individual actinides. To begin, processes such as URanium EXtraction (UREX) exploit the large differences between the chemistry of the actinides and fission products to accomplish separations [39]. The exception to this generalization is the separation of the transplutonium actinides from the lanthanide fission products. Actinide/lanthanide separations are achieved through processes such as TRansURanic EXtraction (TRUEX) and Trivalent Actinide Lanthanide Separation by Phosphorous reagent Extraction from Aqueous Komplexes (TALSPEAK).

**Table 1:** Summary of used nuclear fuel treatment options [15]

<b><u>Aqueous Processes</u></b>	<b><u>Pyroprocesses</u></b>
<ul style="list-style-type: none"><li>• Solvent extraction (PUREX, UREX, TRUEX, etc.)</li><li>• Ion exchange</li><li>• Electrolysis (Flurex)</li><li>• Precipitation (Bismuth Phosphate)</li></ul>	<ul style="list-style-type: none"><li>• Pyrophysical fractionation (AIROX, CARBOX, fluoride volatility etc.)</li><li>• Pyrochemical fractionation (electrorefining, molten salt electrolysis, etc.)</li></ul>

Over 30 alternative approaches have been suggested for reprocessing used nuclear fuel, but all of these can be classified as either an aqueous processes or pyroprocesses. Solvent extraction, ion exchange, photochemical induced separation, precipitation and electrolytic separation fall within the aqueous process category and these processes are generally geared toward oxide fuels (Table 1). Pyroprocesses, both pyrophysical and pyrochemical, are molten salt electrorefining techniques applied to metal fuels [40]. Although there are such a large number of reprocessing options, in the U.S. advanced technologies were investigated with the goals of safely and economically reducing the volume and heat generation of material requiring geologic disposition by separating key radionuclides from used fuel [41]. Therefore, processes such as UREX and TRUEX have been studied more extensively than other options as they are expected to have greater potential for application in the U.S.

### 2.3.1 UREX

The UREX process is based on the PUREX (Plutonium Uranium EXtraction) process. In the first extraction step of UREX, U and Tc in the feed are extracted into the solvent, then in the scrub section, other extractable species are scrubbed from the solvent and finally in the strip section, the solvent is stripped of the U and Tc yielding an aqueous product stream [42]. The solvent for the UREX process itself is the typical PUREX solvent, tributyl phosphate (TBP) in n-dodecane, however the feed of dissolved UNF is held at a lower concentration of nitric acid and acetohydroxamic acid (AHA) is added to enhance the complexation of Pu and Np and increase the extractability of pertechnetate ion (Table 2). These differences (acid, nitrate and AHA concentration) between PUREX

and UREX are what will be exploited in this work. Further process details are presented in Chapter 4.

**Table 2:** PUREX and UREX comparison [43-46]

Component	UREX	PUREX
[H <sup>+</sup> ]	0.5 – 2.0 M	3.5 – 5.0 M
[NO <sub>3</sub> <sup>-</sup> ]	3.0 – 4.5 M	6.0 – 8.0 M
[AHA]	0.1 - 1 M	0 M

As PUREX and UREX have been at the forefront of reprocessing efforts, the extraction of uranyl nitrate by TBP has been studied extensively [47, 48]. Generally, nitrates are extracted by TBP in the neutral form, always solvated by a definite number of TBP molecules. The compounds formed range from hydrated to almost unhydrated [47]. As for the oxidation state of U, in addition to the dominant U(VI) in used fuel, any U(IV) will also complex to TBP and be extracted from a nitric acid solution in a reprocessing scheme, and this resulting uranyl(IV) nitrate in TBP system has been studied [48, 49]. In fact, seven different U (IV) species have been identified in TBP solutions via absorption spectroscopy including U(NO<sub>3</sub>)<sub>4</sub>(TBP)<sub>2</sub>, UOH(NO<sub>3</sub>)<sub>3</sub>(TBP)<sub>2</sub>, [U(NO<sub>3</sub>)<sub>6</sub>]<sup>2-</sup>, a species containing the U<sup>4+</sup> ion solvated with TBP and three distinct uranium perchlorate species [49]. The extraction behavior and expected oxidation state of U in UREX is of importance to this work as the process monitoring concepts proposed are sensitive to chemical environment and coordination chemistry of metals.

### 2.3.2 TRUEX

The UREX process is often proposed to precede other extraction processes, such as TRUEX [50]. In TRUEX, a CMPO (Octyl(phenyl)-N,N-

diisobutylcarbamoylmethylphosphine oxide)/TBP (TriButylPhosphate) in n-dodecane diluent is used to extract actinides and lanthanides from fission products (Figure 4 and Figure 5), a scrub section removes any fission products that may have extracted into the organic phase, and a strip section returns the extracted metals to the aqueous phase product.

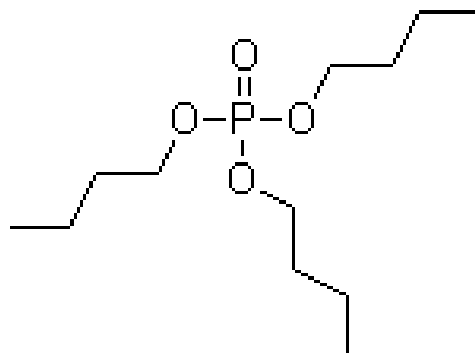


**Figure 4:** TBP molecule [51]

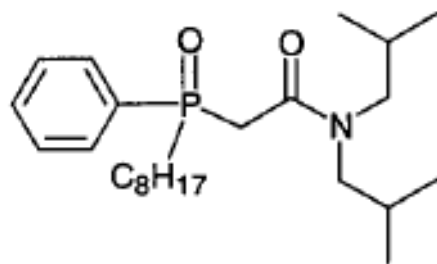


**Figure 5:** CMPO molecule [51]

Extensive TRUEX process details are presented in Chapter 5. One of the systems that has been studied extensively for used fuel treatment is the UREX+ process (Figure 6) which is fundamentally a series of 5 solvent-extraction flowsheets that perform the following separations. The first flowsheet accomplishes recovery of Tc and U (UREX). Next, Cs and Sr are recovered in FPEX. NPEX follows, which recovers Pu and Np. Next, Am, Cm and the rare-earth fission products are separated from other fission

products through TRUEX. Finally, separation of Am and Cm from the rare earths is achieved through Cyanex 301 or TALSPEAK. In general, each of the processes shown in Figure 6 has an extraction, scrub and strip section.

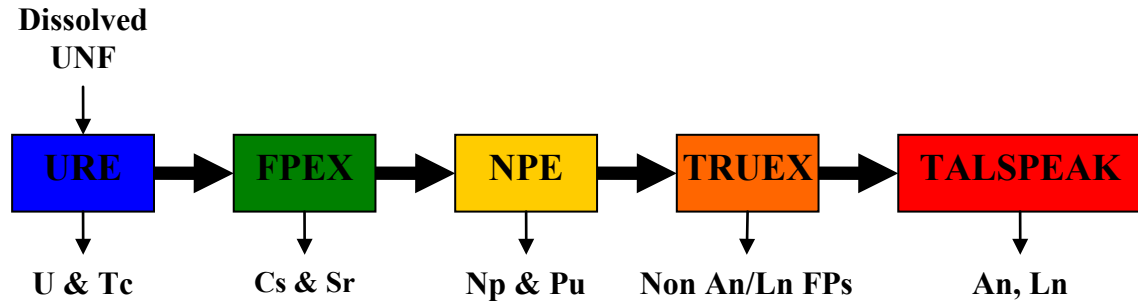


**Figure 6:** Schematic of potential solvent extraction UNF reprocessing scheme

Individual processes such as UREX, FPEX and NPEX are often linked together to form a complete flowsheet for used fuel treatment. When connected together, these flowsheets are designated as UREX+ and several combinations of processes and resulting flowsheets are possible (Table 3). Several of these proposed flowsheets such as UREX+1a, UREX+2 and UREX+3a have been demonstrated at the bench scale at Department of Energy labs in the U.S. with both simulated used fuel and actual used fuel [44, 45, 50].

**Table 3:** UREX+ Suite of Processes [52]

Process	1 <sup>st</sup> Product	2 <sup>nd</sup> Product	3 <sup>rd</sup> Product	4 <sup>th</sup> Product	5 <sup>th</sup> Product	6 <sup>th</sup> Product	7 <sup>th</sup> Product
UREX+1a	U	Tc, I	Cs, Sr	FPs	TRUs		
UREX+2	U	Tc, I	Cs, Sr	FPs	Pu, Np	Am, Cm, Ln	
UREX+3a	U	Tc, I	Cs, Sr	FPs	Pu, Np	Am, Cm	
UREX+3b	U	Tc, I	Cs, Sr	FPs	U, Pu, Np	Am, Cm	
UREX+3c	U	Tc, I	Cs, Sr	FPs	U, Pu	Am, Np, Cm	
UREX+4a	U	Tc, I	Cs, Sr	FPs	U, Pu, Np	Am	Cm
UREX+4b	U	Tc, I	Cs, Sr	FPs	U, Pu	Am, Np	Cm

Head-end steps are often proposed for treatment of UNF before introduction into the processes and flowsheets such as UREX and UREX+3a. These head-end steps allow for physical separation of UNF from cladding, removal of volatile and gaseous fission products, and pulverization for easier dissolving into the aqueous feed of the solvent extraction flowsheet. AIROX is one such head-end step, and has also been proposed as a used fuel treatment process in itself, without subsequent solvent extraction operations.

### 2.3.3 AIROX

As an addition or alternative to solvent extraction based separations for used nuclear fuel treatment, dry recycle technologies have been researched as part of the Integral Fast Reactor (IFR) program, for general fuel cycle use, for application in the DUPIC/CANDU fuel cycle and as a disposition pathway for weapons stockpiled materials (AIROX, Dmitrograd Dry process, CARBOX, OREOX, etc). In each process, fission products are partially removed and there is limited segregation between the TRUs [39, 53, 54]. The Dmitrograd Dry Process (DDP) and IFR processes rely on selective electrotransport of mixed TRU, whereas the AIROX/OREOX/CARDIO/DUPIC rely on oxidation-reduction at pyrochemical temperatures of 400-600°C, with some ventures to higher temperatures, depending on the application. The DDP has been demonstrated with many thousands of fuel pins recycled with a variety of burnups including up to 173,000 MWd/t [55]. The more common dry processing technologies such as AIROX and OREOX have been investigated at various theoretical and experimental levels for decades by countries such as South Korea, Canada and the United States [56]. Research efforts in this dissertation focus on processes that have shown potential for deployment, so the demonstration of dry processing technologies at the laboratory and larger scales is an important criterion.

Dry processing schemes have an inherent benefit over wet processing schemes in that the proliferation resistance is greatly increased due to no chemical separations, flowing fissile material or fissile-fertile separations. Additionally, the processes cannot be easily modified to allow U/Pu separations and due to the higher radioactivity in the used fuel that is dry recycled, even after blending with virgin fissile material, the fuel must be remotely handled. In turn, this can be seen as a downside to dry processing as it also means that fuel fabricated and inspection must proceed remotely as well [57]. Also, after a dry processing recycle, a slightly higher fissile content of fuel is required for blending with the processed used fuel as compared to wet reprocessing [58].

A general dry process as applied to the LWR oxide case, used fuel pins are mechanically removed from the fuel assembly, mechanically punctured and then exposed to oxygen at 400°C where the  $\text{UO}_2$  is converted to  $\text{U}_3\text{O}_8$ , achieving a volume expansion of approximately 30% which completely ruptures the cladding. Volatile and semi-volatile fission products are removed in various fractions by flowing gas over the oxidized used fuel under a variety of temperatures. The  $\text{U}_3\text{O}_8$  is reduced under hydrogen at 600°C to  $\text{UO}_2$ , at which point the powder can be mixed with enriched  $\text{UO}_2$ , resintered and refabricated into new fuel. The oxidation and reduction steps may be repeated multiple times to ensure complete pulverization of the used fuel and release of volatile fission products [59]. Higher temperature treatments with a variety of flowing gases can be utilized to achieve additional fission product removal beyond conservative fission product removals (Table 4). When applied to LWR discharge, dry processing can reduce the current inventory of material destined for geologic repository burial, with the exact amounts being dependent on the selected process and UNF composition.

**Table 4:** Conservative estimates of elemental removal by dry processing [60, 61]

Element	Removal %
K, Xe, I, C	100
Cs, Ru	90
Te, Cd	75

Overall, the goals of any fuel cycle are to reduce the mass of UNF needing to be disposed of as HLW, extract more energy from the original U ore and potentially deplete weapons-material inventories, while maintaining a high level of proliferation resistance [62]. Regardless of wet or dry processing method, demonstrable safeguards, materials accountability and diversion detection capabilities will be necessary.

#### 2.4 Proliferation Resistance and Safeguards

The International Atomic Energy Agency (IAEA) is the world's center of cooperation in the nuclear field. It was set up in 1957 as the "Atoms for Peace" organization within the United Nations family, and now works worldwide to promote safe, secure and peaceful nuclear technologies [63, 64]. The IAEA has established international safeguards standards for fissionable materials at used fuel reprocessing plants. The overarching goal is to ensure that significant quantities of weapons-grade nuclear material are not diverted over a specified time frame. As a result of the international emphasis on nuclear safeguards, characterization and comparison of the proliferation resistance of reactors, used fuel treatment options and fuel cycles in general is commonplace [65-69]. Process monitoring and analysis of collected samples, along with containment and surveillance, can maintain U and Pu accountancy through a reprocessing scheme. Theoretical proliferant diversions would be accomplished via deliberate

modification of the flowsheet chemistry, so by confirming proper operational performance and verifying process integrity throughout the reprocessing scheme, these diversions can be avoided. Online, real time, multiparametric monitoring of the radiochemical streams in any reprocessing flowsheet can provide rapid detection of unwanted and/or suspect deviations from normal operation conditions. In order for this type of monitoring to have the potential for deployment in an actual reprocessing plant, the monitor must be robust, not interfere with the process, be nondestructive and relatively straightforward to apply and maintain.

#### 2.4.1 Process Monitoring

Process monitoring has already been used in various aspects of the nuclear industry, such as in the tracking of radioactive gaseous waste released at Rokkasho and in the in situ X-ray absorption spectroscopy of U(VI) in molten LiCl-KCl eutectic [70, 71]. Investigation of failed fuel elements has been proposed through online monitoring of reactor coolants [72, 73]. Online determinations of acid, nitrate and metal concentrations have been studied through various titrimetric and photometric techniques, with varying success [74-77]. The emphasis in these previous online spectrophotometric studies has been to simply determine concentration, not correlate data with process conditions or quantify changes in situ over time. Additionally, simulation studies without supporting experiments have investigated the potential for gamma- and neutron- based detection as used nuclear fuel process monitors [78, 79]. UV-Visible spectroscopy has been utilized in the measurement of solubilities in supercritical fluid extraction which has the potential to provide a solvent-free extraction process [80]. At the Savannah River Site, U concentration measurements have been conducted for monitoring of tank waste

conditions [1-4]. Applications of Raman spectroscopy have included pharmaceutical analysis and quality control of pesticide formulations [81-83]. In electronic industries, the online monitoring of etching solutions using spectroscopy directly through existing Teflon lines is highly beneficial and accomplished through a Teflon-based Near-Infrared measurement system [84]. More generally, the demand for in situ and online, real time analysis of process streams is present in chemical, biological and nuclear industries from the developmental science stage to the applied manufacturing level [85-87].

**Table 5:** Oxidation states, Raman and UV-Visible wavelengths of common process stream actinides [88]

Oxidation State	Complex Ion	Raman	UV-Vis, nm ( $\epsilon$ , M <sup>-1</sup> cm <sup>-1</sup> )
U(VI)	UO <sub>2</sub> <sup>2+</sup>	870 cm <sup>-1</sup>	415 (10)
Pu(VI)	PuO <sub>2</sub> <sup>2+</sup>	833 cm <sup>-1</sup>	833 (550)
Pu(IV)	Pu <sup>4+</sup>		476 (65), 815 (20)
Pu(III)	Pu <sup>3+</sup>		560 (35), 602 (40)
Np(VI)	NpO <sub>2</sub> <sup>2+</sup>	850 cm <sup>-1</sup>	1223 (45)
Np(V)	NpO <sub>2</sub> <sup>+</sup>	767 cm <sup>-1</sup>	980 (350)
Np(IV)	Np <sup>4+</sup>		953-973

In order to effectively monitor a solvent-extraction based reprocessing scheme, the key signatures, namely concentration and speciation of the main components, of the separations under normal conditions must be identified to have a reference case. Additionally, the stream pH, flow rate, and temperature can be monitored and compared with chemical libraries of spectroscopic, chemical and physiochemical properties [88]. Overall, online monitoring at various points in a process is feasible as most flowsheets contain Raman and/or UV-Visible spectroscopically active species (Table 5), and

immediate information on radiochemical stream composition and flow status is available with off-the-shelf technologies.

If any used nuclear fuel treatment option is adopted by the U.S., regardless of flowsheet or design, it will certainly be required to meet stringent nuclear materials accountability and safeguards standards. Furthermore, the U.S. could set the precedent for other countries who want to develop a commercial reprocessing program by providing full transparency and integrated safeguards. By evaluating a selection of dry and wet used fuel treatment options, opportunities for process monitoring by an application of spectroscopic techniques can be identified.

## CHAPTER 3

### INSTRUMENTATION AND METHODS

Descriptions of the instrumentation and general methods used in this work are presented in this chapter. Details on instrument fundamentals, system specifics, sample preparation and measurement are provided. The techniques of UV-Visible spectroscopy, X-Ray Absorption Fine Structure spectroscopy, Inductively Coupled Plasma Atomic Emission Spectroscopy, Titration, Centrifugal Countercurrent Contactors and Raman Spectroscopy are covered. It should be noted that no experiments utilizing Raman Spectroscopy were performed in this research, but it is proposed for application in future work and is relevant in Chapter 6, and thus an overview of the method is included.

#### 3.1 UV-Visible Spectroscopy

In this dissertation, UV-Visible spectroscopy is used to both quantify U metal concentration in solution and as the main method for detecting changes in the uranyl nitrate molecular structure.

##### 3.1.1 Fundamentals

When exposed to light in the UV-Visible region, molecules undergo electronic transitions which can be investigated by measuring the light intensity before and after passing through a sample of interest [89]. The absorbance ( $A$ , unitless) of a solution is related to the molar absorptivity ( $\epsilon$ , usually in  $M^{-1}cm^{-1}$ ), concentration ( $c$ , usually in moles/liter) and pathlength ( $b$ , usually in cm) by the Beer-Lambert Law (Equation

$1 A = \epsilon bc$  ), and is proportional to the transmission (T) and light intensities (I) as shown in Equation 2 [90].

**Equation 1**

$$A = \epsilon bc$$

**Equation 2**

$$A = -\log T = -\log\left(\frac{I}{I_o}\right)$$

The molar absorptivity or molar extinction coefficient is a measure of how strongly a chemical species absorbs light at a specific wavelength. There are three general arrangements of UV-Visible spectroscopy instruments (Figure 7). In the single beam geometry (a), incident light passes through the monochromator/grating which separates the wavelengths. The separated light then goes through the sample (width of the sample is the pathlength), then a photodetector and amplifier. Any reference measurements in single beam geometry must be made by taking the sample out of the beamline and inserting the reference, taking a reference spectrum and storing it for later correction (or automated software correction) [91].

In the double beam geometry, the setup is similar to the single beam, however after the monochromator or grating, there is a shutter which splits the beam into two. Thus, one part of the light goes through a reference or background sample while the other beam is simultaneously going through the sample to be measured. After each beam goes through its respective cell, each is collected by a photodetector and a difference amplifier is used to determine the reference corrected spectrum. This type of double-beam geometry is considered double-beam separated in space (b), there is also double-beam separated in time (c, a chopper is used to alternate between reference and sample beams).

In this work, two instruments were used for UV-Visible spectroscopic measurements, an Ocean Optics USB200+ and a Varian Cary 6000i UV-Vis-NIR.

The Ocean Optics USB2000+ setup is similar to Figure 7 (a) where a fiber optic dip probe is used for collection of spectra, and reference spectra must be measured separately from the sample of interest. A  $^2\text{H}$ -W halogen light source is connected to the dip probe, and collected light is passed to the spectrometer which uses a fixed grating and silicon charge-coupled device (CCD). Two software interfaces were used, SpectraSuite for the majority of data collection and OmniDriver for integration of the UV-Visible spectroscopic data acquisition into LabVIEW.

The Cary 6000i setup is similar to Figure 7 (b), however in this case the chopper separates the beam into thirds with one going to the sample, one going to the reference and one being blocked. The UV and visible light sources are a  $^2\text{H}$  and a W lamp, respectively, providing a range of 175-1800 nm. Both the sample and reference beams are passed through a photomultiplier tube, with the Cary WinUV software interface providing output results. The standard cuvette size of 12.5 x 12.5 x 45 mm is used in the Cary 6000i, and several options are available for cuvette material and sample pathlength.

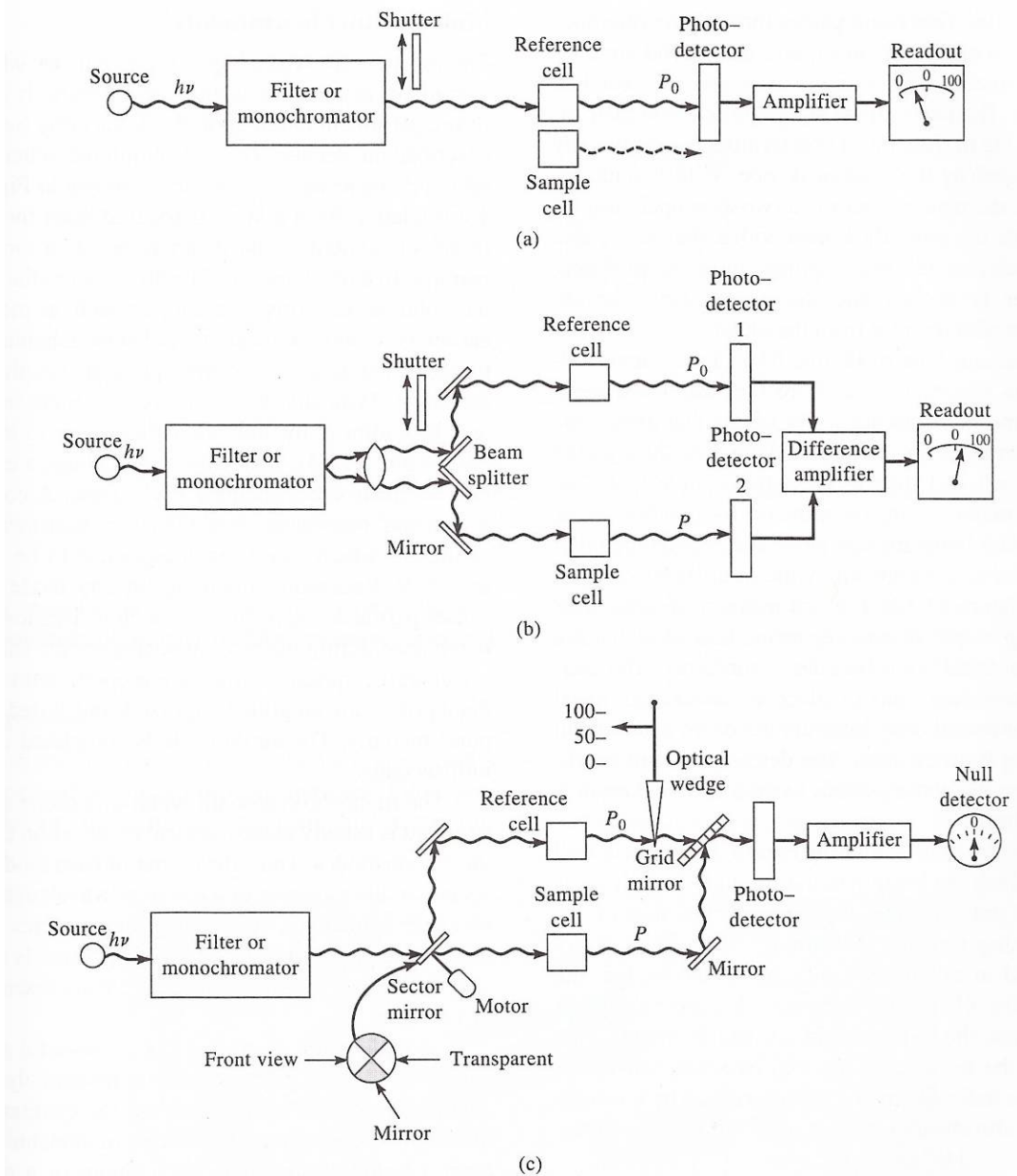


**Figure 7:** Diagram of UV-Visible system [91]

The UV-Visible spectroscopy result is generally a spectrum displayed as absorbance over a range of scanned wavelengths, where instrument calibration and sample quantification are possible. A sample uranyl spectrum is shown in Figure 8 illustrating the various effects of sample geometry (cuvette versus fiber optic dip probe) and

pathlength (2 mm versus 10 mm) on resulting spectra. The characteristic U peaks at approximately 404, 415 and 426 nm should be noted.

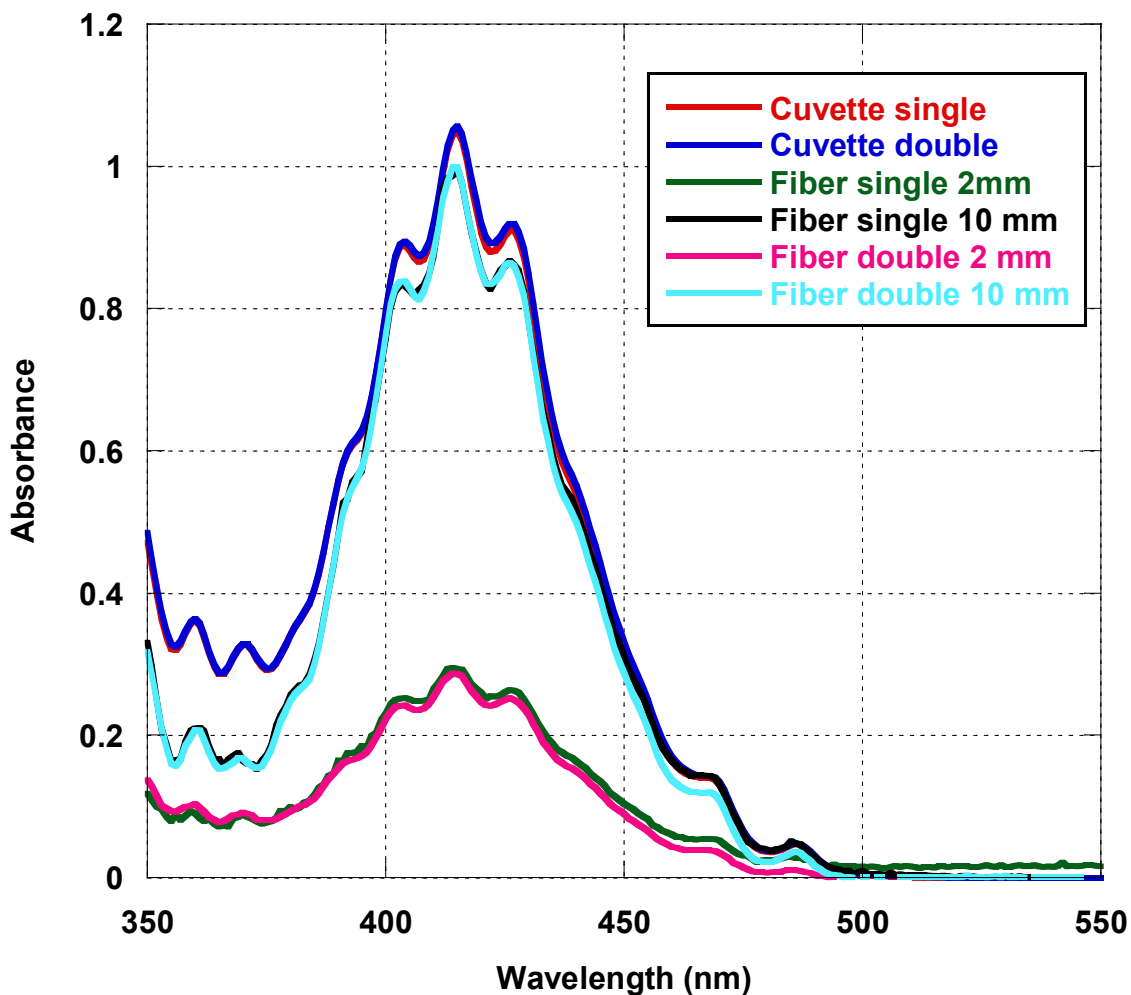


**Figure 8:** UV-Visible spectra of 0.11 M U in  $\sim$ 2 M HNO<sub>3</sub>

As the chemical form of the element impacts the absorbance spectra, speciation can be determined from this technique. UV-Visible spectroscopy is an excellent method for application to the actinides, as elements such as U, Np, Pu and Am are spectroscopically rich due to their different oxidation states.

### 3.1.2 Sample Preparation and Data Analysis

When the Varian Cary 6000i UV-Visible-NIR Spectrophotometer was used for spectroscopic measurements, the pathlengths used for sample measurement varied from 1 mm to 1 cm, and were chosen as appropriate for the molar absorptivity and concentration of the solution under examination. Sample preparation is straightforward – the solution sample is placed in a cuvette, the faces of the cuvette are cleaned so as to not interfere with the passage of light, and the cuvette is placed in the sample holder in the spectrophotometer. Both polymethyl methacrylate and quartz cuvettes were used in this work, however in a given experiment the same type was always used for both the sample and reference cells. In data acquisition, the Cary 6000i allows for the selection of measurement parameters including the wavelength range, speed of scanning and wavelength interval. Generally, the wavelength range scanned was 300-800 nm with 1 nm step size and a scan rate of 300-500 nm/minute. At the beginning of each experiment, the system was zeroed and background and blank spectra were recorded. The background spectrum was taken with a blank in the sample and reference positions. When attempting to observe matrix changes, the reference was kept as a blank rather than a sample matrix. In all cases, the detector was zeroed before every sample collection. When using Hellma flow-through cuvettes, no sample was placed in the reference position, as no identical flow-through cuvette was available. As such, background sample collection before sample measurement was used for spectra correction.

As an alternative to placing the samples directly in plastic or glass cuvettes, a fiber optic dip probe was inserted into a sample, or the sample was flowed through a quartz cuvette flow cell. Again, wavelength range, scan speed and integration time can be

specified for each experiment. Initially the full 300-800 nm spectra were collected, however for most of the uranyl nitrate work, the area of interest is limited so generally these spectra were collected from 350-500 nm, with an acquisition time ranging from 250  $\mu$ s – 1s and an integration time ranging from 500  $\mu$ s to 5 s. As the fiber optic dip probe does not have a beam splitter to provide for a simultaneous reference measurement, background spectra were recorded prior to sample measurement, and blank matrix samples were also recorded in the range pertinent to experiments.

Data analysis of UV-Visible spectra is straightforward. It is important to take a background spectrum of the media of the sample if media effects are to be subtracted. Additionally, the spectrometer's absorbance should be zeroed after the sample chamber is closed but before spectra collection. As long as this general procedure is followed, the resulting plot of absorbance versus wavelength can then be analyzed for peak shifts, absorbance changes or other spectral perturbations.

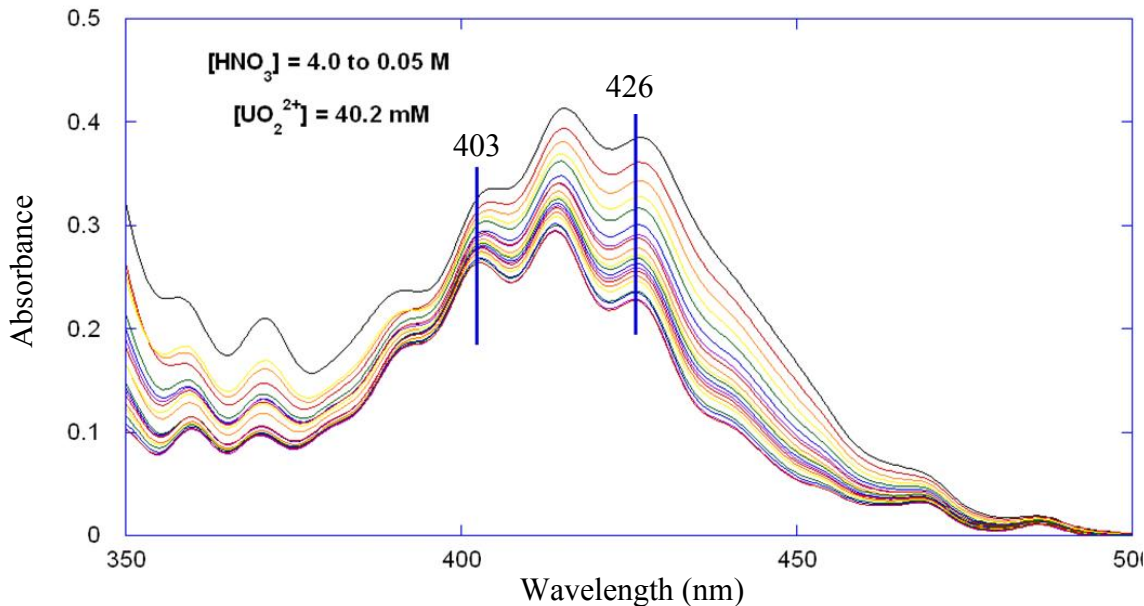


**Figure 9:** Peak ratio example comparing 403 and 426 nm over a range of  $[\text{HNO}_3]$  [89]

In addition to the analysis of the raw spectral output, ratios of absorbance peaks can be used for data breakdown. The peak ratio comparison method is demonstrated in Figure 9, with the lines at 403 and 426 nm drawing attention to the quantitative changes occurring in peak heights as the nitric acid concentration is varied. This method is useful because peak ratios are dependent on molar absorptivities which yield information on speciation, in turn providing process chemistry data. The importance of the peak ratio comparison is that the ratio is no longer dependent on concentration; therefore the ratios are a direct indication of the speciation that is occurring [92-94]. Another benefit of this peak ratio method is that due to the direct relationship between changes in speciation and peak ratio differences, the technique can yield close to real-time feedback in process as a confirmation of chemistry or check for diversion.

### 3.2 X-ray Absorption Fine Structure (XAFS) Spectroscopy

A variety of actinides have been studied with XAFS, both as solids and in solution, as they are relevant to environmental conditions, nuclear wastes and used nuclear fuel reprocessing [95]. Often XAFS experimental techniques are coupled with Density Function Theory (DFT) or other theoretical modeling to both calculate expected XAFS results and interpret experimental data [95-98]. There are several XAFS studies that relate directly to this work on uranyl nitrate [99-102], and other actinides in acidic nitrate conditions [103-111]. In addition to the coupling of XAFS with molecular dynamics simulations, some studies have laid the foundation for adding UV-Visible spectroscopy to the suite of teamed investigative methods [104, 112].

### 3.2.1 Fundamentals

X-ray Absorption Fine Structure spectroscopy is a technique that probes the absorption of x-rays by atoms at energies near and above its core binding energy levels [113]. When an atomic core-level electron absorbs an x-ray, if its incident energy is greater than the binding energy, the electron may be removed from its quantum level and a photo electron with excess energy ejected (photo electric effect). The resulting spectra are sensitive to oxidation state, coordination chemistry and nearest neighbor distances and species. XAFS is generally utilized in two more specific regimes - X-ray Absorption Near Edge Spectroscopy (XANES) and Extended XAFS (EXAFS). XANES typically yields information on oxidation state and extends 30-50 eV beyond the edge energy, while EXAFS provides more data on the neighboring atoms and coordination chemistry (distances, coordination number, and speciation) and probes up to 1000 eV above the edge. All measurements begin at energies below the absorption edge of the element of interest. The absorption coefficient ( $\mu$ ) describes the probability of x-ray absorption (Equation 3), and is a function of x-ray energy (E), sample density ( $\rho$ ), atomic number (Z) and atomic mass (A). XAFS spectroscopy is fundamentally measuring the  $\mu(E)$  for a sample, and resulting spectra are displayed as absorption coefficient versus energy [113].

#### **Equation 3**

$$\mu = \frac{\rho Z^4}{AE^3}$$

For this research, XAFS spectroscopy was performed at the Advanced Photon Source (APS) synchrotron at the Argonne National Laboratory. A schematic of the synchrotron setup is shown in Figure 10. To produce x-rays, electrons are emitted from a cathode, passed through a linear accelerator, injected into a booster synchrotron and then

accumulated in the large synchrotron storage ring. Electromagnets are used throughout the synchrotron to provide acceleration, bending and focusing of the photons, and to provide several beamlines tangential to the storage ring where XAFS experiments can take place. The Basic Energy Sciences Synchrotron Radiation Center Collaborative Access Team Bending Magnet 12 at the APS was used for experiments in this work.

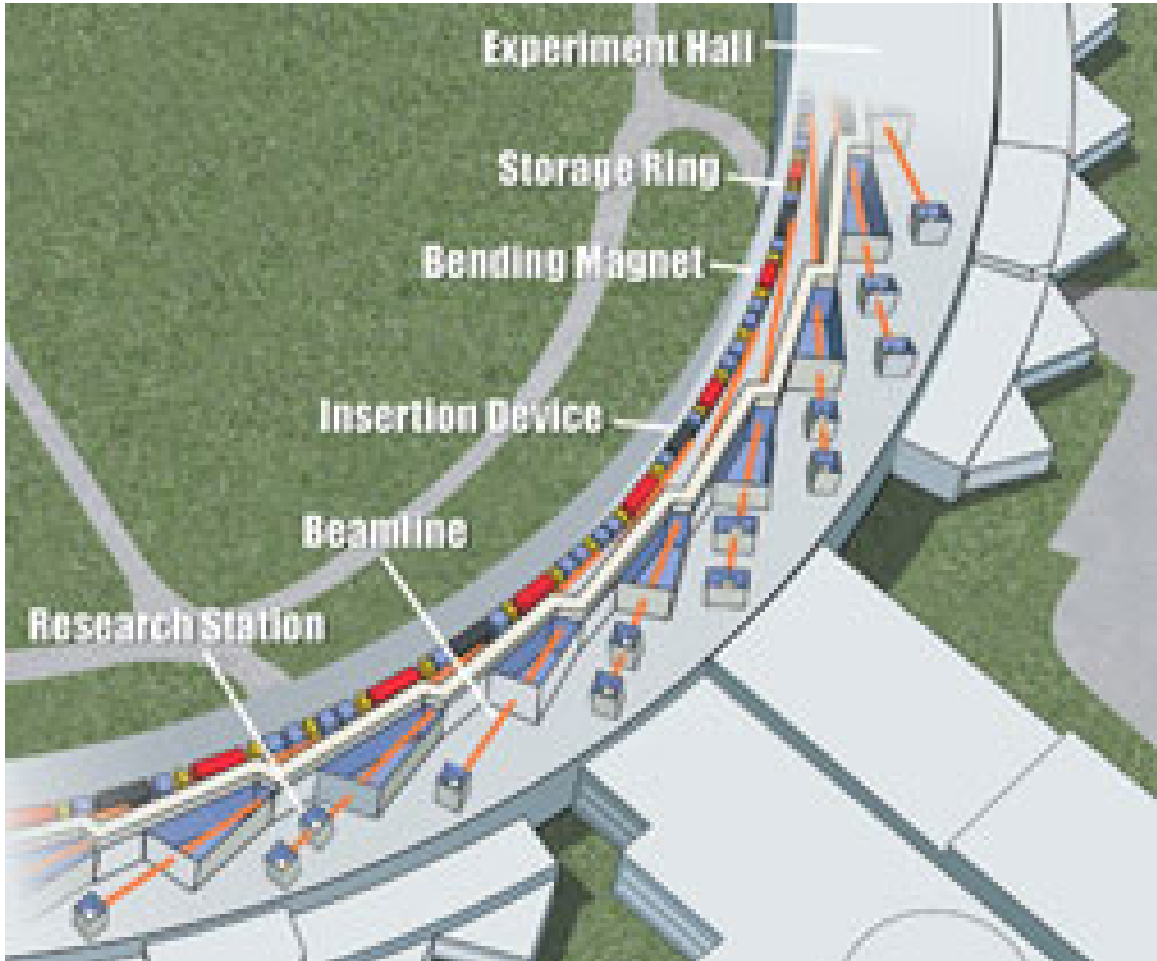


**Figure 10:** Segment of Advanced Photon Source synchrotron [114]

### 3.2.2 Sample Preparation and Data Analysis

As XAFS is an atomic probe, provided a proper and tunable x-ray source is available, it can basically be used on any element and with solid or solution samples. For this work,

liquid samples were prepared in the 1-10 mM concentration range and placed into XAFS sample holders, shown in Figure 11. Transmission or fluorescence measurements are available as long as the beam is properly tuned to a homogeneous sample, with fluorescence preferred for very thin or thick, dilute sample geometries. For U XAFS, samples were measured in fluorescence mode at room temperature with x-rays tuned for the L<sub>III</sub> edge at 17.166 keV, where energy calibration was achieved using an in-beam Zr foil. While taking XANES or EXAFS measurements is fairly simple (once the beam is tuned and the sample aligned), interpretation and analysis of XAFS signals is not as straightforward. In general, 10-16 scans are collected per sample, they are averaged, measured intensities converted to  $\mu(E)$ , and then background subtracted (also called the pre-edge function). The plot of  $\mu(E)$  can then be normalized and used for XANES, or for EXAFS, weight  $\chi(k)$  by  $k^3$  then perform a Fourier transform into R-space [113]. Programs such as Athena, WinXAS, TKatoms and FEFF are useful in XAFS data reduction [115].

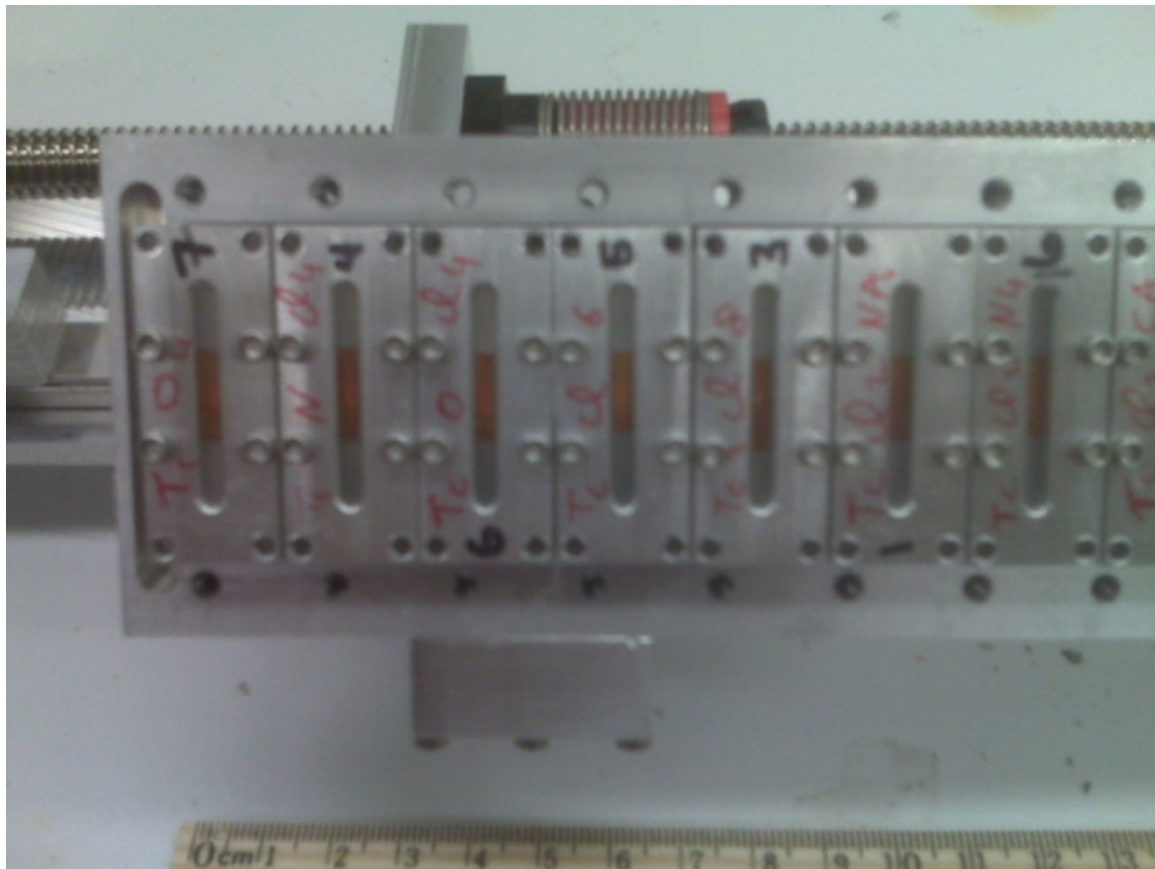


**Figure 11:** XAFS sample holders

### 3.3 Inductively Coupled Plasma – Atomic Emission Spectroscopy (ICP-AES)

#### 3.3.1 Fundamentals

ICP-AES is used to determine metal concentration in solution samples. A schematic of a typical inductively coupled plasma atomic emission spectrometer system is shown in Figure 12. The liquid sample is introduced to the system via a nebulizer, then made into a plasma with an argon carrier gas by a torch with temperatures ranging from 6,000 to 10,000 K [91]. The plasma is initialized when the argon atoms are ionized with a Tesla coil, while the RF induction coil produces a magnetic field. As the torch breaks up the molecules in the sample and ionizes each atom, the excited atoms emit photons at

characteristic wavelengths in order to de-excite, and spectroscopy is used to detect these photons and relate the signal to the concentration of each element. A diffraction grating is used to separate the emitted light spectrum into individual wavelengths. The intensity of photons at each specified wavelength is amplified with a photomultiplier tube (PMT), where photon interactions produce electrons which are amplified by a system of dynodes, yielding an electronic signal. The signal is then sent to a detector, where the intensity of this signal is directly proportional to the concentration of the element and can be used to provide quantitative results when a calibration curve from solutions of known concentrations is utilized.

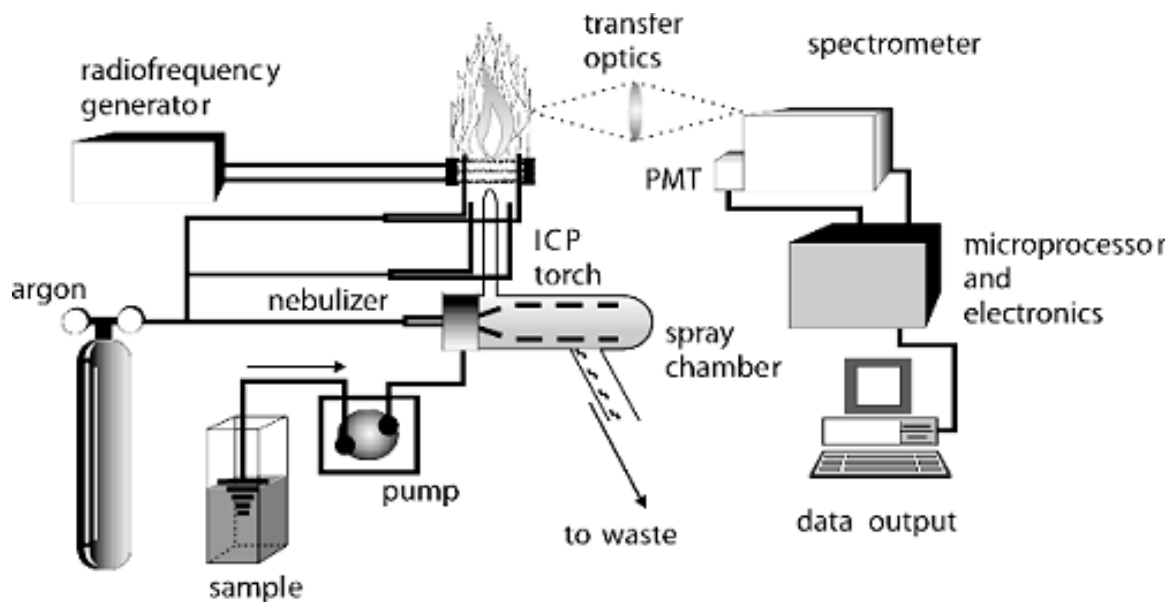


**Figure 12:** ICP-AES diagram [116]

### 3.3.2 Sample Preparation and Data Analysis

A Thermo Scientific iCAP 6000 Series ICP-AES with Thermo iTeva software was used, and for U measurements the 419 nm emission wavelength was monitored. The calibration standards used for this project ranged from  $2.1 \times 10^{-5}$  to  $4.2 \times 10^{-4}$  M uranium and were prepared in a 2% nitric acid matrix. The samples for analysis were diluted in 2% HNO<sub>3</sub> by appropriate factors (40-5000) in order to achieve U concentrations within the range of the standard calibration, generally 1-100 ppm which corresponds to approximately 0.004-0.4 mM U. A calibration was run at the beginning of each use of the instrument, and this calibration curve was used to correlate the counts/second detected by the ICP-AES to elemental concentration in solution. All samples were run in triplicate, and when more than 10 samples were being analyzed using the auto-sampler, calibration checks were inserted at the end of the deck to ensure proper instrument operation throughout data collection.

## 3.4 Titration

### 3.4.1 Fundamentals

Titration is based on the concept of an equivalence point, where the concentrations of acid and base are equal, and this occurs where the change in pH is greatest. Titrations actually measure the end point, a very close approximation of this equivalence point, as the ideal equivalence point is in an infinitely dilute solution. When titrating a strong acid with a strong base, the endpoint should occur at a pH of 7 [117]. The acid concentration of the sample can then be calculated based on the moles of base needed to reach the end point, assuming sample and titrant volume as well as titrant concentration are known.

### 3.4.2 Sample Preparation and Data Analysis

A Brinkmann Instruments Metrohm Titrino 799 with a 685 Dosimat and Tiamo software was used for titrations in this work. In most cases, the Micro pH Glass Electrode 178 mm (6.0234.110) was used as its long length is appropriate for use with the autosampler. Before titration, the electrode was calibrated with three buffers of pH 4, 7 and 10 to ensure proper operation. Next, an excess of 0.45 M  $C_2K_2O_4$  reagent, preadjusted to pH 5.55, was added to the titration cell along with a stir bar. Potassium oxalate, like ammonium oxalate, binds to and prevents the hydrolysis of U(VI) [74]. The pH electrode was lowered into the stirring solution and allowed to equilibrate for approximately 3 minutes. The pH of the solution was tested to ensure it was in the range of 5.50-5.60, if not, appropriate amounts of NaOH or HNO<sub>3</sub> were added to achieve the desired pH. Next, an amount of sample was pipetted into the oxalate solution in order to adjust the pH to less than 5.3, the solution was allowed to stir for a brief period, then the pH was measured. If the pH of the solution was below 5.3, titration continued with 0.100 M NaOH as in a standard titration up to the initial pH observed (between 5.50 and 5.60). If the pH of the solution after adding the sample was greater than 5.3, more sample was added in order to adjust the pH to lower than 5.3 [118]. The software calculated the endpoint value, which was used to determine the original acid concentration of each sample. The calculation was performed by the software by finding the inflection point of the titration curve.

## 3.5 Centrifugal Countercurrent Contactors

In a solvent extraction process, two immiscible phases (aqueous and organic) are mixed, allowing the soluble species to distribute, then separated. At the bench scale,

small samples can be prepared manually, vortexed and then centrifuged. When scaled up to the laboratory or demonstration level, vessels such as mixer-settlers, pulsed columns or centrifugal contactors facilitate the contacting and separating of the phases [119]. Some advantages that contactors have over other vessels are that they have a smaller footprint, lower total volume for a process, shorter contact time, faster approach to steady-state, process upset tolerance, clean-in-place capability and rapid stage change out [120]. One downside of the contactors is that they do not tolerate solids, so care must be taken to properly maintain the vessels by thoroughly cleaning after use. Generally the small samples are on the order of milliliters, while solvent extraction vessels such as centrifugal contactors can accommodate flow rates of liters/minute and run continuously. Contactors can be used for flowsheet development, mass transfer testing, and demonstration and evaluation of potential commercial processes. A cutaway view is provided in Figure 13.

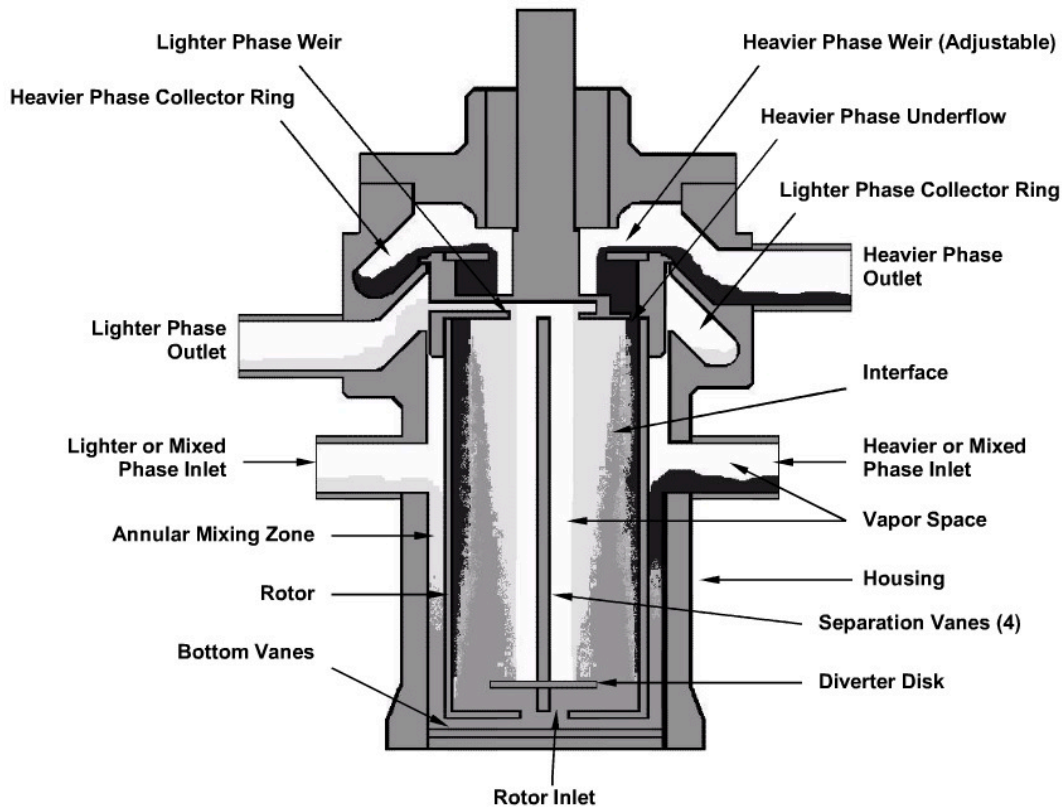


**Figure 13:** Cutaway view of CINC V-02 contactor [121]

### 3.5.1 Fundamentals

Development and demonstration of solvent extraction equipment has been ongoing in the U.S. national laboratory system for almost 40 years. The first centrifugal contactors, consisting of a vertical centrifuge allowing the mixing and separating of liquids, were developed at Savannah River National Laboratory. Contactors have also been used in studies of solvent extraction processes for used nuclear fuel reprocessing internationally [122, 123]. Contactors can be easily interconnected to allow multistage processing with two immiscible liquids fed into the annulus, formed by the spinning rotor and the stationary housing wall, of each contactor through inlets toward the top of the device.

The liquids mixed in the annular region or are pumped into the rotor bottom, then into the separation zone where the liquids are accelerated to the wall with the heavier fluid going to the outside and exiting the contactor first. Figure 14 illustrates the counter-current nature of the contactors as well as how they can be connected as to improve total process efficiency and separation factors. The efficiency of the solvent extraction, the transfer of a species between the two phases, depends on the total contacting surface, on the separation between the two phases, and the time of contact between the phases [124].

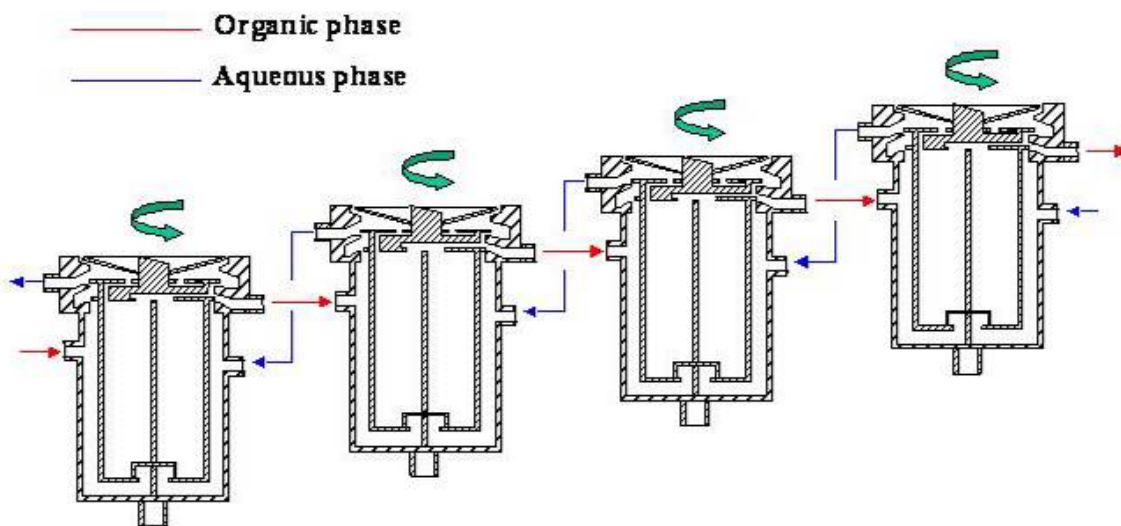


**Figure 14:** Example Diagram of Countercurrent Centrifugal Contactors [125]

Argonne National Laboratory has developed systems of centrifugal contactors that are reliable, and relatively inexpensive to build, operate and maintain. Due to the compact contactor stages, the overall liquid holdup is low, the systems can undergo fast startup and shutdown, and high mass transfer efficiency can be achieved. The interstage lines are external to the contactor body so that both the aqueous and organic liquids are accessible as they enter and leave each stage, making stream interrogation physically easy (Figure 14). There are some undesirable effects seen when the flowrate of liquids is

low in the 2-cm contactor, the interstage lines are not fully wetted, thus producing slugs of solution rather than continuous, steady-state operation. Such flow, which is controlled by the surface tension of the liquid, is a concern since it will reduce stage efficiency [126]. Centrifugal contactors have also been used to extract Am(III) with somewhat low separation factors, however increasing the number of contactors for each stage is known to increase the overall separation factor [127].

### 3.5.2 Settings and Options

The contactors used in this work are a set of 3 model V-02 from CINC Manufacturing, LLC. The V-02 model has a 2 inch rotor, is approximately 9 inches long, 9 inches wide and 25 inches tall, can hold up to 1.9 liters/minute, weighs 25 pounds and uses a 1/8 horsepower 110 VAC motor [121].

Each of the 3 contactors can be operated independently, allowing flexibility in experimental design. Masterflex pumps are used to feed solutions into the contactors, and flowrates are adjusted manually via the pump control console. The pumps and interstage connections are made with Tygon tubing and stainless steel fittings. Total flowrates (sum of organic and aqueous flows) through the system are nominally less than 2 liters/minute. Residence time is an important factor to consider when decided on flowrate for aqueous and organic flows, as it affects both the holdup volume and the contact/separation time (Figure 15). The selection of flowrate directly affects the residence time, in this work solutions are pumped through the UNLV contactors in the range of 300-600 milliliters/minute.

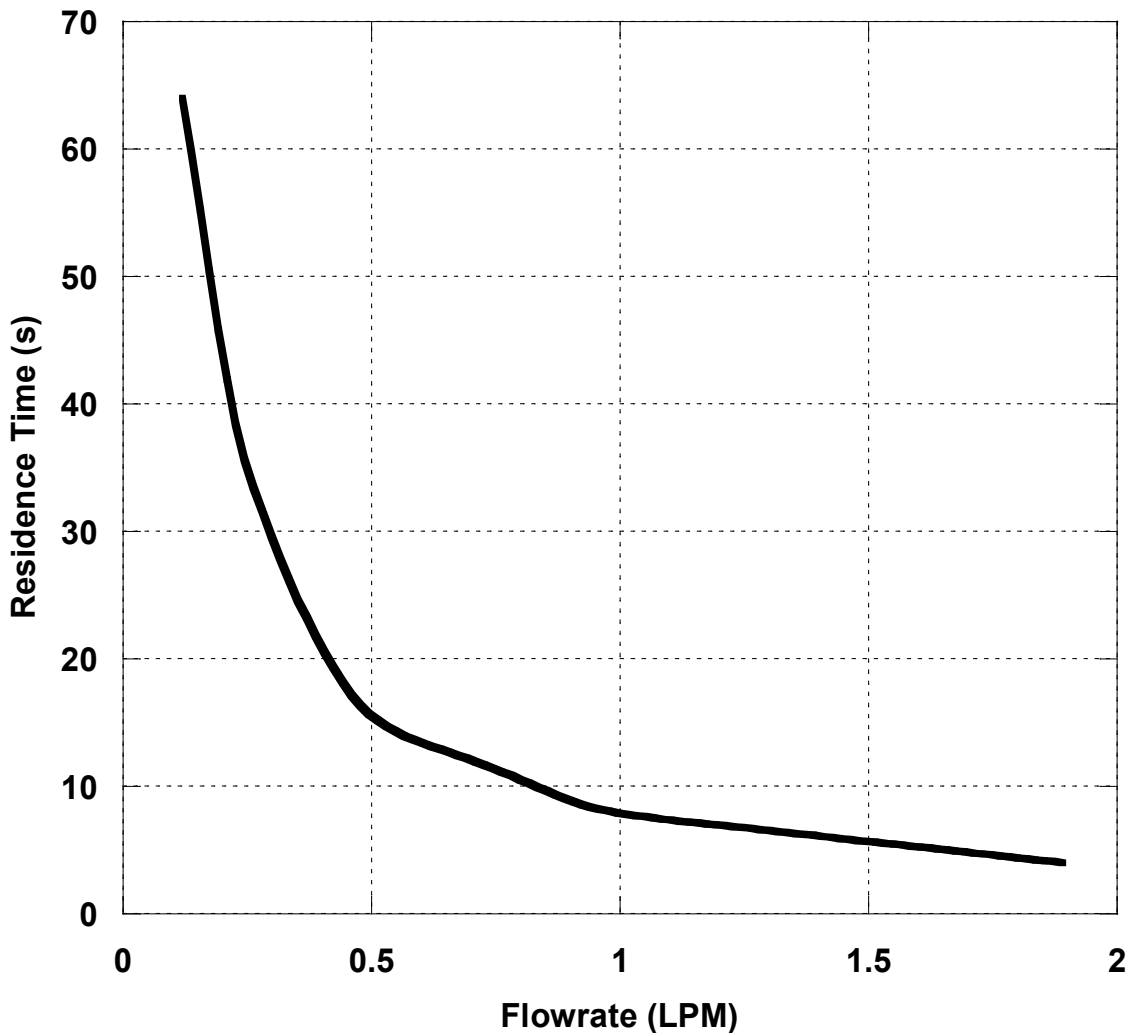


**Figure 15:** Residence time as a function of flowrate in the V-02 CINC contactor [121]

The organic and aqueous phase outlets are all vented to protect against pressurization inside the vessels, and so flow between contactors and through the outlets is driven by gravity. The feed aqueous and organic solutions were stored in covered containers either underneath the contactor bench or directly adjacent. Sampling from the contactor outlets can be achieved through the valves attached to the outlet tubing, and sampling from all contactors is possible through the stage drains.

### 3.6 Raman Spectroscopy

No Raman spectroscopy experiments were performed in this work, however it is proposed as a method of process monitoring in Chapter 7, therefore instrument fundamentals and a brief overview of sample preparation and data analysis are provided.

#### 3.6.1 Fundamentals

Raman spectroscopy provides information about the structure and symmetry of molecules, as well as some data on their vibrational energies. It relies on the inelastic (Raman) scattering of monochromatic light (not absorption as in UV-Visible spectroscopy), as from a laser, usually in the visible, near visible or infrared range. The light interacts with the vibrations of the molecule causing small shifts in the laser photons' energy. These shifts are dependent on the chemical structure of the molecules causing the scattering [128]. Infrared spectroscopy is a complementary technique to Raman spectroscopy, as molecules that are Raman active are IR inactive, and vice versa. Raman species are active if the vibrations cause a change in the polarizability of the molecule, whereas species are IR active if the vibrations yield a change in the dipole moment [129]. Stretching and bending vibrational modes are shown in Figure 16. Water does not cause interferences in Raman spectra as it does in IR spectra, allowing for the potential application of Raman spectroscopy as an online process monitor in areas where UV-Visible spectroscopy is ineffective or inappropriate.

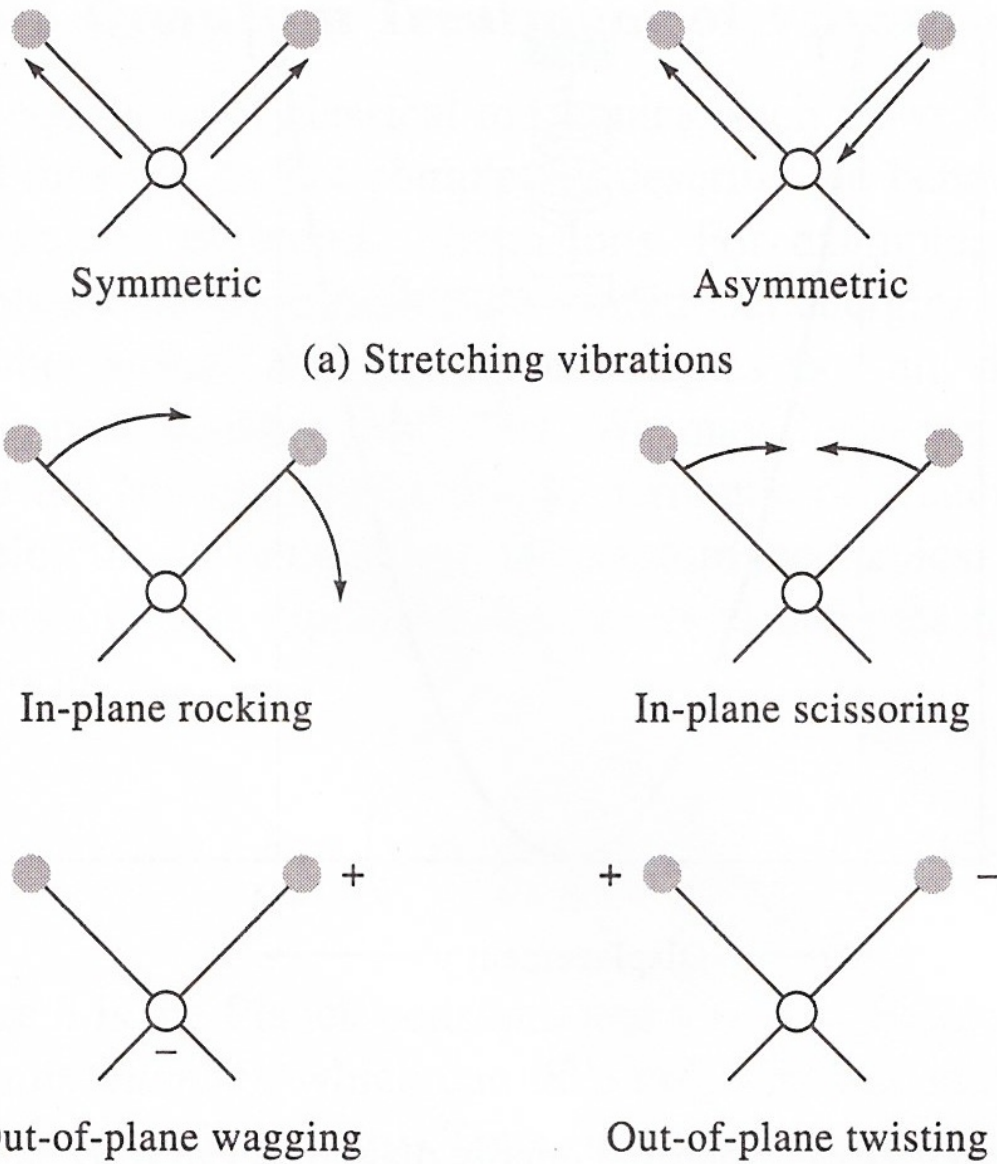


**Figure 16:** Molecular vibration modes [91]

Raman is not a destructive technique, spectral acquisition is very fast (seconds), it is adaptable to various sample types (gas, liquid, solid), can be used in relatively extreme environments (high temperature) and can utilize fiber optic systems for measurement.

Thus, Raman spectroscopy has the potential for use as a process monitor in used fuel reprocessing type scenarios.

### 3.6.2 Sample Preparation and Data Analysis

Solid, liquid or gas samples can be studied with Raman spectroscopy, with solid sample preparation including grinding to a fine powder. Generally gaseous samples have a very low concentration of analyte, in which case a long path length would be necessary. For liquid samples, spectra can be obtained through glass or plastic sample holders, where subtraction of a blank spectra can then provide the analyte Raman spectra. In any case, the sample is irradiated with a source of monochromatic light, often a laser, and the spectrum of the scattered radiation is measured with a spectrometer, often at a right angle to the incident beam [91]. Collected Raman spectra are often referred to as “fingerprints” of the sample, and collections, databases and books of spectra are available for identification of spectral peaks [130, 131]. Often, however, software such as OMNIC or LabSpec is used to deconvolute or separate spectra and search spectral libraries to aid in qualitative Raman spectral analysis (identification). When quantitative Raman spectral analysis is necessary, peak ratios can be compared as the relative intensities of peaks are directly proportional to the concentrations in the sample.

## CHAPTER 4

### PROCESS MONITORING UNDER UREX CONDITIONS

Speciation by spectroscopic methods has been demonstrated to have applications to materials accountability and process monitoring by providing a route to evaluate radionuclide concentrations and solution conditions [132]. As the chemical form of the element impacts the absorbance spectra, speciation can be determined from this technique. UV-Visible spectroscopy is an excellent method for application to the actinides, as elements such as U, Np, Pu and Am are spectroscopically rich due to their different oxidation states. Taking this application one step further, speciation by spectroscopic methods has been demonstrated to have applications to materials accountability and process monitoring by providing a route to evaluate radionuclide concentrations and solution conditions [132]. The spectroscopically determined information can then be used to both verify the extraction system and detect diversion attempts. Namely, differentiation between PUREX and UREX is of prime importance. The approach to this differentiation is straightforward as the uranyl UV-Visible spectrum is shown to change with varying nitrate concentration, which is one of the main differences between the PUREX and UREX systems [3, 13].

#### 4.1 Introduction

##### 4.1.1 Uranyl Spectroscopy

UV-Visible spectroscopy is directly related to electronic transitions in a species, where allowed transitions will have a much higher molar absorptivity than forbidden

transitions (which can still be detected spectroscopically) [133]. The uranyl nitrate complex usually exists as the mononitrate or dinitrate, however the uranyl trinitrato complex has been prepared at upwards of 16 M HNO<sub>3</sub> and found to be fairly stable in the absence of water [134, 135]. The molar extinction coefficient of the tetranitrato salt is much higher than that of the trinitrato salt or aqueous uranyl nitrate solutions and is reported to reach upwards of 57 M<sup>-1</sup>cm<sup>-1</sup>, as compared to 8-10 M<sup>-1</sup>cm<sup>-1</sup> for the latter [136]. Uranyl's molar absorptivity dependence on nitrate is a fundamental premise of the project. While neither the trinitrato nor tetranitrato species are expected in this work, it should be noted that the presence of these salts would substantially affect the UV-Visible absorption spectra. It is assumed that in acidic solutions from pH~0.1 to pH~2, the uranyl ion UO<sub>2</sub><sup>2+</sup> is exclusively formed [134]. Additionally, uranyl nitrate is strongly complexed in nitric acid solutions and inhibits Pu(VI) formation when present in high concentrations, but enhances the formation when present in low concentrations [137].

The spectroscopy of the uranyl ion can be explained by examination of atomic and electronic structures. The uranyl ion is formally a 5f<sup>0</sup> system and consists of a U atom covalently bound to two oxygen atoms in a linear arrangement. The electronic structure of the uranyl ion can be described in terms of the molecular orbitals formed by the 5f and 6d valence orbitals of U and the 2s and 2p orbitals of the O atoms (Figure 17). The bonding molecular orbitals σ<sub>g</sub><sup>+</sup>, σ<sub>u</sub><sup>+</sup>, π<sub>g</sub>, and π<sub>u</sub> accommodate the 12 valence electrons of UO<sub>2</sub><sup>2+</sup>, with σ<sub>u</sub><sup>+</sup> being the highest occupied molecular orbital (HOMO). The lowest unoccupied molecular orbitals (LUMO) are the nonbonding δ<sub>u</sub> (f<sub>xyz</sub>, f<sub>z(x2-y2)</sub>) and φ<sub>u</sub>, originating from the 5f orbitals of U. The UV-Visible absorption spectra of uranyl compounds can be explained in terms of excitations from the σ<sub>u</sub><sup>+</sup> orbital to the δ<sub>u</sub> and φ<sub>u</sub>

orbitals:  $(\sigma_u^+)^2 \rightarrow \sigma_u + \delta_u$  and  $(\sigma_u^+)^2 \rightarrow \sigma_u + \varphi_u$ . In the free uranyl ion, i.e., in the uranyl ion without any ligands in its equatorial plane, the nonbonding orbitals  $\delta_u$  and  $\varphi_u$  have approximately the same energy. However, when ligands are surrounding the uranyl ion in the equatorial plane, the energy of the  $\varphi_u$  orbital increases due to interaction with the equatorial field. All electronic transitions in uranyl spectra are parity forbidden by the Laporte selection rule (allowed requires a change in parity), therefore, intensity must be induced either by the static ligand field (e.g.,  $[\text{UO}_2(\text{NO}_3)_3]^-$   $D_{3h}$ ) or by the dynamic ligand field, also referred to as vibronic coupling (e.g.,  $[\text{UO}_2\text{Cl}_4]^{2-}$   $D_{4h}$ ) [138].

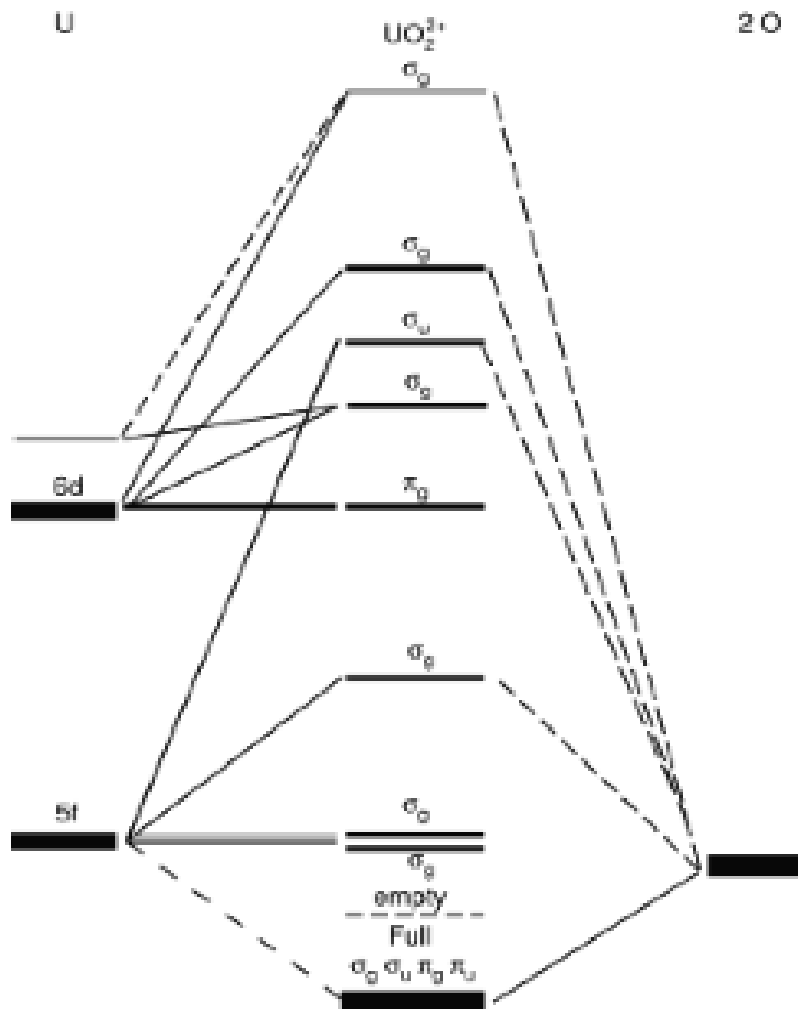


**Figure 17:** Molecular orbital diagram of uranyl ion [139]

The uranyl ion has characteristic absorption spectra containing three fingerlike peaks at 403, 414 and 426 nm (Figure 18). The uranyl absorption spectra change shape and shift absorbance maxima with shifts in speciation, since the spectrophotometer detects variations in the U electron configuration and transition energies. Changes in speciation can occur due to ligand and metal concentration variation, with previous work showing that as nitric acid concentration increases from 2 to 6 M the characteristic uranyl peaks broaden and merge into one large peak [140]. In the visible U spectrum, the 426 nm absorption line possesses the greatest sensitivity to nitrate conditions, whereas the 359 nm line exhibits a sensitivity which is only one-third of this value. Overall, the absorption at all wavelengths increases with nitric acid concentration, the 403, 426, and 416 nm U triplet becomes less defined, as the 426 nm line broadens into a shoulder. In the literature, the slopes of the curves obtained with varying nitrate were found to be identical to those obtained with changing nitric acid, with uranyl absorbance demonstrating a linear relationship with nitrate throughout the U concentration range. Quantitatively, the absorbance increases linearly at a rate of 0.00145 absorbance units per degree centigrade for both the 416 and 416 maxima [139].

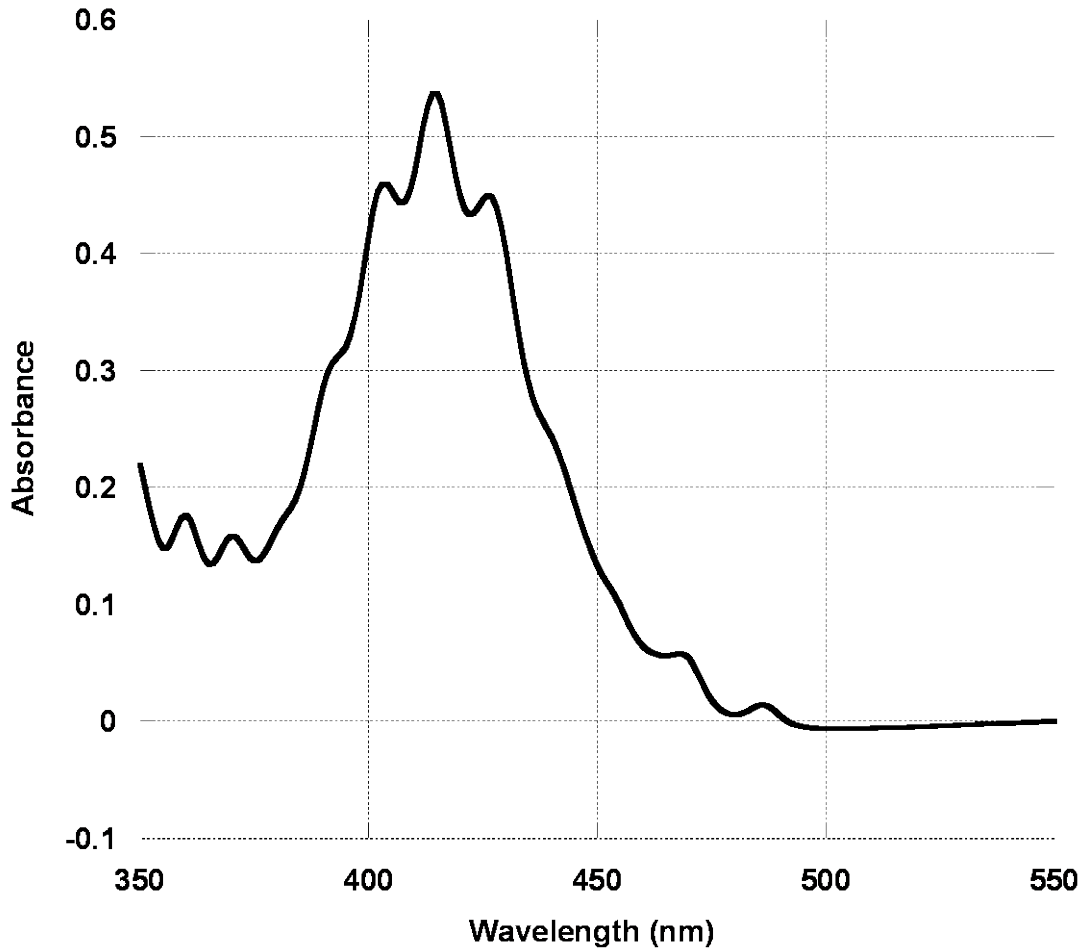


**Figure 18:** UV-Visible Absorbance of 0.63 M U at 0.01 M HNO<sub>3</sub>, 0.1 cm pathlength

In general, UV-Visible spectroscopy is a reliable method for U concentration determination. However, this work exploits a main caveat to this generalization, which is that uranyl measurement by UV-Visible spectroscopy in nitrate matrices is complex due to nitrate concentration altering uranyl speciation, and therefore its absorption spectrum [141, 142]. Thus, the UV-Visible spectroscopy of uranyl nitrate is extremely sensitive to solution conditions.

#### 4.1.2 Relevance to reprocessing

The reprocessing of irradiated fuel from LWRs was initially intended to produce separated Pu and U products. The speciation of the U and Pu in solution is directly relevant to the application of UV-Visible spectroscopy as a process monitor. While no reprocessing is currently underway in the U.S., the Barnwell Nuclear Fuel Plant stored highly concentrated Pu nitrate solutions and conducted studies to determine the physical and chemical properties of concentrated (approximately 500 and 700 grams/liter of Pu(IV) in  $\text{HNO}_3$ ) Pu solutions [143]. Typical output streams from the PUREX fuel recycling process contain from 20-200 grams/liter U, in addition to approximately 4 M nitric acid and 1 M nitrate. The UV-Visible spectroscopic spectrum of uranyl in TBP in the presence of acetohydroxamic acid has been studied [144]. This information, including data on density, viscosity and materials corrosion rates, can be used in conjunction with any process monitoring of Pu-bearing streams in a reprocessing plant.

In considering the application of spectroscopy in a separations scheme, typical output streams from the PUREX/UREX fuel recycling process contain up to 300 grams/liter U ( $\leq 1.26$  M), in addition to approximately 0.1-6 M nitric acid and corresponding ranges of nitrate. In both UREX and PUREX, the organic phase is 30 % tributylphosphate in an organic diluent, normally dodecane. In UREX, acetohydroxamic acid (AHA) is utilized along with a reduced acid concentration as compared to PUREX in order to prevent the extraction of Pu(IV) with U. The difference in the aqueous phases for UREX and PUREX are summarized in Section 2.3.1. The interaction of AHA with tetravalent Pu decreases extraction into the organic phase by either complex formation or reduction of Pu to the trivalent state [145]. In UREX the Tc(VII) is extracted into the organic phase

along with U(VI). UREX is generally proposed to be the initial component of a range of used nuclear fuel reprocessing flowsheets (Section 2.3).

Continuing the consideration of the application of spectroscopy in a separations scheme, controlling Pu in a reprocessing scheme has been a goal throughout the history of nuclear fuel cycles [146]. Of relevance to this work, Pu oxidation behavior has been studied and absorption spectroscopy has been used to characterize nitrate complexes of Pu(IV) [137, 147, 148]. For UV-Visible spectroscopic applications in cases of low concentrations of Pu, liquid core waveguides (LCW) can be used to effectively increase the pathlength of the sample cell. With the lower detection limits of a LCW, the identification of oxidation states in dilute Pu solutions is possible [149]. A 1.0 meter LCW was utilized to detect and quantify Pu(III, IV, VI, V) in perchloric acid. Due to the nature of the LCW, the sample must be pumped through the system, in this case at a flow rate of 5 milliliter/minute, and through spectral averaging, no flow-rate effects were seen. The measured molar absorption coefficient for the Pu band at 600 nm was found to be approximately  $34 \text{ M}^{-1} \text{ cm}^{-1}$ , and this results in a lower limit of detection for Pu(III) of  $8.0 \times 10^{-6} \text{ M}$ . The absorbed wavelengths for the various oxidation states of Pu and their respective molar absorptivities can be seen in Table 6.

**Table 6:** Molar absorptivities and Lower Limit of Detection (LLD) for Pu major absorption bands in 1 M HClO<sub>4</sub>, diluted from 0.005 M Pu stock

Pu Ion	Abs. Wavelength (nm)	Molar Absorptivity ( $\text{M}^{-1}\text{cm}^{-1}$ ) [149]	Molar Absorptivity ( $\text{M}^{-1}\text{cm}^{-1}$ ) [150]	LLD for 1 cm ( $\mu\text{M}$ )
III	600	33.8	38	236
IV	470	49.0	55	158
V	568	18.8	19	518
VI	830	288	550	12.4

Detection limits for the UV-Visible spectroscopy of Pu were found to be  $10^{-5}$ - $10^{-6}$  M for a 1 cm pathlength cell, and this LLD was brought down to the  $10^{-7}$  M range for a LCW UV-Visible spectroscopy setup [151].

Centrifugal contactors have been found to be reliable and relatively inexpensive to build, operate and maintain; therefore have been considered for use in a reprocessing plant. Due to the compact contactor stages, the overall liquid holdup is low, the systems can undergo fast startup and shutdown, and high mass transfer efficiency can be achieved [124, 126, 152, 153]. The contactor interstage lines are external to the contactor body so that both the aqueous and organic phases are accessible as they enter and leave each stage, making stream interrogation physically straightforward. Thus, the process monitoring system described in this work is applied to a contactor setup for a demonstration of the technology and methodology.

Theoretical proliferant diversions in separations would be accomplished via deliberate modification of the flowsheet chemistry. Therefore, by confirming proper operational performance and verifying process integrity throughout the PUREX/UREX scheme, these diversions can be identified. Online, real time, multiparametric monitoring of the radiochemical streams in a reprocessing flowsheet can provide rapid detection of unwanted deviations from normal operation conditions. In order to effectively monitor a reprocessing scheme, concentration and speciation of the main components under normal conditions must be identified to have a reference case of key signatures. Additionally, the stream pH, flow rate, and temperature can be monitored and compared with chemical libraries of spectroscopic, chemical and physiochemical properties [4, 21, 70, 88, 132]. The work presented in this chapter can be used with other commercial off the shelf

technologies that monitor other process variables to provide a robust, comprehensive process monitor in a reprocessing setting.

#### 4.2 Scoping Experiments and Preliminary Application to Reprocessing

There are two methods for the UV-Visible spectroscopy of the moving solutions: a fiber optic dip probe can be inserted into the stream or the stream can be diverted to a cuvette flow-cell placed in a spectrophotometer. Before the fiber optic system was integrated into a flowing stream, fundamental studies with both a benchtop spectrophotometer and the fiber optic dip probe were performed to characterize the uranyl nitrate UV-Visible system. Following these studies, flowing experiments were carried out with both the fiber optic dip probe and cuvette flow-cells.

The Cary 6000i was used to measure a set of U samples ( $[U]=1.13, 0.566, 0.113, 0.0566, 0.0113,$  and  $0.00566\text{ M}$ , all at  $2\text{ M }[\text{H}^+]$ ) in the single and double beam configuration with the samples in 1 cm cuvettes. Next, the same instrument was used to measure the samples with the fiber optic dip probe in the single and double beam configurations. In this way, effects of the differing setups could be seen and a comparison of the cuvette to fiber probe measurements revealed any fiber losses of light.

Figure 8 shows an example of the spectra collected from the Cary 6000i. Here, the same sample ( $[U] = 0.113\text{ M}$ ) is measured in a cuvette in both single and double beam geometries (black and dark green lines). Then the same sample is measured by the fiber optic dip probe in a centrifuge tube with the 2 mm tip in both single and double beam geometries, and then with the 10 mm tip in both the single and double beam geometries. It is evident that within each method – cuvette, 2 mm, 10 mm – quite similar results are shown in single and double beam settings. For greater detail on the single and double

beam methods of UV-Visible spectroscopy, see Section 3.1.1. Previously shown data (Figure 8) identifies the issue of variation in molar absorptivities. For example, the fiber optic dip probe with 2 mm tip measurement at the 414 peak (green line, absorbance ~0.29) yields a molar absorptivity of approximately 13. The 414 peak in the single beam cuvette with 1 cm pathlength (purple line, absorbance ~0.85) arrangement yields a molar absorptivity of 9.3. The variation here is an experimental introduction to uranyl's molar absorptivity dependence on nitrate which is a fundamental premise of the project.

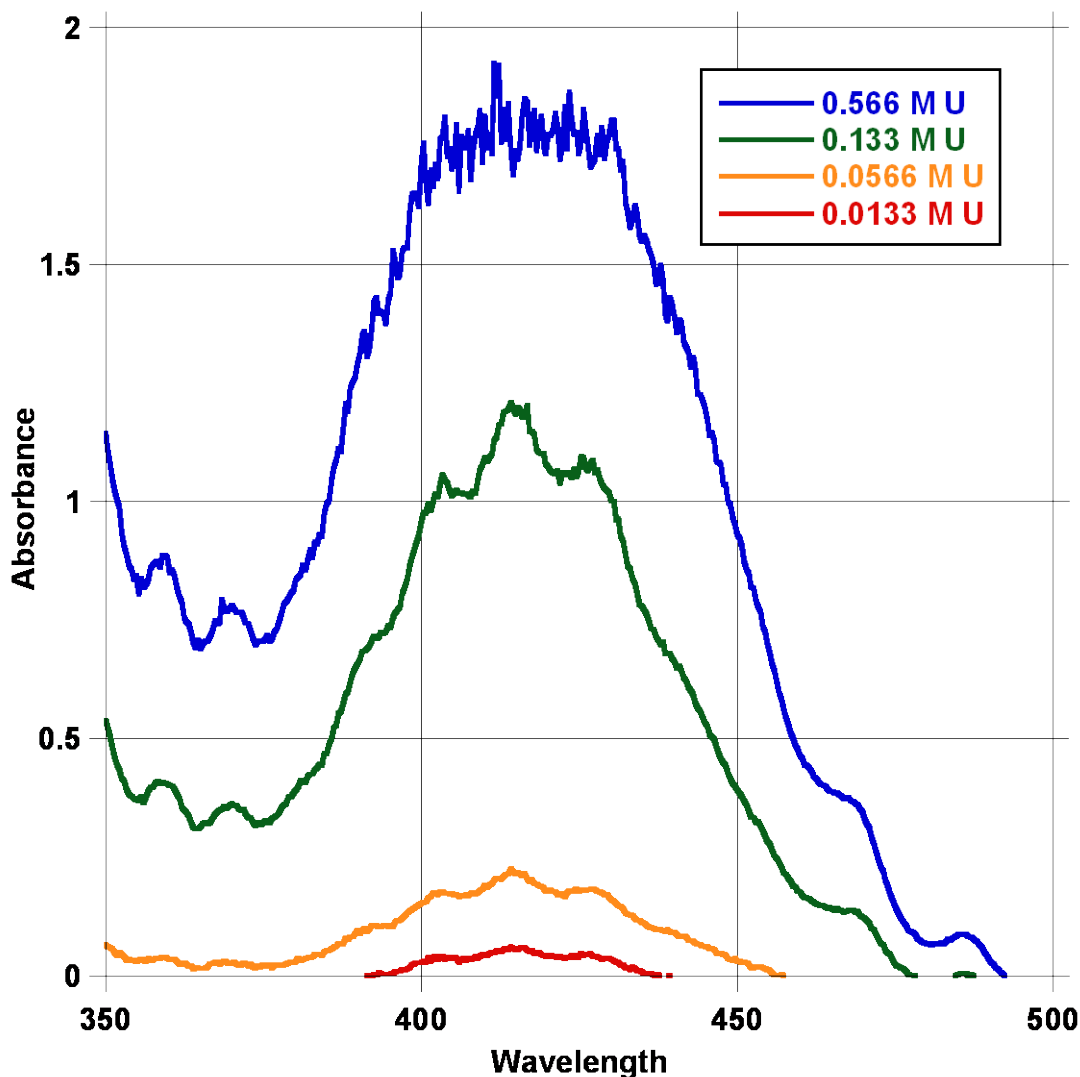


**Figure 19: Fiber optic dip probe range study with  $\text{UO}_2^{2+}$**

In studies for preparation of flowing system measurements, an Ocean Optics fiber optic dip probe with a 2 mm pathlength tip was inserted into a Swagelok tee. A diaphragm pump provided solution flow, and the system spanning 0.0113-0.566 M  $[\text{UO}_2^{2+}]$  was investigated with the Ocean Optics USB2000+ UV-Visible spectrometer system. As seen in Figure 19, the Ocean Optics setup can easily and distinctly resolve 0.04 M differences in  $\text{UO}_2^{2+}$  concentration at levels as low as 0.01 M  $\text{UO}_2^{2+}$ . It can also provide some spectral information at concentrations upwards of 0.5 M  $\text{UO}_2^{2+}$ , however the characteristic uranyl shape is lost and peaks cannot be resolved. Thus, the resolution of this specific Ocean Optics setup is greater than 0.04 M  $\text{UO}_2^{2+}$  over the effective range of 0.01-0.15 M  $\text{UO}_2^{2+}$ .

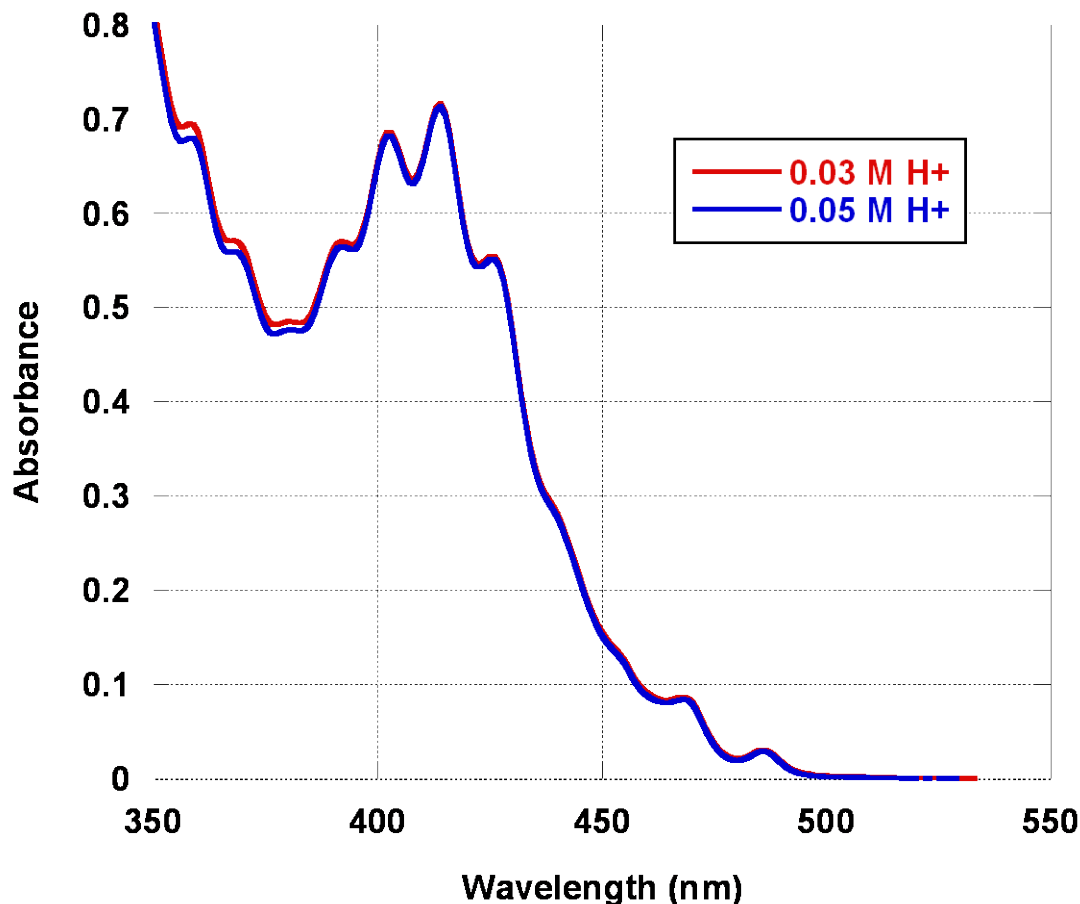


**Figure 20: Effect of addition of  $\text{NH}_4\text{OH}$  on UV-Visible spectra**

In order to determine the effect on UV-Visible spectra from a titration with base, a 0.05 M HNO<sub>3</sub>/0.12 M UO<sub>2</sub>(NO<sub>3</sub>)<sub>2</sub> sample and a 0.03 M H (0.05 M HNO<sub>3</sub> + 0.02 M NH<sub>4</sub>OH) 0.12 M UO<sub>2</sub>(NO<sub>3</sub>)<sub>2</sub> sample were prepared and compared. Figure 20 shows the overlay of the spectra produced in the Cary 6000i UV-Visible spectrometer. While some changes are noticeable below 390 nm, in the area of interest for the uranyl species (400-430nm), the spectra appear to overlap entirely.

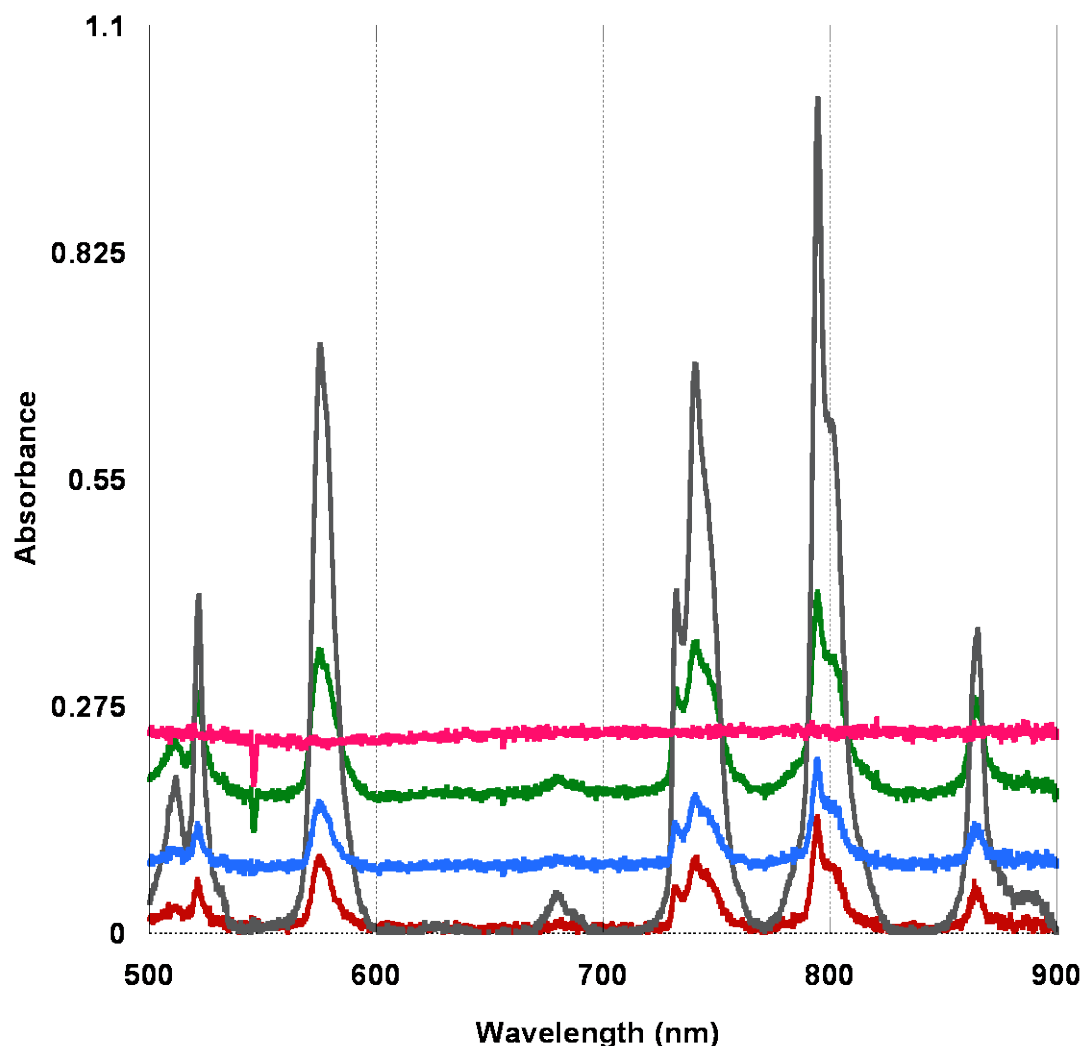


**Figure 21:** UV-Visible absorption spectra of Nd solution showing the time response study with fiber optic dip probe

To continue studies with the fiber optic probe UV-Visible spectroscopy system, solutions with varying concentrations of Nd were used in order to determine the time response of the probe in solution. Results indicate instantaneous response from the probe when presented with 0.02 M differences in concentration of  $\text{Nd}(\text{NO}_3)_3$  (Figure 21). Another time response experiment was conducted with the fiber optic probe setup, however varying concentrations of uranyl nitrate were used, and the resolution (minimum distinguishable concentration difference) was found to be 0.002 M  $\text{UO}_2(\text{NO}_3)_2$  (Figure 22).

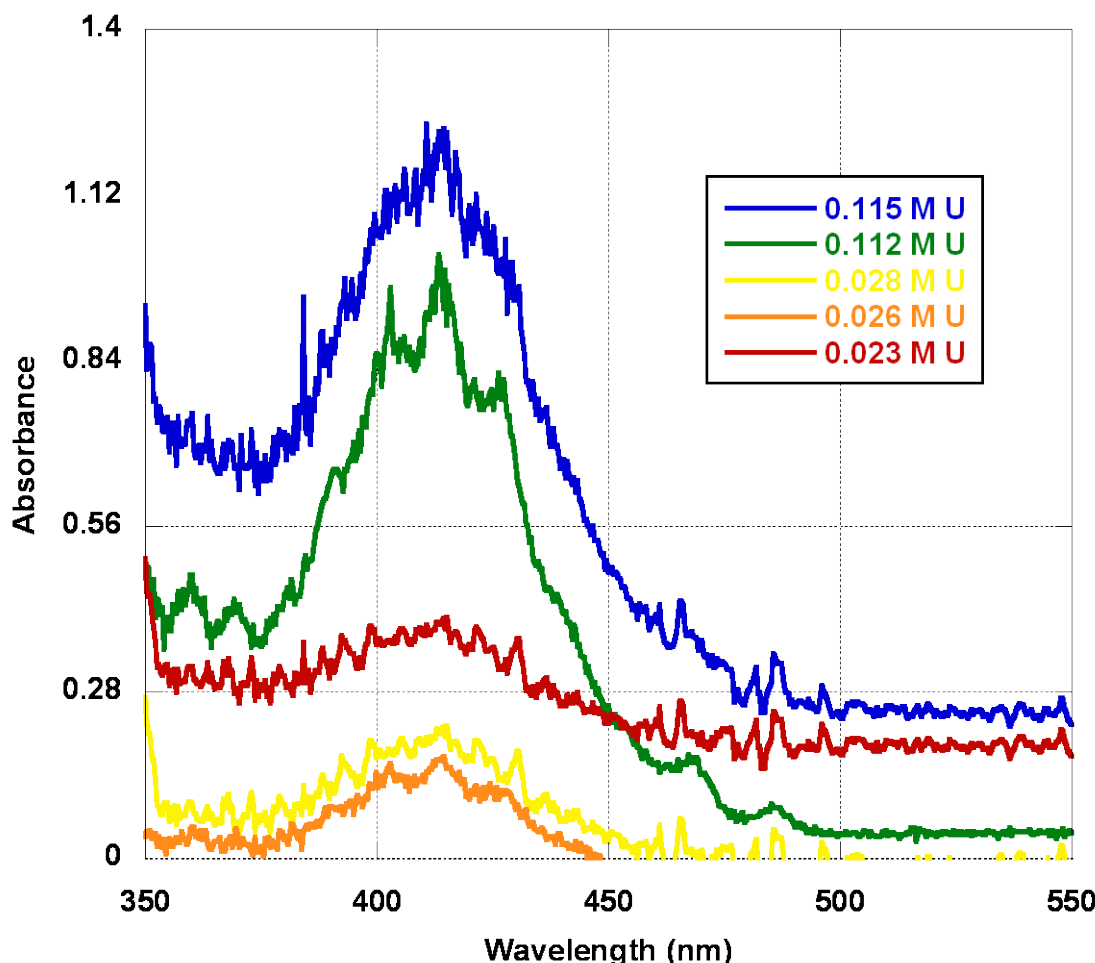


**Figure 22:** Resolution studies of uranyl nitrate solutions (0.023 to 0.115 M) with the fiber optic dip probe in Swagelok flow cell

After scoping studies with the Swagelok tee and single pump system, the fiber optic probe was mounted in the same Swagelok tee design in the aqueous product stream of bank of twenty 2-cm contactors at ANL for a U-only UREX demonstration (Figure 23).



**Figure 23:** Fiber optic dip probe mounted in aqueous product outlet

The introduction and growth of the spectra as  $\text{UO}_2^{2+}$  enters the product stream exiting the last strip stage after approximately 30 minutes is shown in Figure 24. The fiber optic probe behaved as expected in this demonstration, and the relationship between solution flow rates and UV-Visible spectra was brought to attention. While there was no effect of flow rate on spectra in previous experiments with single solution flow, the countercurrent nature of the contactors combined with the use of multiple solution inlets complicates the relationship.

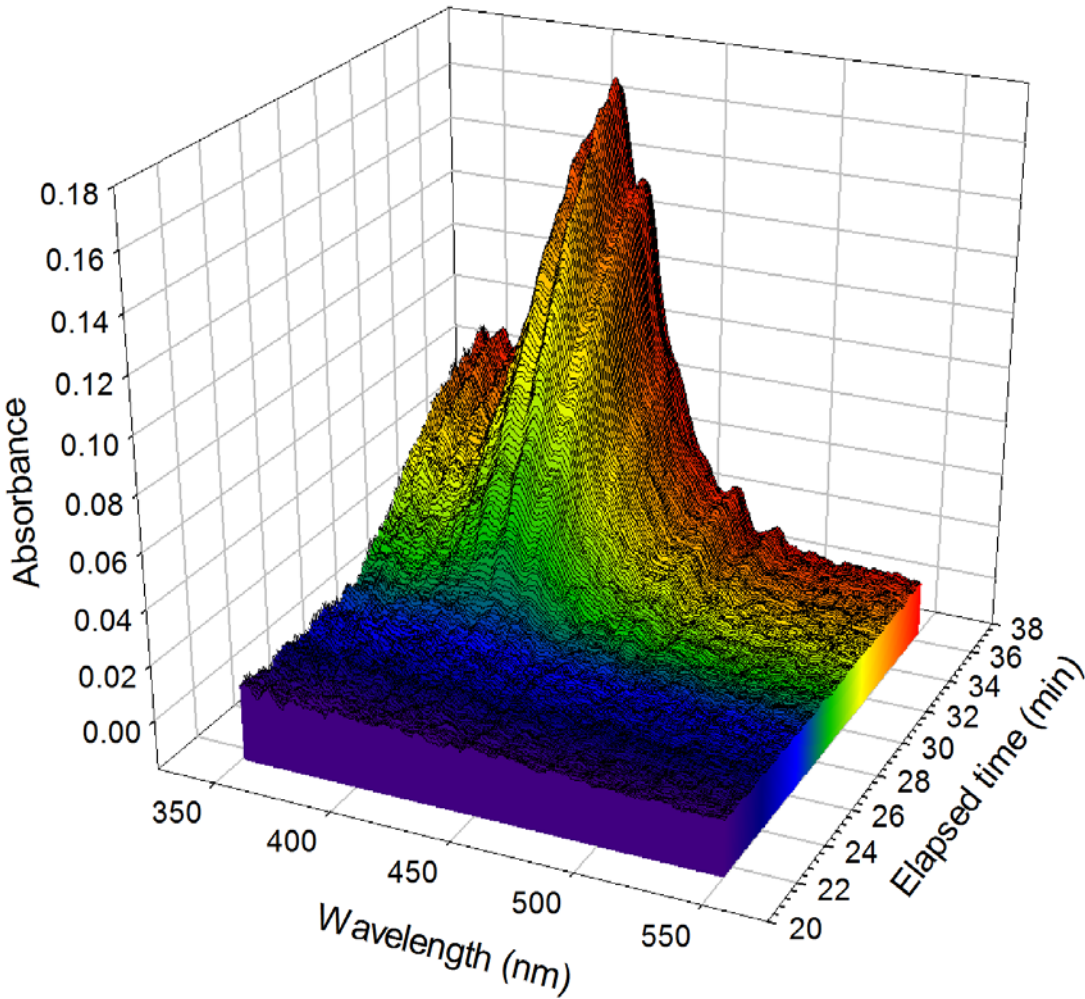


**Figure 24:**  $\text{UO}_2^{2+}$  growth in UREX product stream [154]

Specifically, changes in the strip flow rate were found to be inversely proportional to the concentration changes in the product as seen by the UV-Visible spectrometer (Figure 25). In general, the flowrate of the solution under fiber optic dip probe investigation should be explicitly related to the other flowsheet flowrates, and this determined relationship can be used to explain UV-Visible absorbance value changes due to flowrate variance. One observation from this setup is that the high surface tension of the aqueous flow dictates the flow through the tubing, oftentimes pulling a slug of product through, leaving the aperture of the probe empty.

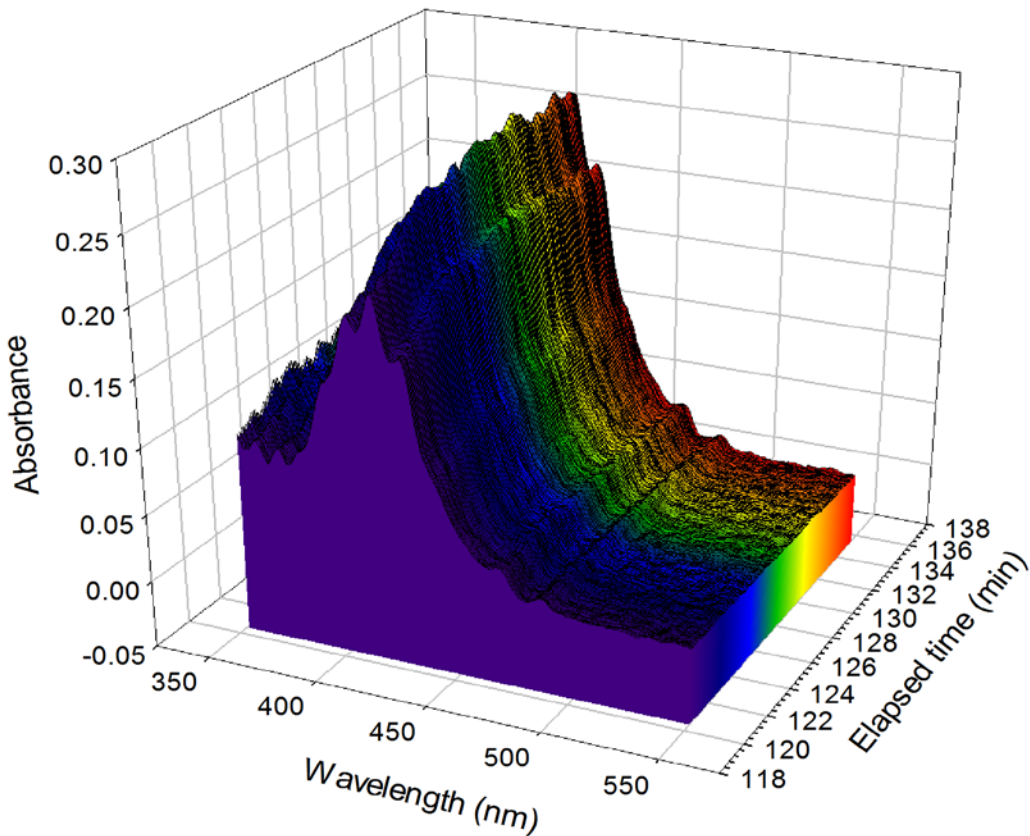


**Figure 25:** Inverse relationship between strip flow rate adjustment and  $\text{UO}_2^{2+}$  concentration seen in aqueous product stream [154]

#### 4.3 High Fidelity Uranyl Nitrate System Studies

As an alternative to the fiber optic dip probe technique, quartz Hellma flow-through cuvettes with pathlengths of 0.1, 0.5 and 1.0 cm were coupled with a peristaltic pump (flowrate  $\leq 2.5$  milliliter/minute) and a Cary 6000i Spectrophotometer. These cuvettes are very similar to standard cuvettes for UV-Visible spectrophotometric measurements. However, the concept is that a slipstream of the solution of interest can be directed into a benchtop spectrophotometer to provide higher resolution data. Samples of 0.01, 0.126, 0.262, 0.63, 1 and 1.26 M U at 0.01, 0.1, 0.5, 1, 3, and 6 M  $\text{HNO}_3$  were prepared via dilution of a single stock uranyl nitrate solution. The solution was prepared

gravimetrically by dissolving 141.11 grams of  $\text{UO}_2(\text{NO}_3)_2 \cdot 6\text{H}_2\text{O}$  in 200 milliliters of DI  $\text{H}_2\text{O}$  to make a 1.4 M stock from which samples were prepared by volumetric dilution with concentrated  $\text{HNO}_3$  and DI  $\text{H}_2\text{O}$ . Prepared samples were analyzed by ICP-AES using a NIST traceable standard at  $9962 \pm 37$  ppm for calibration with  $R^2=0.9997$  and all samples were found to have less than 1.5% error across triplicates (selected data shown in Table 7). The samples were then pumped through the Hellma cuvettes using the peristaltic pump, and UV-Visible spectra were obtained in triplicate at a flowrate of approximately 2 milliliters/minute with the Cary 6000i in double beam mode with a quartz cuvette of DI  $\text{H}_2\text{O}$  as a background. Reported spectra are averaged and background subtracted (Figure 26 and Figure 28).

**Table 7:** Comparison of calculated and averaged ICP-AES determined values for U concentration

Calculated	Averaged ICP-AES	STDEV	% Difference
0.01	0.0096	0.0005	4.17
0.126	0.1246	0.0028	1.12
0.262	0.2609	0.0078	0.42
0.63	0.6302	0.0216	0.03
1	1.012	0.0549	1.18
1.26	1.257	0.0781	0.24

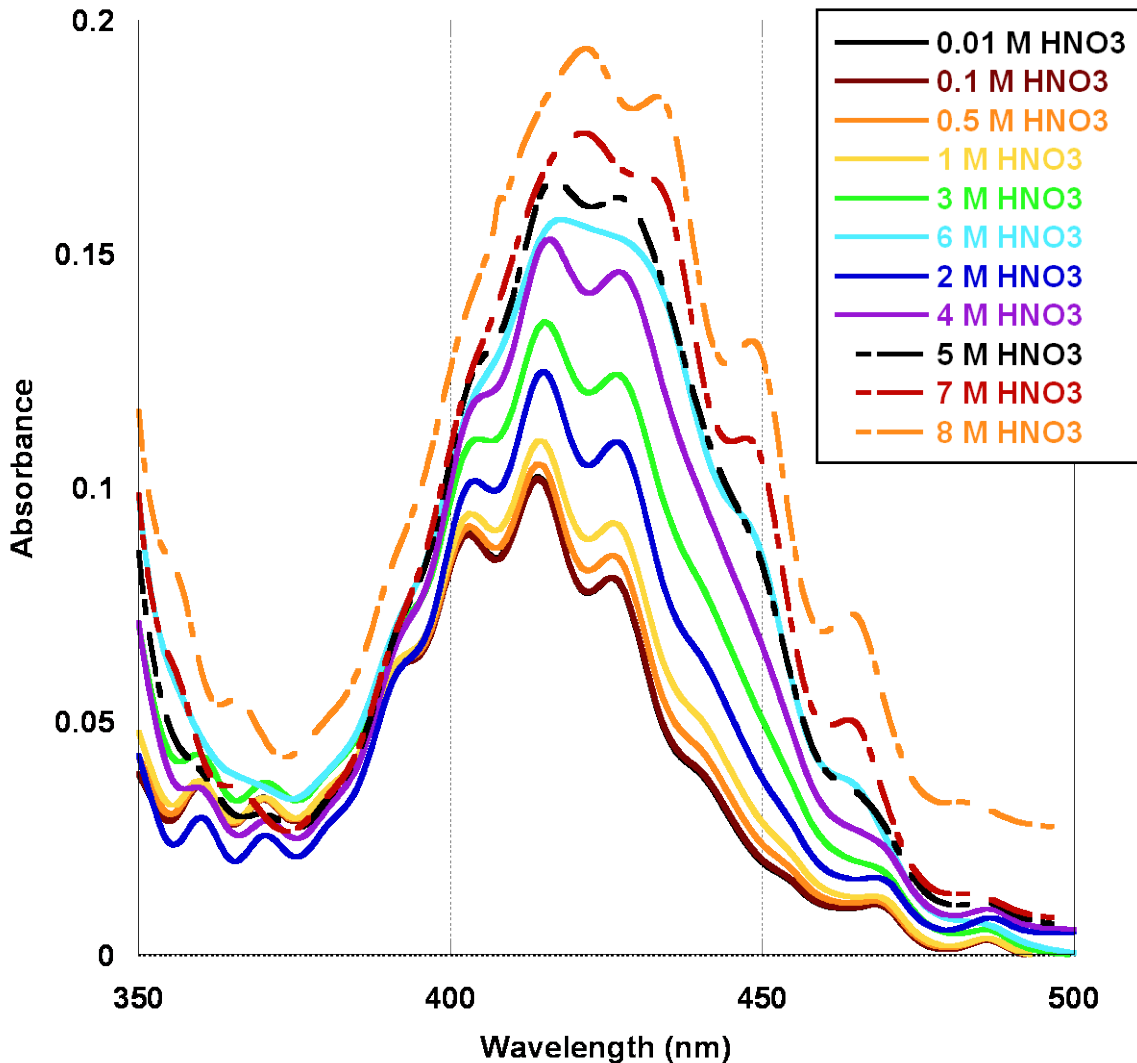


**Figure 26:** UV-Visible Absorbance of  $0.126 \pm 0.02$  M U at  $0.01\text{-}8$  M HNO<sub>3</sub>, 0.1 cm pathlength

**Table 8:** Prepared sample conditions

[HNO <sub>3</sub> ]	2, 4, 5, 7, 8
[UO <sub>2</sub> <sup>2+</sup> ]	0.01, 0.126, 0.262, 0.63, 1

Next, samples were prepared at the conditions in Table 8 via volumetric dilution of a single stock uranyl nitrate solution. In preparation for dilution, the stock solution was characterized as 1.9 M UO<sub>2</sub>(NO<sub>3</sub>)<sub>2</sub> by ICP-AES and as 0.9 M HNO<sub>3</sub> by titration. Again,

all samples were analyzed by ICP-AES using a NIST traceable standard at  $9962 \pm 37$  ppm for calibration with  $R^2=0.9998$  (Figure 27) and less than 2.8 % error was found across triplicates.

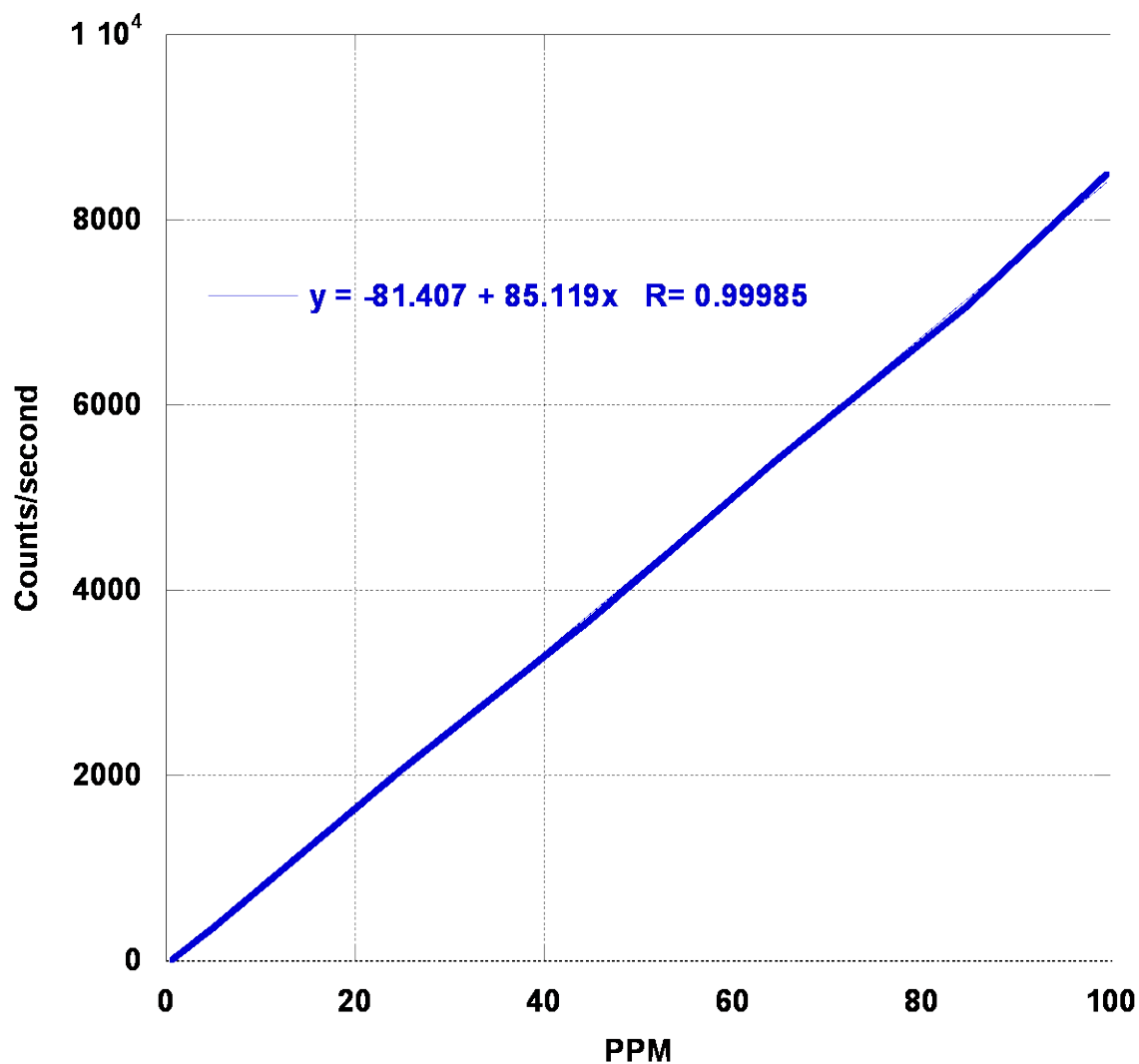


**Figure 27:** Example ICP-AES calibration curve

These samples were titrated along with samples previously prepared using a potassium oxalate complexation method and a standardized 0.1 M NaOH solution. The average disagreement between expected and titrated acid concentrations for all samples was found to be 7.77%. As nitric acid was the only acid used in these experiments, acidities

are directly correlated to nitric acid and therefore nitrate concentrations. Again, the samples were then pumped through the Hellma cuvettes using same experimental setup and conditions as used previously, with reported spectra averaged and background subtracted (Figure 26 and Figure 28).

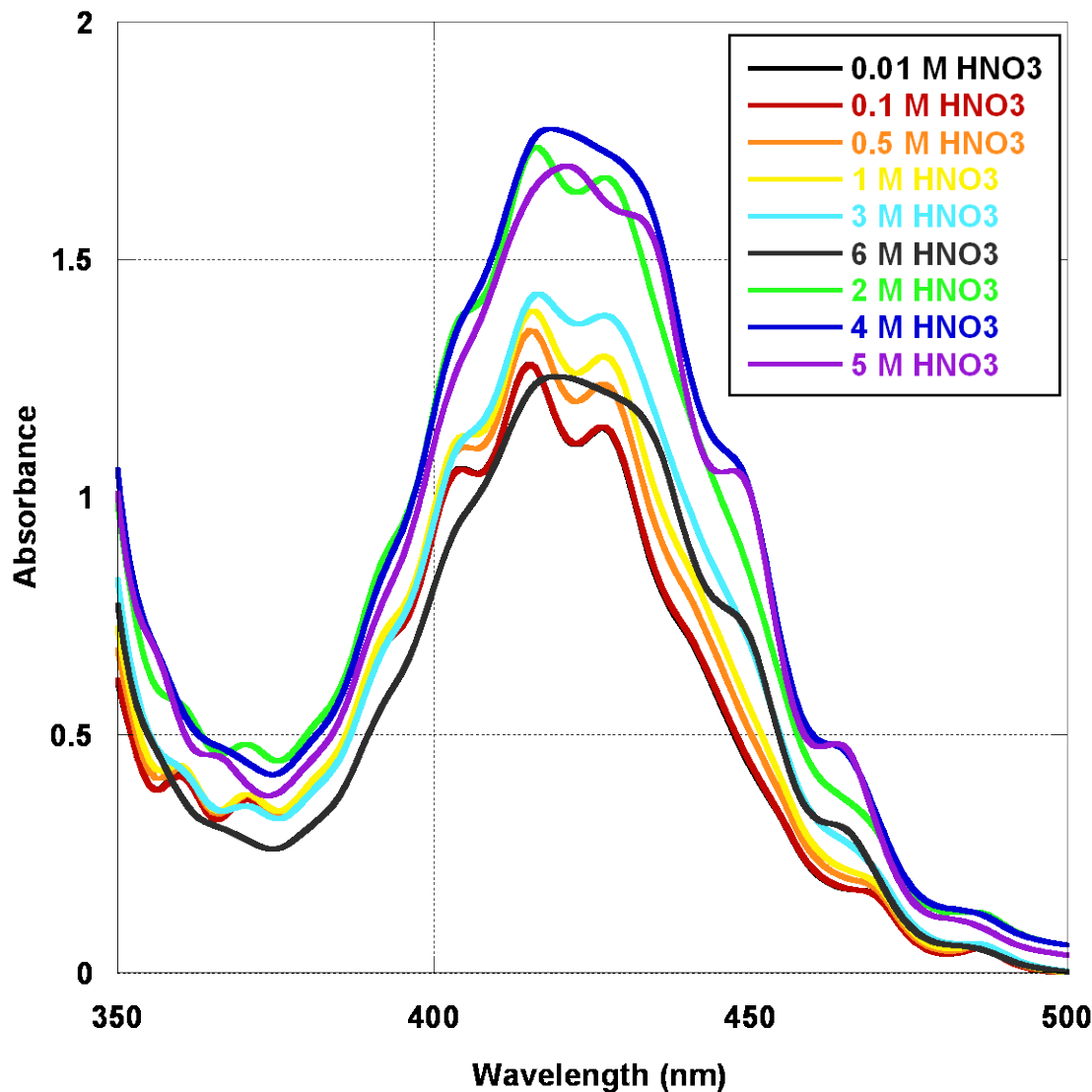


**Figure 28:** UV-Visible absorbance of  $1.26 \pm 0.10$  M U at  $0.01\text{-}5$  M HNO<sub>3</sub>, 0.1 cm pathlength

Although the calculation of uranyl nitrate speciation is unknown and complex, the speciation changes can be investigated spectroscopically. In Figure 26, some semblance of the characteristic uranyl spectra can be seen throughout the range of nitric acid concentrations (0.01-8 M). However, at 1.26 M  $\text{UO}_2^{2+}$  (Figure 28), the characteristic uranyl spectrum begins to lose shape immediately as nitric acid concentration increases, indicating prominent changes in speciation. The combination of 1.26 M  $\text{UO}_2^{2+}$  and 5 M  $\text{HNO}_3$  demonstrates the most defined spectral contrast when compared with the 0.126 M at 0.01 M  $\text{HNO}_3$ . Furthermore, changes in peak ratios are evident even in a cursory comparison of these figures. In Figure 26, the 403 peak is larger than the 426 peak in the low acid ( $\leq 1$  M  $\text{HNO}_3$ ) spectra whereas the opposite is true of the same peak comparison in Figure 28. A calculation of the unit-less peak ratio from Figure 26 yields approximately 1.125 for the 0.01 M  $\text{HNO}_3$  data, whereas the same calculation from Figure 28 yields 0.913. The spectral changes are so great, in addition to free uranyl, mono-, di-, perhaps even tri- nitrate speciation changes, uranyl-uranyl coordination may contribute [141, 142]. The complexity of the uranyl nitrate speciation and sensitivity to chemical environment allow for this method of process monitoring to provide detailed information on solution chemistry and thus process operations and performance.

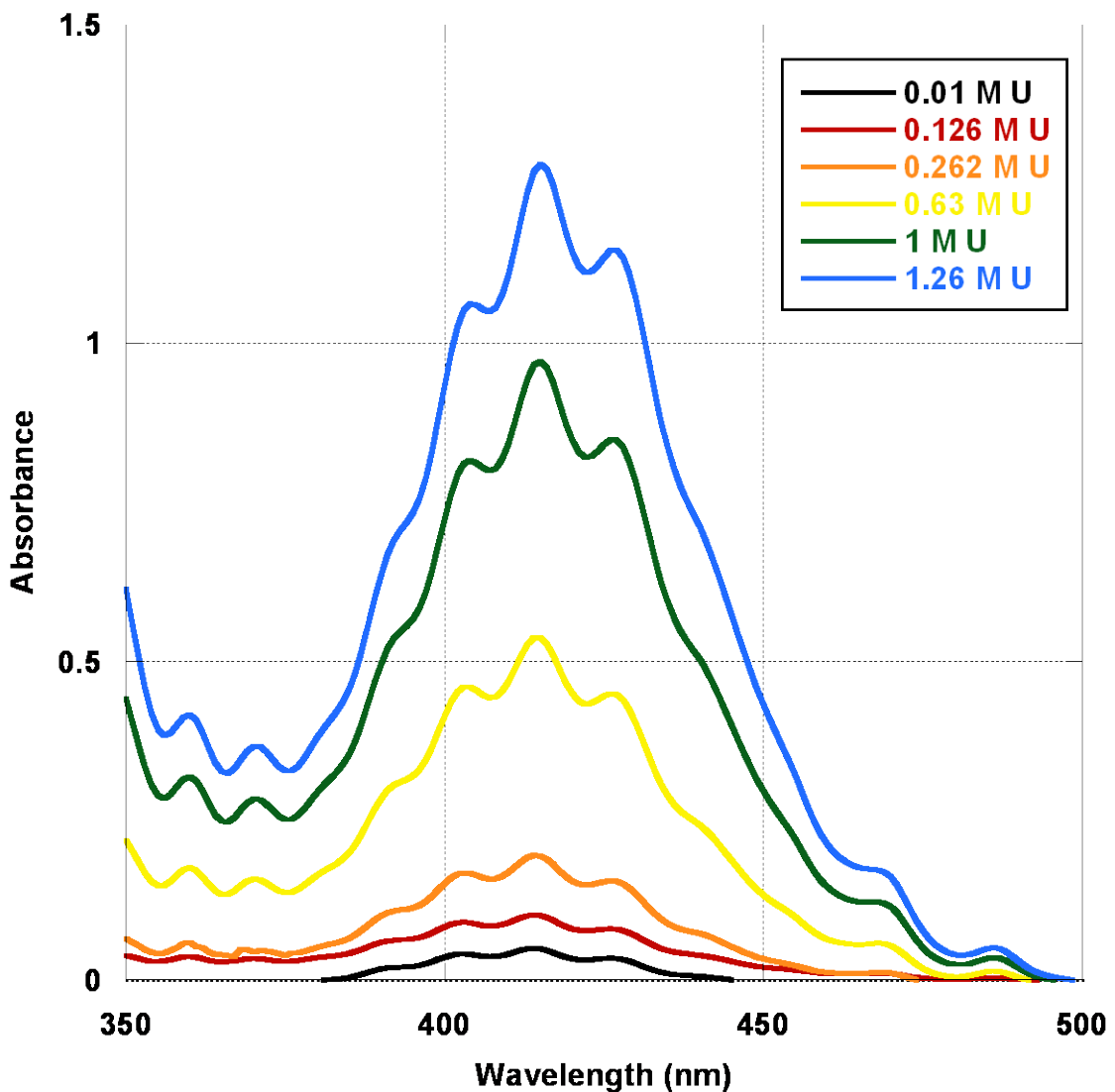


**Figure 29:** UV-Visible Absorbance of 0.01-1.26 M U concentrations at 0.01 M HNO<sub>3</sub>, 0.1 cm pathlength

Overall spectral shape and peak definition are of primary concern in the comparison across nitric acid concentrations, not absolute absorptivity values as there is a slight variance in uranyl concentration introduced in sample preparation. Figure 29 demonstrates the consistent characteristic uranyl spectra found at 0.01 M HNO<sub>3</sub> across all uranyl concentrations studied. In sharp contrast, Figure 30 shows the complete lack of peak definition in the 380-410 nm range and the formation of defined peaks in the

previously smooth 440-470 nm region for all uranyl concentration values.

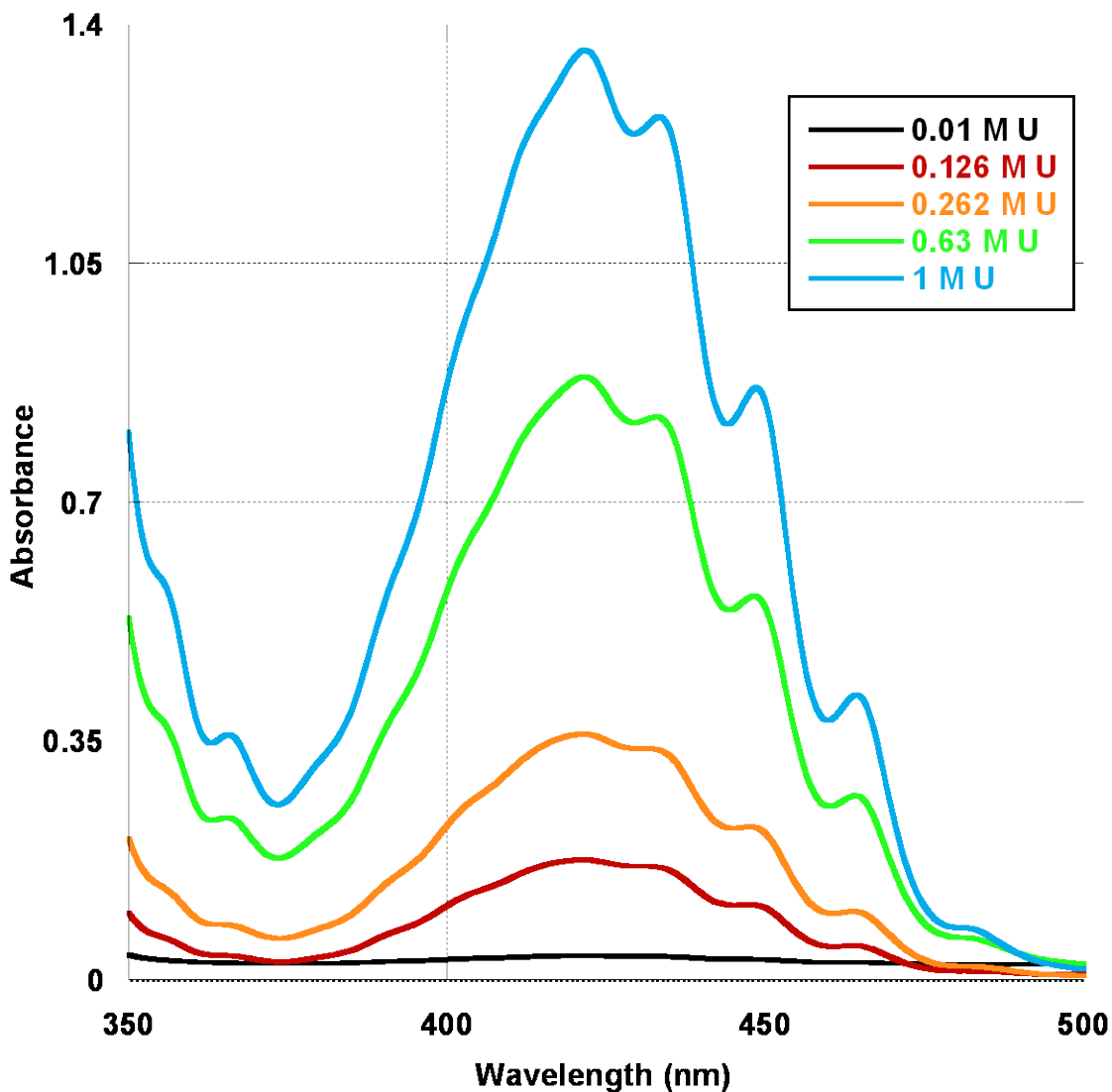


**Figure 30:** UV-Visible Absorbance of 0.01-1 M U concentrations at 7 M HNO<sub>3</sub>, 0.1 cm pathlength

Figure 31 describes the uranyl spectra at 3 M HNO<sub>3</sub> in mid-transformation from the characteristic shape observed at 0.01 M HNO<sub>3</sub> (Figure 29) to the shifted, unresolved profile from the 7 M HNO<sub>3</sub> condition (Figure 30), with shape atypical of a U system. From Figure 31, it can be seen that higher U concentrations also negatively affect peak resolution. Thus, the UV-Visible process monitor would provide the greatest resolution

of individual peaks when placed in an environment relatively dilute in U and nitric acid. However, if used to track peaks and peak ratios over time, the UV-Visible process monitor can be effective at much higher U and nitric acid concentrations.

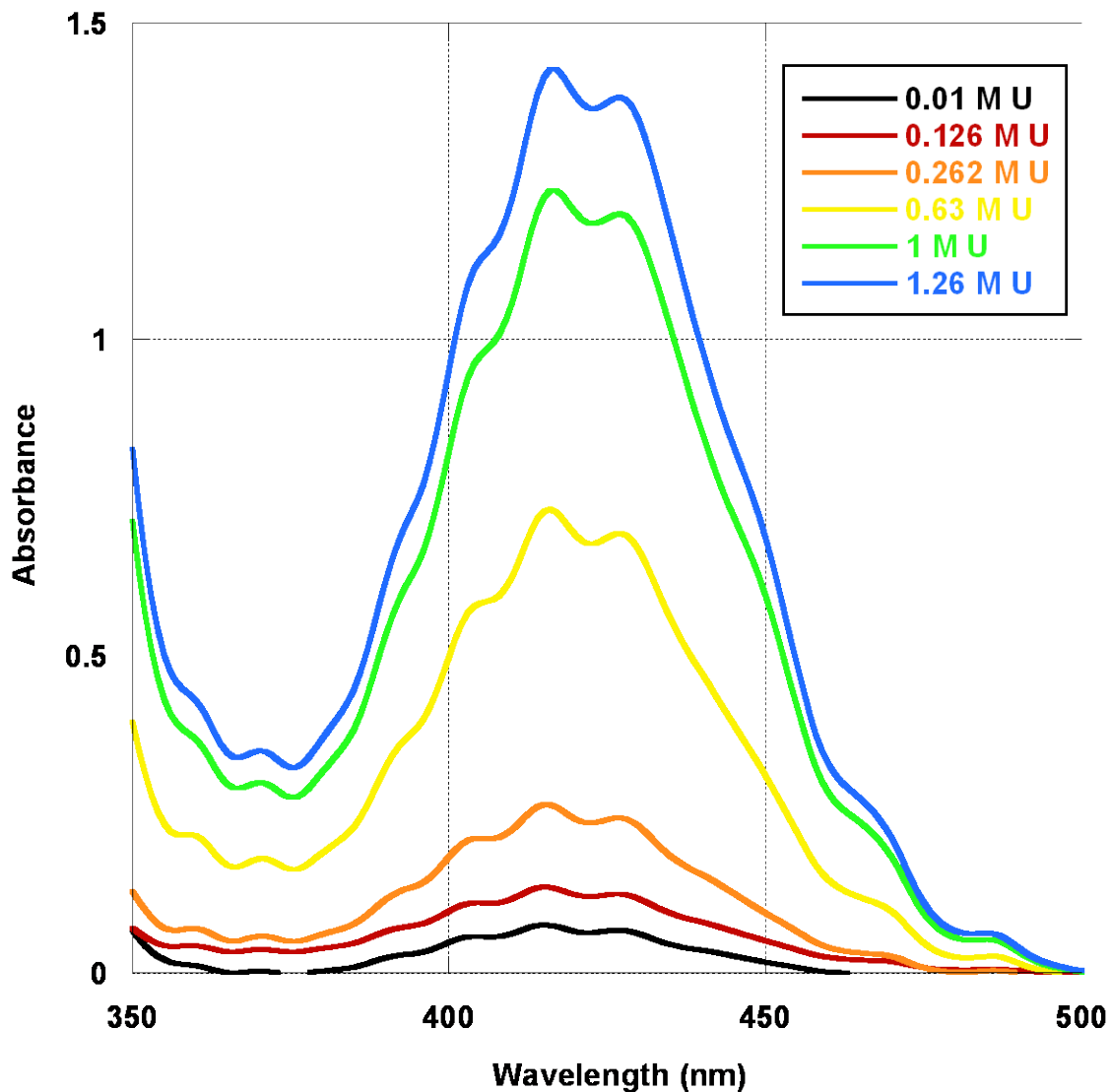


**Figure 31:** UV-Visible Absorbance of 0.01-1.26 M U at 3 M HNO<sub>3</sub>, 0.1 cm pathlength

A calculation of molar absorptivities from UV-Visible absorbance values and known uranyl concentrations shows the dependence on nitric acid concentration. The trends seen in Figure 32 are present at the 403 and 426 nm peaks as well, indicating that changes in nitrate influence all uranyl nitrato species formation in a similar fashion.

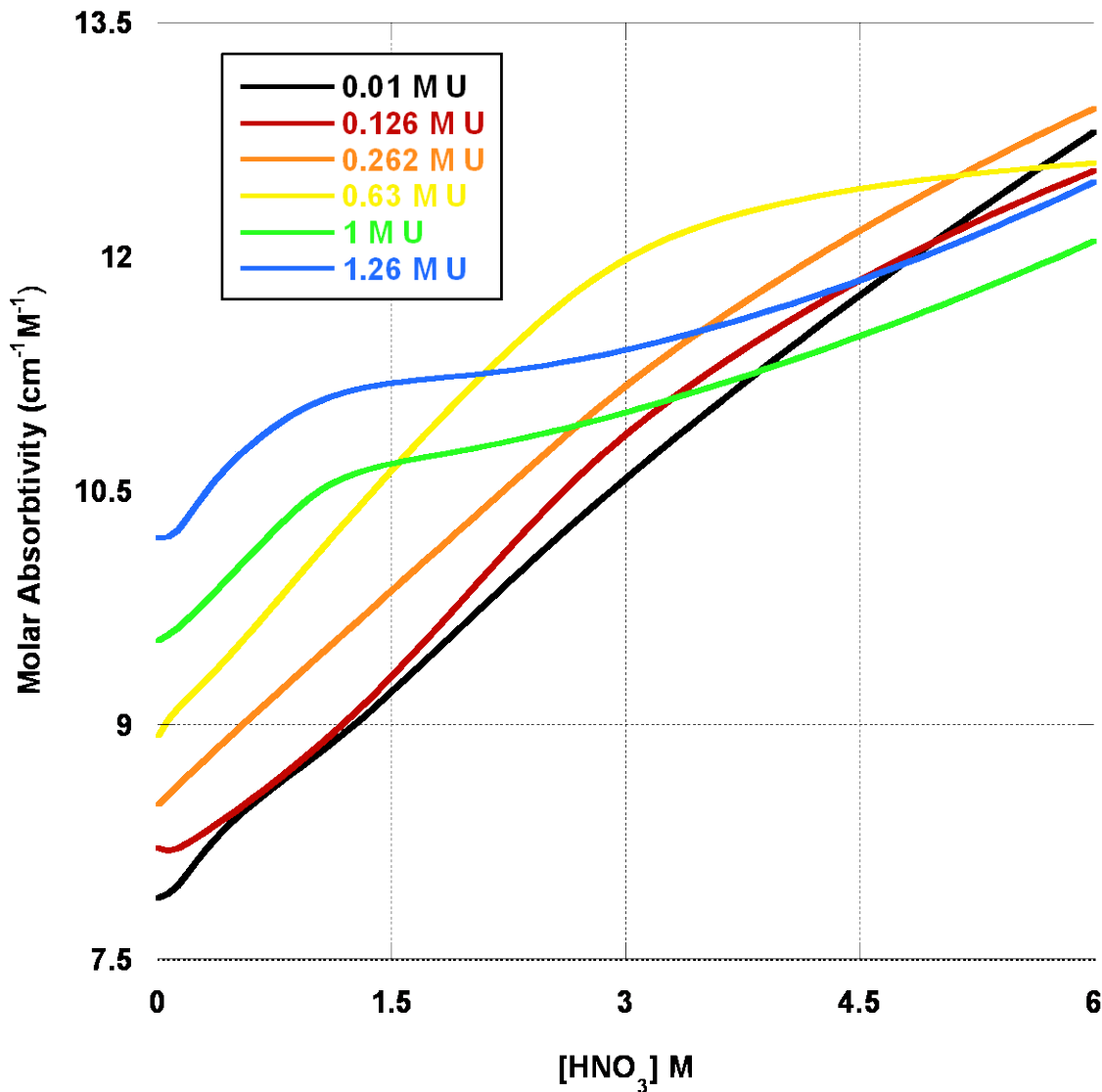


**Figure 32:** Molar absorptivities at 414 nm for uranyl in varied nitric acid solutions

#### 4.4 Experimental Implementation of UV-Visible Process Monitor

A bench of 3 V-02 contactors is seen in Figure 33, and was used to perform a UREX demonstration with U, Nd, Fe and Zr metals in concentrations 1/5<sup>th</sup> of expected actual UREX process conditions (Table 9).



**Figure 33:** Bench of 3 V-02 contactors at UNLV

Four different aqueous feeds were used, the first being a 1 M HNO<sub>3</sub> startup solution with no metals, the second was meant to simulate an actual UREX feed at 1 M HNO<sub>3</sub> and 0.1 M AHA. The third aqueous feed did not contain AHA but was kept at 1 M HNO<sub>3</sub>, and the fourth feed contained 4 M HNO<sub>3</sub> (Table 10).

**Table 9:** Metal concentration in UREX aqueous feeds

Metal	Concentration (M)
U	0.252
Nd	0.0026
Fe	0.00022
Zr	0.0002

**Table 10: Summary of UREX aqueous feed variables**

Aqueous Solution	[HNO <sub>3</sub> ]	[AHA]
Cold startup	1 M	0 M
Aqueous feed #2	1 M	0.1 M
Aqueous feed #3	1 M	0 M
Aqueous feed #4	4 M	0 M

The purpose here was to simulate a change from a UREX to PUREX feed. Two liters of each aqueous solution was prepared, and the aqueous flowrate was approximately 300 milliliters/minute with an organic flowrate of 600 milliliters/minute. After the cold startup solution was pumped through the contactors and began to exit the aqueous product port, the organic phase pump was started. Once solvent was seen exiting the organic phase outlet port, the pumps were temporarily suspended and aqueous feed was switched to Aqueous feed #2. This feed lasted approximately 7 minutes, at which point the pumps were suspended again and the feed was switched to Aqueous feed #3. Again, after approximately 7 minutes, the pumps were suspended and aqueous inlet was switched to Aqueous feed #4. Grab samples were collected from the aqueous and organic outlets every minute by opening a valve installed at the bottom of the outlet tubing.

The UV-Visible spectra of the 403, 414 and 427 uranyl peaks are shown in Figure 34, plotted every minute for the duration of the 39 minute test. Deviation in metal concentration in aqueous product are immediately detectable, however the flowrates were adjusted at several points throughout the test for various reasons. Thus, raw changes in absorbance values are not simply attributed to the change in aqueous feeds.

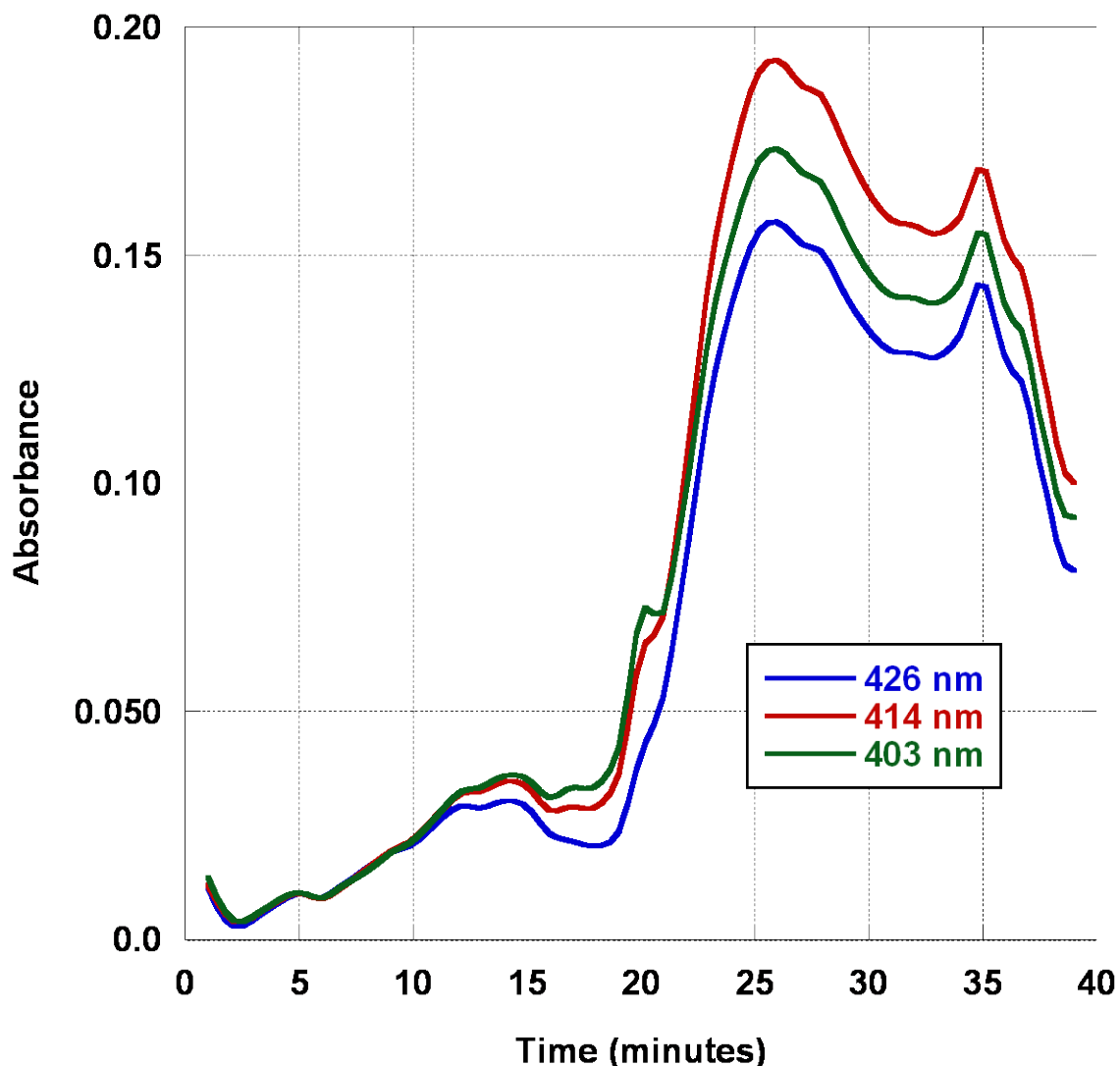


**Figure 34:** UV-Visible absorbance of uranyl peaks over time under UREX process conditions

ICP-AES results for the same 1 minute grab samples are plotted to confirm metal concentration changes as seen by the UV-Visible spectrophotometer (Figure 35). The ICP-AES detection of U metal concentration over time does correlate well with the UV-Visible absorbance measurements. Essentially, the ICP-AES measurements confirm the movement of metals from the aqueous feed solution to the organic phase in the extraction portion of the experiment (0-17 minutes) and the back-extraction of metals from the organic to the aqueous phase in the strip portion of the experiment (17-37 minutes).

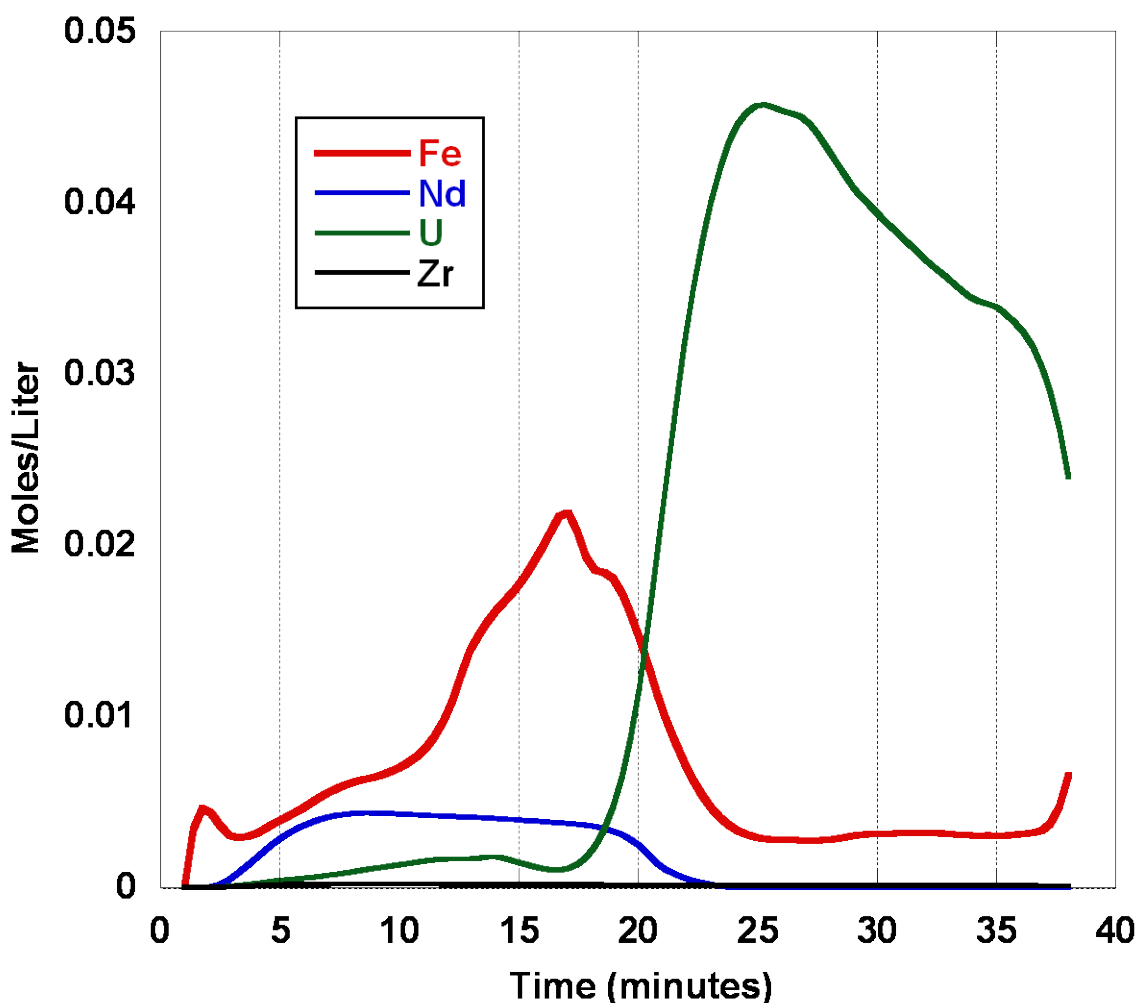


**Figure 35:** ICP-AES measured metal concentrations over time in the aqueous product of a UREX extraction (0-17 minutes) and strip (17-37 minutes)

The non-steady-state behavior of the U and Fe indicate that the total amount of metal was either not fully extracted or not fully stripped, respectively, and in either case process equilibrium was not achieved. Peak to peak ratio measurements help elucidate what peak absorbance changes can be attributed to change in nitric acid concentration (Figure 36).

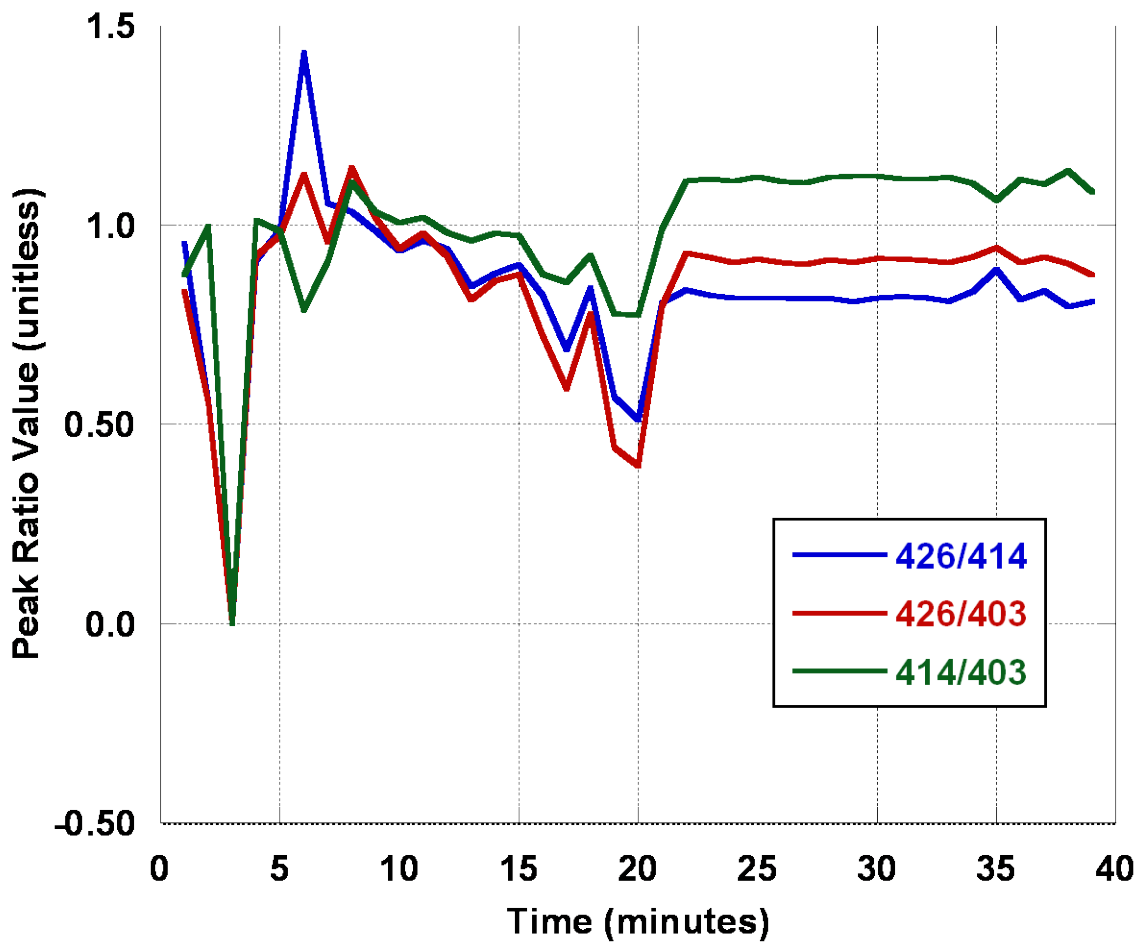


**Figure 36:** Peak ratios over time in UREX extraction and strip



**Figure 37:** Foaming in organic interstage tubing

As in the TRUEX test (Chapter 5), organic phase foaming began within minutes of two phase flow and continued throughout the duration of the test (Figure 37). No foaming was observed in the aqueous interstage tubing however, and carryover of organic into aqueous was minimal (Figure 38). A small amount of aqueous carryover was observed at the bottom of the solvent outlet tank, on the order of 250 milliliters.

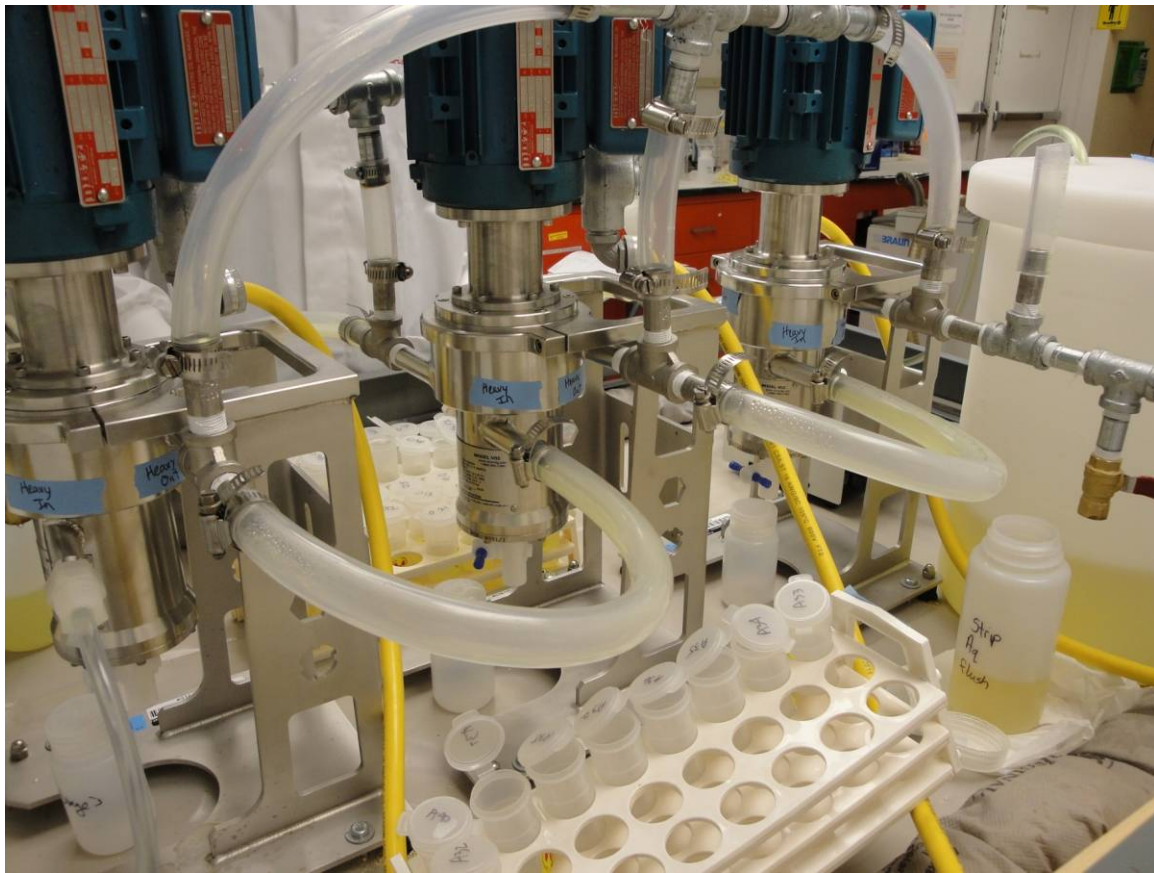


**Figure 38:** No foaming in aqueous interstage tubing

#### 4.5 Conclusions

UV-Visible spectroscopy can be used effectively to discriminate changes in uranyl and nitric acid concentrations in the 0.01 – 1.26 M U and 0.01 – 8 M nitric acid system. Alterations of the characteristic uranyl UV-Visible spectral shape at high nitric acid suggest significant speciation changes, and peak shifts in the high uranyl system similarly imply an ingrowth of uranyl nitrate species not present at lower uranyl concentrations. The presence of the differing uranyl nitrate species is expected to substantially affect the UV-Visible absorption spectra, therefore by coupling with additional spectroscopic studies, UV-Visible spectral variations can be attributed directly to specific speciation

changes. Additionally, uranyl-uranyl coordination may be the basis of the UV-Visible spectral shifts seen at high U concentrations [93, 141, 142]. By defining uranyl and nitrate parameters for the various uranyl nitrate species, a continuous model for the UV-Visible spectra can be developed and used in a process monitoring application. A milestone for this work is a successful demonstration of the UV-Visible spectroscopy process monitoring concept in centrifugal contactors under solvent extraction conditions. On the whole, the continuation of these efforts will enable an online materials accountability system as well as provide an attribution methodology for identifying diversion scenarios.

Future work should include the incorporation of other actinides such as Pu, lanthanides and fission products into the simulated used fuel aqueous feed for UREX type studies. Following successful benchtop scale studies, experiments can be scaled up to the metal concentrations expected in process. Collaborations with the national laboratories should prove to be extremely useful for troubleshooting issues with centrifugal countercurrent contactors, and utilizing codes such as AMUSE to provide models for future flowsheet demonstrations. Modeling that incorporates information such as aqueous feed composition and number of contactors can output expected separation factors for metals, and aid in rotor speed and flow rate settings for optimum flowsheet behavior. This prediction of aqueous products and raffinates will allow more accurate correlation between UV-Visible spectroscopic online monitor results and specific process changes or upsets.

## CHAPTER 5

### TRUEX EXPERIMENTS

In order to effectively monitor a given solvent extraction process, both the flowsheet and the related system instrumentation must be well understood and characterized. This chapter provides detailed information on the setup and testing of a centrifugal countercurrent contactor system and TRUEX process demonstration. Important factors for pilot plant and flowsheet development are identified and discussed. The effect of physical parameters such as holdup volume and solution temperature are relevant both to flowsheet design and resulting performance, thus their study allows for the optimization of both physical setup and chemical compositions in processes. Previous works on flowsheets and centrifugal contactors have seen unexpected results or identified areas for further research, so another goal of this research is to build upon previous relevant studies and elucidate discrepancies. Demonstrations such as the one presented in this chapter are the link between benchtop scale laboratory work and industrial scale commercial operation. This chapter provides the connection between other benchtop studies presented in this dissertation and the applicability to industry. The work discussed here is also used as a basis for the construction of the contactor bank at UNLV (CHAPTER 4) as well as for identifying potential areas for safeguards in the TRUEX solvent extraction flowsheet.

Official Use Only is a classification given to information that has the potential to damage governmental, commercial, or private interests [155]. Applied Technology is a category given to material in order to preserve the foreign trade value of certain engineering, development, design, construction, and operational information [156]. In

flowsheet testing, design parameters such as number of stages for each process section, flowrates, organic to aqueous ratio and specific solution compositions are often characterized as Official Use Only (OUO) or Applied Technology (AT). Therefore, certain portions of information relevant to the research presented in this chapter will not be included as they fall under the OUO or AT designation. Generally, results can be presented if the OUO/AT portion of information is not provided, i.e. the TRUEX flowsheet can be shown as long as the specific flowrates and concentrations of feed solutions that fall under OUO/AT are not given.

## 5.1 Introduction

A pilot plant of 30 annular centrifugal 5 cm CINC V-02 contactors has been constructed to evaluate various solvent extraction flowsheet applications [157]. In this work, a TRUEX flowsheet was tested, and both the solvent extraction and contactor performances were evaluated. Relevant collected data include contactor holdup volumes, hydraulic performance, temperature profiles, real-time single-stage sampling and metal distribution values at various locations during transient and at steady-state process conditions.

The goal of TRUEX is to recover and purify the actinides and lanthanides from fission products and to prepare a solution for the next separation process (TALSPEAK) which will separate the actinides from the lanthanides [158, 159]. Previous TRUEX tests utilized oxalic acid to complex Zr and found that the complexation was incomplete, resulting in the presence of Zr in most of the process streams including the organic phase. The resulting organic phase Zr would be fed to the subsequent TALSPEAK in a full UREX + scheme. Additionally, it was found that significant amounts of the hydrolizable

elements in the process precipitated and redissolved at various points during UREX, TRUEX and TALSPEAK testing [160, 161]. Process monitoring is based on the concept that a materials accountability and control system can be utilized to detect excursions from steady-state or expected conditions. Discrepancies between expected flowsheet results and actual performance mean that these steady-state or expected conditions are not fully known, therefore any process monitoring system has no control or base case for a benchmark.

Previous testing of the 30 stage pilot plant included temperature profile measurements recorded across the cascade using both single-phase and two-phase flow regimes [158, 162]. Previous pilot scale centrifugal contactor studies have been limited to single-stage performance measurements [163-166]. Most flowsheet tests performed with actual spent fuel feed solutions are limited to 1 or 2 cm mini-contactors, yielding fairly low reported stage efficiencies due to flow inconsistencies related to their small size [158]. In addition, stage-wise sampling at low flows can upset process equilibrium so it is avoided in mini-contactors. This means that single stage distribution values cannot be analyzed, leading to an over-estimation of the number of stages required for a particular flowsheet. In attempts to optimize the flowsheet, one effort is to utilize the minimum necessary number of contactor stages for the mass transfer efficiencies required, as this reduces size and cost of the plant as well as volumes of solution for testing. Cold pilot scale testing provides design data for steady-state operating parameters and stage-wise efficiency for flowsheets, allowing for the testing of proposed flowsheets and validation of modeling data from codes such as AMUSE [157]. Again, these studies provide information needed to enhance solvent extraction flowsheet understanding and performance. This

understanding is fundamental to the concept of process monitoring and materials control, as a process monitor cannot provide useful information on confirmation of flowsheet chemistry or materials accountability if the steady-state behavior of the method under investigation is unknown.

### 5.1.1 Equipment

The mechanical equipment making up the pilot plant includes thirty CINC V-02 centrifugal contactors with frequency drives, five liquid supply pumps, four process solution heaters with controllers, multiple thermocouples, and assorted fluid flow components (Figure 39). All of this is mounted on a stainless steel support structure and is located within a spill containment system. Inlet/outlet interconnective tubing for this evaluation was 5/8 inch I.D. chemically compatible Tygon tubing. Feed and product tanks are located directly below the contactor cascade, still within the spill containment system.

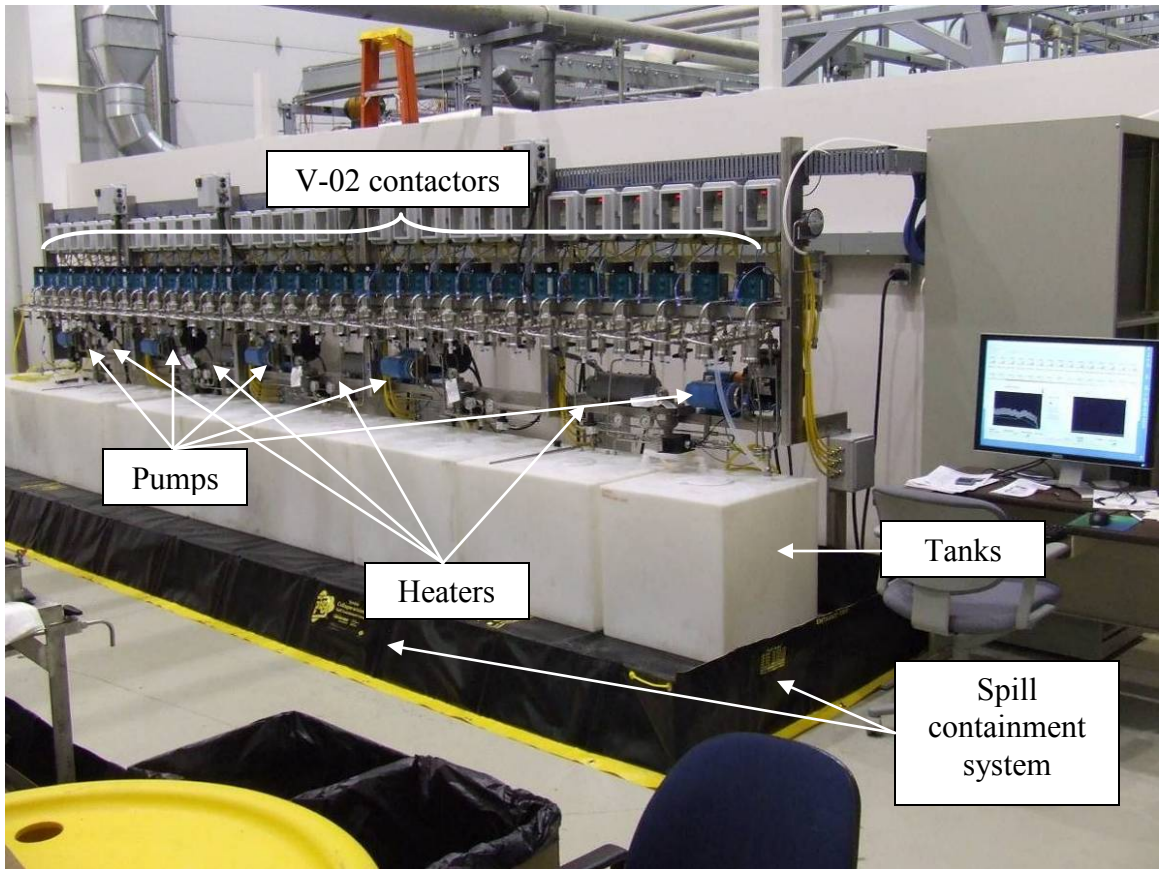


**Figure 39:** Thirty stage centrifugal contactor pilot plant

Each contactor has a 5 cm diameter rotor and a light/heavy phase weir package attached to a shaft and bearing assembly connected to the motor. The V-02 contactors have an operating range of 0.1 to 2.0 liters/min and have a variable rotor speed ranging from 0 to 6000 rpm. The fan-cooled 1/3 horsepower motors are explosion-proof rated and operate on 208 volt three-phase power. The pilot plant has automated process control capabilities coupled with a data acquisition system which allow LabVIEW command of contactor startup and shutdown, rotor speeds, pump flow rates, heater control and real-time feedback from thermocouples and flowmeters (Figure 39). Additional information specific to the pumps, flowmeters, signal processing, back

pressure valves, heaters, in-line filters, thermocouples, fittings, off-gas vents, process control and data acquisition systems is available elsewhere [157].

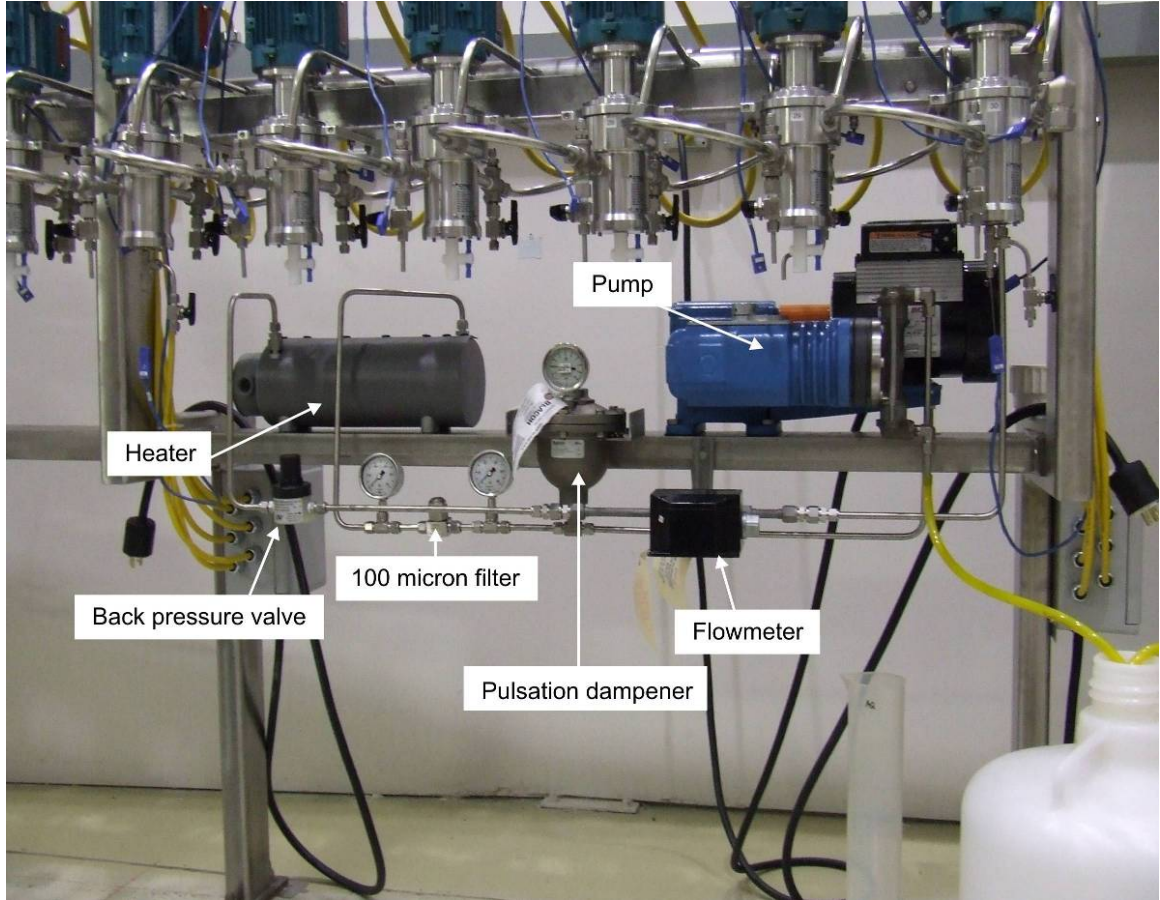


**Figure 40:** Typical fluid feed system with components

## 5.2 Experimental Techniques and Setup

### 5.2.1 TRUEX Flowsheet

The flowsheet tested was a slightly modified version of a previously tested TRUEX flowsheet [160]. The finalized flowsheet contained organic (light) and aqueous (heavy) phases that flowed in a counter-current fashion, employed all 30 stages in the pilot plant,

and included extraction, scrub, strip, solvent wash and solvent reacidification sections (Figure 41). It should be noted that all solution inlets are often termed “Feed” and outlets are “Product” or “Raffinate.” Generally the Extraction section aqueous outlet is the flowsheet “Raffinate” and the Strip section aqueous outlet is the flowsheet “Product.” Specific stage numbers and flow rates for the aqueous and organic solutions are Applied Technology, so will not be included in this document.

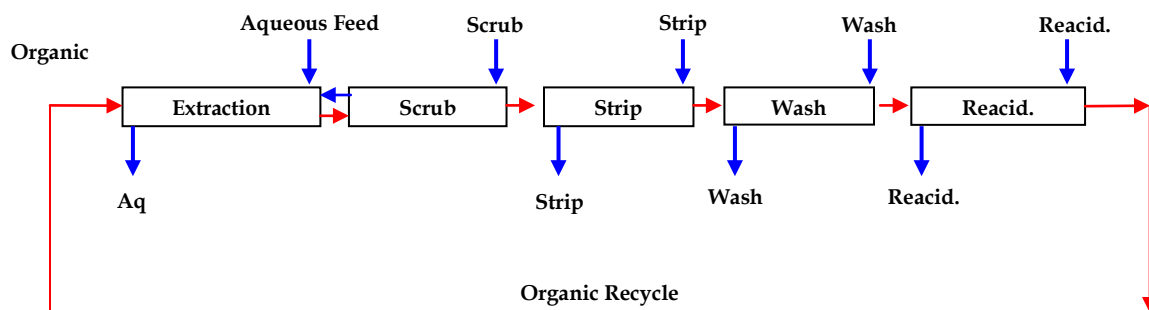


**Figure 41:** Contactor pilot plant flowsheet diagram

The TRUEX solvent used for this test consisted of 0.2 M CMPO (octyl (phenyl)-N,N-diisobutylcarbamoyl-methylphosphine oxide) in 1.4 M TBP (tri-butyl phosphate) in n-dodecane hydrocarbon diluent. All chemicals were reagent grade and used as received, with information on their acquisition from vendors available elsewhere [157]. In a previous experiment, the TRUEX solvent had been washed with sodium carbonate and reacidified with dilute nitric acid, with the solvent composition and purity confirmed using an  $^{241}\text{Am}$  purity test [167]. The starting solvent volume for testing was 10 liters. Based upon previous tests, the aqueous feed solution used was a  $\sim 4.4$  M nitric acid solution adjusted with  $\sim 0.07$  M oxalic acid to complex the Zr thus minimizing extraction

[161]. The target and actual concentrations of the lanthanides and fission product surrogates in the aqueous feed are listed in Table 11.

**Table 11:** Aqueous feed target and actual compositions

Component	Target Concentration (M)	Actual Concentration (M)	Parent chemical
Oxalate	0.07	0.07	Oxalic acid
H <sup>+</sup>	4.2	4.4	Nitric acid
La <sup>-3</sup>	0.0011	0.0012	La(NO <sub>3</sub> ) <sub>3</sub> · 6H <sub>2</sub> O
Ce <sup>-3</sup>	0.0024	0.0025	Ce(NO <sub>3</sub> ) <sub>3</sub> · 6H <sub>2</sub> O
Nd <sup>-3</sup>	0.0033	0.0035	Nd(NO <sub>3</sub> ) <sub>3</sub> · 6H <sub>2</sub> O
Eu <sup>-3</sup>	0.0002	0.0002	Eu(NO <sub>3</sub> ) <sub>3</sub> · 5H <sub>2</sub> O
Cs <sup>-1</sup>	0.0017	0.0017	CsNO <sub>3</sub>
Sr <sup>-2</sup>	0.0057	0.0059	Sr(NO <sub>3</sub> ) <sub>2</sub>
Zr <sup>-2</sup>	0.0023	0.0024	ZrO(NO <sub>3</sub> ) <sub>2</sub>

A nitric acid scrub solution was used to mimic the previous TRUEX test studies [160]. A TRUEX flowsheet test [159, 168-172] consisted of three scrub sections which included oxalic acid for Zr complexation followed by a more concentrated nitric acid for removal of residual oxalic acid then a final dilute nitric acid to reduce acid concentration prior to the solvent entering the strip section. By addition of the oxalic acid directly to the aqueous feed, only a single scrub solution consisting of 1.4 M nitric acid was incorporated.

The loaded solvent was stripped with a buffered diethylenetriaminepentaacetic acid/lactic acid solution that was pH adjusted. A dilute sodium carbonate wash and dilute nitric acid reacidification were used to prepare the solvent for recycle, after which it was reintroduced into the extraction section of the pilot plant.

### **5.2.2 Demonstration and Data Collection**

Prior to the actual demonstration, all pumps were calibrated and low-mix sleeves were installed on the raffinate and strip aqueous phase outlets and the wash and reacidification organic phase outlets. Low-mix sleeves restrict solution flow to the rotor portion of the contactor, therefore they are employed to increase phase disengagement and decrease carryover (aqueous phase in organic phase and vice versa) [173]. The contactor rotors were started at 3750 rpm initially, with the exception of the low-mix sleeve contactors which were started at 4000 rpm, as previous hydraulic tests suggested rotor speeds in the range of 3500-4000 rpm assisted with smooth interstage flow profiles [153, 163].

For startup, aqueous feed solutions were pumped to their input stages and allowed to flow through their entire section prior to starting the solvent flow. All aqueous solutions used for initial startup had the same makeup as the actual experimental test solutions, with the exception of the aqueous extraction feed which was a blank (no metals) nitric acid solution representative of the actual experimental extraction feed. Organic phase foaming was observed almost immediately after solvent flow was introduced, at which point all rotor speeds were reduced to 3500 rpm. The foaming persisted so the rotor speeds were further reduced to 3350 rpm and finally 3000 rpm for the remainder of the testing. Foam was seen in the interstage tubing throughout the pilot plant (Figure 42). Time zero of the demonstration occurred when the solvent flow first exited the cascade, approximately 15 minutes from the start of organic flow, at which point the blank aqueous feed solution was switched to the actual aqueous feed solution with metals.

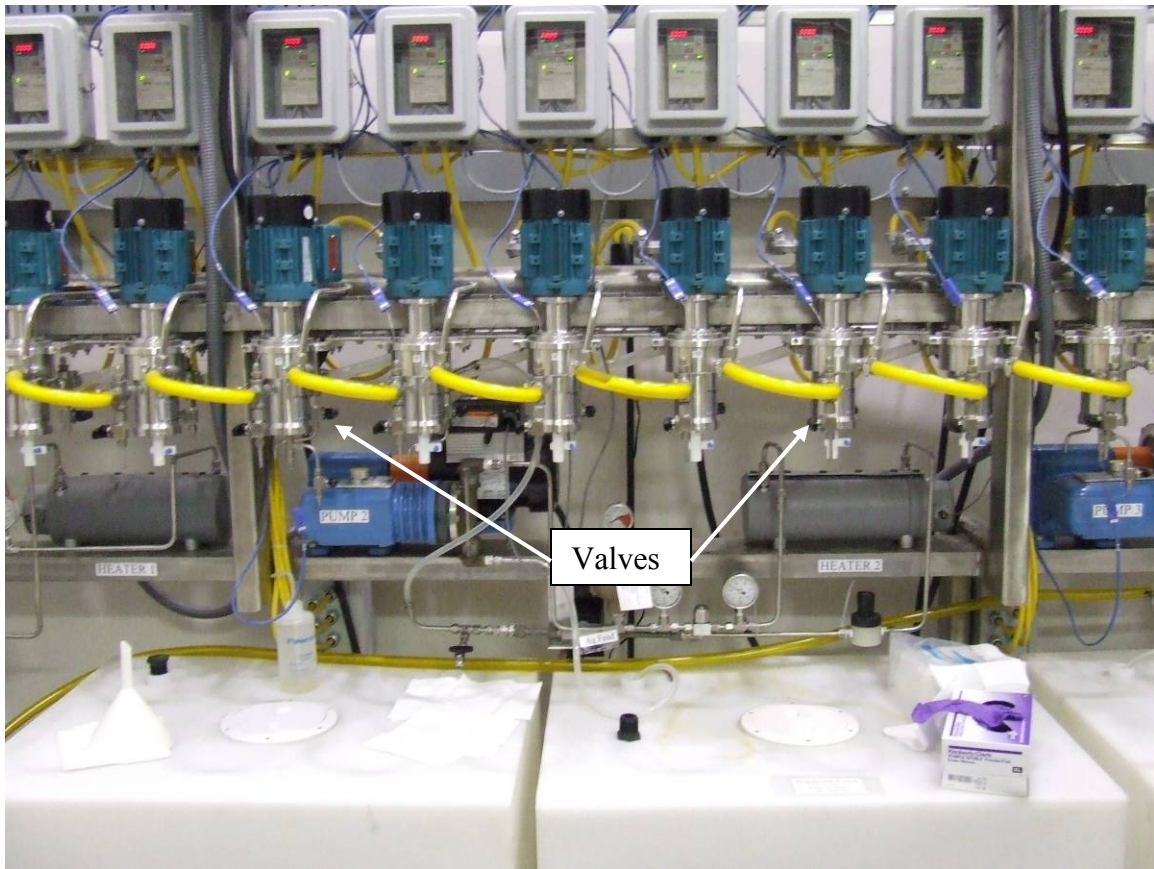


**Figure 42:** Foaming evident in interstage tubing throughout pilot plant

As a result of the continuous foaming and resulting organic carryover into the aqueous phase, it became evident that the total solvent volume being recycled was decreasing noticeably as seen in the solvent tank. Therefore, an additional 2.5 liters of fresh solvent was added to the recycle tank. This introduced some uncertainty in solvent turnover rates as calculated for steady-state conditions, therefore steady-state samples were taken 40 minutes later than originally planned to ensure the system had reached steady-state. Generally, five solvent turnovers are the estimation for when a solvent extraction process with recycled organic reaches steady-state [174].

In order to assess the performance of the specific flowsheet and the physical setup of the contactor pilot plant, over 200 samples were taken throughout the process demonstration (Table 12). Valves installed at the contactor aqueous and organic inlet/outlet ports allowed for sampling of individual stages, and valves on the solvent recycle, aqueous product and raffinate streams provided for their sampling. Selected stages were sampled very early in the test during the transient phase to support kinetic modeling efforts to determine approach to steady-state. Following that, samples were taken from each aqueous product stream every 20 minutes and an entire profile was taken at 140 minutes, meaning samples from every stage from both phases. This was to evaluate steady-state conditions and calculate individual stage efficiencies.

**Table 12:** TRUEX demonstration sample plan summary

Section	Phase	Time (min)
Extraction	Aq Product	20, 40, 60, 80, 100, 120, 140, 160
Extraction	Both	2, 3, 4, 5, 7
Extraction	Feed Inlet	1, 2, 3
Scrub	Both	2, 3, 4, 5, 7
Strip	Both	2, 3, 4, 5, 7, 20, 40, 60, 80, 100, 120, 140, 160
Wash	Aq	20, 40, 60, 80, 100, 120, 140, 160
Reacid.	Both	20, 40, 60, 80, 100, 120, 140, 160
All	Both	140, 180
All Feed Tanks		0
All Product Tanks		180

Logistically, sampling was achieved by first clearing the valves (see black knobs on either side of contactor housings in Figure 42) of any stagnant solution purging into waste container, then collecting a 10-15 milliliter sample of flowing process solution by opening the valve for approximately 2-3 seconds. The expectation is that this sample volume will not upset the process during transient, steady-state or shut down operation. This is true if the proper volumes and organic to aqueous ratios in the contactor setup are

maintained during sampling as to not affect extraction, scrub or strip efficiencies. The steady-state samples obtained at 140 minutes were recontacted at process temperatures for several hours, separated and analyzed. A total of 176 samples were collected and analyzed for metal concentrations via Inductively Coupled Plasma-Mass Spectrometry (ICP-MS). The flowsheet testing lasted for a total of 172 minutes of continuous two phase flow. To conclude the test, all solution feed pumps and contactor rotors were shutdown simultaneously. Solutions were collected from each contactor drain and archived.

### 5.3 Results and Discussion

The flowsheet test lasted for a total of 172 minutes and generally operated as expected, with the exception of the organic foaming in light phase interstage tubing throughout the test. With the addition of the extra 2.5 liters of fresh solvent, the solvent experienced an estimated 6-8 turnovers, where turnover time is calculated by estimating the phase holdup volume (liters) of the contactor vessels and interstage tubing, and dividing by the flowrate of the phase (liters per time). The addition of fresh solvent did not impact solvent flow between stages and foaming was not observed in the heavy phase interstage tubing.

Samples taken during testing showed that solvent carryover into the aqueous phase was occurring, likely due to the foaming (approx. 2% in aqueous raffinate, 0.8% in the strip product and 0.02% in the reacidification product). This was estimated by placing select samples in a volumetric flask and observing phase carryover. Organic phase carryover into the carbonate wash and reacidification effluent as well as aqueous phase carryover in the solvent was not measurable. As discussed previously, the use of low-

mix sleeves is intended to increase phase separation and thus decrease phase carryover. However, the low-mix sleeves at the raffinate outlet and strip product outlet did prevent the carryover of solvent in aqueous phase as it was caused by the foam forming in the lower collection ring of the affected stages.

### 5.3.1 Steady-State Determination

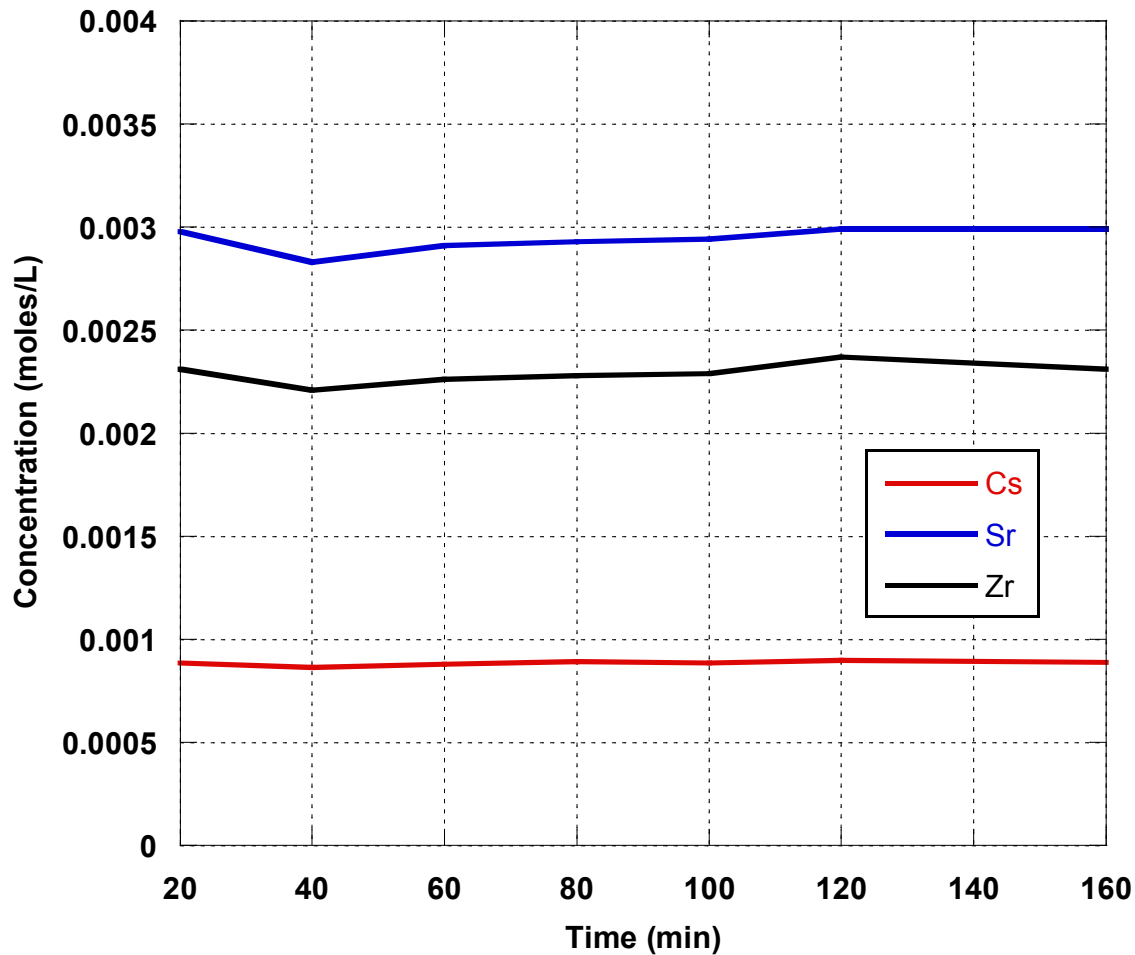
Metal concentrations in all samples were analyzed with ICP-MS, detection limits given in Table 13. Figure 43 and Figure 44 display the approach to steady-state plotted data for the metal concentrations in raffinate outlet and strip product outlet, respectively.

**Table 13:** Detection limits for ICP-MS metals analysis

<b>Isotope</b>	<b>Detection Limit (Mol/Liter)</b>
<sup>140</sup> Ce	2.51E-09
<sup>133</sup> Cs	1.93E-10
<sup>151</sup> Eu	1.46E-09
<sup>153</sup> Eu	1.22E-09
<sup>139</sup> La	1.65E-09
<sup>143</sup> Nd	3.47E-09
<sup>145</sup> Nd	3.08E-09
<sup>146</sup> Nd	3.40E-09
<sup>88</sup> Sr	4.58E-10
<sup>90</sup> Zr	1.19E-07
<sup>91</sup> Zr	1.15E-07

The steady-state plots shown in Figure 43 indicate that Cs, Sr and Zr reach steady-state conditions within 20 minutes. The lanthanides were not included in this graph due to sample results at or below detection limits indicating they were effectively extracted by the TRUEX solvent. The samples taken during the transient startup period of the test indicated that the extraction section was nearly at steady-state conditions after 7 minutes

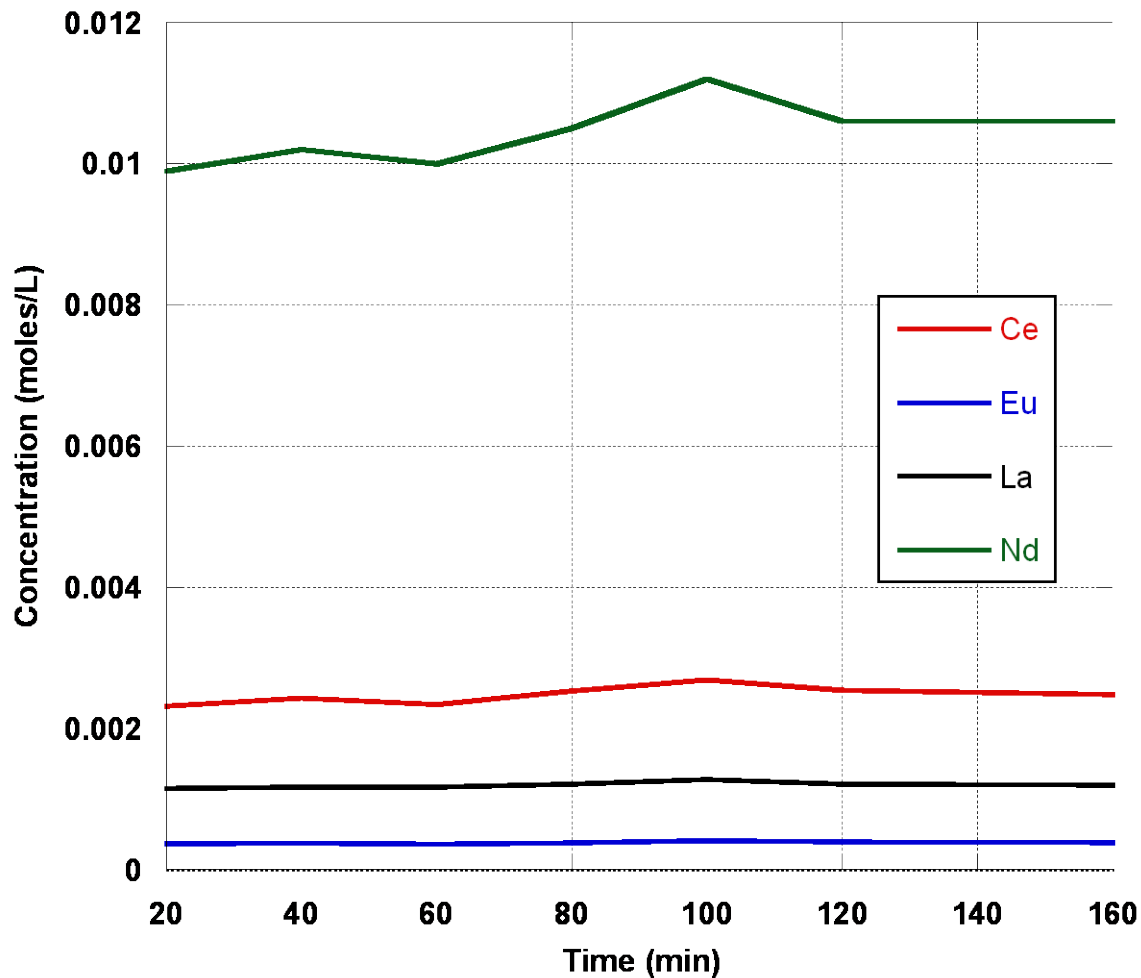
of runtime. The estimation of steady-state can be given when metal concentration variance over time is less than 10% [174].



**Figure 43:** Steady-state plots for raffinate outlet

The plots of the strip product lanthanide concentrations in Figure 44 show sample results under steady-state conditions. The noticeable increase in Ce and Nd concentrations after 60 minutes may be attributed to the increase in system temperatures as shown in the strip section temperature profiles found in Figure 47 or possible

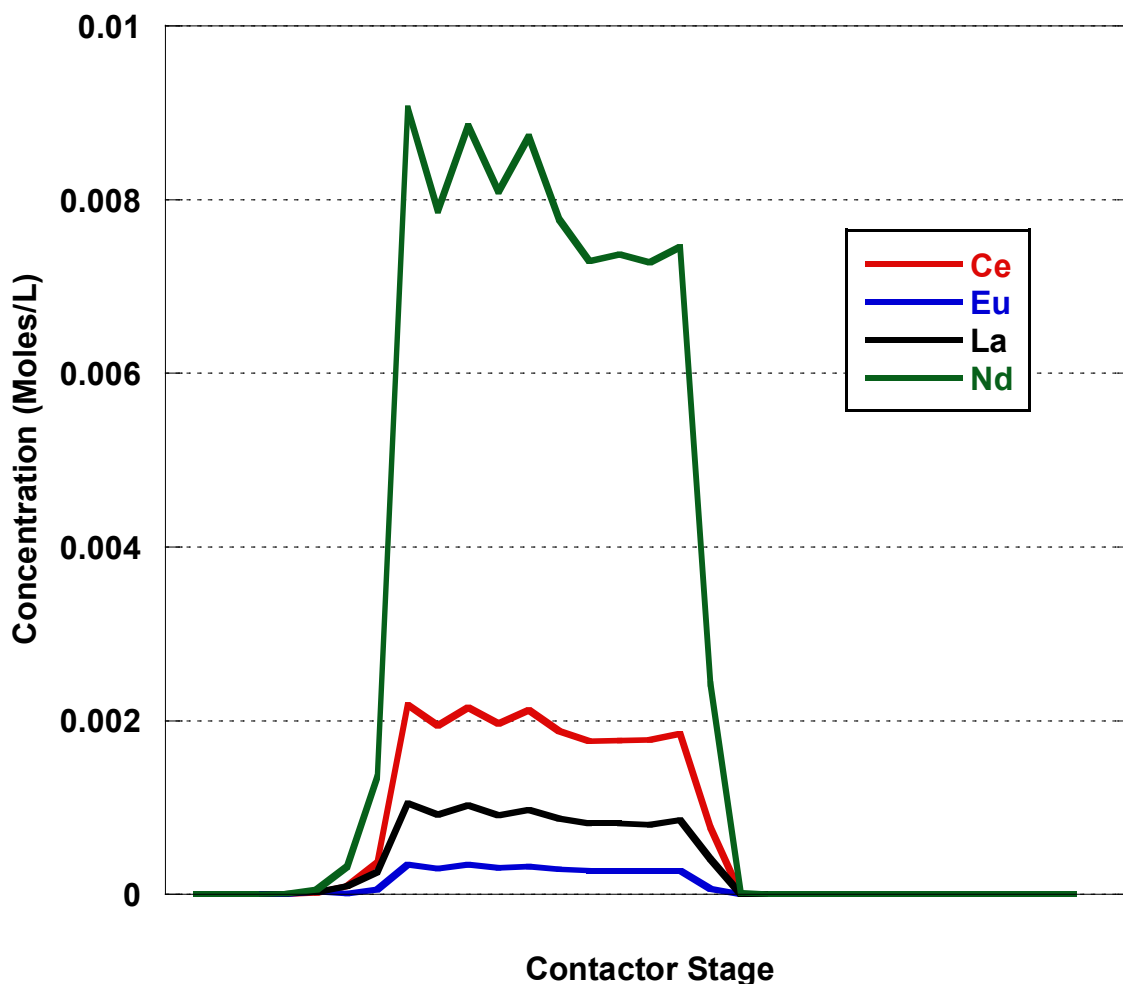
analytical error. Stripping efficiency increases with increasing temperature with the TRUEX strip solution.



**Figure 44:** Approach to steady-state at strip product outlet

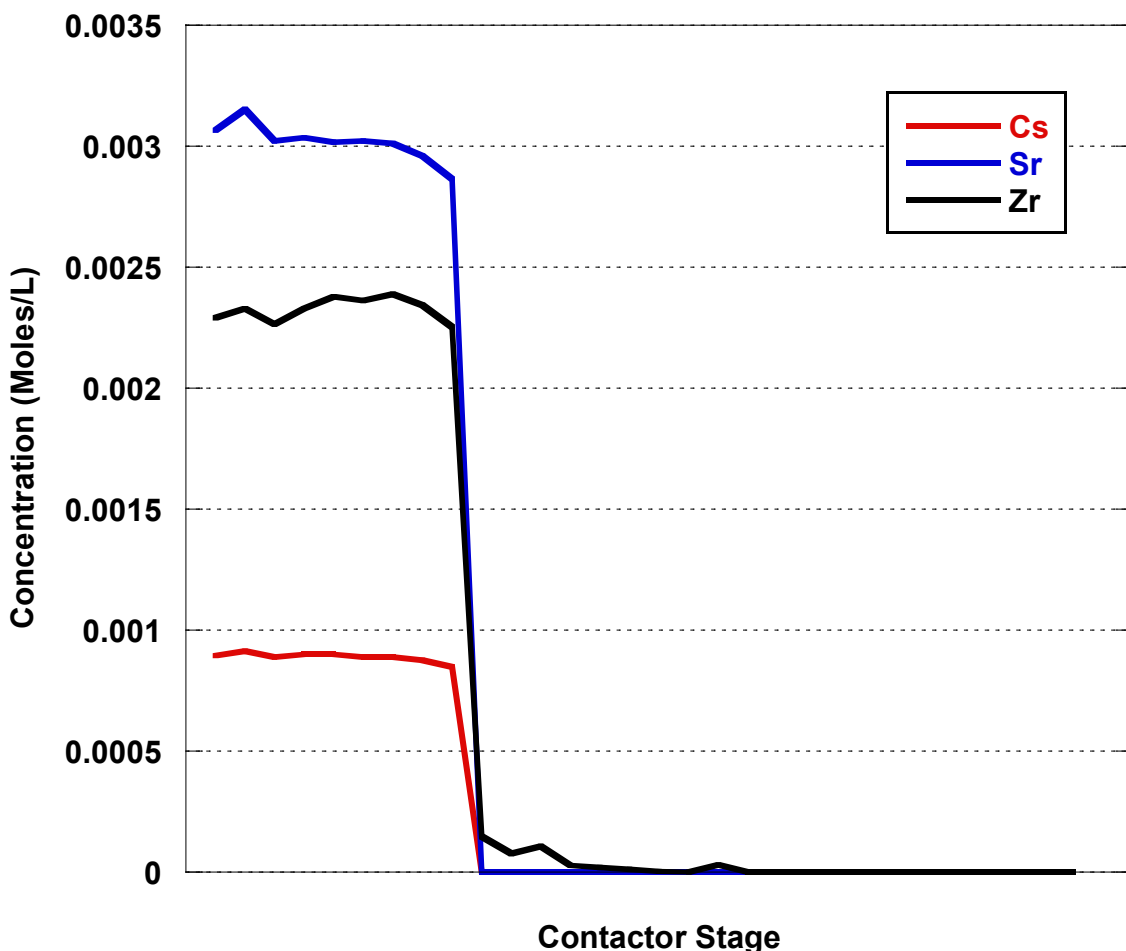
Concentration profile plots shown in Figure 45 for Ce, Nd, Eu and La indicate the lanthanides were efficiently extracted and stripped with the number of stages used for this flowsheet evaluation. The contactor stage numbers cannot be presented in Figure 45 or Figure 46 as they are OOU, however the presence of metals in the organic phase shown in the middle section of the plot correspond to the scrub portion of the flowsheet. From

Figure 41, it follows that the extraction section precedes the scrub, and the strip section follows the scrub. The data in Figure 45 suggest that fewer extraction and strip stages would have been adequate to achieve desired removal efficiencies as the maximum loading of the organic is seen in the first few scrub stages – immediately after solvent loading in the extraction section. In addition, the organic phase concentration drops off immediately in the strip section, indicating that the first few stages are sufficient to strip the loaded lanthanides from the solvent.



**Figure 45:** Lanthanide concentration profile across the cascade in organic phase at steady-state

Figure 46 shows the concentration profile for Cs, Sr and Zr using aqueous phase sample results only and indicate the TRUEX solvent did not extract significant quantities of these metals (fission products). The Zr data indicated it was present in the aqueous phase of the scrub section in the flowsheet. This would suggest a small fraction of Zr may have been extracted by the solvent; however, this fraction was scrubbed by the scrub solution.



**Figure 46:** Concentration profiles for fission products across the cascade in aqueous phase at steady-state

### 5.3.2 Removal Efficiencies

Sample results taken from both phases for the full cascade profile were used to calculate the percentage of metals found in respective effluent streams and the removal efficiencies ( $R_{Eff}$ ) for those metals [157]. Table 14 shows the calculated results. The percentages of metals found in the raffinate and strip product (both aqueous outlets) were calculated using Equation 4.

$$\%Metals_{Aq\ outlet} = 100\% \times \frac{(Concentration \times Flowrate)_{Aq\ outlet}}{(Concentration \times Flowrate)_{Feed}} \quad \text{Equation 4}$$

The metal removal efficiency results were calculated using Equation 5, where for the lanthanides the numerator is calculated for the raffinate (extraction aqueous outlet) and for the fission products the numerator is calculated for the strip product.

$$REff_{Metal} = 100\% \times \left[ 1 - \frac{(Concentration \times Flowrate)_{Aq\ outlet}}{(Concentration \times Flowrate)_{Feed}} \right] \quad \text{Equation 5}$$

**Table 14:** Percentage of metals in effluent streams just prior to shutdown and calculated removal efficiencies.

Effluent stream	Ce	Eu	La	Nd	Cs	Sr	Zr
Raffinate	< 0.002	< 0.014	< 0.007	< 0.002	>100	98.1	95.5
Strip Product	90.0	91.2	91.5	92.7	< 0.001	< 0.001	0.6
R Eff	> 99.9	> 99.9	> 99.9	> 99.9	100.	100.	99.4

The calculated quantity of lanthanides in the strip product indicated nearly a 10 % loss, however there was no detected lanthanide concentration in the raffinate or in the

organic leaving the strip section. The 10 % material loss is likely due to a combination of flowrate inaccuracies associated with the data acquisition system in conjunction with flowmeter measurement and analytical error due to matrix interferences. All pump flowrate calibrations were performed at ambient laboratory temperature, and flowmeters were designed for measuring water at 20° C. Thus, considerable flowmeter error is expected for measurement of organic phase at elevated temperatures. The Cs and Sr were not extracted and thus ended up in the raffinate. Removal efficiencies indicated very good performance of the tested TRUEX flowsheet with > 99.9% extraction of the lanthanides without extraction of the Cs and Sr and with minimum Zr extraction (0.6%). Overall, these results indicated the flowsheet performed well and is suitable for lanthanide extraction, however future work may include the investigation of a slightly higher concentration of oxalate to fully suppress Zr extraction. While it is possible that some small amount of Zr in the organic phase may not adversely affect the solvent extraction flowsheet, efforts to keep Zr out of the organic phase will continue as part of flowsheet optimization studies [157].

### 5.3.3 Mass Transfer Stage Efficiency

Individual stage efficiency calculations were made to further evaluate the overall performance of the TRUEX flowsheet in the contactor pilot plant. The re-equilibration samples were prepared by heating the original steady-state samples to test temperatures recorded at 140 minutes, then contacting appropriate volumes to match organic to aqueous ratios utilized in the appropriate section of the flowsheet. Analyzed metal concentrations from aqueous and solvent phase steady-state samples and the re-equilibrated steady-state samples were used to calculate stage efficiencies. The mass

transfer stage efficiencies for selected extraction and strip stages were calculated using Equation 6 [157].

$$\eta = 100\% \times \frac{(X - X_{in})}{(X_{eq} - X_{in})} \quad \text{Equation 6}$$

In this case,  $X$  is the metal concentration of the effluent,  $X_{in}$  is the inlet metal concentration, and  $X_{eq}$  is the metal concentration of the effluent following re-equilibration, where inlet is the stage inlet and effluent is the stage outlet. Lanthanide stage efficiency results for select stages in the extraction section and in the strip section are included in Table 15.

**Table 15:** Individual stage efficiencies for selected stages.

Stage #	Ce (%)	Eu (%)	La (%)	Nd (%)
Ext <sub>1</sub>	88.9	93.6	93.3	92.0
Ext <sub>2</sub>	93.3	91.8	94.5	93.5
Ext <sub>3</sub>	61.4	88.5	29.4	89.2
Ext <sub>4</sub>	~100 <sup>1</sup>	85.1	92.5	88.3
Ext <sub>5</sub>	90.2	90.0	89.5	89.9
Strip <sub>1</sub>	60.0	70.6	59.0	62.7
Strip <sub>2</sub>	~100 <sup>1</sup>	84.7	~100 <sup>1</sup>	99.5
Strip <sub>3</sub>	~100 <sup>1</sup>	97.9	~100 <sup>1</sup>	~100 <sup>1</sup>

1. Calculated Efficiency was greater than 100% likely as a result of analytical and/or experimental uncertainty

Individual stage efficiencies in the extraction section range from 85 % to 95 % excluding Ext<sub>3</sub> results for Ce and La and Ext<sub>4</sub> results for Ce. The low and greater than 100% results are likely due to erroneous analytical results as good agreement was obtained for the individual lanthanide stage efficiencies throughout the rest of the

analyzed stages. The efficiencies are slightly lower than the expected range of 95% to 100% [157]; however, they are certainly high enough to achieve good separation and thus the flowsheet performance is considered successful. The strip section stage efficiencies range from 59 % to 100 %. It is unclear why Strip<sub>1</sub> efficiencies are lower but it is speculated that they may be due to analytical error, again because good agreement was seen through the rest of the section and measured stage efficiencies increase to near 100% in later strip stages.

#### 5.3.4 Temperature Profiles

Temperature profile data recorded with the data acquisition system was plotted for the duration of the flowsheet testing. Aqueous phase temperature profiles for the extraction, scrub, and strip sections are included in Figure 47.

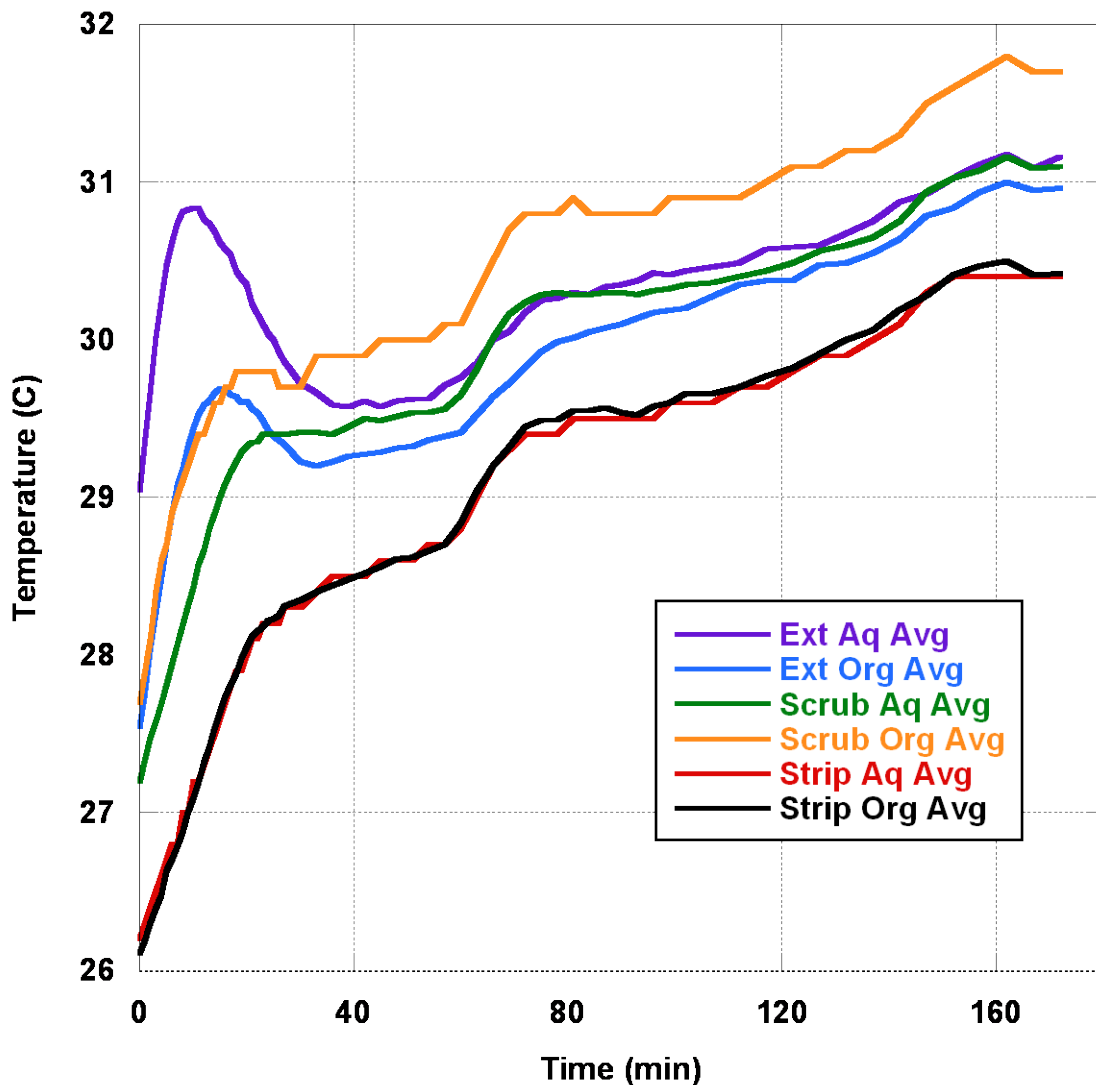


**Figure 47:** Aqueous and organic phase temperature (°C) profile averaged across respective extraction, scrub and strip sections

Generally, temperatures in all stages increased during the first 20 minutes of testing, which is attributed to the test startup procedure where freshly prepared (elevated temperature) nitric acid solutions were used. After the initial temperature increase at about 20-30 minutes, stage solution temperatures leveled off and started to trend slightly upward as the averaged ambient laboratory temperature increased throughout the morning. The increase of temperature over time is likely due to a combination of

contactor heat and increase in ambient laboratory temperature. The maximum temperature for stage 1 reached after three hours of testing was  $\sim 33$  °C.

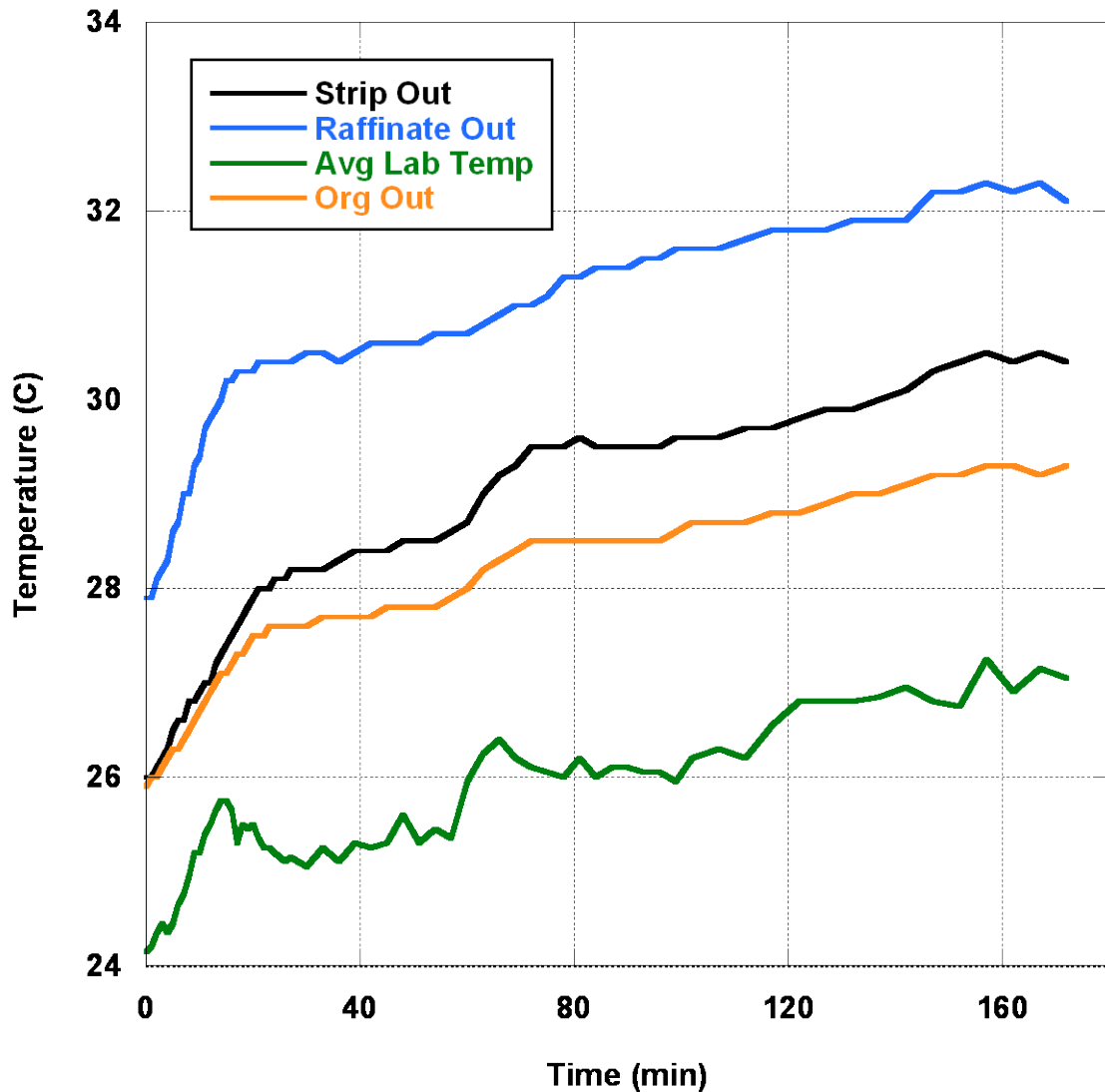


**Figure 48:** Temperature profile of solution outlets and ambient laboratory

Temperature profiles for the solution outlets (organic, strip and raffinate) are shown in Figure 48. After the initial increase in temperature during the first 20 minutes (as a

result of freshly prepared startup solution entering the system), the continuous trend of increasing solution temperature with increasing ambient laboratory temperature is evident. Again, the temperature profiles are extremely relevant to flowsheet testing as extraction parameters and efficiencies are based on temperature. Flowsheet parameters, operation and chemistry under steady-state and transient conditions must be known for an online process monitor to have a benchmark for comparison. Expected flowsheet behavior must be known for a materials accountability and process control system to be able to notify of a deviation from normal. The similarity between the contactor temperature trend and the averaged laboratory temperature indicates that after initial temperature equilibrium is reached, solution temperatures across the cascade are more dependent on ambient laboratory temperature than equipment-generated heat. Evidenced by comparing the average laboratory temperature plot with flowsheet section temperature plots, there was a small but comparable temperature increase that occurred within 20 minutes followed by a very similar upward temperature gain of ~ 2-3° C over the remainder of the testing. The maximum solvent temperature was determined to be below 35 °C for the duration of the test. The intermittent addition of ambient temperature aqueous solutions throughout the cascade minimizes temperature increases, and the recycling of organic provides for some normalization of temperature increase in that phase.

Results from previous ambient lamp oil/water, two-phase temperature profile testing indicated the maximum solution temperature measured was approximately 32° C, under a total flowrate of 1.4 liters/minute, rotor speeds of 4000 rpm, and an average laboratory

temperature of 25° C [162]. Thus, the results from this TRUEX demonstration are in agreement with previous literature values under similar operating conditions.

#### 5.4 Conclusions

An evaluation of the performance of the TRUEX process in a 30 stage centrifugal contactor pilot plant has been completed. The overall equipment operation, actual flowsheet performance including steady-state data, removal efficiencies, individual stage mass transfer efficiency, as well as temperature profiles were measured and reported. Overall the flowsheet performed as expected, and all equipment operated as designed. Metal concentration data indicate the cascade was operating at steady-state condition within twenty minutes. Removal efficiencies indicate > 99.9% of the Ce, La, Eu, and Nd was partitioned to the strip product stream. TRUEX is not designed for Cs/Sr separation, and as expected these metals were not extracted by the TRUEX solvent. The calculated removal efficiency for Zr indicates that ~ 0.6 % of the metal may have extracted.

Organic phase foaming was observed in the light phase interstage tubing almost immediately after solvent flow had begun, with the expected cause being high rotor speed causing air to be mixed with solvent. Other causes of foaming are high solvent flowrates or if the contactors are inadequately vented. Foaming in the light phase collector ring was also verified by inspection of samples taken of the aqueous raffinate and strip product streams. These aqueous samples contained small amounts of solvent. Foam volume can build in the light phase collector ring and eventually be pushed up to the heavy phase collector ring where it is discharged with the organic constituent. At 3000 rpm the solvent flow remained steady; however, some foaming was still observed. The use of low-mix sleeves did not alleviate organic in aqueous carryover. No foaming was

observed in the heavy phase interstage tubing. An estimated solvent in aqueous carryover of ~ 2% was measured in the raffinate while ~ 0.8% carryover was measured in the strip product (approximations from pumping out solution tanks). These foaming and carryover issues suggest further evaluation of pilot plant operating conditions and/or equipment design, specifically the installed off-gas ventilation tubing and the solution flow path design.

The flowmeter measurements of the organic phase did indicate a continuous small increase in solvent flowrate throughout the entire TRUEX demonstration, with the maximum reaching approximately 117% of the target flowrate. In contrast, aqueous solution recorded flowrates indicated minimal increases (all <5%) over the demonstration, with the exception of the aqueous feed which increased by approximately 7%. Again, the increases in flowrates were likely due to changes in solution properties as temperatures increased, resulting in a deviation from pump calibration conditions and reduction in flowmeter accuracy.

Individual stage mass transfer efficiency results ranged from 85 % to 95 % in selected extraction stages and from 59-100 % in selected strip stages. It is speculated that the lower efficiencies reported for a stage in the strip section are attributed to analytical uncertainty, as higher efficiencies were calculated throughout the remainder of stages. Temperature profile graphed data for the TRUEX flowsheet testing agreed with previous temperature profile data reported using a lamp oil/water solvent pairing at ambient solution operating temperature.

The success of the TRUEX demonstration was used directly for the setup and demonstration of a UREX flowsheet (Chapter 4). Lessons learned from the TRUEX test

include slight physical changes to the contactor setup such as employing a steeper angle flow path between contactors is desired an adjustment of offgas outlets to minimize foaming. Through the TRUEX experimental demonstration, these improvements can be incorporated into the contactor system and following flowsheet tests for demonstration of online process monitoring. The foaming issues and anomalies in stage mass transfer efficiencies show that further flowsheet testing is warranted. These issues, along with the temperature profile, can be used as the basis for further research and analysis of flowsheet data such as from the UREX demonstration. Moreover, a flowsheet must be fully characterized and understood in order for an appropriate process monitor to be developed and successful at detecting diversion scenarios. For example, deviations in flowsheet performance due to temperature changes must be documented and attributed to specific temperature values so that when deployed, a process monitor (or user) can differentiate between expected changes in process conditions due to physical circumstances and actual material diversion or process upset.

# CHAPTER 6

## DEVELOPMENT OF A DRY PROCESSING FLOWSHEET AND SAFEGUARDS

### APPROACH

The motivation for the work presented in this chapter is to develop a dry process for recycling of used fuel for General Atomics' Energy Multiplier Module ( $EM^2$ ) reactor. The goal is to recycle both existing LWR used fuel stockpiles and  $EM^2$  discharge. Towards this end, the technical feasibility of dry fuel treatment options previously studied must be considered. From an extensive review of previous dry processing technologies, an  $EM^2$  flowsheet was developed and corresponding options for materials accountability and safeguards were proposed. The composition of recycled used fuel from this flowsheet was modeled and used to aid in next generation  $EM^2$  core calculations. The waste materials from the proposed flowsheet were also modeled and categorized according to the existing nuclear waste framework. As the  $EM^2$  reactor is a proposed design from a commercial vendor, straightforward engineering and favorable economics are highly valued. Though the proposed  $EM^2$ -based dry processing fuel cycle has not been experimentally tested yet, the goal of this development study is to reduce the used fuel generated per kWe as compared with the current open fuel cycle while incorporating a higher level of proliferation resistance than closed fuel cycles utilizing wet reprocessing technologies.

#### 6.1 Introduction to $EM^2$

As in solvent-extraction based reprocessing, dry recycling technology can be applied to used LWR fuel to remove certain fission products, allowing the bulk of used nuclear

fuel to be recycled into new nuclear fuel. One option for the utilization of this recycled LWR fuel is the General Atomics EM<sup>2</sup> reactor design. In this work, EM<sup>2</sup> is representative of one of the newest trends in nuclear reactors, the small modular reactor, and is used to provide the basis for a dry processing based modified open fuel cycle. The EM<sup>2</sup> is a modified version of General Atomics' high-temperature, He-cooled reactor, with each module producing about 240 MWe of power at 850°C. The initial "starter" section of the EM<sup>2</sup> core would be enriched to approximately 12% <sup>235</sup>U and provide the neutrons required to convert used nuclear fuel or depleted U into fissile fuel. The core life expectancy is ~30 years (using used nuclear fuel and depleted U) without refueling [175]. Reactor specifics beyond these general characteristics and those relevant to fuel composition will not be discussed. Safeguards will be necessary in the utilization of any used fuel reprocessing technology, but are technology- and flowsheet- specific, so proliferation resistance methods must be developed for each used fuel treatment option. In order to design safeguards for a used fuel treatment process, the process itself must be understood, and from there areas for materials accountability and process monitoring can be identified.

The scope of this work is to evaluate the fuel cycle of LWR discharge dry processed for recycling, and identify potential areas for safeguards in the dry processing scheme. A thorough review of the literature provides confirmation of the dry processing (AIROX/OREOX) technical feasibility, while a study of experimental conditions and fission product removal percentages allows a dry processing scheme to be developed and tailored for LWR discharge for recycle into an EM<sup>2</sup> reactor, and for EM<sup>2</sup> discharge for recycle into a new EM<sup>2</sup> core. Benefits of this advanced fuel cycle include reducing the

mass and possibly the number of waste packages of current UNF needing to be disposed of as HLW, minimizing nuclear waste in general, reusing valuable parts of used nuclear fuel to maximize the energy derived from U ore and potentially deplete or control weapons-material inventories, while maintaining proliferation resistance [62].

#### 6.1.1 EM<sup>2</sup> fuel cycle goals

Several universal goals among used fuel processing technologies include maximization of energy recovery, minimization of radioactive waste that needs long-term disposal, economic feasibility and proliferation resistance [53, 176-178]. The EM<sup>2</sup>-based modified-open fuel cycle proposes to meet all of these goals through recycling of U, Pu and transuranics (TRU) and minimizing the amount of used fuel needing long term management. Additionally, the need for HLW repositories is directly linked to the production and accumulation of UNF from commercial nuclear power production, with the current inventory estimated to match the legislated repository capacity of 70,000 MTHM [24].

EM<sup>2</sup> deployment is proposed to utilize existing UNF stockpiles while meeting U.S. energy demands, so the current proportion of electricity generated by nuclear power is used as a benchmark. Three nuclear marketshare scenarios are considered in Figure 49, with information on current U.S. energy demand and nuclear proportion of electricity generation taken from literature [179]. Shown in blue are continued 2010 levels with no annual growth. Shown in green are a maintenance of 20% marketshare and 1% annual energy demand growth. Shown in red is an increase to 35% marketshare with 1% annual energy demand growth. Two nuclear reactor deployment scenarios are presented. The solid lines represent all the LWRs generation of all nuclear energy. The dotted lines

represent all LWRs being replaced by EM<sup>2</sup>s in an incremental fashion: 100% LWRs from 2010-2030, 50% LWRs and 50% EM<sup>2</sup>s from 2030-2050 and 100% from 2050-2100. The fundamental assumption for generation of UNF from LWRs is that at the 2010 nuclear energy level, the production of UNF is 2000 MT/year. Key points to note are that if existing LWR technologies are used to continue to provide nuclear power at 2010 levels, the accumulation of UNF will require at least 3 repositories in the next 90 years.

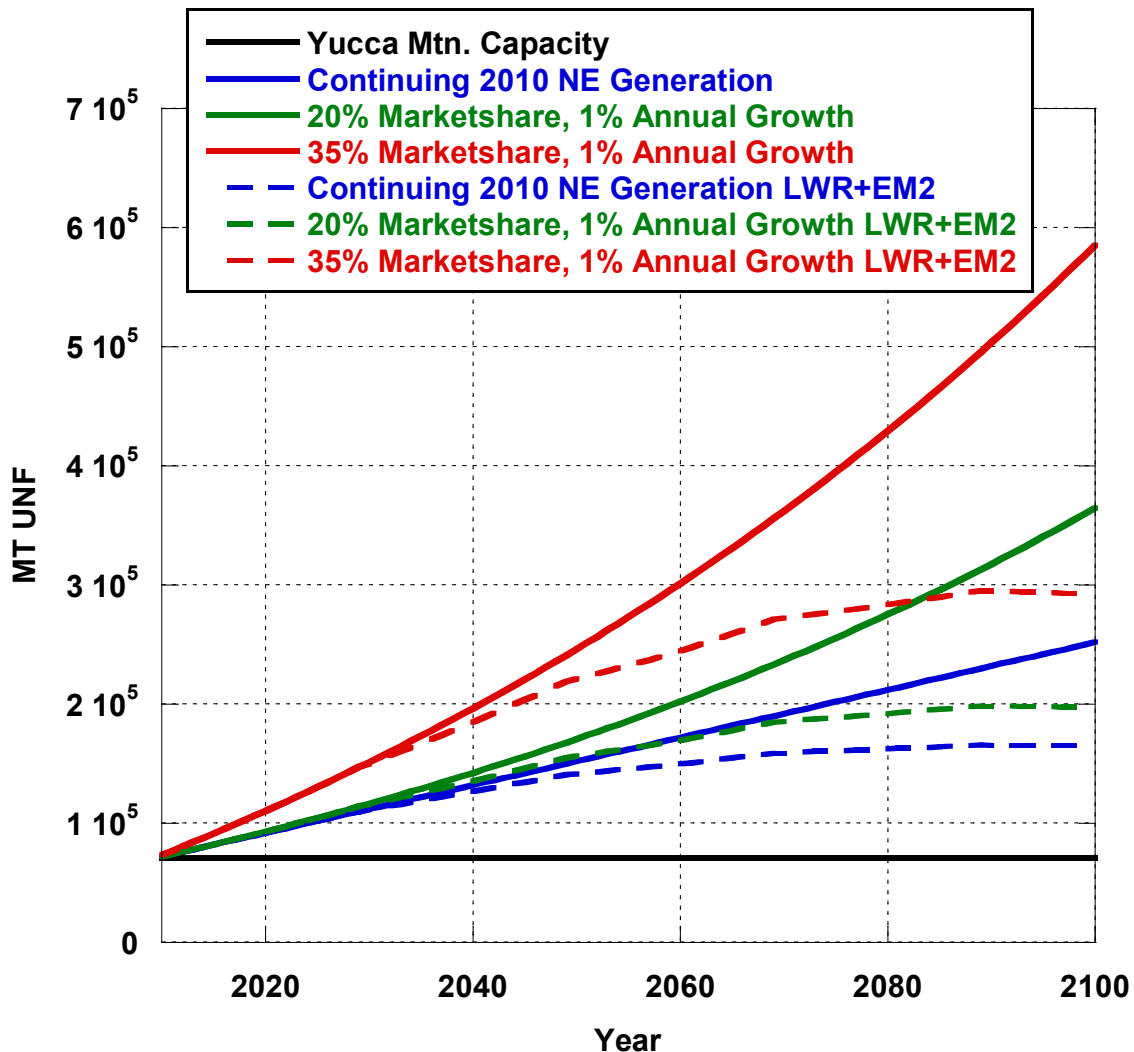


**Figure 49:** Used nuclear fuel accumulation scenarios

If existing LWR technologies are deployed to keep up with a 20% nuclear marketshare and a 1% annual energy demand growth, it is likely that 5 repositories will be necessary within a century. If existing LWR technologies are deployed more aggressively to attain a 35% nuclear marketshare and keep up with a 1% annual energy demand growth, at least 8 repositories will be needed by 2100. Generally, the combination fleet of LWRs and EM<sup>2</sup>s produces UNF at a slower rate than the all-LWR fleet case. As EM<sup>2</sup>s burn LWR used fuel and have a much longer core life than LWRs (~30 years), more aggressive EM<sup>2</sup> deployment would increase the reduction rate of UNF total inventory.

As EM<sup>2</sup> is proposed to exploit LWR UNF as a new fuel supply as well as recycle its own discharge, the elemental makeup of both resources must be characterized. Approximately 96% of LWR used nuclear fuel mass is recyclable material, 95% as U and 1% as the TRUs (Np, Pu, Am, Cm) with the remaining 4% being the fission products (FPs). A full elemental breakdown of LWR and EM<sup>2</sup> UNF is shown in Figure 50 [180].

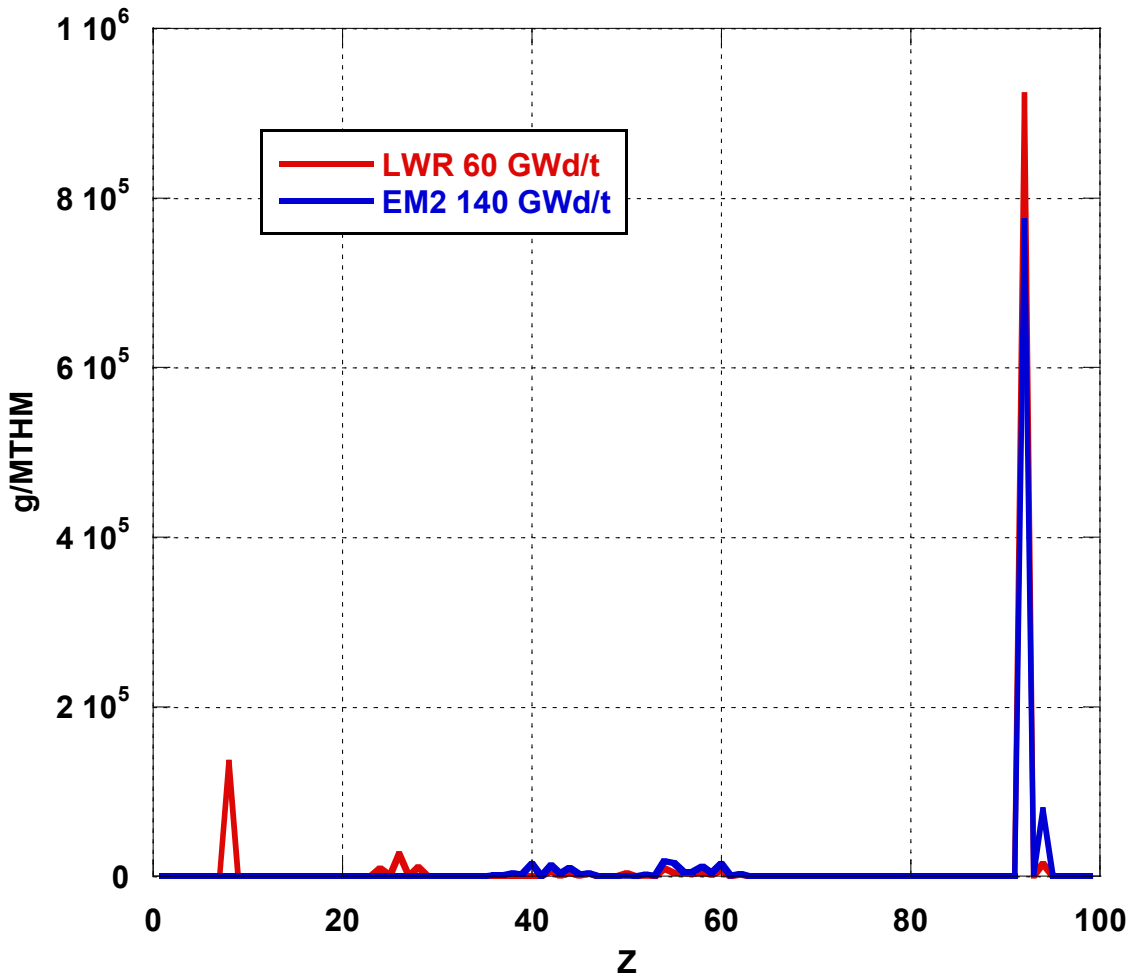


**Figure 50:** Elemental makeup of LWR and EM<sup>2</sup> used fuel [180]

For EM<sup>2</sup> discharge, the fission products make up approximately 15% of the mass, due to higher burnup (nominally 140 GWd/t). A dry fuel cycle that recycles used LWR fuel can provide maximum utilization of energy from the original mined U ore, reduction of potential repository source term, simplified processing design and robust proliferation resistance.

## 6.2 Previous dry processing studies

Discharged LWR fuel can be recycled in a dry process and utilized as fuel for future nuclear reactor cores. The general dry process is based on voloxidation, AIROX,

OREOX and DUPIC technologies previously studied for recycle of used LWR fuel. After dry processing, if further separations are desired, solvent extraction systems can be coupled with AIROX/OREOX/DUPIC to produce highly separated used fuel [160, 181]. Voloxidation is often proposed as a head-end step for multiple types of fuel to precede more extensive used fuel separations such as electrorefining or solvent extraction [182-184]. In addition to studies on dry processing as related to used nuclear fuel treatment, contamination of areas such as the Hanford site have led to studies focused on the extraction of  $^{137}\text{Cs}$ ,  $^{90}\text{Sr}$ ,  $^{60}\text{Co}$  and U from Portland cement by means of volatility processes. However, to date these studies have shown limited success with only  $^{137}\text{Cs}$  successfully being removed at temperatures of 1200°C or greater [185].

Fission products are often classified as volatiles or semivolatiles in dry processing literature. Volatilization depends on the chemical form and volatility of fission products, which is determined by Gibbs-energy minimization. Semivolatiles (Cs and Ru) have boiling points above that of water, while volatiles have boiling points of less than 200°C and include  $^3\text{H}$ , Xe, Kr and I. Metals such as Sr, Y, Zr, Nb, Mo, Tc, Rh, Pd, Ba, La, Ce, Pr and Nd are considered to be relatively nonvolatile, however they can form volatile species [186, 187]. Volatiles generally are able to diffuse through the fuel matrix, while low-volatile fission products depend on the partial pressures of the chemical forms of the fission products in order to be released from the used fuel. An additional mechanism of release results from the volatilization of the fuel matrix itself as  $\text{UO}_3$ . Other release behaviors can be restricted (such as that of Te and Sb) due to chemical trapping in Zircaloy cladding [29].

Following the voloxidation and volatilization of fission products from used fuel, the radionuclides must be trapped from the gas for effective wasteform production. A relevant study focused on an off-gas treatment system proposed to trap volatile fission products present from the oxidation of irradiated (PWR ~37 GWd/t, 27 year cooled) UO<sub>2</sub> to U<sub>3</sub>O<sub>8</sub> [188]. Individual filters in distinct zones were used to trap I, Tc and Cs in order to separate the radionuclides from the used fuel and each other. Granular zeolites or aluminosilicate disks were used to selectively trap the fission products, with multiple tests demonstrating up to 100% I trapping, 71% Cs trapping and 72% Tc trapping. The physical setup had 2.5 cm sections of UO<sub>2</sub> oxidizing at the bottom of a column under flowing oxygen or air (0.5 liters/minute) at 500 °C for 3 hours. As the fission products moved up the column, they passed through a 800-1000 °C zone which trapped the Cs, a 600 °C zone which trapped the Tc and lastly a 150 °C zone trapping the I [188]. These trapping technologies will need to be utilized to capture AIROX/OREOX volatilized fission products to provide a comprehensive EM<sup>2</sup> flowsheet for used fuel treatment.

### 6.2.1 AIROX

AIROX was initially developed in the 1960s as a dry, pyrochemical, low-decontamination method for recycling used LWR fuel and has gone through several cycles of process demonstration including fuel refabrication and irradiation [189-191]. It simultaneously declads and pulverizes the spent fuel, which is then reenriched (depending on reactor, not shown in figure), repelletized and recycled to the reactor. One benefit of AIROX processing, on top of the fairly straightforward process design, is the reduction in radioactivity. As a reference, used fuel cooled for 20 years AIROX-processed has about the same total dose for used fuel cooled for 93 years [192].

Variations in the literature exist for AIROX process conditions such as temperature, pressure, and gas atmosphere and as a result a wide variety of fission product removal percentages are reported. Generally, the process begins with removing used LWR UO<sub>2</sub> fuel pins from the fuel assembly and mechanically puncturing them every 1-4 cm in order to allow gaseous reactants access to the fuel. Then, the used fuel is exposed to an oxygen rich atmosphere at about 400°C where the UO<sub>2</sub> is converted to U<sub>3</sub>O<sub>8</sub>. A sample AIROX flowsheet is provided (Figure 51).

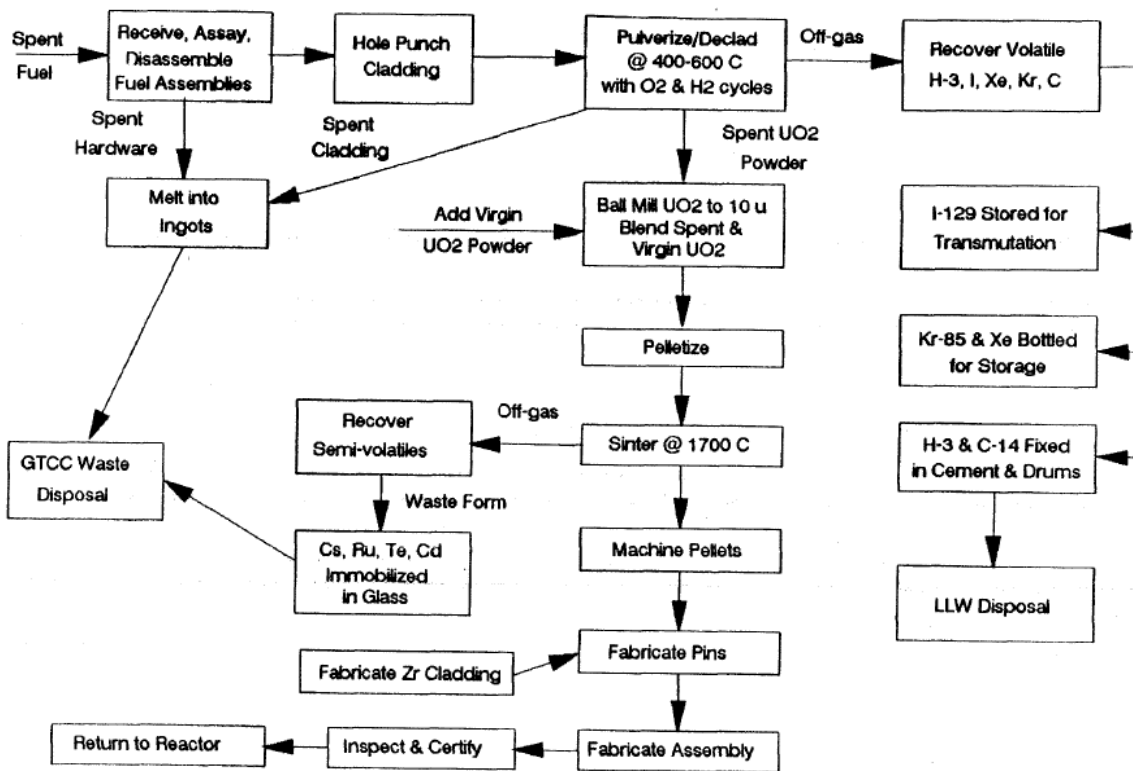


**Figure 51:** Sample AIROX flowsheet [57]

Complete oxidation to U<sub>3</sub>O<sub>8</sub> is not necessary to obtain sufficient volume expansion of approximately 30%, which ruptures the clad and cracks the fuel. If oxidation is carried out too rapidly, the U<sub>3</sub>O<sub>8</sub> on the surface of the fragments inhibits further oxidation and pulverization. One study showed that pulverization with complete decladding could be

accomplished in less than 1 hour when oxidation began at 480°C and then decreased to 425°C [59]. Care should be employed during oxidation, as U<sub>3</sub>O<sub>8</sub> begins to sinter at temperatures around 450°C [193]. Sintering would result in the fusing of U<sub>3</sub>O<sub>8</sub> powder, which is undesirable as it still needs to be blended with enriched U or Pu oxides before being fabricated into new fuel.

While one oxidation stage has been proposed to achieve complete decladding, oxidation and reduction cycles may be repeated multiple times to ensure complete pulverization of the used fuel and release of volatile fission products. After treatment, the fuel can be ball-milled to ensure pulverization to 2 mm particle size and complete fuel-cladding separation. Volatile and semivolatile fission products can be removed by flowing various gases over the used fuel at temperatures of 400-1800°C. After the processing for fission product removal is complete, the U<sub>3</sub>O<sub>8</sub> is put under a hydrogen-rich (hydrogen in argon, hydrogen in nitrogen) atmosphere at approximately 600°C to reduce it back to UO<sub>2</sub>. The reduced UO<sub>2</sub> is then mixed with enriched U or Pu oxides, resintered and refabricated into new fuel. Studies show that AIROX recycling of LWR used fuel produces a new LWR fuel that is approximately 75% by volume used nuclear fuel [193].

The size of the used fuel powder that is AIROX-processed affects the success of volatile and semivolatile fission product removal, and therefore the results of the preliminary oxidation and reduction steps on used fuel powder must be considered. While different processing conditions have led to variations in pulverization effectiveness, all of the resulting used fuel is less than 2 mm in particle size, with over 70% being smaller than 297 microns [58]. Very little product is less than 297 microns

and greater than 74 microns. This indicates that once pulverization begins, the used fuel rapidly goes to powder <74 microns. In contrast, the amount of material less than 5 microns is negligible [58].

While a number of AIROX studies have been published, discrepancies exist in the fission product removal data, such as removal fractions for Ag, Cd, Cs, In, Ir, Mo, Pd, Rh, Ru, Se, Tc and Te (Figure 53 and Figure 54). A substantial portion of the neutron absorbing fission products, especially lanthanides and Rh, in used fuel should be removed. One study found that the volatile fission products removed during AIROX processing decrease the parasitic neutron absorption by about 25% in the LWR scenario [189]. However, the effect of AIROX processing in a fast reactor used fuel recycling scheme is expected to be significantly higher. In one reference case for 20 year decayed fuel, the large elemental negative reactivity contributors are rare earth fission products including Gd, Sm, Nd and Eu, followed by the metallic inclusions of Mo, Ru, Rh, Tc and Pd. As applied to fast reactors, the presence of fission products both increases the parasitic neutron absorption but also results in the physical displacement of fertile material, decreasing the breeding ratio [189]. Fertile material percentage is important as it is converted to fissile material during reactor operation, and fast reactors rely on this to provide longer burnup times and core life. The breeding ratio is the number of fissile atoms created per fission event, thus when fertile material is converted to fissile material, the breeding ratio would increase.

Overall, commonly agreed-upon (in the literature) AIROX removals include 100% of Xe, Kr and I, 90% of Cs and Ru, 75% of Cd, Te and In, and 30% of the slowly saturating lumped fission products [193]. Detailed studies on fission product removals suggest

that oxidative vaporization can remove Tc, Mo and some Ru. Due to lanthanides being incorporated into a solid solution with UO<sub>2</sub>, any separation requires complete pulverization of used fuel. Chlorination of a pulverized oxide at 1100-1200 °C has been shown to vaporize substantial portions of Nd, Eu, Gd and Rh. A fraction of the U would also likely vaporize, however no significant loss of Pu during dry processing and refabrication has been found [189]. In another study employing used fuel with a burnup of 50 MWd/kg HM, up to 99% of <sup>3</sup>H, 75% of I and 98% of the Kr and Xe were expected to be released from a single oxidation cycle. This study also put forth that Cs, Te, Ru, Tc, Cd and In were also removed to a significant extent during pellet sintering. Overall, through the oxidation and reduction cycles, more than 99.9% of the UO<sub>2</sub> was removed from cladding. Other experiments of note include one in which Te was partially removed, Ru could be volatilized by having one oxidation step above 725 °C and rare earths remain with the U. In these studies, medium and low volatility fission products such as Ba, Sr, Ce, La, Pd and Zr remained in the fuel along with the U, Pu and higher actinides. The thermodynamic data relevant to volatility processing for some fission products is lacking, however some reported boiling points for certain fission product species are available (Table 16). The two boiling points for Tc are presented for Tc<sub>2</sub>O<sub>7</sub> (311 °C) and TcO<sub>2</sub> (1000 °C) species expected to be relevant in used nuclear fuel.

**Table 16:** Selected boiling points reported for fission products [192]

Element	Boiling Point (°C)
Ag	2200
Cd	770
Cs	670
In	2072
Ir	4428
Mo	4639
Pd	2963
Rh	3695
Ru	4150
Se	685
Tc	311, 1000

Kilogram-scale experimental studies were performed on unirradiated UO<sub>2</sub>, both with and without simulated fission products and small scale hot experiments were conducted on pellets with burnups up to 31,000 MWd/MTU [57]. Experimental results indicated that simulated high burnup and multiple recycles did not significantly affect the pulverization of the UO<sub>2</sub> pellets and actually enhanced pellet sintering. Cold small scale decladding experiments were conducted on sections of UO<sub>2</sub> pellets clad in stainless steel and zircaloy tubes, and larger sections of UO<sub>2</sub> pellets in stainless steel cladding. Results indicated that fuel rods punctured at 2.5 cm intervals and exposed to oxygen at 400 °C for 2 hours were completely declad. Repeating the cycle of oxidation and reduction provided 99.9% mechanical separation of fuel from cladding. Hot tests indicated that oxidation, reduction and decladding rates for irradiated UO<sub>2</sub> pellets are similar to unirradiated UO<sub>2</sub> pellets, and that <sup>3</sup>H, Kr and I were released during the oxidation and reduction cycles, with large fractions of semivolatile fission products (95% of Cs and 50% of Ru) released during pellet sintering. Smaller amounts of Te, Tc, Cd and In were also volatilized

during the sintering [193]. In another set of experiments, stable fission products equivalent to 20,000 MWd/MTU burnup were added during five cycles to yield an equivalent burnup of 100,000 MWd/MTU. In this case, about 58% of the volatile fission products were removed when the fuel capsule was ruptured (punctured and oxidized), with the remainder of the volatile fission products removed during AIROX [58]. As an alternative to adding stable fission products to produce an equivalent burnup of used fuel, SIMFUEL was produced for some time to simulate the composition and microstructure of high burnup UO<sub>2</sub> [193].

The lanthanides in new fuel physically displace fertile fuel, and they are also especially important to remove in the fast spectrum due to their neutron absorption properties. Several attempts at lanthanide removal from used fuel have been studied, such as fluoride volatility, supercritical fluids, glass solubility, plasma-based separations, magnetic separation, high temperature fluorination, and electrostatic separation. The electrostatic separation technique is promising for the separation of Rh and other noble metal poisons such as Mo, Tc, Ru and Pd, from the U oxide [192]. However, one study in particular reported removal percentages of up to 69% for Sm, 68% for Nd and 89% for Gd, demonstrating experimentally the promise of the dry processing practice [194].

After all fission product removal is complete, the AIROX-processed used fuel must be mixed with virgin enriched fuel which can come from diluted weapons grade material (either HEU previously destined for a reactor or weapons stockpiled material). In this way, AIROX not only extends U reserves by better utilization of the original U ore, it can also allow for the depletion of stockpiled weapons material and HEU globally [57]. The dependence on weapons grade material is not sustainable, however disposition of this

material and the transition away from HEU-fueled reactors are currently priorities in U.S. policy [20, 22].

### 6.2.2 OREOX and DUPIC

The Direct Use of PWR fuel In CANDU (DUPIC) process has been investigated. CANDU reactors generally utilize natural U as a fuel, so LWR used fuel, though less enriched than fresh LWR fuel, contains enough  $^{235}\text{U}$  to be effective as a CANDU fuel. In general, the  $^{235}\text{U}$  content in used LWR fuel is less than the content of freshly enriched fuel (3-5%), but greater than the content of natural U (0.72%) [195]. However, the used LWR fuel does contain fission products which must be removed to some extent in order for the fuel to be effective in the CANDU reactor. The existence of residual fission products in fresh DUPIC fuel also means that due to the high radioactivity, all the manufacturing processes must be performed remotely in a highly shielded facility. While increasing cost, this enhances proliferation resistance simply due to the difficulties of physical access and diversion of materials in a self-contained processing facility with all special nuclear material (SNM) contained in hot cells or other highly shielded facilities. In the LWR regime, the DUPIC process generates approximately 20% less HLW than other wet reprocessing and 60% less HLW than direct disposal. It also uses two times higher burnup fuel meaning overall reduction in waste production and better utilization of energy resources [18].

For fission product removal, DUPIC adopts volatilization followed by three cycles of Oxidation and REduction of OXide fuel (OREOX). Oxidation occurs at 450°C under an air atmosphere and reduction under 4% H<sub>2</sub> in Ar at 700°C [179]. As in AIROX, volatile fission products are released along with some semivolatiles. The goal for OREOX in

DUPIC is for Cs, Ru, Mo and Tc removal in order to reduce operating cost and radioactivity level. Removal of the long-lived  $^{99}\text{Tc}$  and  $^{129}\text{I}$  is beneficial because this reduces the time that the used fuel must be actively monitored and protected in storage [56].

The OREOX process has been tested with voloxidation performed for 5-10 hours at 500°C in air, followed by three oxidation and reduction cycles [196]. High burnup used fuel rods were mechanically slit open, and then oxidized at 700°C for 5 hours in order to completely retrieve spent fuel material. With this method, over 99.9% recovery was achieved. Experimental testing has shown that the density of sintered pellets fabricated with high burnup used fuel was lower than those fabricated with conventional burnup used fuel. This indicates that fuel fabricated from higher burnup materials will have different material properties than conventional fuel. Two burnups, 65,000 MWd/tU, and 27,300 MWd/tU, 15 years older, of used PWR fuel were studied. Sintering was performed at 1800°C for 7 hours in 4%  $\text{H}_2/\text{Ar}$ . It was found that these higher temperatures were needed to remove fission products. In all tests,  $^{85}\text{Kr}$  started to be released at 350°C during the first voloxidation, with its release behavior showing strong dependence on temperature and not gas atmosphere. It was found that when processing used fuel with higher burnups, a longer process time was required to completely release  $^{85}\text{Kr}$  [197]. The release behavior of  $^{14}\text{C}$  was found to be similar to that of  $^{85}\text{Kr}$ , with release beginning at 300°C. Higher burnup used fuel required longer operation time for complete removal of  $^{14}\text{C}$ .

In another study, release fractions during a voloxidation at 500°C showed over 99% for  $^3\text{H}$ , 17-22% for  $^{14}\text{C}$ , 7-17% for  $^{85}\text{K}$  and <8% for  $^{129}\text{I}$ . The release of  $^{137}\text{Cs}$  during a

voloxidation at 500°C was not observed; however at 800°C, Cs release began with estimated fraction of 16% after reaching 1000°C. Approximately 90% of Cs was released after reaching 1250°C in air. The percent of UO<sub>2</sub> successfully oxidized to U<sub>3</sub>O<sub>8</sub> has been shown to directly affect the release percentages of <sup>85</sup>Kr and <sup>14</sup>C fission gases during voloxidation at 500°C, but the effect may be less pronounced at higher voloxidation temperatures. Additionally, for certain radionuclides, a higher burnup used fuel showed higher voloxidation release fractions than lower burnup fuel [196].

Fission products were removed from 25 year old PWR oxide fuel through OREOX. These experiments found that the extent of fission product removal increased with increasing operating temperature and decreasing pressure. Rh, Ru, Tc, Mo, Te and Cs were removed to some extent through the oxidation process, with less than expected removal fractions attributed to partial vaporization, incomplete oxidation or the formation of non-volatile complex oxides. Molybdenum volatility was found to be especially dependent on the pressure of the system, with no removal under pressures greater than 0.789 atmospheres, however partial removal was observed below 0.001 atmospheres [181].

In another OREOX experiment, 500 PSI O<sub>2</sub> at 600°C was used to produce a U<sub>3</sub>O<sub>8</sub>+PuO<sub>2</sub> phase from which more than 99% of the <sup>3</sup>H was released. About 98% of I and Kr were volatilized from highly irradiated fuel specimens, but more typical releases were around 45% Kr and 75% I. In an attempt to achieve complete removal of <sup>3</sup>H, I, Xe and Kr, tests were conducted in a hot cell with temperatures up to 850°C with He, air or O<sub>2</sub>, on short and long-cooled fuel with burnups up to 100,000 MWd/t. The Pu concentration of the used fuel and the type of fabrication were found to affect the amount

of fuel disintegration and release of noble gases. Other relevant factors were found to be the homogeneity of U-Pu mixture, chemical form of the fuel, anion to metal ratio, method of fuel preparation, physical fuel form, burnup, neutron energy, enrichment, temperature of irradiation and degree of fuel restructuring [59]. Successful oxidation and pulverization of a homogeneous U/PuO<sub>2</sub> ceramic fuel was determined to be dependent on Pu/M ratio, quality of the ceramic and physical size of sample. Sol-gel pellets and microspheres were found to be the most difficult to pulverize. This is pertinent to the EM<sup>2</sup> fuel cycle because the proposed fuel fabrication process is based on a sol-gel technique. Voloxidation was found to have no effect on Pu dissolution [59], meaning that dry processing does not limit further fuel treatment options in the event that Pu recovery is desired.

#### 6.2.3 CARBOX/CARDIO

The EM<sup>2</sup> design requires a carbide fuel, so the few dry processes investigated for application to these fuels are especially relevant. The CARBOX process is essentially the AIROX process applied to carbide fuels, with oxidation converting U carbide to the oxide, then further oxidation to achieve UO<sub>2</sub> to U<sub>3</sub>O<sub>8</sub> conversion. After fission product volatility, the U<sub>3</sub>O<sub>8</sub> is reduced back to UO<sub>2</sub> in the presence of carbon, and then converted to the carbide [15].

The CARDIO process was also investigated as relating to carbide fuels (CARbon DIOxide oxidation) under a CO<sub>2</sub> atmosphere. A CARDIO processing experiment examined removal fractions for Ag, Cs, Mo, Ru, Gd, Nd, Rh and Sm. Two runs at 1000°C and two runs at 1600°C were both held at temperature for 5 hours with 80 mg of

powder in a platinum foil lined alumina furnace boat, heated at 8°C/min under flowing CO<sub>2</sub>. A summary of the results of these studies is presented in Table 17 [194].

**Table 17:** Mean observed removal fractions of selected elements under CARDIO [194]

Element	1000°C	1600°C
Ag	0.99	1.00
Cs	1.00	1.00
Eu	0.71	0.09
Gd	0.89	0.39
Mo	1.00	1.00
Nd	0.68	0.09
Sm	0.69	0.05

#### 6.2.4 Summary of processing conditions and results

Literature studies have been conducted on a variety of dry processing techniques, utilizing varied experimental conditions, simulated and real used fuel compositions. For development of the EM<sup>2</sup> dry process, these previous works are used as the guideline for bounds of experimental conditions. Dry processing experiments have utilized temperatures ranging from 400-1850°C, pressures generally at atmospheric but some below 1 atmosphere, and flow gases of oxygen, oxygen and ozone, “wet” oxygen (water present), dilute oxygen in argon, dilute hydrogen in argon, chlorine, fluorine (fluorination processes) and air.

A generalization of the maximum removal percentages achieved through the various experimental conditions is shown in Figure 52. Although this presents a useful summary of the maximum removal percentages reported in the literature, there is a wide distribution in experimentally reported removal percentages even in these colored groups.

H																			He	
Li	Be														B	C	N	O	F	Ne
Na	Mg														Al	Si	P	Se	Cl	Ar
K	Ca	Sc	Ti	V	Cr	Mn	Fe	Co	Ni	Cu	Zn	Ga	Ge	As	Se	Br		Kr		
Rb	Sr	Y	Zr	Nb	Mo	Tc	Ru	Rh	Pd	Ag	Cd	In	Sn	Sb	Te	I		Xe		
Cs	Ba	La	Hf	Ta	W	Re	Os	Ir	Pt	Au	Hg	Tl	Pb	Bi	Po	At		Rn		
Fr	Ra	Ac	Rf	Db	Sg	Bh	Hs	Mt												
					Ce	Pr	Nd	Pm	Sm	Eu	Gd	Tb	Dy	Ho	Er	Tm	Yb	Lu		
					Th	Pa	U	Np	Pu	Am	Cm	Bk	Cf	Es	Fm	Mo	No	Lr		

**Figure 52:** Summary of maximum removal percentages reported in the literature for dry processes: green $\geq 75\%$ , yellow $\geq 65\% > 75\%$  and red $\leq 5\%$

For example, a summary of the experimental data for the removal percentages of elements with reported maximum values of  $\geq 75\%$  is shown in Figure 53. Similarly, a summary of the experimental data for the removal percentages of elements with reported maximum values between 65% and 75% is shown in Figure 54. As seen in these figures, any dry process must be developed and tailored specifically to a fuel cycle because depending on the reactor, desired fuel type and burnup, the desired composition of the input fuel will vary. Thus, the dry process treatment of UNF must be adapted to provide a fuel input for a reactor in order to provide the desired composition under any cost, input material, waste output or fabrication constraints.

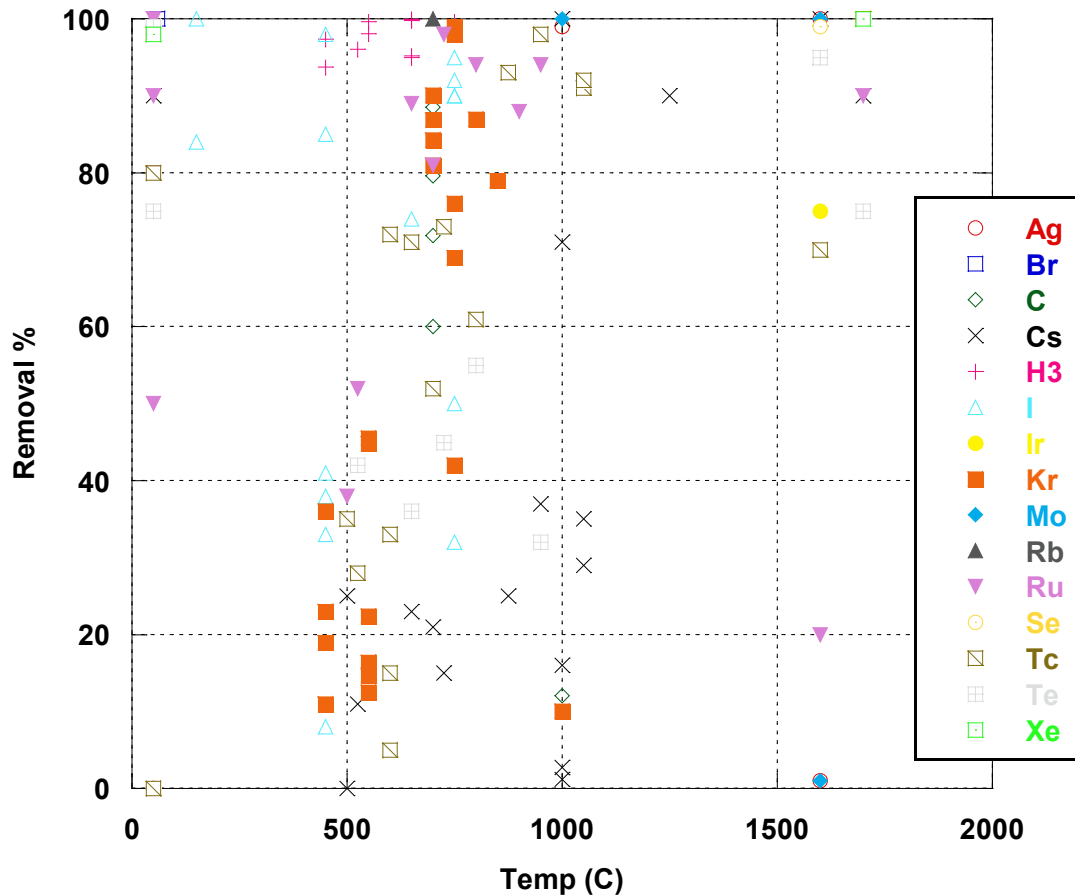


**Figure 53:** Literature reported removal percentages for elements with maximum reported percentages of  $\geq 75\%$

The reported removal percentages of Am, Ba, Ce, La, Np, Pr, Pu, Sr, and Y are all between 0% and 5%. Due to the variety of experimental conditions studied, there is no clear-cut temperature dependence of removal percentages for any element. In order to elucidate a trend or pattern from this data, unsuccessful or inappropriate data points are removed from the data sets. In this way, the removal percentages of Ag, C, Cs,  $^3\text{H}$ , I, In, Kr, Mo, Rh, Ru, Tc and Te all demonstrate some form of positive dependence on temperature – that is, as temperature increases, so does the removal percentage. In many cases, there is not enough data to demonstrate a temperature dependence. Some elements

show no temperature dependence and some even show a correlation between increasing fission product removal and decreasing temperature.

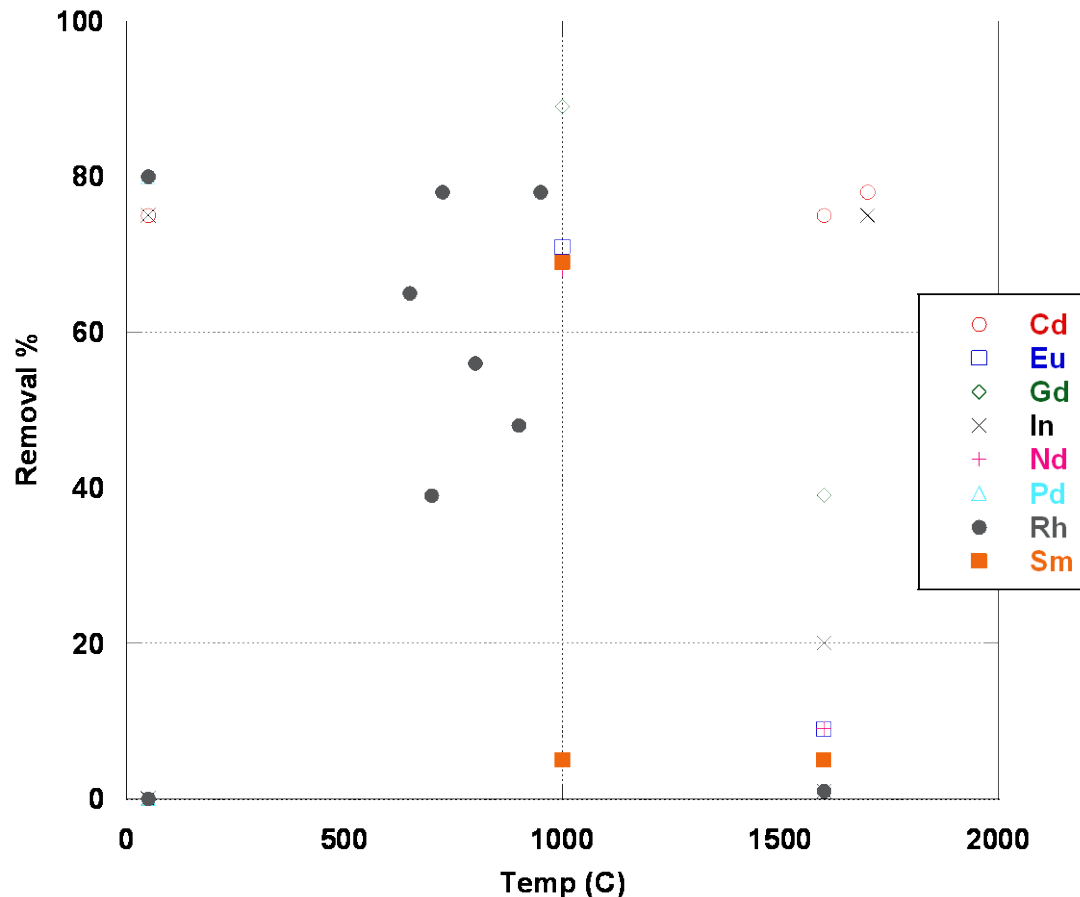


**Figure 54:** Summary of removal percentages for elements with maximum removal percentages between 65% and 75%

### 6.3 Development of EM<sup>2</sup> flowsheet

This task included the development of a dry processing flowsheet specific to the EM<sup>2</sup> reactor design. Additionally, this flowsheet can be used to assess areas for safeguards and process monitoring. The dry processing options presented in Section 6.2 can be applied to the LWR and EM<sup>2</sup> used nuclear fuels described in Section 6.1.1 order to

produce such used fuel treatment flowsheets. These flowsheets are generally developed with the aim of achieving specific goals, such as those outlined in Section 6.1.1. In addition to these, overall goals of a fuel cycle can include balancing removal percentages with new LWR core needs and waste streams generated [60, 61, 198]. Also, the decay times for LWR discharges need to be considered. A longer decay time results in total activity reduction, but must be weighed with cost of on-site storage and new core needs.

**Table 18:** EM<sup>2</sup> dry process flowsheet fission product removal goals

<b>% Removal</b>	<b>Element</b>	<b>Proposed Wasteform</b>	<b>Waste Classification</b>
100	<sup>3</sup> H, <sup>14</sup> C	cement	LLW
90	Te	glass	GTCC
75	Cd, lanthanides	glass	GTCC

With these considerations in mind, the sample process flowsheet (Figure 55) is designed to achieve at a minimum the removal percentages shown in Table 18. During these processes, likely other radionuclides will volatilize as well including 90% of the Tc, 100% of the I, 90% of the Cs and 100% of the Kr and Xe. Another possibility to consider is to remove as little as possible Tc and I and keep in the fuel for transmutation as these are the main environmentally mobile concerns in wasteforms, however under certain processing conditions, volatilization will be inevitable.

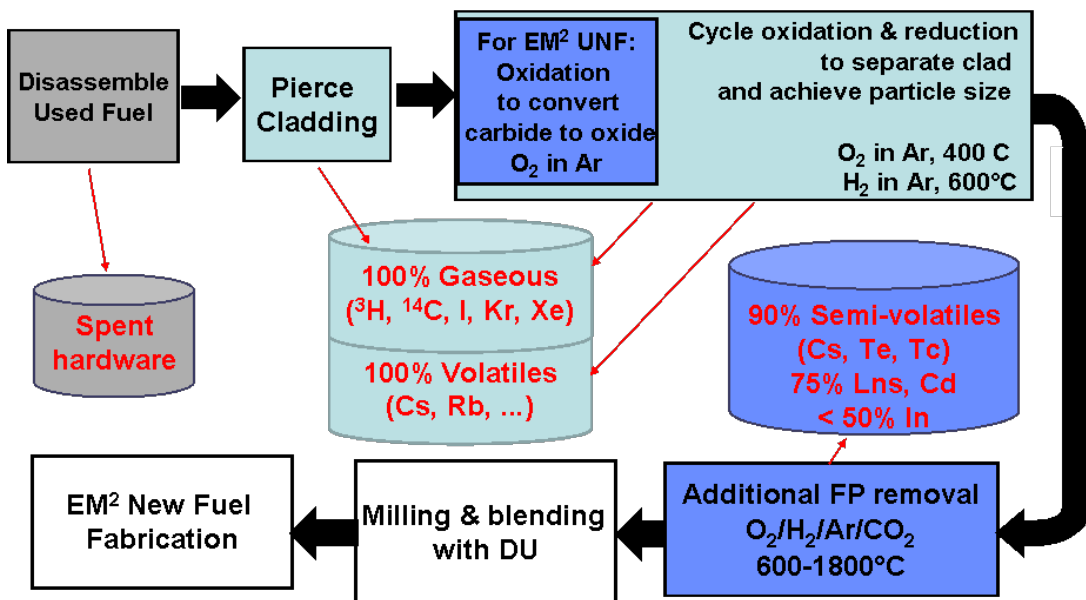


**Figure 55:** Flowsheet for dry processing of used nuclear fuel for recycle into EM<sup>2</sup>

As shown in Figure 55, proposed dry processing of EM<sup>2</sup> used fuel begins with a conversion from the carbide to the oxide under an oxygen atmosphere in argon. After this step, the dry treatment of EM<sup>2</sup> used fuel is the same as material from other reactor types. Three cycles of oxidation with O<sub>2</sub> in Ar or air at 400°C and reduction with H<sub>2</sub> in Ar at 600°C are used to remove the fuel from the cladding. In these first oxidation and reduction steps, it is expected that 100% of the <sup>3</sup>H, I, Kr, and Xe will volatilize. Due to the fairly low fission product content of LWR used fuel, additional FP removal yields are not expected to be high. However, with the larger presence of fission products in EM<sup>2</sup> used fuel, further dry processing will likely result in added fission product volatilization. In either case, to produce the best product for new fuel fabrication, higher temperature removal steps are proposed. Thus, the used fuel will be exposed to CO<sub>2</sub> at approximately 1000°C to yield 75% removal of Eu, Gd, Nd, Sm, and perhaps other lanthanides. This CO<sub>2</sub> step can be cycled multiple times in an effort to achieve greater removal

percentages. High temperature fuel sintering would volatilize additional fission products, so an 1800°C processing step before sintering should remove approximately 90% of the Cs, Tc and Te, 75% of the Cd and <50% of the In and minimize fission product volatilization during fuel fabrication.

#### 6.4 Characterization of waste and recycled streams

The products and wastes from dry processing must be identified and assessed for materials accountability and to identify potential safeguards approaches. A summary of the expected elemental composition of the volatilized fission products and recycled heavy metals and non-volatile fission products from the LWR recycle process is shown (Figure 56).

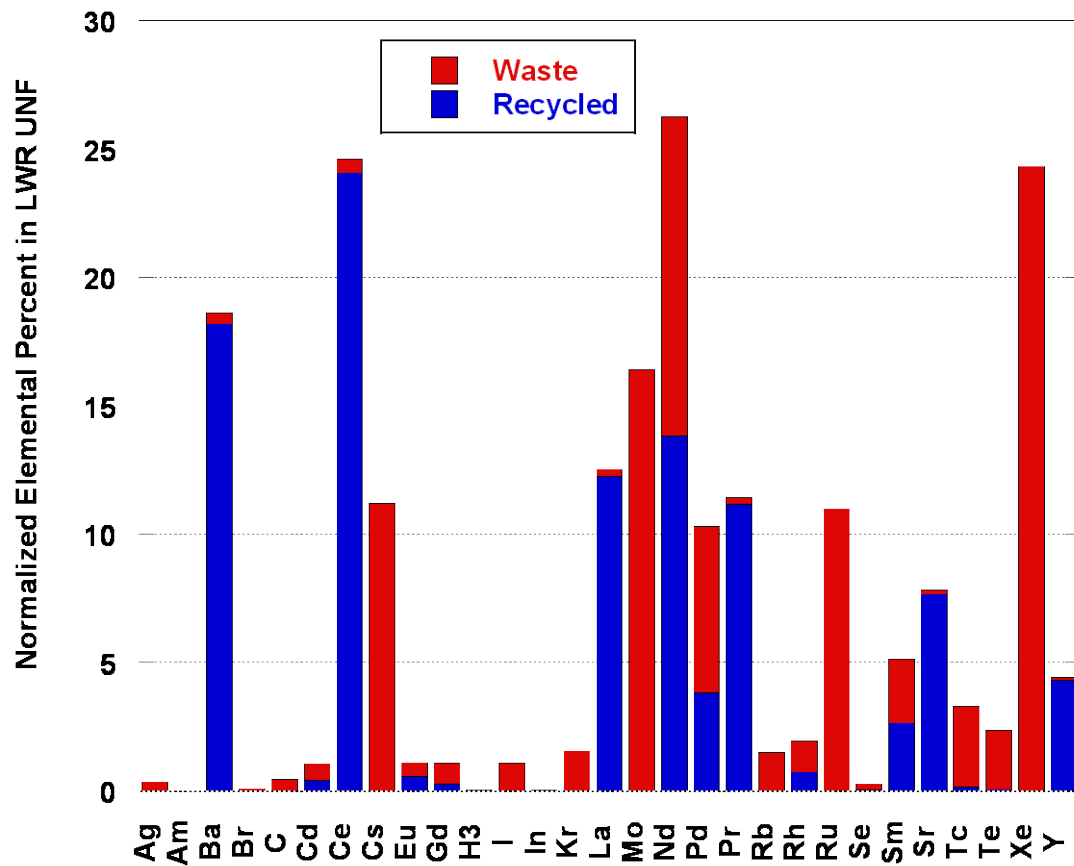


**Figure 56:** Normalized elemental composition of recycled and waste streams from dry processing of LWR discharge

The ORIGEN computer code has been used to provide isotopes, related activities, masses and thermal power for EM<sup>2</sup> fuel (assuming 140 GWd/t burnup over 30 years) at discharge, and after 5 and 10 years of decay time (Table 19). As values for over 1000 isotopes are produced, a summary of the elements present in highest mass percentage in EM<sup>2</sup> discharge fuel is shown in Table 20 [180].

**Table 19:** Selected summary of EM<sup>2</sup> used fuel at Discharge, 5 and 10 years

<b>Isotope</b>	<b>Activity(Ci)</b>			<b>Mass (g)</b>			<b>Thermal Power (W)</b>		
	Disch.	5 yr	10 yr	Disch.	5 yr	10 yr	Disch.	5 yr	10 yr
<sup>14</sup> C	5.0E-04	5.0E-04	5.0E-04	1.1E-04	1.1E-04	1.1E-04	1.5E-07	1.5E-07	1.5E-07
<sup>242</sup> Cm	3.7E+03	4.6E+00	2.9E+00	1.1E+00	1.4E-03	8.8E-04	1.4E+02	1.7E-01	1.1E-01
<sup>137</sup> Cs	4.3E+05	3.8E+05	3.4E+05	4.9E+03	4.4E+03	3.9E+03	4.8E+03	4.2E+02	3.8E+02
<sup>3</sup> H	3.3E+03	2.5E+03	1.9E+03	3.4E-01	2.6E-01	2.0E-01	1.1E-01	8.5E-02	6.4E-02
<sup>129</sup> I	1.5E-01	1.6E-01	1.6E-01	8.7E+02	8.8E+02	8.8E+02	7.1E-05	7.2E-5	7.2E-05
<sup>94</sup> Nb	6.8E-04	6.8E-04	6.8E-04	3.6E-03	3.6E-03	3.6E-03	6.9E-06	6.9E-06	6.9E-06
<sup>241</sup> Pu	6.6E+04	5.2E+04	4.1E+04	6.4E+02	5.0E+02	4.0E+02	2.1E+00	1.6E+00	1.3E+00
<sup>90</sup> Sr	3.1E+05	2.7E+05	2.4E+05	2.3E+03	2.0E+03	1.8E+03	3.6E+02	3.2E+02	2.8E+02
<sup>99</sup> Tc	5.7E+01	5.7E+01	5.7E+01	3.3E+03	3.4E+03	3.4E+03	2.8E-02	2.9E-02	2.9E-02

**Table 20:** Summary of selected elements present in EM<sup>2</sup> discharge fuel

<b>Element</b>	<b>Mass (g/MT)</b>	<b>Element</b>	<b>Mass (g/MT)</b>
U	7.74E+05	Pr	4.52E+03
Pu	7.82E+04	Pd	4.31E+03
Xe	1.82E+04	Sr	3.97E+03
Cs	1.56E+04	Np	3.55E+03
Zr	1.49E+04	Sm	3.40E+03
Zr	1.49E+04	Tc	3.34E+03
Nd	1.48E+04	Te	2.36E+03
Mo	1.31E+04	Rh	2.27E+03
Ce	1.18E+04	Y	2.02E+03
Ru	1.07E+04	Kr	1.65E+03
Ba	5.83E+03	Rb	1.46E+03
La	5.13E+03	I	1.24E+03

For the waste stream, the isotopes of the fission products must be examined to determine half life, heat produced and radiotoxicity, as all relate to the choice of waste form and ultimate disposal options. Short lived fission products such as  $^{137}\text{Cs}$  and  $^{90}\text{Sr}$ , both with approximate half lives of 30 years, are expected to decay quickly enough that they are the significant contributors to heat loading in a wasteform but can be stored separately for a relatively short time (~300 years) and do not need long term geologic burial [199]. Long lived fission products (Table 21) however, do need a long term management plan. As some of these isotopes are not present in any significant quantity and may be ignored at present, those listed in Table 21 are noteworthy contributors. In addition to long lived fission products in the waste stream, any tramp or carry-over of heavy metals will affect the classification and therefore disposition of process wastes. In Table 21, while some elements listed are naturally occurring and/or stable, if they are present with a radioactive isotope of the same element, they will be included in the waste stream (as separations are non-isotopic) and thus contribute the waste and recycled products.

**Table 21:** Isotopes expected in LWR dry processing waste and recycled streams in quantities greater than g/MTHM with half lives greater than 100,000 years

Waste Stream		Recycled Stream	
Isotope	Half-life (yr)	Isotope	Half-life (yr)
<sup>142</sup> Ce	5.00E+16	<sup>142</sup> Ce	5.00E+16
<sup>129</sup> I	1.57E+07	<sup>50</sup> Cr	1.80E+17
<sup>115</sup> In	4.41E+14	<sup>135</sup> Cs	2.30E+06
<sup>100</sup> Mo	1.00E+19	<sup>144</sup> Nd	2.29E+15
<sup>144</sup> Nd	2.29E+15	<sup>150</sup> Nd	1.10E+19
<sup>150</sup> Nd	1.10E+19	<sup>237</sup> Np	2.14E+06
<sup>87</sup> Rb	4.75E+10	<sup>107</sup> Pd	6.50E+06
<sup>79</sup> Se	1.13E+06	<sup>242</sup> Pu	3.73E+05
<sup>82</sup> Se	1.08E+20	<sup>147</sup> Sm	1.06E+11
<sup>147</sup> Sm	1.06E+11	<sup>148</sup> Sm	7.00E+15
<sup>148</sup> Sm	7.00E+15	<sup>149</sup> Sm	2.00E+15
<sup>149</sup> Sm	2.00E+15	<sup>126</sup> Sn	1.00E+05
<sup>99</sup> Tc	2.11E+05	<sup>99</sup> Tc	2.11E+05
<sup>128</sup> Te	2.20E+24	<sup>128</sup> Te	2.20E+24
<sup>130</sup> Te	7.90E+20	<sup>130</sup> Te	7.90E+20
<sup>136</sup> Xe	2.36E+21	<sup>234</sup> U	2.46E+05
		<sup>183</sup> W	1.10E+17
		<sup>184</sup> W	3.00E+17
		<sup>93</sup> Zr	1.53E+06
		<sup>96</sup> Zr	3.80E+19

## 6.5 Proliferation resistance in dry processing

While reduction in UNF inventories and production is a mainstay of a future nuclear fuel cycle, proliferation resistance is of utmost importance, as no system will be adopted unless proven to meet rigorous U.S. nonproliferation objectives [19]. Additionally, reduction of proliferation risk relative to wet reprocessing has been stated as a DOE nuclear fuel cycle goal [20]. The internationally accepted definition of proliferation resistance describes “that characteristic of a nuclear energy system that impedes the diversion or undeclared production of nuclear material or misuse of technology by States in order to acquire nuclear weapons or other nuclear explosive devices [68].” Essentially,

proliferation resistance is describing the extent to which the characteristics and safeguards of a nuclear energy system impede proliferation, with the understanding that a proliferation-proof system does not exist. The dry processing system described in this chapter must be examined with proliferation resistance criteria in mind and potential safeguards developed.

A basic premise of SNM safeguards is that all nuclear materials, regardless of how attractive, are candidates for diversion, therefore all require steps toward avoiding proliferation. Dry processing increases proliferation resistance by allowing the fuel material to retain a full component of fission products. The material remains highly radioactive requiring fully remote handling. Further, dry processing with enrichment permits utilization of residual Pu in fuel without complete separation [189]. Safeguarding dry fuel cycles is inherently simpler than wet fuel cycles mainly because when material is moved it is a discrete mass. Even waste and scrap are handled as discrete, tracked and weighed items [55]. Therefore, throughout the dry process, inspection and accountancy are straightforward. There is also a scale difference between the dry and wet recycle technologies. Dry recycle processes utilize relatively small scale process equipment, meaning transportation of the material is reduced to a minimum and physical security is enhanced [58, 68, 189, 200-202].

In general, dry processing for used nuclear fuel recycling is considered to be inherently more proliferation resistant than wet processing due to several factors. Dry processing requires discrete, batch treatments of used fuel, allowing for direct materials accountancy and prohibiting some of the flowsheet modifications possible in a wet recycling scheme [58]. Also, dry processing does not allow for U/Pu separations

chemistry, and all streams originating from a dry process will have fission product contamination. This means there is some level of self-protection due to radioactivity. The fission product contamination in the product stream of a dry process makes the material less desirable for diversion and easier to detect. While all of these characteristics make a dry process more proliferation resistant, the introduction of process monitoring to a dry process scheme should be considered as a safeguard and path to increase proliferation resistance. Just as UV-Visible spectroscopy can be applied as an online process monitor in a wet reprocessing scheme, Raman spectroscopy provides the same potential for dry processing of used nuclear fuel [83, 203, 204].

Dry processing reduces the attractiveness of used fuel as a weapons feedstock due to the inclusion of transuranics and fission products [68]. Qualitatively, nonproliferation assessment methodology depends on attractiveness of nuclear material, proliferation technical difficulty, proliferation time and cost along with detection probabilities. Quantitatively, values for neutron emission, heat generation, gamma emission and bare sphere critical mass can be used to assess proliferation risks, with higher values complicating weapons physics and making detection of proliferation attempts easier [205]. To improve physical security, the transuranics should be kept together as much as practical due to their higher heat, gamma and neutron emission rates, and the inclusion of U with the recycled transuranics increases the bare sphere critical mass [62]. In all dry processing scenarios the actinides are kept together, further enhancing proliferation resistance of the fuel cycle.

In the AIROX/OREOX scheme, approximately 40-60% of the fission product radioactivity escapes as volatile materials [201]. The remaining fission products and

minor actinides in used fuel provide substantial decay heat and self-protect with alpha, beta, gamma and neutron emitters (self protection criterion of 1 W of gamma power or 1 Sv/h at 1 meter) [206, 207]. In addition to meeting the self-protection requirement, the material itself is more easily detected than various HEU and  $^{239}\text{Pu}$  sources due to the presence of multiple sources of radiation. In the event of a diversion of fast reactor used fuel, any PUREX type processing plant would need to be physically modified to meet more stringent criticality limits and provide for greater heat removal in order to perform separations on the material [55].

In a comparison study with MOX, PWR once through, and PWR/MOX combination used fuel, the DUPIC/dry processed fuel was considered to be the most proliferation resistant [57, 58]. Among these used fuels, MOX contains the largest Pu per MTHM, with DUPIC containing the lowest fissile Pu content. Dry processed fuel with a high Pu content has the highest dose rate of the used fuels under consideration here. This means that shielding would be necessary during all phases of diversion of this material [200]. Another study quantitatively examined proposed protracted and abrupt proliferation scenarios for dry processing. Material is diverted over several months in the protracted case and days or weeks in the abrupt case [64]. Again, for any diverted used fuel powder from dry processing, further reprocessing facilities would be necessary to recover pure Pu. Using IAEA units and criterion to look at a protracted diversion scenario: to obtain 8 kg of Pu in 3 months, 2-3 PWR assemblies or 50 CANDU bundles would be necessary. On top of requiring a PUREX facility to process the diverted materials, sophisticated remote operation would be necessary to divert powder from the hot cells. Additionally, the high temperature furnaces and controlled atmospheres would be disrupted and the

accountancy systems would be disturbed, all increasing the probability of detection. The diverter could not extract the Pu from the powder while still in the hot cell as the aqueous reagents required would be incompatible with AIROX/OREOX cell designs. This would certainly disrupt temperatures, controlled atmospheres and accountancy systems. In addition, during a protracted diversion attempt, the transport of small amounts of used fuel material over a long period of time would be fairly easy to detect due to the high radiation field. An abrupt diversion scenario would mean diversion of 8 kg of Pu in approximately 1 MT of material in the process line. This is a considerable mass and volume of material and its loss would be readily detectable by mass balances, pressure changes, off-gas systems, or other methods [201].

#### 6.5.1 Raman spectroscopy for dry process monitoring

An evaluation of the elemental makeup of the waste and recycling streams from dry processing is used to identify potential targets for process monitoring. Due to their relatively high concentration in used nuclear fuel, elements considered as candidates for process monitoring through online Raman spectroscopic measurements are shown in Table 22.

**Table 22:** Selected elements in used nuclear fuel and relative concentrations

>1000 g/MT UNF	>100g/MT UNG but <1000 g/MT UNF
Xe, Cs, Nd, Mo, Ru, Tc	Te, Pd, Rh, Rb, Sm, I, Kr, Gd, Eu, C, Ag, Ba, Cd, Ce, La

Raman spectroscopy has been used for process monitoring in fields such as pharmaceuticals, agrochemistry and quality control [81, 82, 208, 209]. Also, in the quality control of commercial pesticide formulations, vibrational spectroscopy has been

used for the quantitative analysis of certain formula components. These techniques are used because of the short analysis time, non-destructive nature, accuracy and opportunity for direct analysis of solid and aqueous samples, similar to UV-Visible spectroscopy. Therefore, it follows that Raman spectroscopy is also quite relevant to these process monitoring and safeguards in reprocessing studies and can be applied to a dry process or even a wet reprocessing scheme. The investigation of Raman spectroscopy as a process monitor is meant to augment the proposed UV-Visible spectroscopy safeguards work.

Fiber optic samples probes, compact designs, high efficiency detectors and fast electronics all allow for Raman spectroscopy to be used for real-time, multi-component chemical analysis, as in this proposed application of process monitoring. Raman requires no sample preparation, can be used noninvasively to test materials in containers, requires minimally trained personnel and as water is a weak Raman scatterer, aqueous solutions can be analyzed along with the gaseous and solid phases [83, 128, 203, 204]. Raman spectroscopy of aqueous solutions has been reported in conditions greater than 180 °C [209], which is relevant to the application to used fuel processing as the waste and product streams coming out of a dry process will inherently be above room temperature (400-1800 °C). Raman experimental spectra have also been shown, in ideal situations, to have excellent agreement with theoretical calculations, indicating a possible avenue for continued research and development of this subject [209]. Near Infrared (NIR) was used in a process monitoring application to probe an In-Sn-oxide etching solution, and in this case the spectroscopic monitoring was actually achieved directly through existing Teflon lines [84]. Naturally, the nuclear industry would prefer not having monitoring or safeguards equipment interfere directly with process flow [210], so any spectroscopy that

can be achieved without perturbing the system under consideration will be favored. Even if a slipstream is necessary, the ability to spectroscopically probe a system without removing samples from the gaseous or liquid solution, and therefore without opening up a potential avenue for diversion, is highly valuable.

As for monitoring of the actinide-rich recycled stream from a dry process, U chemistry has been researched extensively due to its mining industry and nuclear fuel reprocessing. In mining, a variety of uranyl minerals have been studied with Raman, NIR and IR spectroscopy [211]. Uranyl's IR spectra are found to be complex. However, coupling multiple spectroscopic methods allows for elucidation of spectral results [212]. A variety of uranyl nitrate complexes in solid and solution phases have been studied with IR and Raman spectroscopy. The degree of dentateness, IR and Raman vibrational frequencies in both solid and in CCl<sub>4</sub> and CH<sub>3</sub>OH have are reported for the uranyl nitrate tributyl phosphine oxide complex (UO<sub>2</sub>(NO<sub>2</sub>)·2TBPO, Table 23) [213]. Specifically, the bands associated with the vibrations of the nitrate groups are isolated in IR spectra, and the resulting structure of the coordination sphere of uranyl is extrapolated. Similar to TBP, TBPO can be used as a ligand for transition metal separations.

**Table 23:** Vibrational frequencies ( $\text{cm}^{-1}$ ) of  $\text{UO}_2(\text{NO}_2)_2\cdot 2\text{TBPO}$  [213]

Solid		Solution in $\text{CCl}_4$	Solution in $\text{CH}_3\text{OH}$
IR	Raman	IR	IR
		2930, 2920, 2885	
1530, 1505	1527, 1507		1525
1398, 1355, 1300	1452, 1314	1480, 1465, 1402, 1380, 1345	1465, 1400, 1380, 1345, 1305
1290, 1275		1280	1270
1230, 1220, 1098	1108	1225, 1110	1225, 1120
1020, 1070	1096, 1076	1100	1070
1052	1056	1050	1050
1030	1032	1030	1025
965		965	965
923, 918		930	930, 925
903	900, 905	903	905
	866, 842		845
825	823		
808, 810			810
745, 740		752	745
720			725
470, 450, 440, 420		480, 465	
380, 375		390	395
259, 250			
200	202		

Previous to this work, Raman spectra for  $\text{UO}_2(\text{NO}_3)_2\cdot 6\text{H}_2\text{O}$  and  $\text{UO}_2(\text{ClO}_4)_2\cdot 7\text{H}_2\text{O}$  solids and aqueous salt solutions were reported over a wide range of solution composition. The lack of ion-pair formation was noted in uranyl perchlorate as was the weak complex of uranyl nitrate [49, 92, 105, 214]; for reference, molecules of  $[\text{UO}_2(\text{NO}_3)_3]^-$  and  $[\text{UO}_2\text{Cl}_4]^{2-}$  are shown in Figure 57 and Figure 58. Raman depolarization experiments indicated monodentate and bidentate linkage of nitrate to uranyl [214]. Electron redistribution in the uranyl nitrate complexes resulting in large changes in the molar scattering efficiencies of the nitrate modes, which, combined with the spectral information on dentateness, indicates the potential of this type of

spectroscopy for online process monitoring of dry and wet used fuel reprocessing streams.

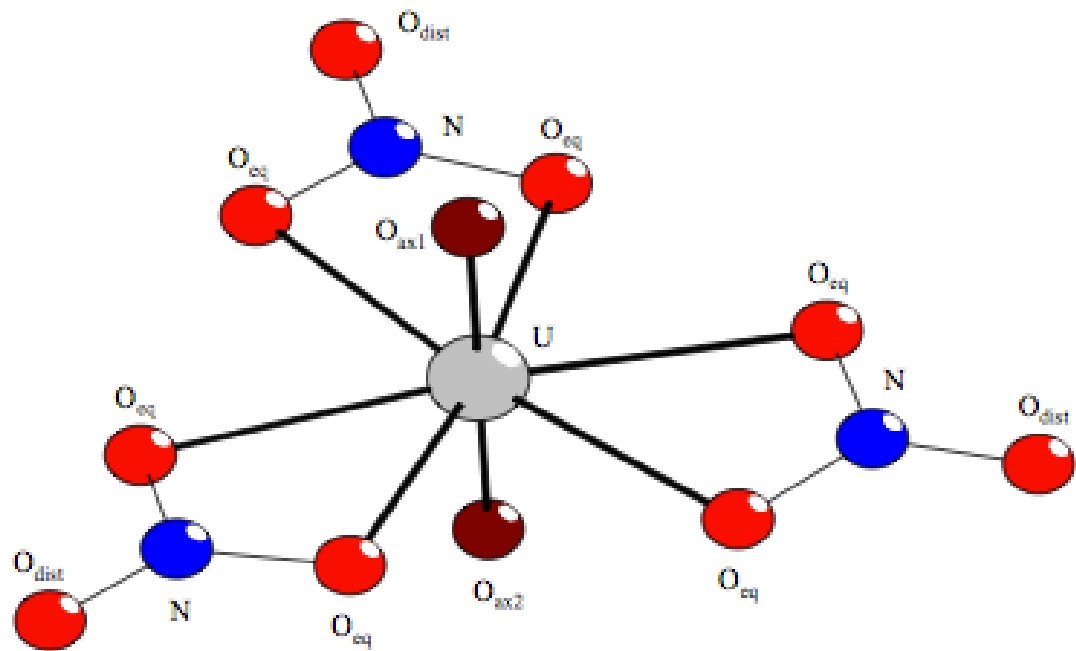


**Figure 57:**  $[UO_2(NO_3)_3]^-$  molecule [14]

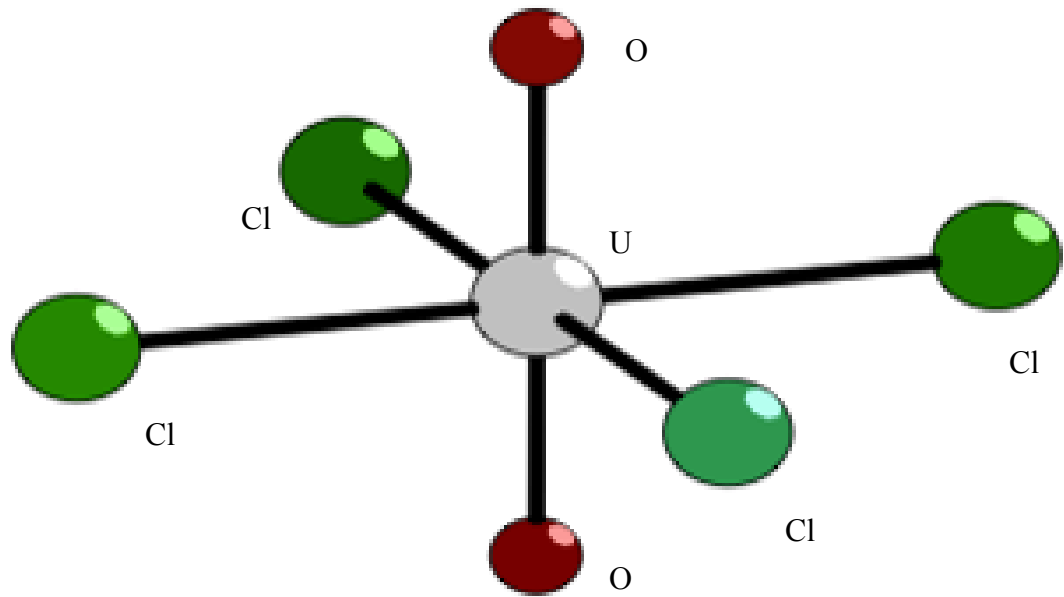


**Figure 58:**  $[UO_2Cl_4]^{2-}$  molecule [14]

Together, Raman and NIR spectroscopies can be complementary process analytical technology tools and previous work on uranyl nitrate in aqueous and organic media have been reported [83, 203, 211]. These fast, noninvasive, nondestructive techniques were used to provide online monitoring of a freeze-drying process. Both Raman and NIR measurements were taken in a freeze dryer chamber, with the resulting spectra analyzed with both principal component analysis and multivariate curve resolution. The importance of the positions of the probes was demonstrated, as certain positioning of the NIR probe resulted in saturated Raman spectra, and the complementary nature of the techniques allowed for mutual confirmation of online monitoring results [83].

Raman spectroscopy has also been used in analysis of gaseous phases including relevant lanthanides and fission products [128, 130, 204, 215-220]. Raman spectra of the trivalent lanthanide sesquioxalates were reported. From the results, information on metal-ligand coordination, lanthanide contraction and changes in the coordination of water molecules was obtained [204]. Again, this approach is directly relevant and parallels the suggested method of utilizing Raman, NIR and IR spectroscopies as complements to existing UV-Visible spectroscopy work and as online process monitors. The goal is to produce a reprocessing flowsheet with techniques and spectroscopically active species identified throughout for online monitoring, safeguards and process control. Methods of principal component analysis and multivariate curve resolution must then be used to analyze the spectroscopic data and provide meaningful, real-time information relevant to process streams. Using polarized Raman data and the depolarization ratio (DPR) appears promising as a way to extract more molecular

information. The DPR is the intensity ratio between the perpendicular component and the parallel component of the Raman scattered light, and thus is sensitive to molecular properties and insensitive to sample and experimental variations. For dispersive vibrational modes, a wavenumber-dependant change of the DPR may result from a small energy shift of an allowed electronic transition [208]. These analysis approaches must be investigated further in order to propose a more detailed plan for using Raman, NIR and IR data to obtain useful molecular information from used fuel reprocessing.

## 6.6 Classification of dry processed waste products

In order to provide a comprehensive analysis of the proposed EM<sup>2</sup> flowsheet for treatment of used fuel, the classification for the waste stream from recycling must be investigated. As the exact flowsheet has not been experimentally tested, possible variations in waste stream composition and resulting benefits and/or drawbacks in waste classification are also discussed.

The regulatory framework for classification of waste is largely governed by the Nuclear Waste Policy Act, however other regulations such as the Atomic Energy Act, the Uranium Mill Tailings Radiation Control Act, the Code of Federal Regulations (10CFR40.4, 10CFR61.55, 10CFR61.56), the Low Level Waste Policy Act, the Resource Conservation and Recovery Act, the EPA and the NRC all play parts in nuclear waste classification and management [221]. The Nuclear Waste Policy Act of 1982 states that highly radioactive material resulting from reprocessing of spent nuclear fuel is high level waste and as such must be stored in a repository. If not classified as high level waste, nuclear waste is classified according to 10 CFR 61.55 text and tables, which demonstrate the complexity and comprehensiveness of waste classification guidelines [222].

U recovery from UNF can reduce the mass of waste and possibly the number of waste packages that require geologic disposal. Recycle of all TRU reduces long term environmental burden, reduces heat load to repositories, extracts more energy from the original U ore and has significant proliferation resistance and physical security advantages. Recovery of the short lived (half lives approximately 30 years) fission products  $^{137}\text{Cs}$  and  $^{90}\text{Sr}$  can allow them to be managed separately due to their high decay heat and activity, likely decaying to LLW in facilities tailored to that need, rather than geologic disposal. Recovery of the dominant and long-lived  $^{99}\text{Tc}$  and  $^{129}\text{I}$  can allow them to be sent to a geologic disposal in improved waste forms (i.e. borosilicate glass). Transmutation of Tc and I is also an alternative. For LWR UNF, recycling the actinides can reduce the mass of waste by a factor of 20, with HLW volume reduced by keeping long lived contaminants such as Tc and I out of short lived wastes. Pu and Am comprise about 90% of the long-term heat commitment in a repository, and removing them along with the TRUs, Cs and Sr would reduce the commitment by a factor of 100 [62].

In 1987, the NWPA was amended, selecting Yucca Mountain as the geologic repository site. While specific limits for Yucca Mountain are discussed here, any proposed repository design will include statutory capacity limits, dose limits and space capacity limits. Yucca's statutory capacity is 70,000 MTHM, and the technical space capacity limits are undetermined as they are based on mass of the waste, volume of waste packaging, tunnel wall temperature and temperature in the rock between tunnels. Temperatures for the technical space capacity should be considered from decades to centuries [62]. Yucca's proposed dose limits are 15 mrem/yr from when waste is emplaced to 10,000 years, and 350 mrem/yr from 10,000 years to 1,000,000 years.

Radiotoxicity and mobility factor in to calculating potential contribution to dose limits, with  $^{99}\text{Tc}$  and  $^{129}\text{I}$  being the main examples of more mobile but less radiotoxic component of used nuclear fuel.

While these guidelines are extremely intricate and dependent on waste isotopic composition and radioactivity, wasteform, wasteform loading and mixing of radionuclides, several studies have attempted to determine the classification of AIROX-produced wastes. Included in the extensive laboratory testing of AIROX as applied to the LWR fuel cycle in the early 1960s, a fuel cycle picture, complete with hypothetical AIROX processing plant and resulting waste streams, was developed. In this scheme, used LWR hardware and cladding would be Greater Than Class C (GTCC) waste due to  $^{59}\text{Ni}$ ,  $^{61}\text{Ni}$  and  $^{94}\text{Nb}$  and would be crushed/melted into ingots for disposal. Isotopes such as  $^{129}\text{I}$  would be trapped and stored for transmutation. Recovered noble fission product gases would be trapped in a similar fashion to that of I, then be cryogenically distilled, bottled and stored, prior to LLW disposal.  $^3\text{H}$  and  $^{14}\text{C}$  would also be trapped in a manner similar to that of I, then combined and immobilized in cement or grout wasteform as LLW. Any remaining mixture of  $\text{I}_2$ , Xe, or Kr would be passed over a heated bed of silver-impregnated zeolite to chemisorb silver iodide/iodate. The remaining Xe and Kr would then be passed through a cryogenic distillation unit to condense from the Ar carrier gas. Semivolatiles would be recovered by high temperature metal filters and high temperature HEPA filters, then immobilized together in a borosilicate glass waste form as GTCC waste with all of the used  $\text{UO}_2$  recycled and reconstituted in process. Assumptions include 100% volatilization of  $^3\text{H}$ , Kr, Xe, I and C, 90% removal of semivolatiles  $^{134}\text{Cs}$ ,  $^{137}\text{Cs}$  and  $^{106}\text{Ru}$ , and 75% removal of Te, Cd, and In (volatilized

during pellet sintering). This study also modeled an AIROX plant with capacity of 200 MTIHM/yr with 0.9 MTIHM/day processing, where the production rate of new PWR and BWR assemblies would be 1.5 and 1.8 assemblies/day, respectively. The resulting wastes, per MTHM used fuel and at the end of one year of operation, are summarized in Table 24.

**Table 24:** Resulting wastes from AIROX plant [57]

Quantity/MTHM UNF	Composition	Waste type	Form	After 1 year
0.29 MT	Cladding and hardware	GTCC	Ingot	145 MT
0.103 MT	Semivolatiles	GTCC	Glass	30.5 canisters
41 moles	K and Xe	Cylinder storage	Gaseous	330 cylinders
0.19 m <sup>3</sup>	<sup>14</sup> C	LLW	Concrete	5000 drums
1.89 m <sup>3</sup>	Rags, ash, etc.	LLW	Trash	
221 g	I	LLW	Zeolite	0.6 m <sup>3</sup>

For all of the flowing systems, the use of low off-gas flow rates and Ar as carrier would be highly advantageous for designing off-gas cleanup system. Approximately 1 drum of LLW per MTHM would be generated from process off-gases [57]. Overall, while AIROX-processed fuel would have approximately twice the decay heat of conventional fuel, there would be one half of the number of AIROX-recycled used fuel assemblies and several orders of magnitude less HLW waste.

For disposal paths, any radioactive waste that does not qualify as LLW would go to a federal repository, and extra care should be taken to minimize this waste stream (GTCC and HLW). Investigations into recycling of cladding and hardware could yield a reduction in HLW and higher heat loadings for GTCC glass wasteforms would be

possible if Cs was allowed to decay (must compare cost of storage and decay time vs. direct disposal of GTCC).  $^{129}\text{I}$  could be disposed of as LLW or as GTCC, but due to water transport mechanisms,  $^{99}\text{Tc}$  and  $^{129}\text{I}$  are estimated to account for more than 99.99% of hypothetical population dose from repository [57].

## 6.7 Conclusions

A flowsheet to recycle used LWR and used EM<sup>2</sup> fuel via dry processing was developed based on previous literature (Figure 55). It is expected that the volatile fission products are released during processing, and some of the semivolatile fission products are released during higher-temperature pellet sintering [57]. Medium and low-volatility fission products generally remain in the fuel along with the actinides (Section 6.2). The waste stream from the flowsheet was characterized in order to provide a comprehensive analysis of the EM<sup>2</sup> fuel cycle.

Benefits of the dry processing scenario proposed in this chapter include waste volume minimization, avoiding the production of high level liquid waste streams, reduced U demand allowing extension of U reserves and increasing the proliferation resistance and nuclear security of the U.S. nuclear fuel cycle [58]. Proliferation resistance is increased due to the discrete nature of a dry process, lack of chemical separation of Pu, utilization of a hot cell for all processing and the accelerated buildup of  $^{238}\text{Pu}$ . Although the need for a repository does not disappear with dry processing, the waste radiotoxicity is reduced, diminishing potential environmental release and public exposure [57]. In the event that further separations beyond dry processing are desired in the future, reducing the amount of fuel requiring chemical separation could lead to simplified aqueous or pyrochemical reprocessing approaches that could be integrated directly into the dry

processing fuel cycle [189]. Additionally, one study has found that in fuel cost analysis, dry processing with zone separation based on fuel location in the core (and thus burnup) reduces fuel cost as compared with the once through cycle [202]. The dry processing fuel cycle is an advanced concept to meet ever-increasing energy demands while addressing nonproliferation concerns and reducing waste management burdens [223].

All of these benefits are accomplished in a highly proliferation-resistant manner as the dry processes do not allow U/Pu or isotopic separations and yield self-protecting product and waste streams. Additionally, the process design that cannot be easily manipulated to allow SNM separations, so a clandestine reprocessing plant would be necessary following a diversion in order to extract pure U or Pu. The addition of Raman spectroscopy as a process monitor of both the waste and recycled streams of a dry process further the robust safeguards in this system. As Raman spectroscopy has already been used as a process monitor in other industries, has been applied to fission product, actinide and lanthanide elements and is a commonly used laboratory technique, its application in this scenario is straightforward. Depending on experimental results, the EM<sup>2</sup>-based dry processing fuel cycle may offer a reduction of used fuel generated per kWe as compared with the current open fuel cycle and is may be more proliferation resistant than closed fuel cycles utilizing wet reprocessing technologies.

## 6.8 Future work

Experimental testing of the discussed processes needs to be performed. While much research has been conducted on dry processing technologies, disagreements are in the literature. Laboratory experiments are needed to resolve this issue. To begin, this should consist of preparing simulated used fuel and analysis of the volatility of its components

[224]. Following successful demonstration of concepts at the laboratory scale, larger scale experiments with simulated used fuel and then actual used fuel can be demonstrated. Similarly, the development of the Raman spectroscopic process monitor can follow the laboratory-to-bench-scale path forward.

In addition to evaluating experimental parameters such as temperature, carrier gas, time at temperature, and temperature ramp rate, several other areas should be investigated. The actual composition of individual LWR used fuel bundles will be dependent on reactor type, burnup, cooling time and any unique storage or pretreatment steps. The transition from the oxide-based to carbide-based dry processing regime should be explored. Carbide fuels react rapidly with oxygen and moisture. The Gibbs free energy for the possible reactions at room temperature is negative, as expected, since often UC samples must be handled and stored under moisture-free inert atmosphere [225]. Therefore, while the application of oxide-based separations processes to the EM<sup>2</sup> carbide fuels must be proven, no technical issues are expected.

In the same vein, all previous dry processing studies have utilized the fuel pellet and rod design common to LWRs, not the EM<sup>2</sup>-specific fuel design. The application of dry processing to EM<sup>2</sup> UNF must be proven. However, as long as a large fuel surface area can be obtained for interaction with the various oxidizing and reducing conditions, no concerns should arise. An approximate goal for the recycle of EM<sup>2</sup> UNF is the removal of 60% reactivity. Reactivity is a parameter that characterizes a reactor's deviation from criticality and is a function of UNF isotopic composition and related interaction cross sections. Determination of several possible conditions yielding 60% reactivity removal (i.e. sample percentages of isotopes present) will allow for consideration of multiple

options of dry processing and may result in higher waste reduction abilities and/or more favorable economics.

One issue that is mentioned sparsely in the literature is the effect that fissile/fertile distribution in the used fuel has on the temperatures at which volatilization occurs. In the LWR thermal neutron flux, the outer portion of the fuel pellet shields the central portion of the pellet, resulting in a substantially higher Pu content in the outer restructured zone. In the fast neutron regime, the flux is essentially constant across the pellet which results in a much higher temperature near the pellet center. In stoichiometric fuel, Pu has been shown to migrate up the thermal gradient, yielding a much higher concentration in the center of used fast fuel. In addition to this Pu inhomogeneity, restructuring of the fuel occurs in the high temperature region, leaving relatively unstructured fuel in the lower temperature region. In dry processing, restructured fuel pulverizes into larger particles than the unrestructured fuel, and combined with the Pu migration with this restructuring phenomenon, the larger particle fraction will have much higher fissile content [202]. Successive dry processing should continue to increase the fissile content of recycled fuel, but the effect of the restructuring and Pu migration on dry processing removal fractions should be explored further. Lastly, a cost analysis should be conducted to compare HLW reduction and resulting decrease in repository space requirements with the hotter used fuel that will eventually be produced in the higher burnup, dry recycle case [57, 226]. In general, keeping waste classified as LLW is desired as it is less costly to dispose of than HLW or mixed waste. Likely development beyond laboratory scale is necessary to develop an accurate cost-benefit scheme.

## CHAPTER 7

### CONCLUSIONS

Demonstrated concepts for spectroscopic process monitoring for safeguards in used nuclear fuel recycling scenarios are presented in this dissertation. Relevant background information such as the composition of discharged fuel, used nuclear fuel treatment methods and previous research on process monitoring for safeguards is reviewed. UREX, TRUEX and dry processing used fuel treatment methods are evaluated specifically, and opportunities for process monitoring by applications of spectroscopic techniques identified.

#### 7.1 Process Monitoring Under UREX Conditions

In order to detect a process change from the UREX to PUREX flowsheet, differences in their chemistry are presented, along with corresponding UV-Visible spectroscopy for application in process monitoring for safeguards. UREX uses the same basic solvent extraction flowsheet as PUREX, but has a lower acid concentration throughout and adds AHA as a complexant/reductant to the feed solution to prevent the extraction of Pu [39]. By evaluating the impact of process conditions, such as acid concentration, metal concentration and flow rate, on the sensitivity of the UV-Visible detection system, the process-monitoring concept is developed from an advanced application of fundamental spectroscopy. Systematic benchtop-scale studies investigated the system relevant to UREX or PUREX type reprocessing schemes, encompassing 0.01-1.26 M U and 0.01-8 M HNO<sub>3</sub>. Based on this foundation, a laboratory-scale UREX experiment was performed. A fiber optic dip probe for UV-Visible spectroscopy was integrated into a

bank of three counter-current centrifugal contactors to demonstrate the online process monitoring concept. Nd, Fe and Zr were added to the uranyl nitrate system to explore spectroscopic interferences and identify additional species as candidates for online monitoring. Changes in metal concentration and solution chemistry were successfully detected in a counter current contactor system with a UV-Visible spectroscopic process monitor. This milestone is a demonstration of the potential of the developed spectroscopic technique which lies in the ability to simultaneously and directly monitor the chemical process conditions in a reprocessing plant, providing inspectors with another tool to detect nuclear material diversion attempts.

Future work in the UREX regime includes addition of more fission products, actinides and lanthanides, followed by a scale up to actual expected metal concentrations. UV-Visible spectroscopic investigations can be expanded to the organic phase, and perhaps online process monitors inserted between contactors for materials tracking through the contactor bank. It should be noted that many UNF solvent extraction flowsheets in the U.S. and abroad are similar to UREX, therefore much of the work discussed here could be extrapolated and applied to other TBP-nitric acid extraction systems [40, 41]. A solvent extraction code such as AMUSE can be used to provide a model for further flowsheet demonstrations, and thus give a guideline for expected aqueous product compositions and extraction efficiencies. The presence of foam in the countercurrent contactor system is an issue that needs to be resolved as all solvent extraction studies are based upon liquid-liquid interactions, however this likely requires an engineering and design modification from the contactor vendor. Collaborations with other CINC V-02 contactor users could help elucidate specific design changes to alleviate

foam production.

## 7.2 TRUEX Experiments

An evaluation of the performance of the TRUEX process in a 30 stage centrifugal contactor pilot plant has been completed. The overall equipment operation, actual flowsheet performance including steady-state data, removal efficiencies, individual stage mass transfer efficiency, as well as temperature profiles were measured and reported. Overall the flowsheet performed as expected, and all equipment operated as designed. Metal concentration data indicate the cascade was operating at steady-state condition within twenty minutes. Removal efficiencies indicate > 99.9% of the Ce, La, Eu, and Nd was partitioned to the strip product stream. The Cs and Sr separation was negligible as these metals were not extracted by the TRUEX solvent. The calculated removal efficiency for Zr indicates that ~ 0.6 % of the metal may have extracted. Organic phase foaming was observed in the light phase interstage tubing almost immediately after solvent flow had begun, with the expected cause being high rotor speed causing air to be mixed with solvent. Other causes of foaming are high solvent flowrates or if the contactors are inadequately vented. Individual stage mass transfer efficiency results ranged from 85 % to 95 % in selected extraction stages and from 59-100 % in selected strip stages. Temperature profile graphed data for the TRUEX flowsheet testing agreed with previous temperature profile data reported using a lamp oil/water solvent pairing at ambient solution operating temperature.

Lessons learned from the TRUEX test include slight physical changes to the contactor setup such as employing a steeper angle flow path between contactors and an adjustment of offgas outlets to minimize foaming. Through the TRUEX experimental

demonstration, these improvements can be incorporated into the contactor system and following flowsheet tests for demonstration of online process monitoring. The foaming issues and anomalies in stage mass transfer efficiencies show that further flowsheet testing is warranted. These issues, along with the temperature profile, can be used as the basis for further research and analysis of flowsheet data such as from the UREX demonstration.

### 7.3 Dry processing flowsheet and safeguards approach

Dry processing of used nuclear fuel is often used as a head-end step before solvent extraction-based separations such as UREX or TRUEX [13, 42, 43]. Reconstituting used LWR and used EM<sup>2</sup> fuel via dry processing is technically feasible. Literature suggests that the volatile fission products (Kr, Xe, I, <sup>3</sup>H) are released during processing, and some of the semi-volatile fission products (Cs and Ru) are released during pellet sintering. Medium and low-volatility fission products (Ba, Sr, Fe, La, Pd, Zr) generally remain in the fuel along with the U, Pu and actinides. Proliferation resistance is increased due to the discrete nature of a dry process, lack of chemical separation of Pu, utilization of a hot cell for all processing and the accelerated buildup of <sup>238</sup>Pu which makes the used fuel isotopically less desirable. The addition of Raman spectroscopy as a process monitor of both the waste and recycled streams of a dry process may further the robust safeguards in this system. As Raman spectroscopy has already been used as a process monitor in other industries, has been applied to fission product, actinide and lanthanide elements and is a commonly used laboratory technique, its application in this scenario is expected to be straightforward.

Future development work should include experimental testing AIROX recycling of used nuclear fuel both from LWRs and EM<sup>2</sup>. Following successful recycling tests, AIROX-recycling of high burnup used fuel should also be examined. In both cases, trapping technologies for volatilized fission products should be evaluated, as well as the integration of process monitoring for safeguards requirements. In addition to evaluating experimental parameters such as temperature, carrier gas, time at temperature, and temperature ramp rate, several other areas should be investigated. The actual composition of individual LWR used fuel bundles will be dependent on reactor type, burnup, cooling time and any unique storage or pretreatment steps. The transition from the oxide-based to carbide-based dry processing regime should be explored. In the same vein, all previous dry processing studies have utilized the fuel pellet and rod design common to LWRs, not the EM<sup>2</sup>-specific fuel design. An approximate goal for the recycle of EM<sup>2</sup> UNF is the removal of 60% reactivity (parameter describing proximity to criticality). Determination of several possible conditions yielding 60% reactivity removal will allow for consideration of multiple options of dry processing and may result in higher waste reduction abilities and/or more favorable economics.

## NOMENCLATURE

AIROX	Atomics International Reduction Oxidation
CANDU	Canadian Deuterium Uranium
CARDIO	Carbon Dioxide oxidation
CMPO	Octyl (phenyl)-N,N-diisobutylcarbamoyl-methylphosphine oxide
CFR	Code of Federal Regulations
DUPIC	Direct Use of PWR In CANDU
EM <sup>2</sup>	Energy Multiplier Module
GTCC	Greater Than Class C
HEU	High Enriched Uranium
HLW	High Level Waste
HM	Heavy Metal
ICP-AES	Inductively Coupled Plasma Atomic Emission Spectroscopy
ICP-MS	Inductively Coupled Plasma Mass Spectrometry
IFR	Integral Fast Reactor
LLW	Low Level Waste
LEU	Low Enriched Uranium
LWR	Light Water Reactor
MA	Minor Actinides
MOX	Mixed OXide
MTHM	Metric Tonnes Heavy Metal
MTU	Metric Tonnes Uranium
MWd/GWd	Megawatt-day/Gigawatt-day
O/A	Organic to Aqueous ratio
OREOX	Oxidation Reduction
PWR	Pressurized Water Reactor
REM	Roentgen Equivalent Man
SNF	Spent Nuclear Fuel
SNM	Special Nuclear Material
SQ	Significant Quantity
SRNL	Savannah River National Laboratory
TBP	TriButyl Phosphate
TGA-MS	Thermal Gravimetric Analyzer Mass Spectrometry
TRU	TRansUranic
TRUEX	TRansUranic EXtraction
UNF	Used Nuclear Fuel
UREX	URanium EXtraction
UV-Vis	UltraViolet-Visible spectroscopy

## REFERENCES

1. Lascola, R.; Sharma, V. Application of Absorption Spectroscopy to Actinide Process Analysis and Monitoring. *Plutonium Futures - The Science Proceedings*, Keystone, CO, September 19-23, 2010, 2010.
2. Lascola, R. J.; Livingston, R. R.; Sanders, M. A.; McCarty, J. E.; Cooper, G. A. *On Line Spectrophotometric Measurement of Uranium and Nitrate in H Canyon*; WSRC-TR-2002-00334; 2002.
3. Lascola, R. J.; Cooper, G. A. *Feasibility of Uranium Concentration Measurements for H Canyon Tank 16.7*; Westinghouse Savannah River Company: Aiken, SC, 2002.
4. Lascola, R.; Livingston, R. R.; Sanders, M. A.; McCarty, J. E.; Dunning, J. L. Online Spectrophotometric Measurements of Uranium and Nitrate Concentrations of Process Solutions for Savannah River Site's H-Canyon. *Journal of Process Analytical Chemistry*. 2002, 7 (1), 14-20.
5. Van Uffelen, M.; Jucker, P.; Fenaux, P. Radiation resistance of fiberoptic components and predictive models for optical fiber systems in nuclear environments. *IEEE Trans.Nucl.Sci.* 1998, 45 (3 pt 3), 1558-1565.
6. Evans, B. D.; Sigel Jr., G. H. Radiation Resistant Fiber Optic Materials and Waveguides. *IEEE Transactions on Nuclear Science*. 1975, NS-22 (6), 2462.
7. Peters, M. T. Advanced Nuclear Fuel Cycles Presentation (unpublished). Argonne National Laboratory, 2008.

8. Deutch, J. M.; Forsberg, C. W.; Kadak, A. C.; Kazimi, M.; Moniz, E. J.; Parsons, J. E. *Update of the MIT 2003 Future of Nuclear Power*; Massachusetts Institute of Technology: Cambridge, MA, 2009.
9. Kazimi, M.; Moniz, E. J.; Forsberg, C. W.; Ansolabehere, S.; Deutch, J. M.; Driscoll, M. J.; Golay, M. J.; Kadak, A. C.; Parsons, J. E.; Regalbuto, M. C.; Apostolakis, G.; Hejzlar, P.; Shwageraus, E. *MIT Study on the Future of the Nuclear Fuel Cycle*; Massachusetts Institute of Technology: Cambridge, MA, 2010.
10. Rohlf, T.; Van Schepen, B.; Zmolek, L. Nuclear Power.  
<http://wiki.uiowa.edu/display/greenergy/Nuclear>, May 29, 2011.
11. Edwards, C. R.; Oliver, A. J. Uranium Processing: A Review of Current Methods and Technology. *Journal of the Minerals, Metals and Materials Society*. 2000, 52 (9), 12-20.
12. Mittag, S.; Kliem, S. Burning plutonium and minimizing radioactive waste in existing PWRs. *Annals of Nuclear Energy*. 2011, 38 (1), 98.
13. Paviet-Hartmann, P.; Benedict, B.; Lineberry, M. J. Nuclear Fuel Reprocessing. *Nuclear Engineering Handbook*, CRC Press, Taylor and Francis Group: USA, 2009; 317.
14. Chandler, S. Thesis: Comparison of Reprocessing Methods for Light Water Reactor Fuel. Master of Science, Georgia Institute of Technology, 2006.
15. Selvaduray, G.; Goldstein, M. K.; Anderson, R. N. Survey of nuclear fuel reprocessing technologies. *CONSERV.RECYCL.* 1979, 3 (2), 93-134.

16. Kobayashi, H.; Amano, O.; Kawamura, F.; Aoi, M.; Hoshino, K.; Sasahira, A.; Kani, Y. Fluorex reprocessing system for the thermal reactors cycle and future thermal/fast reactors (coexistence) cycle. *Prog.Nucl.Energy.* 2005, *47* (1-4), 380-388.
17. Navratil, J. D.; Wei, Y. Z. Actinide ion exchange technology in the back end of the nuclear fuel cycle. *Nukleonika.* 2001, *46* (2), 75-80.
18. Hwang, Y. S.; Kang, C. H.; Kim, S. G.; Park, H. S. Progress of radioactive waste management in Korea. *Prog.Nucl.Energy.* 2003, *42* (2), 159-177.
19. The U.S. Department of Energy's Office of Nuclear Energy Fuel Cycle Research and Development. May 20, 2011.  
[http://www.ne.doe.gov/pdfFiles/factSheets/2012\\_FCRD\\_Factsheet\\_final.pdf](http://www.ne.doe.gov/pdfFiles/factSheets/2012_FCRD_Factsheet_final.pdf)
20. Mullen, M. Nuclear Energy R&D Objective 4: Understanding and Minimizing the Risks of Nuclear Proliferation and Terrorism. *Materials Protection and Control Technology Working Group Meeting*, Gaithersburg, MD, September 15-16, 2010.
21. Orton, C. R.; Fraga, C. R.; Christensen, R. N.; Schwantes, J. M. Proof of concept simulations of the Multi-Isotope Process monitor: An online, nondestructive, near-real-time safeguards monitor for nuclear fuel reprocessing facilities. *Nuclear Instruments and Methods in Physics Research Section A: Accelerators, Spectrometers, Detectors and Associated Equipment.* 2011, *629* (1), 209-219.
22. Holdren, J. P. Radioactive-Waste Management in the United States: Evolving Policy Prospects and Dilemmas. *Annu.Rev.Energy Environ.* 1992, *17*, 235-259.

23. Kikuchi, M.; Yoshida, T.; Matsuda, M.; Kanai, H. Developing Technologies for Nuclear Fuel Cycles: Radioactive Waste Treatment and Spent Fuel Storage. *Hitachi Review*. 1999, 48 (5), 277-284.
24. U.S. Energy Information Administration Total U.S. Commercial Spent Nuclear Fuel Discharges, 2011.  
[http://eia.doe.gov/cneaf/nuclear/spent\\_fuel/ussnfdatal.html#table1](http://eia.doe.gov/cneaf/nuclear/spent_fuel/ussnfdatal.html#table1)
25. U.S. Department of Energy. *Final Environmental Impact Statement for the Disposal of Spent Nuclear Fuel and High-Level Radioactive Waste at Yucca Mountain, Nye County, Nevada, Appendix A*; 2002.
26. GE Reports The Mark I Containment System in BWR Reactors.  
<http://www.gereports.com/the-mark-i-containment-system-in-bwr-reactors/>  
November 1, 2011.
27. Buongiorno, J.; Ballinger, R.; Driscoll, M.; Forget, B.; Forsberg, C.; Golay, M.; Kazimi, M.; Todreas, N.; Yanch, J. *Technical Lessons Learned from the Fukushima-Daichii Accident and Possible Corrective Actions for the Nuclear Industry: An Initial Evaluation*; MIT-NSP-TR-025 Rev. 1; Center for Advanced Nuclear Energy Systems: Cambridge, MA, 2011.
28. AREVA; Mitsubishi Heavy Industries; Japan Nuclear Fuel Limited; Babcock & Wilcox Technical Services; Battelle Energy Technology; URS Washington Division *Integrated U.S. Used Fuel Strategy - Analyses Performed by the International Nuclear Recycling Alliance*; International Nuclear Recycling Alliance: 2008.

29. Lewis, B. J.; Corse, B. J.; Thompson, W. T.; Kaye, M. H.; Iglesias, F. C.; Elder, P.; Dickson, R.; Liu, Z. Low volatile fission-product release and fuel volatilization during severe reactor accident conditions. *J.Nucl.Mater.* 1998, 252 (3), 235-256.
30. Neeb, K. Radionuclides in the Reactor Core. *The Radiochemistry of Nuclear Power Plants with Light Water Reactors*, de Gruyter: Berlin, Germany, 1997; 66-133.
31. Agnew, S.; Garzenne, C.; Gilleland, J.; Greenspan, E.; Papay, L.; Pluche, H.; Wagoner, J.; Lebreton, P. *Potential Applications of the Archimedes Filter Technology to the Nuclear Fuel Cycle - UREX Process and UREX-AFP Process*. Unpublished, 2005.
32. Lebreton, P. *Potential Applications of the Archimedes Filter Technology to the Nuclear Fuel Cycle - Spent Nuclear Fuel Contents Hypothesis and Assessments*. Unpublished, 2005.
33. Notz, K. J.; Carter, W. L.; Kibbey, A. H. Integrated Data Base for Spent Fuel and Radwaste: Inventories. *ANS Proceedings*, Los Angeles, CA, June 6-11, 1982, 1982.
34. Notz, K. J. Characteristics of Spent Nuclear Fuel. *Fourth International Symposium on Ceramics in Nuclear Waste Management*, Indianapolis, IN, 1988.
35. Ando, Y.; Nishihara, K.; Takano, H. Estimation of spent fuel compositions from light water reactors. *J Nucl Sci Technol.* 2000, 37 (10), 924-933.
36. Campbell, D. O.; Burch, W. D. The Chemistry of Fuel Reprocessing: Present Practices, Future Trends. *J.Radioanal.Nucl.* 1990, 142 (1), 303-320.

37. Loveland, W. D.; Morrissey, D. J.; Seaborg, G. T.; *Modern Nuclear Chemistry*; Eds.; John Wiley and Sons: New Jersey, 2005.
38. Schneider, M.; Marignac, Y. *Report: Spent Nuclear Fuel Reprocessing in France*; Princeton University: Princeton, 2008.
39. Nash, K. L.; Barrans, R. E.; Chiarizia, R.; Dietz, M. L.; Jensen, M. P.; Rickert, P. G.; Moyer, B. A.; Bonnesen, P. V.; Bryan, J. C.; Sachleben, R. A. Fundamental Investigations of Separations Science for Radioactive Materials. *Solvent Extraction and Ion Exchange*. 2000, 18 (4), 605-631.
40. Selvaduray, G.; Goldstein, M. K.; Anderson, R. N.: Reprocessing and Recycling: Separation Technologies Reviewed, 35-40, 1978.
41. Regalbuto, M. C.; Copple, J. M.; Leonard, R.; Pereira, C.; Vandegrift, G. F. Solvent Extraction Process Development for Partitioning and Transmutation of Spent Fuel. *Actinide and Fission Product Partitioning and Transmutation Eight Information Exchange Meeting*, Las Vegas, NV, November 9-11, 2004.
42. Vandegrift, G. F.; Regalbuto, M. C.; Aase, S. B.; Arafat, H. A.; Bakel, A. J.; Bowers, D. L.; Byrnes, J. P.; Clark, M. A.; Emery, J. W.; Falkenberg, J. R.; Guelis, A. V.; Hafenrichter, L. D.; Leonard, R. A.; Pereira, C.; Quigley, K. J.; Tsai, Y.; Pol, M. H. V.; Laidler, J. J. Lab-Scale Demonstration of the UREX+ Process. Proceedings of *Waste Management Symposia*. Tucson, AZ, 2004.
43. Lanham, W. B.; Runion, T. C. *PUREX Process for Uranium and Plutonium Recovery*; ORNL-479; Oak Ridge National Laboratory: 1949.
44. Vandegrift, G. F.; Regalbuto, M. C.; Aase, S.; Bakel, A.; Battisti, T. J.; Bowers, D.; Byrnes, J. P.; Clark, M. A.; Cummings, D. G.; Emery, J. W.; Falkenberg, J.

- R.; Gelis, A. V.; Pereira, C.; Hafenrichter, L.; Tsai, Y.; Quigley, K. J.; Vander Pol, M. H. Designing and Demonstration of the UREX+ Process Using Spent Nuclear Fuel. *ATALANTE*, Nimes, France, 2004.
45. Rudisill, T. S.; Thompson, M. C.; Norato, M. A.; Kessinger, G. F.; Pierce, R. A.; Johnson, J. D. Demonstration of the UREX solvent extraction process with Dresden reactor fuel. *Transactions of the American Nuclear Society*, 2003.
46. Schroeder, N. C.; Attrep, M. *Technetium and Iodine Separations in the UREX Process*; Accelerator Transmutation of Waste Program WBS 1.24.01.01; Los Alamos National Laboratory: 2003.
47. Healy, T. V.; McKay, H. A. C. The Extraction of Nitrates by Tri-Normal-Butyl Phosphate (TBP) 2. The Nature of the TBP Phase. *Transactions of the Faraday Society*. 1956, 52 (5), 633-642.
48. Fedorov, Y. S.; Zilberman, B. Y.; Kopyrin, A. A.; Arkhipov, S. A. Uranium(IV) Complexes Formed in Extraction with Tributyl Phosphate from Nitric Acid Solutions. *Radiochemistry*. 2001, 43 (2), 166-171.
49. Woodhead, J. L.; McKay, H. A. C. Uranium (IV) Nitrate and Perchlorate Species in Tri-n-Butyl Phosphate Solutions. *Journal of Inorganic and Nuclear Chemistry*. 1965, 27, 2247-2254.
50. Pereira, C.; Vandegrift, G. F.; Regalbuto, M. C.; Aase, S.; Bakel, A.; Bowers, D.; Brynes, J. P.; Clark, M. A.; Emery, J. W.; Falkenberg, J. R.; Gelis, A. V.; Hafenrichter, L.; Leonard, R.; Quigley, K. J.; Tsai, Y.; Vander Pol, M. H.; Laidler, J. J. Lab-Scale Demonstration of the UREX+2 Process Using Spent Fuel. Proceedings of *Waste Management Symposia*. Tucson, AZ, 2005.

51. Wright, A. D. Thesis: Nitrate Ion Effects on Uranium Chemistry in the TBP-Dodecane System. M. S., UNLV, 2008.
52. Pereira, C. UREX+ Process Overview. Personal communication, September 19, 2008.
53. Laidler, J. J.; Battles, J. E.; Miller, W. E.; Gay, E. C. Development of IFR Pyroprocessing Technology. *Proceedings of GLOBAL 1993*, Seattle, WA, September 12-17, 1993.
54. Nash, K. L. Twenty-First Century Approaches to Actinide Partitioning. *Separations for the Nuclear Fuel Cycle in the 21<sup>st</sup> Century*, American Chemical Society: 2006; 21-40.
55. Hannum, W. H.; Wade, D.; Stanford, G. *Self-Protection in Dry Recycle Technologies*; Argonne National Laboratory: Argonne, 1995.
56. Nuclear Energy Agency. *Pyrochemical Separations in Nuclear Applications - A Status Report*; Organisation for Economic Cooperation and Development: Paris, 2004.
57. Majumdar, D.; Jahshan, S. N.; Allison, C. M.; Kuan, P.; Thomas, T. R. *Recycling of Nuclear Spent Fuel with AIROX Processing*; DOE Idaho Field Office: 1992.
58. Grantham, L. F.; Clark, R. G.; Hoyt, R. C.; Miller, J. R. AIROX Dry Pyrochemical Processing of Oxide Fuels - A Proliferation-Resistant Reprocessing Method. *ACS Symp.Ser.* 1980, (117), 219-232.
59. Baybarz, R. D.; Clinton, S. D.; Farrar, L. G.; Fitzgerald, C. L.; Haire, R. G.; Tennery, V. J.; Vaughen, V. C. A.; Watson, C. D. *Voloxidation-Removal of*

- Volatile Fission Products From Spent LMFBR Fuels*; ORNL-TM-3723; Chemical Technology Division, ORNL: Oak Ridge, Tennessee, 1973.
60. Jahshan, S. N.; McGeehan, T. J. Evaluation of the deployment of AIROX-recycled fuel in pressurized water reactors. *Nucl Technol.* 1994, *106* (3), 350-359.
  61. Allison, C. M.; Jahshan, S. N.; Wade, N. L. *Neutronics and Fuel Behavior of AIROX-Processed Fuel Recycled into Light Water Reactors*; EGG-M--93267; CONF-930913--17; EG&G Idaho, Inc., INEL: 1993.
  62. Piet, S.; Bjornard, T.; Dixon, B.; Gombert, D.; Laws, C.; Matthern, G. Which elements should be recycled for a comprehensive fuel cycle? 2007.
  63. International Atomic Energy Agency. *About the IAEA*.  
<http://www.iaea.org/About/> October 5, 2011.
  64. IAEA. *The Present Status of IAEA Safeguards on Nuclear Fuel Cycle Facilities*; IAEA Bulletin Volume 22 Number 3/4; 1980.
  65. Kang, J. Proliferation resistance of PEACER system. *Progress in Nuclear Energy*. 2007, *49*, 115.
  66. Pereira, C.; Leite, E. M. Non-proliferating reprocessed nuclear fuels in pressurised water reactors: Fuel cycle options. *Ann.Nucl.Energy.* 1998, *25* (12), 937-962.
  67. Hannum, W. H.; Wade, D. C.; Mcfarlane, H. F.; Hill, R. N. Nonproliferation and Safeguards Aspects of the IFR. *Progress in Nuclear Energy*. 1997, *31* (1/2), 203.
  68. Bari, R.; Cheng, L. Y.; Phillips, J.; Pilat, J.; Rochau, G.; Therios, I.; Wigeland, R.; Wonder, E.; Zentner, M. Proliferation Risk Reduction Study of Alternative Spent

- Fuel Processing. *INMM Annual Meeting Proceedings*, Tucson, AZ, July 12-16, 2009.
69. Pomeroy, G.; Bari, R.; Wonder, E.; Zentner, M.; Haas, E.; Killeen, T.; Cojazzi, G.; Whitlock, J. Approaches to Evaluation of Proliferation Resistance of Nuclear Energy Systems. *Proceedings of the 49th Annual Meeting of the Institute of Nuclear Materials Management*, Nashville, TN, July 13-17, 2008.
  70. Ooyama, K.; Keta, S.; Kanou, M.; Moriyama, T.; Okamura, Y.; Ogaki, K.; Noda, K. Monitoring of Radioactive Gaseous and Liquid Wastes at Rokkasho Reprocessing Plant. *Pacific Basin Nuclear Conference*, 2006.
  71. Polovov, I. B.; Volkovich, V. A.; Charnock, J. M.; Kralj, B.; Lewin, R. G.; Kinoshita, J.; May, I.; Sharrad, C. A. In Situ Spectroscopy and Spectroelectrochemistry of Uranium in High-Temperature Alkali Chloride Molten Salts. *Inorg. Chem.* 2008, 47 (17), 7474-7482.
  72. Zhemzhurov, M. L.; Levadnyi, V. A. Gamma Spectrometry in Continuous Monitoring of the Impurity Concentration in the Coolant of a Reactor Circuit. *Atomic Energy*. 1991, 70 (3), 176.
  73. Walker, D. M.; Mullin, D. S. Updating of a Gamma Spectroscopy-based Failed Fuel Monitor. *IEEE Conference Record 1996 Nuclear Science Symposium*, Anaheim, CA, Nov 2-9, 1996.
  74. Sundar, U.; Sivadasan, P. C.; Yadav, R. B.; Gopalan, B.; Syamsundar, S. Rapid titrimetric determination of free acidity in process samples of uranyl nitrate. *Analyst*. 1998, 123, 1875-1877.

75. Moulin, C.; Decambox, P.; Mauchien, P.; Pouyat, D.; Couston, L. Direct Uranium(VI) and Nitrate Determinations in Nuclear Reprocessing by Time-Resolved Laser-Induced Fluorescence. *Anal.Chem.* 1996, 68 (18), 3204-3209.
76. Yamamoto, T. Spectrophotometric determination of plutonium with chlorophosphonazo III. *Mikrochim.Acta*. 1974, 62 (5), 871-877.
77. Moyers, R. Photometric Determination of Uranium Concentration. *INMM Annual Meeting Proceedings*, Baltimore, MD, July 11-15, 2010.
78. Hines, J. W.; Henkel, J. J.; Upadhyaya, B. R. Process Monitoring Techniques for Nuclear Material Diversion Detection. *J.Nucl.Mater.Manage.* 2009, XXXVII (3), 4-13.
79. Goddard, B.; Charlton, W. S.; McDeavitt, S. M. Real-Time Detection of UREX+3a Extraction Streams for Materials Accountancy. *Journal of Nuclear Materials Management*. 2009, 38 (1).
80. Carrott, M. J.; Wai, C. M. UV-Visible Spectroscopic Measurement of Solubilities in Supercritical CO Using High-Pressure Fiber-Optic Cells. *Anal.Chem.* 1998, 70 (11), 2421-2425.
81. Armenta, S.; Quintáns, G.; Garrigues, S.; Guardia, M. d. l. Mid-infrared and Raman spectrometry for quality control of pesticide formulations. *Trends in Analytical Chemistry*. 2005, 24 (8), 772-781.
82. Vankeirsbilck, T.; Vercauteren, A.; Baeyens, W.; Weken, G. V. d.; Verpoort, F.; Vergote, G.; Remon, J. P. Applications of Raman spectroscopy in pharmaceutical analysis. *Trends in Analytical Chemistry*. 2002, 21 (12), 869-877.

83. De Beer, T. R. M.; Vercruyse, P.; Burggraeve, A.; Quinten, T.; Ouyang, J.; Zhang, X.; Vervaet, C.; Remon, J. P.; Baeyens, W. R. G. In-Line and Real-Time Process Monitoring of a Freeze Drying Process Using Raman and NIR Spectroscopy as Complementary Process Analytical Technology (PAT) Tools. *Journal of Pharmaceutical Sciences*. 2009, 98 (9), 3430.
84. Nah, S.; Ryu, K.; Cho, S.; Chung, H.; Namkung, H. Simple and robust near-infrared spectroscopic monitoring of indium-tin-oxide (ITO) etching solution using Teflon tubing. *Anal.Chim.Acta*. 2006, 556 , 208-215.
85. Biddle, P.; Miles, J. H. Rate of Reaction of Nitrous Acid with Hydrazine and with Sulphamic Acid - Its Application to Nitrous Acid Control in 2-Phase Industrial Systems. *Journal of Inorganic & Nuclear Chemistry*. 1968, 30 (5), 1291.
86. Kawamura, K.; Nagayoshi, H.; Yao, T. In situ analysis of proteins at high temperatures mediated by capillary-flow hydrothermal UV-vis spectrophotometer with a water-soluble chromogenic reagent. *Analytica Chimica Acta*. 2010, 667, 88.
87. Bulatov, A. V.; Ivasenko, P. A.; Moskvin, L. N. Simultaneous Stepwise Injection - Photometric Determination of Nitrite and Nitrate Ions in Aqueous Media. *Journal of Analytical Chemistry*. 2010, 65 (8), 816.
88. Bryan, S.; Levitskaia, T. *Monitoring of UREX Radiochemical Processes for Enhanced Safeguards in Reprocessing Plant*; Pacific Northwest National Laboratory: Battelle, 2007.

89. Smith, N. A. UV/Visible Spectroscopy-based Process Monitoring, Fundamental Chemistry for Process Control, MC&A. *GNEP Safeguards Working Group*, PNNL, March, 2008.
90. Strong, F. C. Theoretical Basis of Bouguer-Beer Law of Radiation Absorption. *Anal.Chem.* 1952, 24 (2), 338-342.
91. Skoog, D.; Holler, F. J.; Neiman, T.; *Principles of Instrumental Analysis*; Eds.; Fifth; Harcourt Brace & Company: USA, 1998.
92. Bell, J. T.; Biggers, R. E. The Absorption Spectrum of the Uranyl Ion in Perchlorate Media: Part III. Resolution of the Ultraviolet Band Structure; Some Conclusions Concerning the Excited State of  $\text{UO}_2^{2+}$ . *J.Mol.Spectrosc.* 1968, 25, 312-329.
93. Bell, J. T.; Biggers, R. E. The Absorption Spectrum of the Uranyl Ion in Perchlorate Media: Part II. The Effects of Hydrolysis on the Resolved Spectral Bands. *J.Mol.Spectrosc.* 1967, 1967 (22), 262-271.
94. Bell, J. T.; Biggers, R. E. The Absorption Spectrum of the Uranyl Ion in Perchlorate Media: Part I. Mathematical Resolution of the Overlapping Band Structure and Studies of the Environmental Effects. *J.Mol.Spectrosc.* 1965, 18, 247-275.
95. Steele, H.; Taylor, R. J. A theoretical study of the inner-sphere disproportionation reaction mechanism of the pentavalent actinyl ions. *Inorg.Chem.* 2007, 46 (16), 6311-6318.

96. Tsushima, S.; Wahlgren, U.; Grenthe, I. Quantum chemical calculations of reduction potentials of  $\text{AnO}_2^{2+}/\text{AnO}_2^+$  ( $\text{An} = \text{U}, \text{Np}, \text{Pu}, \text{Am}$ ) and  $\text{Fe}^{3+}/\text{Fe}^{2+}$  couples. *Journal of Physical Chemistry A*. 2006, 110 (29), 9175-9182.
97. Ankudinov, A. L.; Ravel, B.; Rehr, J. J.; Conradson, S. D. Real-space multiple-scattering calculation and interpretation of x-ray-absorption near-edge structure. *Physical Review B*. 1998, 58 (12), 7565-7576.
98. de Jong, W. A.; Apra, E.; Windus, T. L.; Nichols, J. A.; Harrison, R. J.; Gutowski, K. E.; Dixon, D. A. Complexation of the carbonate, nitrate, and acetate anions with the uranyl dication: Density functional studies with relativistic effective core potentials. *Journal of Physical Chemistry A*. 2005, 109 (50), 11568-11577.
99. Barnes, C. E.; Shin, Y.; Saengkerdsub, S.; Dai, S. EXAFS study of uranyl nitrate dimer at high and low temperature. *Inorg. Chem.* 2000, 39 (4), 862-864.
100. Karim, D. P.; Georgopoulos, P.; Knapp, G. S. *EXAFS Studies of Actinide Ions in Aqueous Solution*; Argonne National Laboratory: Argonne, 1979.
101. Allen, P. G.; Shuh, D. K.; Bucher, J. J.; Edelstein, N. M.; Palmer, C. E. A.; Silva, R. J.; Nguyen, S. N.; Marquez, L. N.; Hudson, E. A. Determinations of uranium structures by EXAFS: Schoepite and other U(VI) oxide precipitates. *Radiochimica Acta*. 1996, 75 (1), 47-53.
102. Allen, P. G.; Shuh, D. K.; Bucher, J. J.; Edelstein, N. M.; Reich, T.; Denecke, M. A.; Nitsche, H. EXAFS determinations of uranium structures: The uranyl ion complexed with tartaric, citric, and malic acids. *Inorg. Chem.* 1996, 35 (3), 784-&.

103. Allen, P. G.; Bucher, J. J.; Shuh, D. K.; Edelstein, N. M.; Reich, T. Investigation of Aquo and Chloro Complexes of UO<sub>2</sub><sup>2+</sup>, NpO<sub>2</sub><sup>+</sup>, Np<sup>4+</sup>, and Pu<sup>3+</sup> by X-ray Absorption Fine Structure Spectroscopy. *Inorg. Chem.* 1997, 36 (21), 4676-4683.
104. Gaillard, C.; Chaumont, A.; Billard, I.; Hennig, C.; Ouadi, A.; Wipff, G. Uranyl coordination in ionic liquids: The competition between ionic liquid anions, uranyl counterions, and Cl<sup>-</sup> anions investigated by extended X-ray absorption fine structure and UV-visible spectroscopies and molecular dynamics simulations. *Inorg. Chem.* 2007, 46 (12), 4815-4826.
105. Ikeda-Ohno, A.; Hennig, C.; Rossberg, A.; Funke, H.; Scheinost, A. C.; Bernhard, G.; Yaita, T. Electrochemical and complexation behavior of neptunium in aqueous perchlorate and nitrate solutions. *Inorg. Chem.* 2008, 47 (18), 8294-8305.
106. Di Giandomenico, M. V.; Le Naour, C.; Simoni, E.; Guillaumont, D.; Moisy, P.; Hennig, C.; Conradson, S. D.; Den Auwer, C. Structure of early actinides(V) in acidic solutions. *Radiochimica Acta*. 2009, 97 (7), 347-353.
107. Chan, S. K.; Knapp, G. S. *Extended X-Ray Absorption Fine Structure (EXAFS) Studies of the Actinides*. 3<sup>rd</sup> International EXAFS Conference, Stanford, CA. July 16-20, 1984.
108. Denecke, M. A.; Dardenne, K.; Marquardt, C. M. Np(IV)/Np(V) valence determinations from Np L3 edge XANES/EXAFS. *Talanta*. 2005, 65 (4), 1008-1014.
109. Fillaux, C.; Berthet, J. C.; Conradson, S. D.; Guilbaud, P.; Guillaumont, D.; Hennig, C.; Moisy, P.; Roques, J.; Simoni, E.; Shuh, D. K.; Tyliszczak, T.; Castro-Rodriguez, I.; Den Auwer, C. Combining theoretical chemistry and

- XANES multi-edge experiments to probe actinide valence states. *Comptes Rendus Chimie*. 2007, 10 (10-11), 859-871.
110. Conradson, S. D.; Abney, K. D.; Begg, B. D.; Brady, E. D.; Clark, D. L.; den Auwer, C.; Ding, M.; Dorhout, P. K.; Espinosa-Faller, F. J.; Gordon, P. L.; Haire, R. G.; Hess, N. J.; Hess, R. F.; Keogh, D. W.; Lander, G. H.; Lupinetti, A. J.; Morales, L. A.; Neu, M. P.; Palmer, P. D.; Paviet-Hartmann, P.; Reilly, S. D.; Runde, W. H.; Tait, C. D.; Veirs, D. K.; Wastin, F. Higher order speciation effects on plutonium L-3 X-ray absorption near edge spectra. *Inorg.Chem.* 2004, 43 (1), 116-131.
111. Conradson, S. D.; Manara, D.; Wastin, F.; Clark, D. L.; Lander, G. H.; Morales, L. A.; Rebizant, J.; Rondinella, V. V. Local structure and charge distribution in the UO<sub>2</sub>-U<sub>4</sub>O<sub>9</sub> system. *Inorg.Chem.* 2004, 43 (22), 6922-6935.
112. Servaes, K.; Hennig, C.; Billard, I.; Gaillard, C.; Binnemans, K.; Gorller-Walrand, C.; Van Deun, R. Speciation of uranyl nitrato complexes in acetonitrile and in the ionic liquid 1-butyl-3-methylimidazolium bis(trifluoromethylsulfonyl)imide. *European Journal of Inorganic Chemistry*. 2007, (32), 5120-5126.
113. Newville, M.: *Fundamentals of XAFS Report*. Chicago, IL, pp1-40, 2004.
114. Argonne National Laboratory: Advanced Photon Source For Prospective Users: Learn about X-ray Research. <http://www.aps.anl.gov/Users/Prospective/>, May 19, 2011.
115. Ressler, T. WinXAS: a program for X-ray absorption spectroscopy data analysis under MS-Windows. *Journal of Synchrotron Radiation*. 1998, 5, 118-122.

116. Baltic University Environmental Science Chapter 12: Metal Flows and Environmental Impact, Figure 12.21.  
[http://www.balticuniv.uu.se/environmentalscience/ch12/chapter12\\_g.htm](http://www.balticuniv.uu.se/environmentalscience/ch12/chapter12_g.htm), 2011.
117. Harris, D.C. *Quantitative Chemical Analysis*; Eds,; W.H. Freeman and Co: 2003.
118. *Determination of the Acidity of Aqueous Solutions Containing Hydrolyzable Metal Ions Using Oxalate Complexation*; Allied-General Nuclear Services, Eds,; 1978.
119. Paviet-Hartmann, P. Lecture 8: Notions of Chemical Engineering. Presented at CHEM 793: Reprocessing, UNLV, Spring Semester, 2009.
120. Todd, T. INL Research Fact Sheets: Advanced Separation Technologies.  
<http://www.inl.gov/research/advanced-separation-technologies/>, May 19, 2011.
121. CINC Industries, L. V-02 Operating Manual.  
<http://www.cincmfg.com/v/vspfiles/downloadables/Manual%20V-02.swf>, 2011.
122. Serrano-Purroy, D.; Baron, P.; Christiansen, B.; Glatz, J. -.; Madic, C.; Malmbeck, R.; Modolo, G. First demonstration of a centrifugal solvent extraction process for minor actinides from a concentrated spent fuel solution. *Separation and Purification Technology*. 2005, 45 (2), 157-162.
123. Takeuchi, M.; Ogino, H.; Nakabayashi, H.; Arai, Y.; Washiya, T.; Kase, T.; Nakajima, Y. Extraction and stripping tests of engineering-scale centrifugal contactor cascade system for spent nuclear fuel reprocessing. *J Nucl Sci Technol.* 2009, 46 (3), 217-225.

124. Padial-Collins, N. T.; Zhang, D. Z.; Zou, Q.; Ma, X. Centrifugal Contactors: Separation of an Aqueous and an Organic Stream in the Rotor Zone (LA-UR-05-7800). *Sep.Sci.Technol.* 2006, 41, 1001-1023.
125. Pereira, C. Argonne National Laboratory, General Contactor Slides - Personal Communication, 2008.
126. Leonard, R. A.; Chamberlain, D. B.; Conner, C. Centrifugal Contactors for Laboratory-Scale Solvent Extraction Tests. *Sep.Sci.Technol.* 1997, 32 (1), 193-210.
127. Bilancia, G.; Facchini, A.; Ferrando, M.; Giola, M.; Maluta, F.; Mariani, M.; Mazzuccato, M.; Madic, C.; Sabbioneda, S. Selective actinide extraction with a tri-synergistic mixture using a centrifugal contactor battery. *Solvent Extraction and Ion Exchange*. 2005, 23 (6), 773-780.
128. Weber, A., Eds.; *Topics in Current Physics: Raman Spectroscopy of Gases and Liquids*. Springer-Verlag: Germany, 1979; 11, 318.
129. Siesler, H. W., Ozaki, Y., Kawata, S., Heise, H. M., Eds.; *Near-Infrared Spectroscopy*. Wiley-VCH: Germany, 2002; 348.
130. Nakamoto, K.; Eds. *Infrared and Raman Spectra of Inorganic and Coordination Compounds*. John Wiley & Sons, Inc.: USA, 1997; Fifth Ed. Part A: Theory and Applications in Inorganic Chemistry, 387.
131. Nakamoto, K.; Eds. *Infrared and Raman Spectra of Inorganic and Coordination Compounds*. John Wiley & Sons, Inc.: USA, 1997; Fifth Ed. Part B: Applications in Coordination, Organometallic, and Bioinorganic Chemistry, 384.

132. Smith, N. A.; Cerefice, G. S.; Czerwinski, K. Application of Optical Techniques for On-Line Materials Accountability in the UREX Solvent Extraction Process. *47th Annual Institute for Nuclear Materials Management Annual Meeting*, 2006.
133. Atkins,P.W.; Paula,J.D. *Physical Chemistry*; Eds.,; W.H. Freeman: 2002.
134. Ahrlund, S.On the Complex Chemistry of the Uranyl Ion, Part I. The Hydrolysis of the Six-valent Uranium in Aqueous Solutions. *Acta Chem.Scand.* 1949, 3, 374-400.
135. Ahrlund, S.On the Complex Chemistry of the Uranyl Ion, Part VI. The Complexity of Uranyl Chloride, Bromide and Nitrate. *Acta Chem.Scand.* 1951, 5, 1271-1282.
136. Ryan, J. L.Anion Exchange and Non-Aqueous Studies of the Anionic Nitrate Complexes of the Hexavalent Actinides. *J.Phys.Chem.* 1961, 65 (7), 1099-1107.
137. Crocker, I. H.Oxidation of Pu(IV) to Pu(VI) in Solutions of Nitric Acid, Aluminum Nitrate, Sodium Nitrate, and Uranyl Nitrate. *CRDC-657*. 1957.
138. Nockemann, P.; Servaes, K.; Deun, R. V.; Hecke, K. V.; Meervelt, L. V.; Binnemans, K.; Grller-Walrand, C. Speciation of Uranyl Complexes in Ionic Liquids by Optical Spectroscopy. *Inorg.Chem.* 2007, 46 (26), 11335-11344.
139. Grenthe, I.; Drozdynski, J.; Fujino, T.; Buck, E. C.; Albrecht-Schmitt, T. E.; Wolf, S. F. Uranium. *The Chemistry of the Actinide and Transactinide Elements*, Springer: The Netherlands, 2006; 3, 577.
140. Bostick, D. T.*The Simultaneous Analysis of Uranium and Nitrate*; Oak Ridge National Laboratory Analytical Chemistry Division: Oak Ridge, 1978.

141. Meinrath, G. Uranium (VI) Speciation by Spectroscopy. *J.Radioanal.Nucl.* 1997, 224 (1-2), 119-126.
142. Meinrath, G.; Klenze, R.; Kim, J. I. Direct Spectroscopic Speciation of Uranium (VI) in Carbonate Solutions. *Radiochimica Acta*. 1996, 74, 81-86.
143. Gray, J. H.; Swanson, J. L. *Report: Properties of Concentrated Plutonium Nitrate Solutions*; Allied-General Services: 1978.
144. Tkac, P.; Paulenova, A.; Gable, K. P. Spectroscopic Study of the Uranyl-Acetohydroxamate Adduct with Tributyl Phosphate. *Appl.Spectrosc.* 2007, 61 (7), 772-776.
145. Taylor, R. J.; May, I. Advances in actinide and technetium kinetics for applications in process flowsheet modeling. *Sep.Sci.Technol.* 2001, 36 (5-6), 1225-1240.
146. Birkett, J. E.; Carrott, M. J.; Fox, O. D.; Jones, C. J.; Maher, C. J.; Roube, C. V.; Taylor, R. J.; Woodhead, D. A. Controlling Neptunium and Plutonium within Single Cycle Solvent Extraction Flowsheets for Advanced Fuel Cycles. *J Nucl Sci Technol.* 2007, 44 (3), 337-343.
147. Nitsche, H.; Lee, S. C.; Gatti, R. C. Determination of Plutonium Oxidation States at Trace Levels Pertinent to Nuclear Waste Disposal. *J.Radioanal.Nucl.* 1988, 124 (1), 171-185.
148. Veirs, D. K.; Smith, C. A.; Zwick, B. D.; Marsh, S. F.; Conradson, S. D. Characterization of the nitrate complexes of Pu(IV) using absorption spectroscopy,  $^{15}\text{N}$  NMR and EXAFS. 1993.

149. Wilson, R. E.; Hu, Y.; Nitsche, H. Detection and Quanitification of Pu(III, IV, V and VI) Using a 1.0-meter Liquid Core Waveguide. *Radiochimica Acta*. 2005, 93 (4), 203-206.
150. Silva, R. J.; Nitsche, H. Actinide Environmental Chemistry. *Radiochimica Acta*. 1995, 70/71, 377.
151. Burger, S.; Banik, N. L.; Buda, R. A.; Kratz, J. V.; Kuczewski, B.; Trautmann, N. Speciation of the oxidation states of plutonium in aqueous solutions by UV/Vis spectroscopy, CE-ICP-MS and CE-RIMS. *Radiochimica Acta*. 2007, 95 (8), 433-438.
152. Masaumi, N.; Sano, Y.; Koma, Y.; Kamiya, M.; Shibata, A.; Koizumi, T.; Koyama, T. Separation of actinide elements by solvent extraction using centrifugal contactors in the NEXT process. *J Nucl Sci Technol*. 2007, 44 (3), 373-381.
153. Meikrantz, D.; Garn, T.; Mann, N.; Law, J.; Todd, T. Hydraulic performance and mass transfer efficiency of engineering scale centrifugal contactors. *GLOBAL 2007: Advanced Nuclear Fuel Cycles and Systems*, Boise, ID, September 9-13, 2007.
154. Krebs, J. F. Figures for Warburton, personal communication, September 19, 2008.
155. Department of Energy Understanding Official Use Only.  
<http://www.hss.doe.gov/classification/QualityMgt/understandingouo.pdf>, May 20, 2011.
156. Department of Energy Controlled Unclassified Scientific and Technical Information. <http://www.osti.gov/stip/controlled>, May 20, 2011.

157. Law, J. D.; Garn, T. G.; Meikrantz, D. H.; Warburton, J. Pilot-scale truex flowsheet testing for separation of actinides and lanthanides from used nuclear fuel. *Sep.Sci.Technol.* 2010, 45 (12), 1769-1775.
158. Pereira, C.; Vandegrift, G.; Regalbuto, M.; Bakel, A.; Bowers, D.; Gelis, A.; Hebden, A.; Maggos, L.; Stepinski, D.; Tsai, Y.; Laidler, J. Lab-Scale Demonstration of the UREX+1a Process Using Spent Fuel. *Proceedings of Waste Management '07*, Tucson, AZ, February 25-March 1, 2007.
159. Chamberlain, D. B.; Conner, C.; Hutter, J. C.; Leonard, R. A.; Wygmans, D. G.; Vandegrift, G. F. TRUEX processing of plutonium analytical solutions at Argonne National Laboratory. *Sep.Sci.Technol.* 1997, 32 (1-4), 303-326.
160. Felker, L. K.; Binder, J. L.; Benker, D. E.; Collins, E. D.; Bailey, P. D.; Bell, G. L.; Jubin, R. T.; Spencer, B. B.; Del Cul, G. D.; Vedder, R. L.; Walker, E. A.; Voit, S. L. *Results, Evaluation, and Lessons Learned from the Coupled End to End Project Campaign 1 Using Dresden BWR Used Fuel*; GNEP-SEPA-PMO-M1-DV-2008-000131, ORNL/GNEP/LTR-2008-044; 2008.
161. Jubin, R.; Collins, E.; Felker, K.; Spencer, B.; Walker, E.; Vedder, R.; Taylor, R.; Binder, J. CETE R&D at Oak Ridge National Laboratory Supporting Management of Nuclear Waste. *Proceedings of Waste Management '09*, Phoenix, AZ, March 1-5, 2009, .
162. Garn, T. G.; Meikrantz, D. H.; Greenhalgh, M.; Law, J. D. *Temperature Profile Measurements in a Newly Constructed 30-Stage 5 cm Centrifugal Contactor Pilot Plant*; INL/EXT 08-14861; 2008.

163. Meikrantz, D. H.; Law, J. D.; Herbst, R. S.; Garn, T. G.; Mann, N. R.; Todd, T. A. *Hydraulic and Mass Transfer Testing of Commercial 5 cm Annular Centrifugal Contactors at INL*; INL/EXT 05-00793; 2005.
164. Garn, T. G.; Mann, N. R.; Meikrantz, D. H.; Law, J. D.; Todd, T. A. *Hydraulic and Reliability Tests of the CINC C-05TA-CIP 12.5 cm Annular Centrifugal Contactor*; INL/EXT 06-11958; 2006.
165. Mann, N. R.; Garn, T. G.; Meikrantz, D. H.; Law, J. D.; Todd, T. A. *Clean In Place Testing of a Commercial 12.5 cm Annular Centrifugal Contactor at the INL*; INL/EXT 06-111533; 2006.
166. Garn, T. G.; Meikrantz, D. H.; Law, J. D.; Mann, N. R.; Todd, T. A. *Mass Transfer Efficiency Testing of a Single Stage Commercial 12.5 cm Annular Centrifugal Contactor at the INL*; INL/EXT 07-12739; 2007.
167. Brewer, K. N.; Herbst, S. R.; Tranter, T. J.; Todd, T. A. *CMPO Purity Tests in the TRUEX Solvent Using Americium-241*; WINCO-1177; 2008.
168. Gelis, A. V.; Vandegrift, G. F.; Bakel, A.; Bowers, D. L.; Hebden, A. S.; Pereira, C.; Regalbuto, M. Extraction behaviour of actinides and lanthanides in TALSPEAK, TRUEX and NPEX processes of UREX+. *Radiochimica Acta*. 2009, 97 (4-5), 231-232.
169. Fujii, T.; Aoki, K.; Yamana, H. Effect of nitric acid distribution on extraction behavior of trivalent f-elements in a TRUEX system. *Solvent Extraction and Ion Exchange*. 2006, 24 (3), 347-357.

170. Brewer, K.; Herbst, R.; Tranter, T.; Todd, T. *CMPO Purity Test in the TRUEX Solvent Using Americium-241*; WINCO-1177; Westinghouse Idaho Nuclear Company: 1993.
171. Schulz, W. W.; Horwitz, E. P. The TRUEX Process: Removal/Recovery of TRU elements from acidic waste solutions, *Extraction 87. The Recovery of High Value Materials*. 1987, 103, 245.
172. Vandegrift, G. F.; Chamberlain, D. B.; Conner, C.; Copple, J. M.; Dow, J. A.; Everson, L.; Hutter, J. C.; Leonard, R. A.; Nunez, L.; Regalbuto, M. C.; Sedlet, J.; Srinivasan, B.; Weber, S.; Wygmans, D. G. Development and Demonstration of the TRUEX Solvent Extraction Process. *Technology and Programs for Radioactive Waste Management and Environmental Restoration*. 1993, 2, 1045.
173. Meikrantz, D. H.; Federici, A. G.; Macaluso, L. L.; Sams, H. W. Rotor Sleeve for a Centrifugal Separator. U.S. Patent 5.571.070, 1996.
174. Garn, T. G. Idaho National Laboratory, Estimation of steady-state conditions by calculating solvent turnovers, unpublished, June 2009.
175. General Atomics EM<sup>2</sup> - Nuclear Waste to Energy.  
<http://www.ga.com/energy/em2/> 2011.
176. Lineberry, M. J.; McFarlane, H. F. The EBR-II Spent Fuel Treatment Program. *Proceedings of GLOBAL 1995*, Versailles, France, September 11-14, 1995.
177. Laidler, J. J.; Battles, J. E.; Miller, W. E.; Ackerman, J. P.; Carls, E. L. Development of Pyroprocessing Technology. *Progress in Nuclear Energy*. 1997, 31 (1/2), 131.

178. McPheevers, C. C.; Pierce, R. D.; Mulcahey, T. P. Application of the Pyrochemical Process to Recycle of Actinides from LWR Spent Fuel. *Progress in Nuclear Energy*. 1997, 31 (1/2), 175.
179. US Energy Information Administration Electricity Net Generation: Total (All Sectors), 1949-2009. <http://www.eia.gov/electricity/data.cfm>, 2010.
180. Choi, H. General Atomics, ORIGEN burnup calculations, personal communication, July 2010.
181. Westphal, B. R.; Bateman, K. J.; Lind, B. P.; Howden, K. L.; Del Cul, G. D. Fission Product Removal from Spent Oxide Fuel by Head-End Processing. *Proceedings of GLOBAL 2005*, Tsukuba, Japan, October 9-15, 2005, 2005.
182. Benedict, R. W.; Solbrig, C.; Westphal, B.; Johnson, T. A.; Li, S. X.; Marsden, K.; Goff, K. M. Pyroprocessing Progress at Idaho National Laboratory. *Proceedings of GLOBAL 2007*, Boise, ID, September 9-13, 2007.
183. Westphal, B. R.; Vaden, D.; Li, S. X.; Frederickson, G. L.; Mariani, R. D. Fate of Noble Metals During the Pyroprocessing of Spent Nuclear Fuel. *Proceedings of GLOBAL 2009*, Paris, France, September 6-11, 2009.
184. Lee, J. H.; Shim, J. B.; Kim, E. H.; Yoo, J. H. A Feasibility Study for the Development of Alternative Methods to Treat a Spent TRISO Fuel. *Nuclear Technology*. 2008, 162, 250.
185. Spalding, B. P. Volatility and extractability of strontium-85, cesium-134, cobalt-57, and uranium after heating hardened Portland cement paste. *Environmental Science and Technology*. 2000, 34 (23), 5051-5058.

186. Lewis, B. J.; Andre, B.; Ducros, G.; Maro, D. *A Model For Non-Volatile Fission Product Release During Reactor Accident Conditions*; 30000528; Commissariat a l'Energie Atomique.
187. Lewis, B. J.; Corse, B. J.; Thompson, W. T.; Kaye, M. H.; Iglesias, F. C.; Elder, P.; Dickson, R.; Liu, Z. *Vaporization of Low-Volatile Fission Products Under Severe CANDU Reactor Accident Conditions*; 31006089; Royal Military College of Canada.
188. Westphal, B. R.; Park, J. J.; Shin, J. M.; Park, G. I.; Bateman, K. J.; Wahlquist, D. L. Selective trapping of volatile fission products with an off-gas treatment system. *Sep.Sci.Technol.* 2008, *43* (9-10), 2695-2708.
189. Asquith, J. G.; Grantham, L. F. Low-Decontamination Approach To A Proliferation-Resistant Fuel Cycle. *Nucl Technol.* 1978, *41* (2), 137-148.
190. Hanson, L. A. *Removal of Irradiated UO<sub>2</sub> Fuel From the Cladding by Controlled Oxidation*; NAA-SR-3591; Atomics International: 1959.
191. Brand, G. E.; Murbach, E. W. *Pyrochemical Reprocessing of UO<sub>2</sub> by AIROX Summary Report*; NAA-SR-11389; Atomics International: 1965.
192. Reynard, M. P.; Czerwinski, K. R. MIT Contribution to the LDRD AIROX Project: Examination of Waste Issues. Massachusetts Institute of Technology, 1999.
193. Christian, J.; Sterbentz, J.; Abbott, D.; Czerwinski, K. R.; Caciapouti, R. Concepts for dry processing of spent nuclear fuel for recycling to light-water reactors. *Scientific Basis for Nuclear Waste Management XXIII*, Boston, MA, USA, November 29-December 2, 1999, 2000.

194. Plaue, J. Thesis: Evaluation of Uranium Carbide and Sulfide Fuels for a Gas-Cooled Fast Reactor utilizing Dry Reprocessing. M.S., MIT, 2003.
195. The Nuclear Regulatory Commission: Uranium Enrichment.  
<http://www.nrc.gov/materials/fuel-cycle-fac/ur-enrichment.html>, November 6, 2011.
196. Song, K. C.; Park, G. I.; Lee, J. W.; Park, J. J.; Yang, M. S. Fractional release behavior of volatile and semivolatile fission products during a voloxidation and OREOX treatment of spent PWR fuel. *Nucl Technol.* 2008, 162 (2), 158-168.
197. Park, G. I.; Lee, J. W.; Yang, M. S. Release behavior of Kr-85 from spent fuel during OREOX process. *Transactions of the American Nuclear Society.* 2004, 91, 521.
198. Choi, H.; Baxter, A. A comparative study on recycling spent fuels in gas-cooled fast reactors. *Annals of Nuclear Energy.* 2010, 37 (5), 723.
199. Bresee, J. Advanced Fuel Cycle R&D, Separations and Waste Forms. *Advanced Reactor, Fuel Cycle and Energy Products Workshop for Universities,* Gaithersburg, MD, unpublished.
200. Ko, W. I.; Kim, H. D. Analysis of Nuclear Proliferation Resistance of DUPIC Fuel Cycle. *J Nucl Sci Technol.* 2001, 38 (9), 757-765.
201. Pillay, K. K. S. Safeguards and Nonproliferation Aspects of a Dry Fuel Recycling Technology. *International conference and Technology Exhibition Global 1993,* Seattle, Washington, September 12-17, 1993, 1993.
202. Hoyt, R. C.; Grantham, L. F. A Proliferation-Resistant Method of Recycling Fissile-Rich Spent Fuel. *Transactions of the American Nuclear Society,* 1979.

203. Brooker, M. H.; Huang, C.; Sylwestrowicz, J. Raman spectroscopic studies of aqueous uranyl nitrate and perchlorate systems. *Journal of Inorganic and Nuclear Chemistry*. 1980, *42* (10), 1431-1440.
204. Morris, D. E.; Hobart, D. E. Raman Spectra of the Lanthanide Oxalates. *Journal of Raman Spectroscopy*. 1988, *19*, 231.
205. Baron, P.; Brown, C.; Kaiser, B.; Matthews, B.; Mukaiyama, T.; Omberg, R.; Peddicord, L.; Salvatores, M.; Walter, A. *An Evaluation of the Proliferation Resistant Characteristics of Light Water Reactor Fuel with the Potential for Recycle in the United States*; Pacific Northwest National Laboratory, 2004.
206. Argonne National Laboratory: The Reduced Enrichment for Research and Test Reactors (RERTR) Program. <http://www.rertr.anl.gov/index.html>, November 6, 2011.
207. Pond, R. B.; Matos, J. E. *Photon Dose Rates From Spent Fuel Assemblies With Relation To Self-Protection (Rev. 1)*; ANL/RERTR/TM-25; Argonne National Laboratory RERTR Program: Argonne, IL, 1996.
208. Hassing, S.; Jernshoj, K. D.; Hedegaard, M. Solving chemical classification problems using polarized Raman data. *Journal of Raman Spectroscopy*. 2010, *42* (1), 21.
209. Hanoune, B.; Paccou, L.; Delcroix, P.; Guinet, Y. Raman identification of H<sub>2</sub>CO in aqueous solutions. *Journal of Raman Spectroscopy*. 2010, *42* (3).
210. Murray, P. AREVA, MPACT Working Group Meeting Discussion. Gaithersburg, MD, September 15, 2010.

211. Frost, R. L.; Palmer, S. J.; Reddy, B. J. Raman spectroscopic study of the uranyl titanate mineral euxenite (Y, Ca, U, Ce, Th)(Nb, Ta, Ti)<sub>2</sub>O<sub>6</sub>. *Journal of Raman Spectroscopy*. 2011, 42 (3).
212. Frost, R. L.; Cejka, J. A Raman spectroscopic study of the uranyl mineral rutherfordine - revisited. *Journal of Raman Spectroscopy*. 2009, 40 (9), 1096.
213. Dik, T. A. Spectral Properties of Uranyl Nitrate Complexes with Tertiary Aliphatic Phosphine Oxides. *Journal of Applied Spectroscopy*. 2001, 68 (1), 55-60.
214. Ikeda-Ohno, A.; Hennig, C.; Tsushima, S.; Scheinost, A. C.; Bernhard, G.; Yaita, T. Speciation and structural study of U(IV) and -(VI) in perchloric and nitric acid solutions. *Inorg. Chem.* 2009, 48 (15), 7201-7210.
215. Kruglik, S. G.; Lambry, J. -.; Martin, J. -.; Vos, M. H.; Negrerie, M. Sub-picosecond Raman spectrometer for time-resolved studies of structural dynamics in heme proteins. *J.Raman Spectrosc.* 2011, 42 (3), 265-275.
216. Lucaleau, G.; Le Bacq, O.; Pasturel, A.; Bouvier, P.; Pagnier, T. High-pressure polarized Raman spectra of Gd<sub>2</sub>(MoO<sub>4</sub>)<sub>3</sub>: Phase transitions and amorphization. *J.Raman Spectrosc.* 2011, 42 (3), 452-460.
217. Merten, C.; Li, H.; Lu, X.; Hartwig, A.; Nafie, L. A. Observation of resonance electronic and non-resonance-enhanced vibrationalnatural Raman optical activity. *J.Raman Spectrosc.* 2010, 41 (12), 1563-1565.
218. Okita, Y.; Katagiri, T.; Matsuura, Y. A Raman cell based on hollow optical fibers for breath analysis, *Progress in Biomedical Optics and Imaging – Proceedings of SPIE*, (7559), 2010.

219. Smardzewski, R. R.; Andrews, L. Raman spectra of the products of rubidium and cesium atom argon matrix reactions with oxygen molecules. *J.Phys.Chem.* 1973, 77 (6), 801-804.
220. Selig, H.; Fried, S. Raman spectra of technetium heptoxide. *Inorganic and Nuclear Chemistry Letters*. 1971, 7 (4), 315-323.
221. Cerefice, G. S. Lecture 6: Regulations and Waste Management. Presented at ME656: Nuclear Waste Management, UNLV, 2009.
222. U.S. NRC NRC Regulations, Title 10 Code of Federal Regulations Part 61.55 Waste Classification. <http://www.nrc.gov/reading-rm/doc-collections/cfr/part061/part061-0055.html>, 2011.
223. Barrett, L. H. United States used Nuclear Fuel Management: Future Options. *Proceedings of the Institute for Nuclear Materials Management 51st Annual Meeting*, Baltimore, MD, July 11-15, 2010.
224. Lucuta, P. G.; Verrall, R. A.; Matzke, H. J.; Palmer, B. J. Microstructural features of SIMFUEL - Simulated high-burnup UO<sub>2</sub>-based nuclear fuel. *Journal of Nuclear Materials*. 1991, 178, 48.
225. Asuvathraman, R.; Rajagopalan, S.; Ananthasivan, K.; Mathews, C. K.; Mallya, R. M. Surface studies on uranium monocarbide using XPS and SIMS. *J.Nucl.Mater.* 1995, 224 (1), 25-30.
226. Lee, J.; Lee, J. I.; Chang, W. J.; Chang, S. H. Comparative cost analysis of direct disposal versus pyro-processing with DUPIC in Korea. *Annals of Nuclear Energy*. 2010, 37 (12), 1699.

## VITA

Jamie Lee Warburton

### Degrees:

Bachelor of Science, Nuclear Science and Engineering, 2003  
Massachusetts Institute of Technology

### Special Honors and Awards:

Nonproliferation Graduate Fellow – PNNL contractor to NNSA, 2010-2011  
Nuclear Forensics Graduate Fellow – Sponsored by DNDO and DTRA, 2008-2011  
Roy G. Post Foundation Scholarship Recipient, 2010  
Professional Women in ANS Funding Award, 2010  
Innovations in Fuel Cycle Research Award, 1<sup>st</sup> Place MC&A, 2010  
J. D. Williams Student Paper Award, INMM, 2<sup>nd</sup> Place, 2010  
Women In Nuclear Sponsored Student, 2010

### Internships:

General Atomics, 2010  
Idaho National Laboratory, 2009  
Argonne National Laboratory, 2008

### Publications:

**Warburton, J. L.**; Czerwinski, K.: *Demonstration of UV-Visible Spectroscopic Online Process Monitoring Under UREX Conditions*, Proceedings of the 52<sup>nd</sup> Annual Meeting of the Institute for Nuclear Materials Management, Palm Desert, CA, July 17-21, 2011.

**Warburton, J.**; Smith, N.; Czerwinski, K.: Method for online process monitoring for use in solvent extraction and actinide separations. *Separation Science and Technology*, 45, 1763-1768, 2010.

Law, J. D.; Garn, T. G.; Meikrantz, D. H.; **Warburton, J.**: Pilot-scale TRUEX flowsheet testing for separation of actinides and lanthanides from used nuclear fuel. *Separation Science and Technology*, 45, 1769-1775, 2010.

**Warburton, J.L.**, *Use of UV-Visible Spectroscopy to Determine Solution Chemistry Under Spent Nuclear Fuel Reprocessing Conditions*, Proceedings of the 51<sup>st</sup> Annual Meeting of the Institute for Nuclear Materials Management, Baltimore, MD, July 11-15, 2010.

Dissertation Title: Spectroscopic Methods of Process Monitoring for Safeguards of Used Nuclear Fuel Separations

Dissertation Examination Committee:

Chairperson, Ken Czerwinski, Ph. D.

Committee Member, Patricia Paviet-Hartmann, Ph. D.

Committee Member, Paul Forster, Ph. D.

Committee Member, Mary Anne Yates, Ph. D.

Graduate Faculty Representative, Anthony Hechanova, Ph. D.